Doctoral Thesis

Improvement of (Ultra-) High-Energy Hadronic Interaction Modeling

Rami Oueslati

A dissertation submitted in fulfillment of the requirements for the degree of Doctor of Science

Interactions Fondamentales en Physique et en Astrophysique
Département d'Astrophysique, Géophysique et Océanographie
Faculté de Sciences
Université de Liège
Belgique

2024

This work is dedicated to the memory of my father, Naceur, and my sister, Yosra.
Their love and presence are forever cherished, and their memory continues to inspire and sustain me.

Members of the Thesis Jury

Supervisor:
Jean-René Cudell

President:
Yaël Nazé

Secretary:
Dominique Sluse

Members of the Jury:
Ioana Maris
Adel Trabelsi

Abstract

The primary aim of this thesis was to enhance the modeling of hadronic interactions at high and ultra-high energies. This research delved into the complex dynamics of hadronic interactions, specifically focusing on proton-proton pp and proton-antiproton $p\bar{p}$ scattering. The central issue addressed was the unitarity of the S-matrix, with an emphasis on selecting the most accurate unitarity condition for composite particle interactions at high energies.

To achieve this, two unitarization schemes were thoroughly examined: the eikonal and the U-matrix schemes. These schemes were rigorously tested for their effectiveness in predicting crucial hadronic observables such as total, elastic, inelastic, and diffractive cross-sections, as well as multiplicity distributions. The first study evaluated the implications of high-energy collider data (up to $\sqrt{s} = 13$ TeV) on these cross-sections, demonstrating that the U-matrix scheme provides a fit to the data comparable to the eikonal scheme, with some differences that could impact Monte Carlo simulations.

The second study extended this analysis by incorporating diffractive interactions within a two-channel model, showing that both schemes fit the data well, with a slight preference for the U-matrix. This study also highlighted that the extended versions of these schemes, though slightly improved, still faced challenges in fitting the single diffractive cross-section accurately.

In the third study, a multi-channel model was explored, primarily using the U-matrix scheme. This model accurately described various cross-sections but underperformed in estimating the double-diffractive cross-section, suggesting that an additional pomeron interaction might be necessary. It was also found that the U-matrix scheme better accounts for potential pomeron correlations, which could influence predictions for ultra-high energy cosmic rays.

The fourth study introduced a phenomenological model for multi-particle production based on the geometrical approach and U-matrix scheme. The model provided a reasonable description of multiplicity distributions across

a broad energy range but revealed violations of geometrical and KNO scaling. The study highlighted the role of the U-matrix scheme in understanding the impact of collision geometry on multi-particle production.

Lastly, the fifth study focused on the Pomeron topological cross-section and multiplicity distribution using the Kancheli formalism. It was observed that in the U-matrix scheme, pomerons exhibit geometric correlations, which were not present in the eikonal scheme. This finding could resolve discrepancies between Gribov-Regge theory and string models.

In summary, this thesis contributes to the field of high-energy hadronic interactions by demonstrating the utility of the U-matrix scheme in providing improved predictions and insights into complex phenomena such as multi-particle production and pomeron exchange. The scheme's reliable extrapolation to ultra-high energy regimes makes it a promising candidate for future research and applications, particularly in Monte Carlo event generators for particle colliders and cosmic-ray physics.

This research establishes a solid foundation for further exploration of hadronic interactions at ultra-high energies and offers valuable theoretical perspectives and techniques for advancing particle physics and astrophysics. The thesis marks a significant step in addressing the ongoing challenges in this field.

Résumé

L'objectif principal de cette thèse était d'améliorer la modélisation des interactions hadroniques à haute et très haute énergie. Cette recherche a exploré les dynamiques complexes des interactions hadroniques, en se concentrant spécifiquement sur les interactions proton-proton pp et proton-antiproton $p\bar{p}$. La question centrale abordée était l'unité de la matrice S, avec un accent sur le choix de la condition d'unité la plus précise pour les interactions des particules composites à haute énergie.

Pour ce faire, deux schémas de unitarisation ont été examinés en profondeur : le schéma éikonal et le schéma U-matrice. Ces schémas ont été rigoureusement testés pour leur efficacité à prédire des observables hadroniques cruciales telles que les sections efficaces totales, élastiques, inélastiques et diffractives, ainsi que les distributions de multiplicité. La première étude a évalué les implications des données des colliders à haute énergie (jusqu'à $\sqrt{s} = 13$ TeV) sur ces sections efficaces, démontrant que le schéma U-matrice fournit un ajustement des données comparable à celui du schéma éikonal, avec certaines différences susceptibles d'affecter les simulations de Monte Carlo.

La deuxième étude a étendu cette analyse en incorporant des interactions diffractives dans un modèle à deux canaux, montrant que les deux schémas ajustent bien les données, avec une légère préférence pour le schéma U-matrice. Cette étude a également souligné que les versions étendues de ces schémas, bien que légèrement améliorées, rencontrent toujours des difficultés pour ajuster avec précision la section efficace diffractive unique.

Dans la troisième étude, un modèle multi-canaux a été exploré, principalement en utilisant le schéma U-matrice. Ce modèle a décrit avec précision diverses sections efficaces mais a sous-performé dans l'estimation de la section efficace double-diffractive, suggérant qu'une interaction supplémentaire de pomeron pourrait être nécessaire. Il a également été constaté que le schéma U-matrice rend mieux compte des corrélations potentielles des pomerons, ce qui pourrait influencer les prévisions pour les rayons cosmiques à très haute énergie.

La quatrième étude a introduit un modèle phénoménologique pour la production de multiparticules basé sur l'approche géométrique et le schéma U-matrice. Le modèle a fourni une description raisonnable des distributions de multiplicité sur une large gamme d'énergies, mais a révélé des violations du scaling géométrique et du scaling KNO. L'étude a mis en évidence le rôle du schéma U-matrice dans la compréhension de l'impact de la géométrie de collision sur la production de multiparticules.

Enfin, la cinquième étude s'est concentrée sur la section efficace topologique des pomerons et la distribution de multiplicité en utilisant le formalisme de Kancheli. Il a été observé que, dans le schéma U-matrice, les pomerons présentent des corrélations géométriques, ce qui n'est pas le cas dans le schéma éikonal. Cette découverte pourrait résoudre les écarts entre la théorie de Gribov-Regge et les modèles de cordes.

En résumé, cette thèse contribue au domaine des interactions hadroniques à haute énergie en démontrant l'utilité du schéma U-matrice pour fournir des prévisions améliorées et des aperçus sur des phénomènes complexes tels que la production de multiparticules et l'échange de pomeron. La capacité fiable du schéma à extrapoler aux régimes d'énergie ultra-haute en fait un candidat prometteur pour les recherches et applications futures, notamment dans les générateurs d'événements Monte Carlo pour les collisionneurs de particules et la physique des rayons cosmiques.

Cette recherche établit une base solide pour une exploration plus approfondie des interactions hadroniques à très haute énergie et offre des perspectives théoriques et des techniques précieuses pour faire progresser la physique des particules et l'astrophysique. La thèse marque une étape significative dans le traitement des défis en cours dans ce domaine.

Acknowledgements

I would like to express my heartfelt gratitude to several individuals who have significantly contributed to the completion of this thesis.

First and foremost, I wish to thank my supervisor, Jean-René Cudell, for his invaluable guidance, support, and encouragement throughout the course of this research. As a high-level researcher, his expert advice and insightful feedback have been crucial in refining my work. His commitment to my academic development and his patience in addressing the various challenges I encountered have been truly inspiring. Thanks to his guidance, I have grown significantly as a scientist and have become what I am today.

I am also thankful to my collaborator, Atri Bhattacharya, who initiated me into numerical calculations. His expertise in this area has been beneficial.

My sincere thanks go to Adel Trabelsi, whose unwavering encouragement and belief in my potential have continually inspired me to pursue a scientific career with determination.

I am grateful to all the other members of the thesis committee: Ioana Maris, Yaël Nazé, Damien Hutsemékers, Dominique Sluse. Their valuable feedback and perspectives have been essential in shaping this work.

Lastly, I would like to extend my appreciation to my family and friends for their constant support and understanding. Their encouragement and belief in my work have been a source of strength and motivation.

Thank you all for your contributions and support.

Contents

1 Introduction

1.1 Statement of the problem

The universe is constantly experiencing violent phenomena that result in the production of certain particles whose energy ranges from a few GeV to extremely high energies exceeding 10^{19} eV, namely cosmic rays, neutrinos, and gamma rays. Since these particles are detected on Earth, they are often regarded as excellent astrophysical "messengers" carrying information that could potentially provide solutions to a wide range of physics and astronomy-related concerns.

In particular, cosmic rays incessantly strike the Earth's atmosphere. These high-energy particles are mostly made up of 90% protons. Research has indicated that the cosmic ray flux declines sharply as energy increases. In fact, at energies above 10^{14} eV, the direct detection of these particles is unfeasible. Instead, they are investigated indirectly either by observing the cascades of particles stemming from their interaction with the Earth's atmosphere, commonly known as air showers, or by measuring the secondary particles reaching the ground. Ultra-high-energy cosmic rays (UHECRs), on the other hand, refer to cosmic rays with energies above 10^{18} eV (1 EeV). Their interaction with air nuclei in the upper atmosphere gives rise to extensive air showers (EAS).

The study of these UHECRs has considerably evolved with the advent of large detector arrays. For instance, IceTop, LOFAR, the Pierre Auger Observatory, and the Telescope Array are renowned air shower experiments covering cosmic-ray energies exceeding 10^{16} eV.

In spite of the considerable progress with respect to the detection and characterization of cosmic rays over the last few years, many questions about UHECRs still need to be answered, mainly with regard to their origins, mass composition, as well as the mechanisms accelerating these particles to such extreme energies.

It is worth noting that the observation of these messengers does not only provide valuable information about distant and violent places, but it also checks our understanding of particle physics since the process involving the

production of these messengers at the source, their propagation across the space, till their arrival at Earth, is governed by the laws of particle physics. Cosmic ray physics, for example, uses these particles as a means to probe hadronic interactions at an energy level that goes beyond that possible in terrestrial experiments, such as those conducted at the Large Hadron Collider (LHC). Specifically, as the energy of the UHECRs is significantly higher than that obtained by man-made accelerators, this makes them an ideal laboratory for investigating hadronic interactions at extremely high energies.

Therefore, by extending the energy range of observed interactions, cosmic ray data supplement collider experiments and allow for the study of hadronic interactions, spanning several orders of magnitude. This thorough coverage of energy ensures continuity in the understanding of energy dependence and helps in the improvement of hadronic models.

Air shower data is collected through ground-based detectors, such as those at the Pierre Auger Observatory and the IceCube Neutrino Observatory, which enables the reconstruction of early hadronic interactions. Monte Carlo (MC) simulation codes, based on different hadronic interaction models, such as QGSJET, EPOS, and SIBYLL, are fundamental in this reconstruction process.

It is worthwhile to note that although we have a strong grasp of electromagnetic interactions in the process of cosmic-ray air shower formation, modelling hadronic interactions remains a challenging task. This is mainly due to the paucity of accelerator data within the relevant phase space for air showers, especially in forward particle physics and to the necessity of extrapolating theoretical or phenomenological descriptions of accelerator data to considerably higher energies.

Moreover, modelling hadronic interactions is not devoid of uncertainties, as results vary depending on the specific model employed, and there is a notable discrepancy between predictions and measurements in the description of cosmic-ray observables. For instance, the muon puzzle, referring to the divergence between model predictions and the observed number of muons produced in extensive atmospheric air showers, is one of the long-standing problems in air-shower physics. The reason for this disparity is that the simulation results are not in line with actual measurements. Furthermore, an initial investigation [40] revealed significant variations in the muon spectra predicted by distinct hadronic interaction models at the atmospheric depth where the IceTop surface array of IceCube is located.

Hadronic interactions, involving particles that undergo strong interactions, are at the core of Particle Physics. They are mainly described through Quantum Chromodynamics (QCD), which is now widely recognized as the theory of strong interactions. It is a sophisticated and highly nonlinear quantum field theory describing how quarks and gluons, which are the fundamental building blocks of hadrons, such as protons and neutrons, interact and bind together to create observable particles.

Nevertheless, as a perturbative theory, QCD is most applicable to processes in which the coupling constant is small. Indeed, the QCD coupling constant, α_s, depends on the energy scale of the interaction Q^2 (the momentum transferred between quarks and gluons). Fig. 1.1 illustrates the running coupling constant α_s as a function of the energy scale Q, derived from distinct measurements and QCD calculations.

Owing to the fact that the coupling constant depends on the energy scale, QCD processes can be classified into two regimes, namely Hard QCD and Soft QCD processes.

According to Fig. 1.1, first, it can be seen that at large energy scales when compared to Λ_{QCD}, i.e. small distances, α_s becomes small. This is known as asymptotic freedom and in this regime termed as Hard QCD, perturbative calculations are applicable. Second, for large distances or at the low momentum scale, the QCD coupling constant becomes large, and the perturbation theory breaks down. This regime is known as Soft QCD. In view of the interplay between the two aforementioned regimes, QCD exhibits a depth and complexity that requires a number of theoretical tools so as to properly understand the behavior of the strong interaction at different energy scales.

Despite the considerable advancements in the theoretical description of high-energy hadron collisions during the last few years, we haven't acquired yet a good grasp of all of its facets. This is mainly due to the fact that high-energy hadronic and nuclear collisions are characterized by multi-particle productions, encompassing a wide range of phenomena. Besides, most of the particles produced are soft in nature with low transverse momenta. Thus, an accurate physical description of soft production processes is mandatory.

However, there is a scarcity of methods and/or strategies that can be used to handle these soft production processes based on sound theoretical foundations. For this reason, one must instead turn to effective models, which are abundant in the literature and are primarily based on the

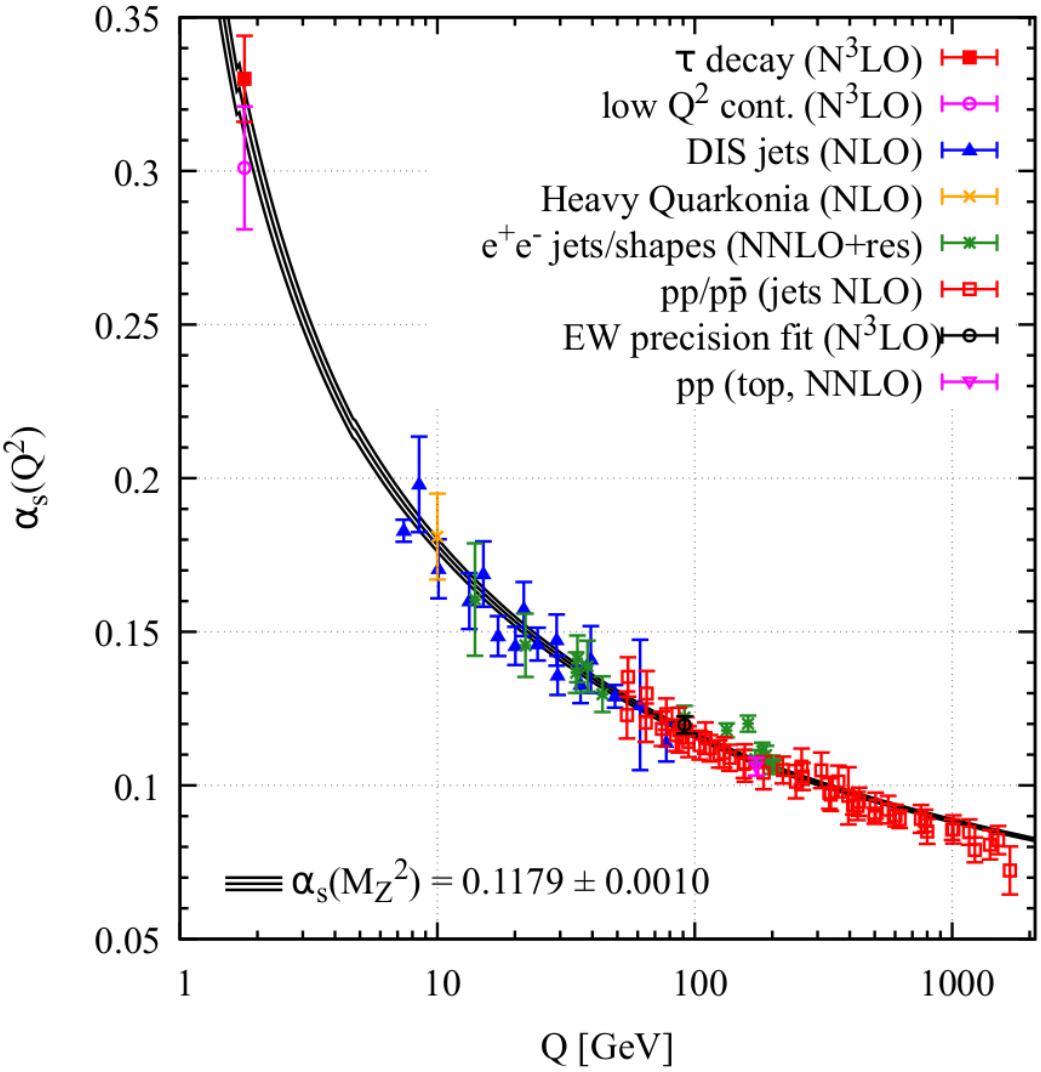

Figure 1.1: Compilation of the measurements and QCD calculations on the running coupling constant α_s as a function of the energy scale Q. Figure taken from [3].

Gribov-Regge phenomenology. They hinge on fundamental principles of quantum field theory – such as unitarity, analyticity and crossing, along with empirical parameterizations. While these models have succeeded, to a certain extent, in describing some of the aspects of hadronic interactions, they still need to be enhanced, especially through testing the hypotheses that are central to their construction, constraining the parametrizations, and fine-tuning the parameters using data comparisons available from both colliders as well as cosmic-ray air showers.

The primary goal of the hadronic interaction models developed within the Gribov-Regge framework is to accurately describe hadronic observables measured by accelerator experiments. Since we heavily rely on them to extrapolate to ultra-high energy scenarios, they should necessarily be internally consistent. It is worth noting that while the foundational assumptions of these models somewhat vary, the majority of them use the eikonal approximation to ensure the unitarization of the scattering hadronic amplitude. As a matter of fact, the unitarization process is key in QFT and particle physics as it ensures that the scattering amplitude satisfies the unitarity condition. This condition guarantees that the total probability of all possible outcomes of a scattering process is one, which preserves physical probabilities.

Technically, the exchange of "Regge poles", such as the pomeron, is the primary contributor to high-energy scattering in these models. Nevertheless, at very high energies, the scattering amplitude is often not well described by a single pomeron exchange. Instead, multiple pomeron exchanges need to be considered. When dealing with them, the eikonal approximation is especially useful for integrating unitarity into these models.

Nonetheless, we believe that the eikonal approximation is not an adequate unitarisation scheme when dealing with composite particle scattering, like hadrons. Thus, we should consider alternative schemes to try to reduce the uncertainties in hadronic interaction modeling, especially when employing these models for ultra-high energy extrapolation.

Gaining a solid understanding of the Soft QCD processes, which are dominated by non-perturbative effects, is essential to comprehending hadronic interactions at high energies. Hadronization— a process involving the formation of observable hadrons by quarks and gluons produced in high-energy collisions—is, in fact, one of the fundamental phenomena in the Soft QCD regime. This intricate process is described by means of string models along with the Gribov-Regge phenomenology, where quark

confinement is represented by flux tubes or "strings" connecting them. To satisfy the unitarity principle, these string models make use of the eikonal approximation.

However, several studies have furnished evidence in support of the insufficiency of the utilized eikonal or its enhanced version, the quasi-eikonal scheme, in providing a comprehensive description of the physics in question. Not to mention the fundamental issues with string models that still need to be solved. In these string models, produced particles are assumed to come from the exchanged Pomerons which are identified from the Gribov-Regge theory, each of which consists of two strings. In this approach, the probability of having configurations with n string pairs is the probability of having a certain number of these n pomerons exchanged, which is Poissonian via the eikonal scheme. Unfortunately, this approach is inconsistent for two main reasons. To begin with, in the string picture, the first and subsequent pairs are of different nature, whereas in the Gribov-Regge approach, all pomerons are identical. Secondly, in the string model, energy is properly shared among the strings, while the Gribov-Regge approach does not consider energy sharing at all.

Overall, the aforementioned issues relating to the modelling of hadronic interactions from collider to cosmic-ray physics have motivated us to undertake this study in hopes of resolving them and particularly reducing the uncertainties in hadronic interaction modelling so as to obtain better and more accurate results.

Our belief is that the eikonal approximation which is a common ingredient in the majority of the hadronic models, is not an adequate unitarisation scheme when dealing with composite particle scattering, such as hadrons, and especially when employing these models for ultra-high energy extrapolation. In this project, we aim to reduce the uncertainties in hadronic interaction modelling by maintaining consistency and coherence with the foundational principles of Quantum Field Theory (QFT) across a range of energies, from those accessible at the LHC to the extremely high energies observed in cosmic rays by considering alternative unitarization schemes and examining the uncertainty attached to them. It has evolved into a detailed study of the U-matrix scheme compared with the eikonal one, and to provide an attempt to explain the fundamental differences between the two schemes, despite that both verify the unitarity constraint principle. Moreover, to prove what unitarisation scheme is more adequate for describing interactions of composite particles like hadrons and highlight how

this approach may provide solutions to the issues in cosmic-ray physics, enhancing our understanding of soft QCD processes and offering a more consistent framework for modeling hadronic interactions.

1.2 Structure of the Thesis

This thesis is divided into eight major chapters. In chapter 1 a general introduction to the research presented in this thesis is provided and the choice of the topic is justified. Chapter 2 will focus on the fundamental formalism related to high-energy hadron scattering, namely the Regge theory and outline the optical theorem which allows for the calculation of the total cross-section. Chapters 3,4,5,6 and 7 contain the articles. Each of these chapters starts with a general context, including the theoretical framework, the main objectives, as well as the methodology adopted. Finally, chapter 8 will summarize the main findings of the thesis. It will also shed light on its strengths and contributions to the field of high-energy hadronic interactions. Moreover, it will suggest possible directions for future research.

2 Theoretical framework of high energy hadron scattering

This chapter reviews the fundamental formalism [53] describing the soft high-energy hadron scattering, which lies at the core of several phenomenological models. More specifically, this formalism is grounded in the S-matrix theory. Indeed, the application of the Quantum Field Theory (QFT) to the study of strong interactions was not thought of before the inception of QCD. As an alternative, physicists focused on examining the implications of a number of tenets about the S-matrix, and mainly comprise; unitarity, analyticity, and crossing symmetry, each of which is associated with basic axioms.

2.1 S-matrix theory

The basic quantity to study in particle physics is the probability that a certain set of particles in a given initial state $|i>$ undergo a collision and scatter into a final state $|f>$.

To this effect, the process is described by the quantity

$$S_{fi} =< f|S|i > \tag{2.1}$$

where S is called the S-matrix (S for scattering) and S_{fi} are the matrix elements. Since the scattering must also include the possibility that nothing occurs, the S-matrix is written in terms of the T-matrix, namely

$$S_{fi} = \delta_{fi} + i(2\pi)^4\delta^4(P_f - P_i)T_{fi} \tag{2.2}$$

where the 4-dimensional δ-function imposes energy-momentum conservation on all particle momenta p_j, and, with obvious notation, $P_{i,f} = \sum_{all} p_{i,f}$. The relevant matrix elements define the scattering and are functions of the momenta of the scattering particles, in particular of the various invariants which can be constructed with the momenta. Let us then turn to the kinematics before going further into the dynamics.

Before the development of QCD nobody dared to apply quantum field theory to the strong interactions. Instead, physicists tried to extract as much as possible by studying the consequences of a (reasonable) set of postulates about the S-matrix :

These general principles were established in the late '50s and consist of unitarity, analyticity and crossing symmetry. Each of them is related to basic axioms:

- unitarity to the conservation of probability in scattering processes;
- analyticity to causality and
- crossing symmetry to the relativistic nature of the interaction.

These basic principles are also at the foundations of relativistic Quantum Field Theory (QFT).

2.2 Unitarity and the scattering amplitude

The measurement of the total cross-section is based on two complementary methods: counting the number of collisions and, measuring the very forward scattering probability. The second method is based on a fundamental physical property i.e., the conservation of probability, which is embedded in the unitarity property of the S-matrix, namely

$$SS^{\dagger} = \mathbf{1} \tag{2.3}$$

In terms of the matrix elements, we have

$$(SS^{\dagger})_{fi} = \sum_{n} S_{fn} S^{*}_{ni} = \delta_{fi} \tag{2.4}$$

where n runs on all possible intermediate states. This condition ensures the normalization and orthogonality of states in the reaction. In particular, for the $i = f$ case, Eq. 2.4 ensures that the sum over all allowed transitions from a given state $|i>$ to any possible final state, is one, namely

$$\sum_{n} |S_{ni}|^2 = 1 \tag{2.5}$$

Eq. (2.5) is the statement of conservation of probability in the scattering.

We can now proceed to derive the optical theorem, by using Eqs. (2.4) and (2.2) to obtain

$$T_{fi} - T_{if}^{*} = (2\pi)^4 \sum_n \delta^4(P_f - P_n) T_{fn} T_{in}^{*} \tag{2.6}$$

Because the left hand side of this equation is linear in T, while the right hand side is quadratic, if the T-matrix can be expanded in a small parameter (say a coupling constant), then unitarity ensures that the T-matrix elements are hermitian. In the general case, one uses Eq. (2.6) to obtain the optical theorem, namely

$$2ImT_{ii} = (2\pi)^4 \sum_n \delta^4(P_i - P_n) |T_{in}|^2 \tag{2.7}$$

where the amplitude T_{ii} indicates elastic scattering in the forward direction and where the right hand side, a part from a normalization factor, gives the total cross-section for scattering from an initial state $|i>$ into any possible final state, as shown in the following subsection. The reader is warned that different authors use different normalizations for the elastic scattering amplitudes and hence due care must be taken in using various unitarity expressions.

2.3 The optical theorem and the total cross-section

The Cutkosky rule (1.7) [Cut60] provides a very interesting relation between the forward amplitude of an elastic process $a(p_1) + b(p_2) - > a(p_3) + b(p_4)$ and the total cross-section. Forward scattering, $t = (p_1 - p_3) = (p_2 - p_4)^2 = 0$, means $p_1 = p_3$ and $p_2 = p_4$. Thus

Here, p_n indicates the total momenta of the final state and n indicates all possible final states. F stands for the flux factor

$$F = 4\sqrt{(p_1 \cdot p_2)^2 - m_1^2 m_2^2}$$

In the center-of-mass frame (c.m.s.) and with negligible masses, we find $F \equiv 2s$, and thus

$$\sigma_{\text{total}} = \frac{1}{s} \text{Im}\left(A(s, t = 0)\right) \tag{2.8}$$

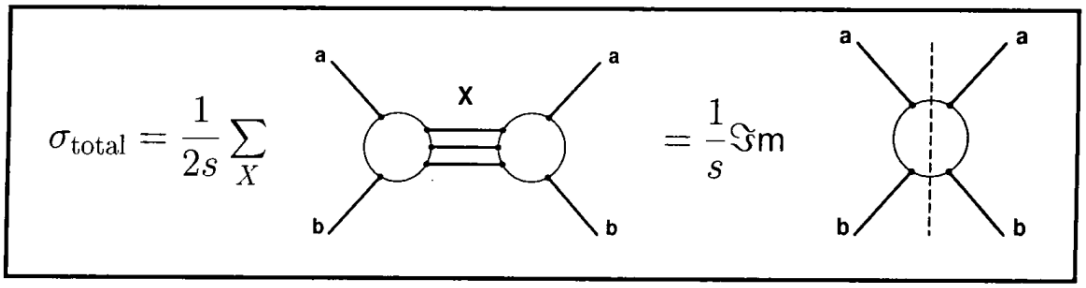

Figure 2.1: The optical theorem.

2.4 Partial-wave Amplitudes and Impact Parameter representation

The scattering amplitude can be efficiently decomposed by identifying the partial-wave amplitudes. The scattering of states having differing angular momenta may be addressed separately and satisfy independent unitarity equations in a relatively straightforward way given that angular momentum is a conserved quantity. For spinless particles, the s-channel centre-of-mass partial-wave amplitudes are determined by

$$A_l(s) \equiv \frac{1}{16\pi}\frac{1}{2}\int_{-1}^{1} \mathrm{d}z_s\, P_l(z_s)A(s,t) \quad l = 0, 1, 2, \ldots \tag{2.9}$$

As for the inverse transformation, it is defined by:

$$A(s,t) = 16\pi \sum_{\ell=0}^{\infty} (2\ell+1)\, P_\ell(\cos\theta)a_\ell(k), \tag{2.10}$$

with the ℓth partial amplitude of momentum k, and the ℓth Legendre polynomial $P_\ell(\cos\theta)$, where $z_s = cos(\theta_s) = 1 + \frac{2t}{s-4m}$ and θ_s is the s-channel centre-of-mass scattering angle.

If we replace this into two-particle unitarity equation, we get

$$A_l^{if}(s_+) - A_l^{if}(s_-) = \frac{4iq_{sn}}{\sqrt{s}} A_l^{in}(s_+)A_l^{nf}(s_-) + \ldots \tag{2.11}$$

which for elastic scattering in which the initial and final states are identical, gives

$$\mathrm{Im}\, A_l^{el}(s) = \frac{2q_{s12}}{\sqrt{s}} \left|A_l^{el}(s)\right|^2 + \sum_{n\neq i} \frac{2q_{sn}}{\sqrt{s}} A_l^{in}(s_+) A_l^{ni}(s_-) + 3 \text{ body channels etc.} \tag{2.12}$$

The elastic scattering is represented by the first term on the r.h.s, the sum over inelastic two particle intermediate states by the second, and the contributions of n-particle intermediate states by the remaining terms. Given that $2q_{s12} = \sqrt{s-4m} \to \sqrt{s}$ for for large s and all the terms on the r.h.s. are positive , the aforementioned equation entails that

$$0 \leq |A_l^{el}|^2 \leq \mathrm{Im}\left\{A_l^{el}\right\} \leq 1 \tag{2.13}$$

which simply illustrates the condition that the probability of the elastic scattering cannot go beyond unity and that no scattering process can be completely inelastic.

The elastic partial-wave amplitudes are most of the time parametrized as follows :

$$A_l^{\mathrm{el}} = \frac{\eta_l e^{2i\delta_l} - 1}{2i\left(\frac{2q_{12}}{\sqrt{s}}\right)} \tag{2.14}$$

clearly meeting the unitarity condition mentioned above, where η_l stands for the inelasticity factor and δ_l refers to the real phase shift. For unitarity to be satisfied $0 \leq \eta_l \leq 1$.

With respect to the partial wave amplitudes, the optical theorem (3.1.12) provides

$$\sigma_T(s) = \frac{8\pi}{q_{12}\sqrt{s}} \sum_l (2l+1)\mathrm{Im}\left\{A_l^{\mathrm{el}}(s)\right\} = \frac{2\pi}{q_{12}^2} \sum_l (2l+1)[1-\eta_l \cos 2\delta_l] \tag{2.15}$$

and when we integrate over all angles, we have

$$\sigma_{\mathrm{el}}(s) = \frac{16\pi}{s} \sum_l (2l+1)|A_l^{\mathrm{el}}(s)|^2 = \frac{\pi}{q_{12}^2} \sum_l (2l+1)[1+\eta_l^2 - 2\eta_l \cos 2\delta_l] \tag{2.16}$$

Consequently

$$\sigma_{\mathrm{inel}}(s) = \sigma_T - \sigma_{\mathrm{el}} = \frac{\pi}{q_{12}^2} \sum_l (2l+1)[1-\eta_l^2] \tag{2.17}$$

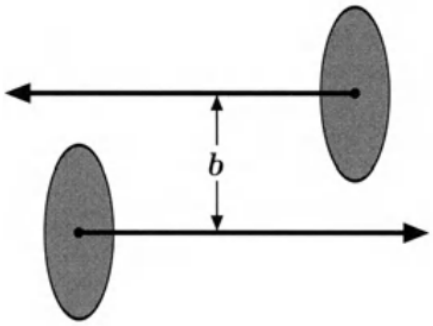

Figure 2.2: Schematic representation of the collision between two hadrons in the impact parameter space.

so that any partial wave's contribution to the total cross-section diminishes as energy grows; and in case this does not happen, then a growing number of partial waves must contribute as energy rises.

At high energies and small angles ($s >> |t|$), where numerous partial waves contribute, we can further simplify the analysis through substituting integrals in impact parameter (b) space for the summations over partial-wave amplitudes.

This follows the the classical relation $l = q_s b - 1/2$ and for large l

$$P_l(z_s) \simeq J_0((2l+1)\sin\frac{\theta_s}{2}), \quad \sum_l \to \int dl \to \int q_s db \tag{2.18}$$

with J_0 being the Bessel function.

and when we write

$$A_l(s) \to A(s,b), \quad \sin\frac{\theta}{2} \simeq \frac{\theta}{2} \simeq \left(\frac{-t}{q_s^2}\right)^{\frac{1}{2}} \tag{2.19}$$

we obtain

$$A(s,t) = 8\pi s \int_0^\infty b db J_0(b\sqrt{-t}) A(s,b) \tag{2.20}$$

with the inverse transformation referring to (3.2.1) is

$$A(s,b) = \frac{1}{16\pi s} \int_{-\infty}^0 dt J_0(b\sqrt{-t}) A(s,t) \tag{2.21}$$

This is merely the scattering amplitude's two-dimensional Fourier transform in impact parameter space with the azimuthal angle integrated out. For the scattering at high energy and small angle, the impact parameter remains constant, replacing the conservation of angular momentum.

The unitarity condition on the elastic partial waves is expressed in terms of the elastic profile function, A(s,b) as follows

$$0 \leq |A(s,b)|^2 \leq Im\, A(s,b) \leq 1 \tag{2.22}$$

and the eikonal phase, $\chi(s,b)$, and the eikonal series are defined by

$$A(s,b) = \frac{e^{i\chi(s,b)} - 1}{2i} = \frac{1}{2i}\sum_{n=1}^{\infty} \frac{(i\chi(s,b))^n}{n!} \tag{3.2.13}$$

in order that $\chi(s,b) 2\delta_l(s)$ for large s and $\chi(s,b)$ is complex with positive imaginary part.

And one obtain the various cross-sections :

$$\sigma_T(s) = 8\pi \int_0^{\infty} bdb\, Im\, A(s,b) \tag{3.2.14}$$

$$\sigma_{el}(s) = 8\pi \int_0^{\infty} bdb |A(s,b)|^2 \tag{3.2.15}$$

$$\sigma_{inel}(s) = 8\pi \int_0^{\infty} bdb G_{\rm inel}(s,b) \tag{3.2.16}$$

where the inelastic profile function $G_inel(s,b)$ is determined by

$$G_{\rm inel}(s,b) = Im(A(s,b)) - |A(s,b)|^2 \tag{2.23}$$

also the "opacity"' $\Omega(s,b)$ is defined by

$$\Omega(s,b) \equiv -i\chi(s,b) \tag{3.2.18}$$

so that

$$G_{\rm inel}(s,b) = 1 - e^{-2Re\,\Omega(s,b)} \tag{2.24}$$

2.5 Regge phenomenology

The partial-wave amplitude is determined for non-integer and complex values of l, as well, enabling us to extend the amplitude into the complex angular momentum plane. For the continuation to be considered unique, the function must vanish for $l \to C \pm \infty$ and be regular for $l > C$ where C is a real constant.

In order to fulfill this for t-channel partial-wave amplitudes, we must break the amplitude down into even and odd components using the interchange $\cos(\theta_t) - \cos(\theta_t)$ (i.e., su). By doing so, we obtain even and odd

signatured amplitudes (S = ±1) with exclusively right-hand cuts in the complex z_t plane.

$$A_l(t) = \begin{cases} A_l^+(t) & \text{for } l \text{ even} \\ A_l^-(t) & \text{for } l \text{ odd} \end{cases} \tag{2.25}$$

The partial-wave series for the signatured amplitude can be expressed as an integral in the complex l-plane through employing a Sommerfeld-Watson transformation.

$$A(s,t) = -\frac{16\pi}{2i} \oint_{C_l} (2l+1) A_l(t) \frac{P_l(-z_t)}{\sin(\pi l)}\, dl \tag{2.26}$$

where C_l is a contour enclosing zero and the positive integers. The expansion of the contour C_l to a semicircle at infinity with its base along the line $Re(l) = C$ is made possible by the analyticity in l of A (t). Due to the convergence features of $A(t)$, only the base contribution remains after the semi-circle's contribution vanishes. Assuming that the signatured partial-wave amplitudes for $Re(l) < C$ only contain isolated singularities (poles and branch cuts), the contour's base line can be moved farther to the left, absorbing distinct contributions from each singularity.

The Legendre function $P_l(z)$ declines most rapidly as a function of z for $l = -1/2$. The contribution to the contour integral along the line $Re(l) = C = -1/2$ will be asymptotically insignificant in comparison to any singularities encountered to the right of the line if the base of the contour is pushed to the left as far as that point. These t-channel singularities, which influence the asymptotic behavior of the s-channel amplitude, are known as the Regge poles and Regge cuts. In fact, we can use the Mandelstam-Sommerfeld-Watson transformation to shift the base of the contour as far to the left as we desire. Since the integral representation is valid across the complex z-plane as long as the partial-wave amplitudes are convergent enough in the l-plane, it is preferred over the partial-wave series, which diverges at the nearest s-channel singularity.

The position of the singularity will be generally a function of t and will describe a trajectory in the l-plane as t varies, $l = \alpha(t)$. A simple pole, R, with signature and residue $\beta(t)$ with the form

$$A_l(t) = \frac{\beta(t)}{l - \alpha_R(t)} \tag{2.27}$$

replaced in eq. 2.26 yields the amplitude

$$A_R^I(z_t,t) = -16\pi^2\,(2\alpha_R(t)+1)\,\beta(t)\frac{P_{\alpha_R(t)}(-zt)}{\sin(\pi\alpha_R(t))}. \tag{2.28}$$

Hence the contribution to the physical amplitude is provided by

$$A_R^S(s,t) = A_R^S(z_t,t) + \mathcal{S}A_R^S(-z_t,t). \tag{2.29}$$

and it has the high energy behaviour in the s-channel

$$A_R^S(s,t) \sim \left(1+\mathcal{S}e^{-i\pi\alpha_R(t)}\right)s^{\alpha_R(t)}. \tag{2.30}$$

According to the disconnectedness principle of the S-matrix theory, the remnant of the pole, $\beta(t)$ factorizes into a product of its couplings to each of the external particle lines, yielding

$$\beta(t) = \gamma_{1,3}(t)\gamma_{2,4}(t) \tag{2.31}$$

The features of a Regge pole in the asymptotic s-channel and the resonance region of the t-channel can be concisely expressed as :

$$A(s,t) = \gamma_{1,3}(t)\gamma_{2,4}(t)\frac{e^{-i\pi\alpha(t)}+\mathcal{S}}{2\sin\pi\alpha(t)}\frac{1}{\Gamma(\alpha(t)+1)}\left(\frac{s}{s_0}\right)^{\alpha(t)} \tag{2.32}$$

The Regge trajectory, $l = \alpha_R(t)$, is demonstrated to be a real analytic function of t and to include the right-hand threshold branch cut. A pole in the physical partial-wave amplitude is produced when a Regge pole with an even signature takes place at an even value of l or with an odd signature at an odd value of l. When this happens below the t-channel threshold, the pole represents a bound state; when it happens beyond the threshold, the trajectory has an imaginary part and represents a resonance. Therefore, the trajectory, $\alpha_R(t)$, generates the asymptotic s-channel behaviour as well as the t-channel poles of the amplitude. For $t > O$, we anticipate that a trajectory with a precise signature will produce a series of bound states and resonances that correspond to observable particles with identical quantum numbers, with the exception of their spins, which vary by two units of angular momentum between consecutive states.

According to the experimental data on particle masses and spins, such series of particles indeed occur and their corresponding trajectories are linear functions of $t(= mass^2)$ with the following the form $\alpha_R(t) = \alpha_R(0) + \alpha_R^{'}t$.

The scattering of particles with spin can be added to the above discussion. In fact, this will further complicate the formalism as we must consider the crossing characteristics and kinematical singularities of the helicity amplitudes. Nevertheless, these issues are manageable, and the outcome is roughly the same as for spin-zero scattering.

2.6 Restoring Unitarity

It is crucial to keep in mind that the parametrization employed in (equation) for the elastic scattering amplitude is not exclusive. Generally speaking, no widely recognized technique exists for restoring unitarity in high-energy hadronic scattering processes.

Furthermore, the choice of a certain unitarization scheme has important physical ramifications, particularly in theories like QCD, where cross-sections rise with energy. It is more than just a matter of preference; it has the potential to alter the behavior and predictions of the theory.

Yet, there are several ways to represent the unit circle, which may yield different insights into the underlying physics [59].

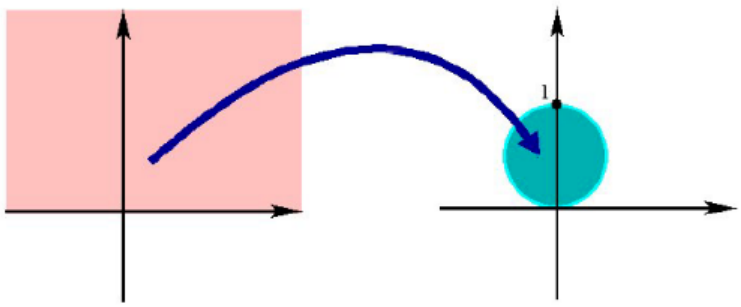

Figure 2.3: Mapping to the Unitary circle (Argand Circle) for the partial wave amplitudes: the amplitudes must lay on the circle to satisfy the unitarity condition for elastic scattering. Figure taken from [54]

First of all, one can map the upper complex plane into a circle via a complex exponential

$$S(s, \mathbf{b}) = \exp(iz(s, \mathbf{b})) \quad \text{with} \quad \text{Im } z(s, \mathbf{b}) \geq 0. \tag{2.33}$$

This maps, in fact, an infinite number of strips with $2n\pi < \text{Re } z(s, \mathbf{b}) < 2(n+1)\pi$ each onto the unit circle.

It is also possible to use a one-to-one map through a Möbius transform

and write

$$S(s,\mathbf{b}) = \frac{1+iz'(s,\mathbf{b})}{1-iz'(s,\mathbf{b})}, \quad \text{with} \quad \text{Im } z'(s,\mathbf{b}) \geq 0. \tag{2.34}$$

The physical amplitude lies within the unitarity circle, so that the associated S matrix can always be represented by Eqs. (2.33) and (2.34). The unitarization scheme comes in once one identifies z or z' with the one-Reggeon exchange amplitude. One then considers (2.33) and (2.34) as series expansions in n-Reggeon exchanges, so that their first term must give $1 + i\chi(s,\mathbf{b})$.

Indeed, if one writes the one-Reggeon exchange amplitude as $\chi(s,\mathbf{b})$, then assuming $z = \chi$ in (2.33) leads to the well-known eikonal representation:

$$G(s,\mathbf{b}) = i(1 - \exp(i\chi(s,\mathbf{b}))). \tag{2.35}$$

This scheme can be derived in QED and other field theories [51] or in potential theory. It leads at asymptotic energies ($s \to \infty$) to the limit $\sigma_{\text{el}}/\sigma_{\text{inel}} = 1$, i.e., to maximum inelasticity.

The other unitarization scheme considered here is the U-matrix representation [45] where one identifies z' in (2.34) with $\chi(s,\mathbf{b})/2$, to match the one-Reggeon exchange

$$G(s,\mathbf{b}) = \frac{\chi(s,\mathbf{b})}{1 - i\chi(s,\mathbf{b})/2}. \tag{2.36}$$

In this scheme, $S(s,\mathbf{b})$ tends to -1 when $s \to \infty$ and $\mathbf{b}$ is finite, so that the inelastic partial wave $\eta_{\text{in}}(s,\mathbf{b})$ tends to 0: the ratio $\sigma_{\text{el}}/\sigma_{\text{inel}}$ vanishes asymptotically. Both schemes have the same development at the second order in χ and differ only in the rest of the series. It must be noted, however, that the resummation must lead to an amplitude within the unitarity circle, but there is no reason to assume that it maps the entire complex plane to the circle. Hence, one can easily extend both schemes through a change in the strength of successive scattering. This gives the extended eikonal schemes.

$$G(s,\mathbf{b}) = \frac{i}{\omega}(1 - \exp(i\omega\chi(s,\mathbf{b}))) \tag{2.37}$$

and the extended U-matrix schemes

$$G(s,\mathbf{b}) = \frac{\chi(s,\mathbf{b})}{1 - i\omega'\chi(s,\mathbf{b})}. \tag{2.38}$$

It is straightforward to check that using $\omega \geq 1$ or $\omega' \geq 1/2$ maps any amplitude χ into the unitarity circle.

3 Unitarisation and non-diffractive interactions

3.1 Context

A pp scattering event may generate a wide variety of phenomena, as portrayed in Figure 3.1:

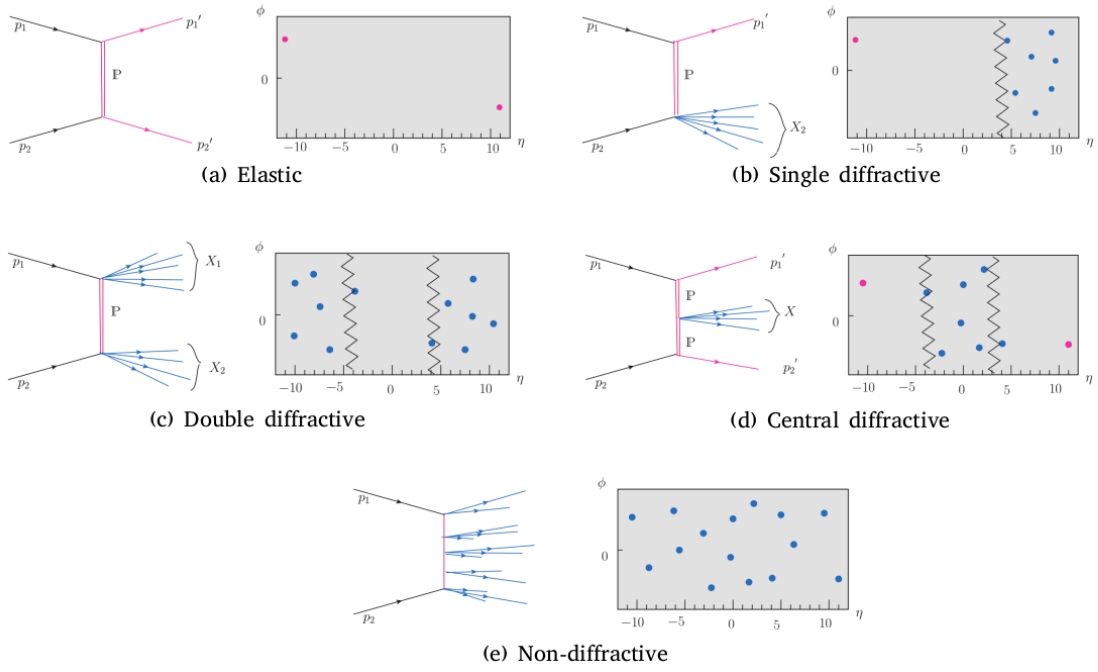

Figure 3.1: a) Diagram for elastic scattering and $\phi - \eta$ map of the distribution of the final state particles. b) Single diffractive for the rapidity window between $-10 < \eta < 3.5$. c) Double diffraction process for the window $-3.5 < \eta < 4$. d) Central diffractive process in two rapidity gaps between $-10 < \eta < -2.5$ and $2.5 < \eta < 10$. e) Non-diffractive process, where there is no rapidity gap, particles are uniformly distributed over ϕ and η. Figure taken from [35].

The first study is concerned with the investigation of the proton inelastic cross section at ultrahigh energies. This was performed by examining high-energy collider data and employing two different unitarization

schemes: the eikonal and the U-matrix. Particularly, it focuses on non-diffractive inelastic interactions. As for diffraction interactions, they will be covered in the subsequent chapter. It specifically seeks to understand how these two schemes affect the predictions of total, elastic, and inelastic cross sections for proton-proton pp and proton-antiproton $p\bar{p}$ scattering up to extremely high energies, reaching beyond the scale accessible by current particle accelerators.

In order to gain deeper insights into the hadronic interactions at ultra-high energies, high-energy collider experiments and cosmic-ray observations are highly needed. For instance, cross-sections,in particle physics, measure the probability of certain interactions between particles. Precisely predicting the behaviour of particles at high energies depends on a proper modeling of these cross-sections, with significant implications for particle physics and astrophysics.

In spite of the efficiency of the 2002 fits to the total cross-section in predicting the LHC pp total cross-section, they failed to relate the total cross-section to the elastic and inelastic ones. The relation between these cross-sections is necessary in the description of extensive air showers, given the prominence of the inelastic cross-section.

In fact, as detailed in the previous chapters, given the challenges in deriving precise cross-sections from quantum chromodynamics (QCD) at these energies, we developed a phenomenological model grounded in the Regge theory.

The elastic scattering amplitude was modeled using a Born-level amplitude with a pomeron exchange, constrained by low-energy data, and a unitarization scheme to account for multiple exchanges at high energies and ensure that the elastic amplitude does not exceed the unitarity limit.

Using our model, high-energy collider data were adopted to determine the best-fit parameters for total, elastic, and inelastic cross-sections, and the predictions of the two unitarization schemes up to energies around the Grand Unified Theory (GUT) scale were compared for the evolution of the ratio of the elastic cross-section to the total cross-section, as well as the extrapolation of the inelastic cross-section at ultra-high energy, which is crucial for understanding cosmic-ray interactions and extensive air showers, was provided and examined.

The high-energy collider data used in this study were mainly from experiments, such as TOTEM, ATLAS, CDF, and others to fit the cross sections.

3.2 ARTICLE 1

The Proton Inelastic Cross Section at Ultrahigh Energies

Atri Bhattacharya, Jean-René Cudell, Rami Oueslati, Arno Vanthieghem

Physical Review D **103** (2021) 5, L051502

arXiv:2012.07970 [hep-ph]

Abstract: We study the consequences of high-energy collider data on the best fits to total, elastic, and inelastic cross sections for pp and $p\bar{p}$ scattering using two very distinct unitarisation schemes: the eikonal and the U-matrix. Despite their analytic differences, we find that the two schemes lead to almost identical predictions up to EeV energies, with differences only becoming significant at GUT-scale and higher energies.

Man-made accelerators and indirect detection methods of high-energy cosmic rays such as extensive air showers, at the core of high-energy and multi-messenger astrophysics, have drawn a particular attention to the modeling of the high-energy hadronic interactions. A comprehensive treatment of the pp and $p\bar{p}$ cross sections with quantum chromodynamics being elusive for the moment, one has to rely on some generic arguments about unitarity and analyticity of the scattering matrix to derive phenomenological estimates of the high-energy total, elastic and inelastic cross sections. In that regard, experimental studies, most notably those related to cosmic-ray showers, often use the 2002 fits to the total cross section that successfully predicted the LHC pp total cross section [55]. Besides the fact that there are a lot of relevant data that have since appeared [22, 25, 24, 23, 28, 5, 3, 4, 110, 6, 11, 26], these fits have the drawback that they cannot self-consistently relate the total cross section to the elastic and inelastic ones. Since the inelastic cross section is key to computing multiple minijet production from cosmic-ray interactions with the atmosphere at ultra-high energies, the relation between the total and inelastic cross sections is therefore essential to the description of extensive air showers. It is at the core of hadronic interaction models adopted in Monte Carlo event generators such as `SIBYLL` [117] and `QGSJET` [113].

In this letter, we want to address this problem [1]. In order to relate

[1] The question of the very forward component of the showers, which is linked to the diffractive cross section, will be considered in a separate paper.

elastic, inelastic, and total cross sections, one needs a physics model of the elastic amplitude. This is typically made of two ingredients: an elastic amplitude at the Born level, which encapsulates the elementary exchange (and can be extracted from low-energy data), and a scheme that takes into account multiple exchanges, which become increasingly important at higher energies and without which the elastic amplitude would exceed the unitarity limit.

The Born term of interest corresponds to pomeron exchange, and is reasonably constrained. We normalize the elastic amplitude $a(s,t)$ so that the differential cross section for elastic scattering is written as

$$\frac{\mathrm{d}\sigma_{el}}{\mathrm{d}t} = \frac{|a(s,t)|^2}{16\pi s^2}\,, \tag{3.1}$$

where $t = -\boldsymbol{q}^2$ is the square of the momentum transfer. The Born term can then be written using the pomeron trajectory $\alpha(t)$, the proton elastic form factor $F_1(t)$ and the coupling pomeron-proton g_p, as

$$a(s,t) = g_p^2\, F_1(t)^2 \left(\frac{s}{s_0}\right)^{\alpha(t)} \xi(t)\,, \tag{3.2}$$

with $\xi(t)$ the signature factor

$$\xi(t) = -e^{\frac{-i\pi\alpha(t)}{2}}\,. \tag{3.3}$$

The pomeron trajectory is close to a straight line [57], and we take it to be $\alpha(t) = 1 + \epsilon + \alpha' t$. Non-linearities in the trajectory for large t may become consequential when considering the differential cross-section $d\sigma/d|t|$, see Ref. [94]; however, this is beyond the scope of the current work.

At high energy, the growth of this pomeron amplitude and eventual violation of unitarity is most clearly seen in the impact-parameter representation, where the Fourier transform of the amplitude $a\,(s,t)$ rescaled by $2s$ is equivalent to a partial wave

$$\chi(s,\boldsymbol{b}) = \int \frac{\mathrm{d}^2\boldsymbol{q}}{(2\pi)^2} \frac{a(s,t)}{2s} \mathrm{e}^{\mathrm{i}\boldsymbol{q}\cdot\boldsymbol{b}}. \tag{3.4}$$

The norm of the partial wave signals two important regimes. When it reaches unity, around $\sqrt{s} = 2$ TeV [60], the model enters the black-disk regime – i.e. maximum inelasticity. When it reaches two, the model begins to violate unitarity. Both regimes start at small impact parameter and spread to higher values of b, and signal that multiple exchanges have to be taken into account [131].

It is thus necessary to introduce unitarization schemes that take into account multiple scatterings by mapping the amplitude $\chi(s, \boldsymbol{b})$ to the physical amplitude $X(s, \boldsymbol{b})$. The latter reduces to $\chi(s, \boldsymbol{b})$ for small s, is confined to the unitarity circle $|X(s, \boldsymbol{b}) - i| \leqslant 1$, and bears the same relation as Eq.(6.15), but this time to the unitarized amplitude $A(s, t)$:

$$X(s, \boldsymbol{b}) = \int \frac{\mathrm{d}^2\boldsymbol{q}}{(2\pi)^2} \frac{A(s,t)}{2s} \mathrm{e}^{\mathrm{i}\boldsymbol{q}\cdot\boldsymbol{b}}. \tag{3.5}$$

The eikonal scheme, — derived for structureless bodies in optics, potential scattering, and QED — is commonly used in the literature. Another proposed scheme is the U-matrix scheme, which can be motivated by a form of Bethe-Salpeter equation [107]. Neither of these may be entirely correct in the context of QCD, but going from one to the other permits an evaluation of the systematics linked to multiple exchanges.

The eikonal scheme assumes [58]:

$$X_E(s, \boldsymbol{b}) = \mathrm{i}\left[1 - \mathrm{e}^{\mathrm{i}\chi(s,\boldsymbol{b})}\right], \tag{3.6}$$

while the U-matrix scheme posits:

$$X_U(s, \boldsymbol{b}) = \frac{\chi(s, \boldsymbol{b})}{1 - \mathrm{i}\chi(s, \boldsymbol{b})/2}. \tag{3.7}$$

In terms of partial waves, the maximum inelasticity is reached in either case for $X(s, \boldsymbol{b}) = \mathrm{i}$, which is also the asymptotic limit of the eikonal scheme at high s.

The total and elastic scattering cross sections may be readily expressed in these representations as

$$\sigma_{\mathrm{tot}} = 2\int \mathrm{d}^2\boldsymbol{b}\ \mathfrak{Im}\left(X(s, \boldsymbol{b})\right), \qquad \sigma_{\mathrm{el}} = \int \mathrm{d}^2\boldsymbol{b}\ |X(s, \boldsymbol{b})|^2. \tag{3.8}$$

We shall now use them to fit all the data in $p\overset{(-)}{p}$ scattering above 500 GeV, for which lower trajectories have a negligible effect. We obtain 3 distinct datasets (for total, elastic and inelastic cross sections) from the following sources, for a total of 37 data points:

- pp total and elastic cross sections from TOTEM [22, 25, 24, 23, 28], and ATLAS [5, 3];
- $p\bar{p}$ total and elastic cross sections from CDF [10], E710 [17, 18], and E811 [30, 31] experiments at TeVatron; and UA4 at Sp$\bar{\mathrm{p}}$S [48];

dataset	number of points	χ^2
σ_{tot}	18	21.7
σ_{el}	11	21.3
σ_{in}	8	4.1

Table 3.1: The values of χ^2 resulting from independent fits to quadratic polynomials in $\log(s)$, illustrating the tensions in some parts of the dataset.

Scheme	ϵ	α'	g_p	t_0	$\frac{\chi^2}{\text{d.o.f}}$
Eikonal	0.11 ± 0.01	0.31 ± 0.19	7.3 ± 0.9	1.9 ± 0.4	1.442
U-matrix	0.10 ± 0.01	0.37 ± 0.28	7.5 ± 0.8	2.5 ± 0.6	1.436

Table 3.2: χ^2/d.o.f and best-fit parameters obtained using the eikonal and U-matrix unitarisation schemes.

- Direct measurements of inelastic cross sections, i.e. not derived from total and elastic measurements, from UA5 at Sp$\bar{\text{p}}$S [15], ATLAS [4, 110], LHCb [6], ALICE [11], and TOTEM [26].

It should be noted that both the total and elastic cross section datasets include discordant data from different experiments. This is quantified by a simple consistency check that fits generic quadratic polynomials in $\log s$ to each dataset and computes the resulting χ^2. Table 4.3 shows the results with both the elastic and total cross sections running up χ^2/d.o.f noticeably greater than 1. Thus, one obtains a minimum combined χ^2 of 47.1. This is a well-known problem with these data, first addressed in [56] and later in [46]. At present, however, the number of data points is simply too small to identify individual outliers, and hence there is little one can do for lack of better experimental results. We shall thus neither filter nor sieve the data, but remember that the best possible χ^2 is rather high.

We use a dipole-like form factor for the proton $F_1 = 1/(1 - t/t_0)^2$. The parameters in our fit thus include ϵ and α' describing the pomeron trajectory, the coupling constant g_p, and finally the form-factor scale t_0.

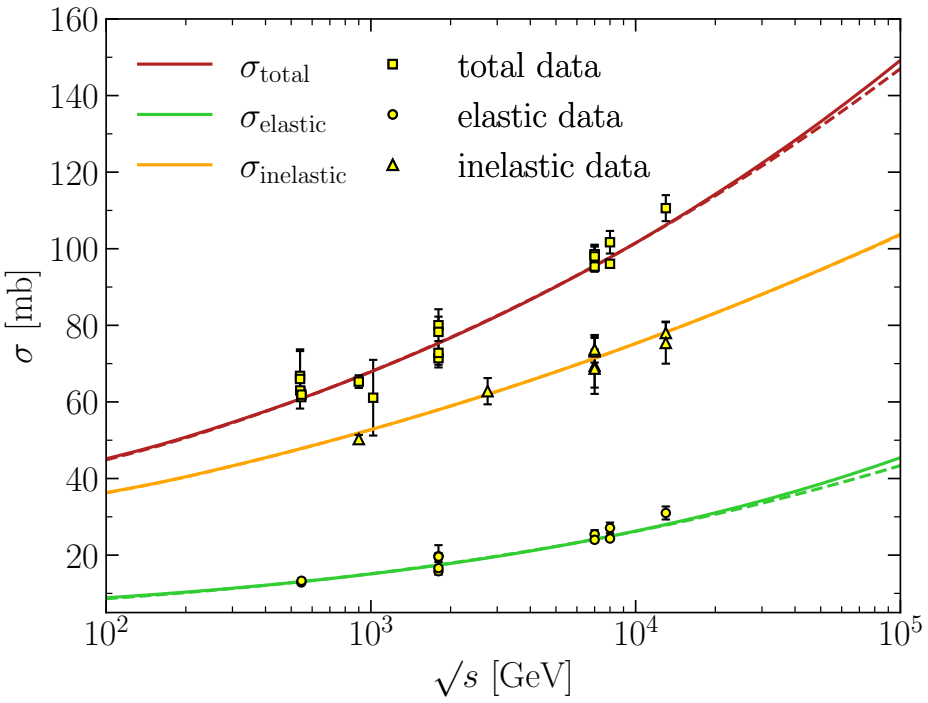

Figure 3.2: Total, elastic and inelastic cross sections obtained with best-fit parameters for the U-matrix scheme (solid curves) and the eikonal scheme (dashed curves).

The results of our fits using either unitarisation scheme are shown in Table 3.2 and in Fig. 3.2. We obtain $\chi^2/\text{d.o.f} = 1.436$ (1.442) when using the U-matrix (eikonal) scheme. Note that, although at face value the fit obtained using either scheme only has a seemingly poor χ^2/d.o.f, the value of the total χ^2 — 47.39 (47.59) for the U-matrix (eikonal) scheme — is very close to the minimum value — 47.1 — obtained earlier.

These values of the parameters are however quite striking. Ref. [57] managed to disentangle the pomeron contribution at low energy from that of lower-t trajectories, and provided estimates of its coupling, intercept and slope. These values are within 1σ of those obtained here for the U matrix, but the eikonal differs significantly from the low-energy results. Hence it seems that for an eikonal scheme, one never recovers the observed one-pomeron simple pole.

Using an exponential form factor $\{F_1 = \exp(R_0 t)\}$, instead of the dipole form, leads to slightly poorer fits $\{\chi^2/\text{d.o.f} = 1.440\ (1.445)\}$; however, the qualitative picture remains unaltered. We have also analysed how the fits improve if one uses the generalised eikonal and U-matrix schemes and we find that these generalisations — at the cost of an additional free parameter (ω or ω') — do not improve the fits significantly.

One particular consequence of the relative independence of the elastic cross section to the choice of the unitarisation scheme is that values of the ρ parameter remain largely unaffected by the choice of the scheme as well. We use our best-fit parameters to compute this parameter across different energies, and find that the corresponding values agree with existing data, except for the latest TOTEM measurement. We indeed obtain $\rho = 0.131$ at $\sqrt{s} = 13$ TeV. Whether this discrepancy is due to the fact that we neglect an odderon contribution, or it comes from a problem in the extraction of ρ from the data [71] is still unclear. As the purpose of this letter is the evaluation of the inelastic cross section, the exact value of ρ is of little importance given than it contributes about 1% to the processes considered here.

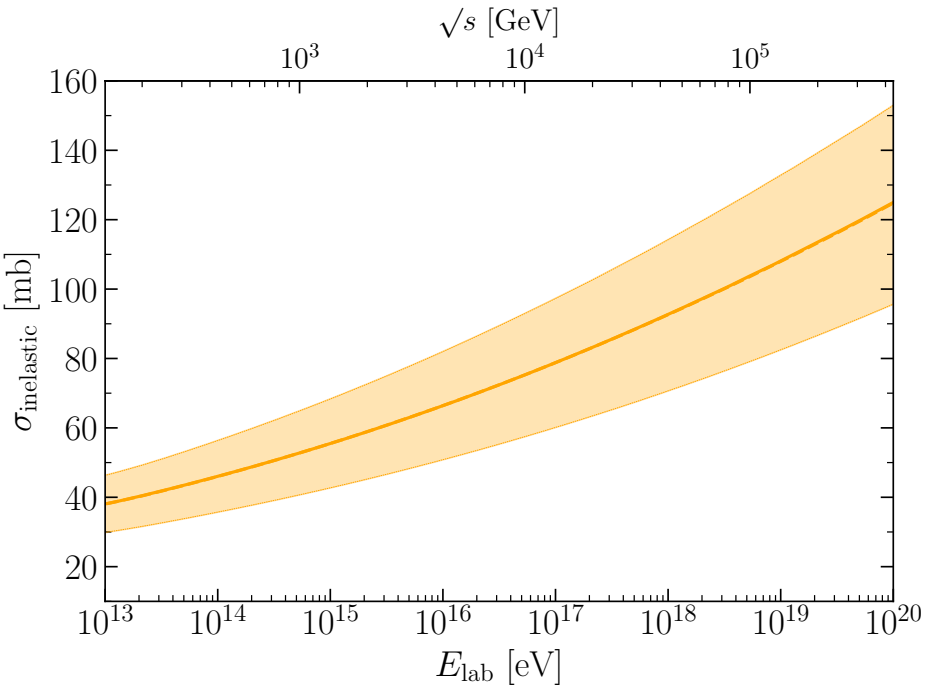

Figure 3.3: The 1σ band for the inelastic cross section at ultrahigh energies. Note that both schemes give almost identical results.

We are now in a position to present our results on the inelastic cross section at ultra-high energies. We obtain them by varying all the parameters of Table 3.2 in a 1σ hyperellipsoid and use the corresponding curves to evaluate the errors at ultrahigh energies. We show the results in Fig. 3.3. The entwinement of the inelastic cross section with the elastic and total cross sections, which are much better known, leads to smaller errors than in the case of a fit to inelastic data alone. Furthermore, despite their

very different analytic properties, the two schemes lead to almost identical predictions. This gives us confidence that the extrapolation to ultra-high energies is well founded.

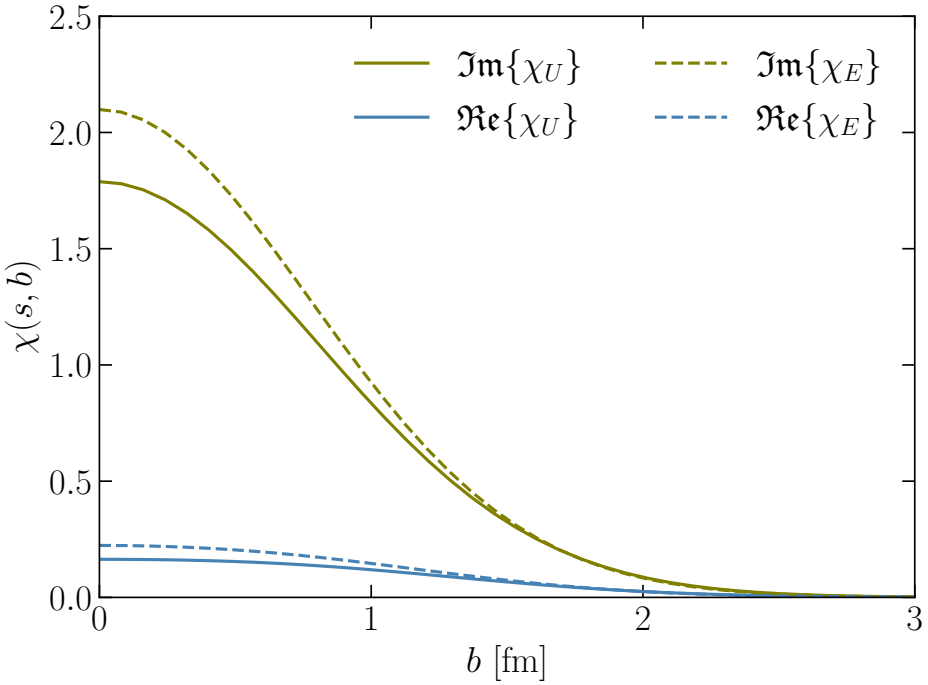

Figure 3.4: Real and imaginary parts of the Born terms $\chi(s,b)$ at $\sqrt{s} = 13$ TeV for the U-matrix (solid curves) and eikonal (dashed curves) schemes.

While the inelastic cross sections using either of the two schemes are almost identical, this alignment happens despite significant differences in the individual order-by-order amplitudes in the expansion. We show this for the specific case of the Born term in Fig. 3.4. Specifically as it pertains to the inelastic cross section, this order-by-order difference can have major consequences, for example, in Monte Carlo showering codes that depend on the n-th term in the Taylor expansion inn χ to weigh the probability of the n minijets. In these codes, switching the traditionally used eikonal scheme to the U-matrix scheme will have an impact on the results, although a full analysis of this impact is beyond the scope of this work.

It is important to note that, although we have shown that the total, elastic, and inelastic cross sections obtained using the two schemes remain nearly identical for $\sqrt{s}$ up to tens of TeV, at extremely high $\sqrt{s}$ approaching the grand unification scale the elastic and inelastic cross sections start differing significantly (see also discussion in [132]). Whereas with the eikonal scheme the elastic cross section reaches parity with the

inelastic cross section at around $\sqrt{s} = 10^{15}$ GeV and remains so at higher energies, the U-matrix scheme instead predicts continuing growth for the elastic cross section — at the cost of the inelastic cross section — until it gradually approaches saturation with respect to the total cross section at some $\sqrt{s} \gtrsim 10^{19}$ GeV. This is illustrated in terms of the ratio of the elastic to total cross-sections in Fig. 3.5. These extremely high energies are of course beyond the reach of experiments; such differences are therefore of limited practical relevance.

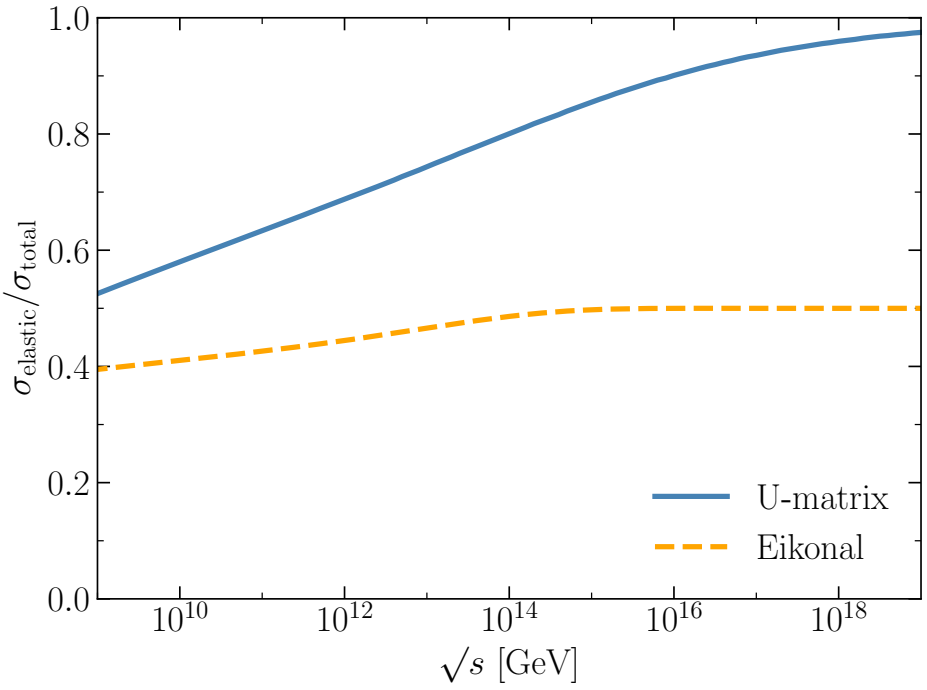

Figure 3.5: The evolution of the ratio of the elastic cross section to the total cross section at the GUT-scale and higher energies based on the unitarisation scheme chosen.

To summarise, we have used non-diffractive experimental data from colliders up to $\sqrt{s} = 13$ TeV to determine the most up-to-date fits to the total, elastic, and inelastic $p^{(-)}p$ cross sections in the literature, both for the eikonal and U-matrix unitarisation schemes. The upshot of our analysis is that the U-matrix scheme leads to cross sections that fit the data as well as the eikonal scheme, which is more conventionally used in most current cosmic-ray Monte Carlo codes. The corresponding total, elastic, and inelastic cross sections from both schemes are nearly indistinguishable at energies relevant to current and near-future colliders; they only start showing differences at energies approaching the grand unification scale. In particular, this allows us to extrapolate the inelastic

cross section up to GZK cut-off energies ($\sim 10^{20}$ eV) uniquely, irrespective of the unitarisation scheme chosen. This alignment between the overall inelastic cross sections notwithstanding, the amplitudes at each order in the series expansions differ significantly, with potential consequences for Monte Carlo showering codes.

Acknowledgments The authors are grateful to O. V. Selyugin and S. M. Troshin for useful discussions. AB is supported by the Fonds de la Recherche Scientifique-FNRS, Belgium, under grant No. 4.4503.19. AB is thankful to the computational resource provided by Consortium des Équipements de Calcul Intensif (CÉCI), funded by the Fonds de la Recherche Scientifique de Belgique (F.R.S.-FNRS) under Grant No. 2.5020.11 where a part of the computation was carried out. This work was also supported by the Fonds de la Recherche Scientifique-FNRS, Belgium, under grant No. 4.4503.19. AV is supported by U.S. DOE Early Career Research Program under FWP100331.

4 Unitarisation and diffractive interactions

4.1 Context of the research study

In the prior study, we thoroughly examined the effects of the eikonal and U-matrix schemes on inelastic non-diffractive interactions at ultra-high energies. Building on these results, we expanded our analysis to include diffractive interactions, which are crucial in high-energy scattering. In such processes, a proton remains intact or dissociates into a low-mass state. Diffractive processes are particularly significant at the high energies probed by the Large Hadron Collider (LHC) and cosmic-ray experiments, accounting for approximately 20 % of the inelastic cross-section at TeV energies [13]. These collisions are key to understanding interaction elasticity, a critical factor in air shower development. During these collisions, momentum is transferred without the exchange of quantum numbers, leading to the generation of new particles. When the energy transfer is small, typically a few GeV, the process is known as low-mass diffraction and is typically modelled using the Good and Walker framework with a 2- or 3-channel approach, depending on the number of diffractive states involved. In contrast, high-mass diffraction involves greater momentum transfer, allowing the exchanged Pomeron to produce additional particles or even a jet, resulting in significantly lower elasticity.

Besides, the inclusion of diffractive processes makes unitarization schemes more thoroughly tested and guarantees that all features of high-energy hadronic interactions are adequately modelled. It also furnishes new evidence that could allow for the improvement of the hadronic interaction modelling. Particularly, in this study, we aimed to evaluate how well the U-matrix and eikonal schemes describe the total, elastic, inelastic, and single-diffractive cross-sections in pp and $p\bar{p}$ interactions and to quantify the uncertainties attached to them. Moreover, the study aimed to explore the potential for generalizing these schemes, known as extended schemes, by introducing an additional parameter, ω. These

generalized forms are expressed as follows:

For the extended eikonal scheme:

$$X_E(s, \boldsymbol{b}) = \frac{\mathrm{i}}{\omega}\left[1 - \mathrm{e}^{\mathrm{i}\omega\chi(s,\boldsymbol{b})}\right], \tag{4.1}$$

For the extended U-matrix scheme:

$$X_U(s, \boldsymbol{b}) = \frac{\chi(s, \boldsymbol{b})}{1 - \mathrm{i}\omega\chi(s, \boldsymbol{b})}. \tag{4.2}$$

In both cases, the asymptotic value of $X(s \to \infty, \boldsymbol{b})$ is $1/\omega$. Thus, the traditional values for ω are 1 for the standard eikonal and 1/2 for the standard U-matrix.

With our optimized model, we also attempted to predict the ρ parameter, the ratio of the real part to the imaginary part of the elastic amplitude, and to compare it with experimental data, particularly at 13 TeV. Another objective of the study was to shed light on the implications of these different unitarisation schemes' effect on the single-diffractive cross-section for current and future cosmic ray data.

In order to fulfil our research purposes, we adopted the following methodology. First, up-to-date collider data on pp and $p\bar{p}$ total, elastic, inelastic and single-diffractive cross sections, including 13 TeV data from recent LHC experiments, have been used to ascertain the best fits to the parameters governing these cross sections. Then, we implemented both the eikonal and U-matrix unitarisation schemes within our theoretical framework, making sure that the unique features of each scheme were appropriately represented. Afterwards, using the collected data, we performed a global fit to determine the best-fit parameters for each unitarisation scheme. This involved minimizing the χ^2/d.o.f to assess the relevance of the fit. Lastly, comparing the generated cross-sections and fitted parameters, we paid particular attention to their concordance with experimental data and their prediction capacity at high energies.

In this context, the Good-Walker formalism is crucial for describing diffractive processes, particularly inelastic diffraction, which arises due to the internal structure of hadrons. At high energies, this phenomenon is more easily understood because the lifetime of fluctuations within a fast hadron is large, $\tau \sim \frac{E}{m^2}$, allowing these fluctuations to be treated as nearly "frozen." During this period, each constituent of the hadron can undergo scattering, disrupting the coherence of the fluctuations. Consequently, the outgoing superposition of states will differ from the incident particle, often resulting in both inelastic and elastic diffraction.

To explore inelastic diffraction, the Good-Walker approach introduces states ϕ_k that diagonalize the T matrix, where these eigenstates undergo only elastic scattering. Since off-diagonal transitions are absent,

$$\langle \phi_j | T | \phi_k \rangle = 0 \quad \text{for} \quad j \neq k, \tag{4.3}$$

a state k cannot diffractively dissociate into a state j. However, for hadronic states, which are not eigenstates of the S-matrix (or T), this condition generally does not hold. To account for the internal structure of hadrons, the set of intermediate states must be expanded beyond just the single elastic channel, introducing a multichannel approach. Before examining such a case, let's express the cross-section in terms of the probability amplitudes F_k of the hadronic process via the various diffractive eigenstates ϕ_k.

Let the orthogonal matrix that diagonalizes $\operatorname{Im} T$ be denoted by a, such that:

$$\operatorname{Im} T = aFa^T \quad \text{where} \quad \langle \phi_j | F | \phi_k \rangle = F_k \, \delta_{jk}. \tag{4.4}$$

Consider the diffractive dissociation of an arbitrary incoming state:

$$|j\rangle = \sum_k a_{jk} \, |\phi_k\rangle. \tag{4.5}$$

The elastic scattering amplitude for this state is:

$$\langle j | \text{Im } T | j \rangle = \sum_k |a_{jk}|^2 \, F_k = \langle F \rangle, \tag{4.6}$$

where $F_k = \langle \phi_k | F | \phi_k \rangle$, and $\langle F \rangle$ represents the average of F over the initial probability distribution of diffractive eigenstates. After diffractive scattering described by T_{fj}, the final state $|f\rangle$ will typically be a different superposition of eigenstates than $|j\rangle$, as shown in the equation above.

At high energies, the real parts of the diffractive amplitudes can be ignored. Then, the cross-sections at a given impact parameter b are:

$$\frac{d\sigma_{\text{tot}}}{d^2b} = 2 \operatorname{Im} \langle j | T | j \rangle = 2 \sum_k |a_{jk}|^2 \, F_k = 2\langle F \rangle, \tag{4.7}$$

$$\frac{d\sigma_{\text{el}}}{d^2b} = |\langle j | T | j \rangle|^2 = \left(\sum_k |a_{jk}|^2 \, F_k \right)^2 = \langle F \rangle^2, \tag{4.8}$$

$$\frac{d\sigma_{\text{el+SD}}}{d^2b} = \sum_k |\langle \phi_k | T | j \rangle|^2 = \sum_k |a_{jk}|^2 \, F_k^2 = \langle F^2 \rangle. \tag{4.9}$$

Thus, the cross-section for single diffractive dissociation of a proton is given by:

$$\frac{d\sigma_{\mathrm{SD}}}{d^2b} = \langle F^2 \rangle - \langle F \rangle^2, \tag{4.10}$$

reflecting the statistical dispersion in the absorption probabilities of the diffractive eigenstates. Here, the average is taken over the components k of the incoming proton that dissociates. If the averages are taken over components of both incoming particles, a second index on F must be introduced, making it F_{ik}, and summing over k and i. In this case, the sum represents the cross-section for both single and double dissociation.

If all the components ϕ_k of the incoming diffractive state $|j\rangle$ were absorbed equally, the diffracted superposition would be proportional to the incident one, resulting in zero inelastic diffraction. At very high energies, if the amplitudes F_k at small impact parameters reach the black disk limit ($F_k = 1$), diffractive production will be zero in this impact parameter domain and will only occur in the peripheral b region. Similar behavior is observed in pp and $p\bar{p}$ interactions at Tevatron energies. Hence, the impact parameter structure of inelastic and elastic diffraction differs significantly when strong s-channel unitarity effects are present. The elastic amplitude primarily originates from the center of the disk (small b), while dissociation occurs at the periphery.

The Good-Walker mechanism effectively handles elastic scattering and single diffractive dissociation by representing the initial state as a superposition of eigenstates that interact with the Pomeron. However, this model assumes that these eigenstates remain unchanged during the interaction, limiting its ability to describe more complex phenomena, such as multiple Pomeron exchanges and diffractive dissociation involving multiple states.

Given the importance of multi-channel interactions at ultra-high energies, we adopted a modified Good-Walker approach. This adaptation extends the original formalism to include additional channels and interaction vertices, such as the $p \to D$, $D \to p$, and $D \to D$ transitions, where D is a diffractive state. These modifications are essential for accurately modelling diffractive dissociation at these energy scales.

A key challenge in this approach is that, at the Born level, the behaviour of the interaction vertices is largely unknown, except for $V_{pp}(t)$, for which the parameterization from non-diffractive inelastic interactions is a good representation at low energy. By assuming a similar functional form for V_{DD}, we retain two parameterizations in our model. Through this careful consideration of vertex behaviour, we can better capture the full range

of diffractive processes that the standard Good-Walker mechanism cannot adequately address.

4.2 ARTICLE 2

Unitarisation Dependence Of Diffractive Scattering In Light Of High-Energy Collider Data

Arno Vanthieghem, Atri Bhattacharya, Rami Oueslati, Jean-René Cudell

Journal of High Energy Physics, 2021(9), 005
arXiv:2104.12923 [hep-ph]

Abstract: We study the consequences of high-energy collider data on the best fits to total, elastic, inelastic, and single-diffractive cross sections for pp and $p\bar{p}$ scattering using different unitarisation schemes. We find that the data are well fitted both by eikonal and U-matrix schemes, but that diffractive data prefer the U-matrix. Both schemes may be generalised by means of an additional parameter; however, this yields only marginal improvements to the fits. We provide estimates for ρ, the ratio of the real part to the imaginary part of the elastic amplitude, for the different fits. We comment on the effect of the different schemes on present and future cosmic ray data.

4.2.1 Introduction

High-energy hadronic scattering may be described by Reggeon exchanges (see, e.g. [63] and references therein) and for center-of-momentum energies $\sqrt{s}$ larger than 100 GeV, the only trajectory that matters is that of the pomeron. However, at energies of a few TeV and higher, the growth of the pomeron term leads to violation of the black-disk limit [87, 123, 120] and eventually of unitarity. Unitarity can be enforced in high-energy pp and $p\bar{p}$ interactions by the inclusion of multiple exchanges, which act as a cut to the elastic scattering amplitude. Different unitarisation schemes have been discussed in the literature [58] but all of them rely on phenomenological arguments in the absence of a comprehensive quantum chromodynamics treatment.

The effect of unitarisation on the growth of $p^{(-)}p$ cross-sections becomes important when considering proton-proton scattering cross sections at the LHC where the centre-of-momentum energies extend up to 13 TeV. Measurements of the total, elastic, inelastic, and diffractive pp cross sections by the different LHC experiments — ALICE [11], ATLAS [5, 3, 4, 110], CMS [125], LHCb [6], and TOTEM [22, 25, 24, 23, 28, 26] — add to existing $p^{(-)}p$ scattering data at lower energies from previous generation experiments at the S$p\bar{p}$S [48, 15] and the TeVatron [10, 17, 18, 9, 30, 31]. This extensive wealth of data allows us to constrain the nature of unitarisation governing these interactions with an improved degree of accuracy.

Differences in cross sections that depend on the choice of the unitarisation scheme are expected to show up at very high energies — at 10 TeV and higher — and therefore may influence predictions for cosmic-ray collisions with atmospheric nuclei at ultra-high energies. Showering codes, such as `SIBYLL` [117] and `QGSJET` [113], used to simulate and reconstruct these events from observations of secondaries have historically used the eikonal scheme (see [20] for a review). In the context of ongoing ultra-high energy cosmic-ray experiments, e.g. the Pierre Auger Observatory [1], the Telescope Array Project [95], and IceTop [8], an investigation of the dependence of cross sections on different unitarisation schemes assumes paramount importance.

In [42], we examined the effect of including up-to-date collider data for total, elastic, and inelastic cross sections. We found nearly identical cross sections for the three irrespective of the unitarisation scheme used. In the current work, we focus on the effect of incorporating diffractive data into the fits. Diffractive scattering in $2 \mapsto 2$ interactions, where either one or both final state particles break up into jets, becomes increasingly important as the interaction energy increases. In these interactions, the final state(s) being no longer expressible in terms of hadronic eigenstates, the calculation of the corresponding scattering amplitudes requires the invocation of a rotated eigenstate basis as described in the Good-Walker mechanism [83].

The present work is organised as follows. In Section 4.2.2, we briefly recapitulate the theory of unitarisation in $p^{(-)}p$ scattering and the different schemes that have been proposed in the literature. In Section 4.2.3 we explain the Good-Walker representation [83]. In section 4.2.4 we list the various parameters defining our fits. Additionally, we list all the $p^{(-)}p$ scattering data that are used to determine our best fits. Finally, in Section

6.2.4 we give our results and discuss them in light of the existing literature, drawing our conclusions.

4.2.2 Brief Survey of Unitarisation Schemes and Fit to Non-Diffractive Forward Data

The differential cross section for elastic scattering may be expressed in terms of the elastic amplitude $A(s,t)$ as

$$\frac{\mathrm{d}\sigma_{el}}{\mathrm{d}t} = \frac{|A(s,t)|^2}{16\pi s^2}\,, \tag{4.11}$$

where $t = -\boldsymbol{q}^2$ is the square of the momentum transfer. At low energy, the term in $A(s,t)$ responsible for the growth of the cross section with s can be parameterised [57] using the pomeron trajectory $\alpha(t)$, the proton elastic form factor $F_{pp}(t)$ and the coupling pomeron-proton-proton g_{pp}, as

$$a(s,t) = g_{pp}^2\, F_{pp}(t)^2 \left(\frac{s}{s_0}\right)^{\alpha(t)} \xi(t), \tag{4.12}$$

with $\xi(t)$ the signature factor

$$\xi(t) = -e^{\frac{-i\pi\alpha(t)}{2}}. \tag{4.13}$$

We shall consider here a dipole form factor, which is close to the best functional form [57], although the exact functional form is not very important as we consider only integrated quantities in this paper:

$$F_{pp} = \frac{1}{(1 - t/t_{pp})^2} \tag{4.14}$$

The pomeron trajectory is close to a straight line [60], and we take it to be

$$\alpha(t) = 1 + \epsilon + \alpha' t. \tag{4.15}$$

At high energy, the growth of this pomeron term and eventual violation of unitarity is most clearly seen in the impact-parameter representation, where the Fourier transform of the amplitude $a\,(s,t)$ rescaled by $2s$ is equivalent to a partial wave

$$\chi(s,\boldsymbol{b}) = \int \frac{\mathrm{d}^2\boldsymbol{q}}{(2\pi)^2} \frac{a(s,t)}{2s} \mathrm{e}^{\mathrm{i}\boldsymbol{q}\cdot\boldsymbol{b}}. \tag{4.16}$$

The norm of this partial wave at small $|\boldsymbol{b}|$ exceeds unity around $\sqrt{s} = 2$ TeV [60].

To solve this problem, one introduces unitarisation schemes which map the amplitude $\chi(s, \boldsymbol{b})$ to the physical amplitude $X(s, \boldsymbol{b})$. The latter reduces to $\chi(s, \boldsymbol{b})$ for small s, is confined to the unitarity circle $|X(s, \boldsymbol{b}) - i| \leqslant 1$, and bears the same relation as Eq.(6.15), but this time to the physical amplitude:

$$X(s, \boldsymbol{b}) = \int \frac{\mathrm{d}^2\boldsymbol{q}}{(2\pi)^2} \frac{A(s,t)}{2s} \mathrm{e}^{\mathrm{i}\boldsymbol{q}\cdot\boldsymbol{b}}. \tag{4.17}$$

The most common scheme is the eikonal scheme, and it has been derived for structureless bodies, in optics, in potential scattering and in QED. Another proposed scheme is the U matrix scheme, which can be motivated by a form of Bethe-Salpeter equation [107]. Probably neither of these is correct in QCD, but going from one to the other permits an evaluation of the systematics linked to unitarisation.

In the following, we shall actually use generalised versions of the schemes, which include an extra parameter ω [58]:

$$X_E(s, \boldsymbol{b}) = \frac{\mathrm{i}}{\omega} \left[1 - \mathrm{e}^{\mathrm{i}\omega\chi(s,\boldsymbol{b})}\right], \tag{4.18}$$

while the generalised U-matrix scheme requires:

$$X_U(s, \boldsymbol{b}) = \frac{\chi(s, \boldsymbol{b})}{1 - \mathrm{i}\omega\chi(s, \boldsymbol{b})}. \tag{4.19}$$

In both cases, the asymptotic value of $X(s \to \infty, \boldsymbol{b})$ is $1/\omega$, hence the traditional values for ω are 1 for the standard eikonal [107], and 1/2 for the standard U matrix [119]. Both schemes map the amplitude $\chi(s, \boldsymbol{b})$ into the unitarity circle for $\omega \geqslant 1/2$. In terms of partial waves, the maximum inelasticity is reached for $X(s, \boldsymbol{b}) = \mathrm{i}$.

The total and elastic scattering cross sections may be readily expressed in these representations as

$$\sigma_{tot} = 2 \int \mathrm{d}^2\boldsymbol{b}\ \mathfrak{Im}\left(X(s, \boldsymbol{b})\right), \qquad \sigma_{el} = \int \mathrm{d}^2\boldsymbol{b}\ |X(s, \boldsymbol{b})|^2. \tag{4.20}$$

Hence these unitarised schemes naturally lead to expressions for the total, elastic, and hence inelastic, cross sections. We shall now use them to fit all the data in $p^{(-)}p$ scattering above 100 GeV, for which lower trajectories have a negligible effect. This includes the following:

- pp total and elastic cross sections from TOTEM [22, 25, 24, 23, 28], and ATLAS [5, 3];

Scheme	ϵ	α' (GeV^{-2})	g_{pp}	t_{pp} (GeV^2)	χ^2/d.o.f
U-matrix	0.10 ± 0.01	0.37 ± 0.28	7.5 ± 0.8	2.5 ± 0.6	1.436
Eikonal	0.11 ± 0.01	0.31 ± 0.19	7.3 ± 0.9	1.9 ± 0.4	1.442

Table 4.1: χ^2/d.o.f and best-fit parameters obtained using the eikonal ($\omega = 1$) and U-matrix ($\omega' = 1/2$) unitarisation schemes without diffractive data [42] .

- $p\bar{p}$ total and elastic cross sections from CDF [10], E710 [17, 18], and E811 [30, 31] experiments at TeVatron; and UA4 at Sp$\bar{p}$S [48];
- Direct measurements of inelastic cross sections, i.e. not derived from total and elastic measurements, from UA5 at Sp$\bar{p}$S [15], ATLAS [4, 110], LHCb [6], ALICE [11], and TOTEM [26].

This gives a total of 37 data points. In the next section, we shall also consider 6 extra data points:

- Single diffractive $p\bar{p}$ cross sections from UA5 [15, 16] and E710 [19]; and
- pp single diffractive cross sections at various energies measured at ALICE [11].

The resulting fit leads to the following parameters of Table 6.1.

4.2.3 Unitarisation and diffraction

The implementation of diffraction within a unitarisation scheme at high energy has to confront two questions: how does one describe the diffractive amplitude at the Born level, and how does one embed that amplitude within a unitarisation scheme?

The first questions has two answers. On the one hand, the asymptotic answer is that , for high-mass final states, one should use the triple-reggeon vertices. However, as the masses considered are not necessarily large, one must consider a variety of reggeons lying on trajectories below that of the pomeron[62], and to include not only subdominant trajectories (with intercept of the order of 1/2) but also sub-subdominant ones (with an intercept of the order of 0). This introduces a multitude of parameters, of the order of the number of high-energy data points available.

On the other hand, it is possible to consider a generic diffractive state D and the vertex $p + I\!P \to D$. A priori, this implies the consideration of a large number of channels for the diffractive state D, and the introduction of many parameters. However, it has been shown in [85] that for inclusive cross section, the consideration of one generic diffractive state $\mid \Psi_D \rangle$ is sufficient, and that adding other states does not significantly improve the description of the data. One however looses the information about the mass of the diffractive state.

We will concentrate in this paper on inclusive quantities, and on a generic diffractive D, which is the seed of high-energy pions, and hence of high-energy muons, in cosmic ray showers. This makes them of particular interest in view of the muon anomaly at ultra-high energies (see [2] and references therein).

The second question concerns the description of multiple exchanges, which are expected to be important at ultra-high energies. The problem is to include insertions that contain the $pI\!PD$, the $DI\!Pp$ and $DI\!PD$ vertices, and re-sum them. Solutions to this problem have been proposed by Gotsman, Levin, and Maor (GLM) [85, 86] and further explored by Khoze, Martin, and Ryskin [96, 97, 99] using the Good-Walker model [83]. We shall adapt their method, originally proposed for the eikonal unitarisation, to any scheme, and more specifically to the U-matrix unitarisation scheme.

At the Born level, the interaction of a proton with a pomeron can leave the proton intact or turn it into a diffractive state D. GLM argue that it is possible to define two states $\mid \Psi_1 \rangle$ and $\mid \Psi_2 \rangle$ which are not modified by the interaction with a pomeron:

$$\mid \Psi_p \rangle = \cos\theta \mid \Psi_1 \rangle + \sin\theta \mid \Psi_2 \rangle \,, \text{ and} \tag{4.21a}$$

$$\mid \Psi_D \rangle = -\sin\theta \mid \Psi_1 \rangle + \cos\theta \mid \Psi_2 \rangle \,, \tag{4.21b}$$

with θ an arbitrary angle. In this representation, the final states for elastic, single diffractive, and double diffractive amplitudes are given by $\mid \Psi_p \Psi_p \rangle$, $\mid \Psi_p \Psi_D \rangle$, and $\mid \Psi_D \Psi_D \rangle$ respectively.

Before we unitarise, we need the Born-level amplitudes $a_{ij}(s,t) = \langle \Psi_i \Psi_j \mid \hat{T} \mid \Psi_i \Psi_j \rangle$, for $i, j = 1, 2$. We shall assume that the pomeron is a simple pole at the Born level, so that the amplitudes can be factorised in t space as e.g.

$$a_{pp\to pp} = \langle pp|T|pp\rangle = V_{pp}(t)^2 R(s,t) \tag{4.22}$$

$$a_{pp\to pD} = a_{pp\to Dp} = \langle pp|T|pD\rangle = V_{pp}(t)V_{pD}(t)R(s,t) \tag{4.23}$$

$$a_{DD\to DD} = \langle DD|T|DD\rangle = V_{DD}(t)^2 R(s,t) \tag{4.24}$$

with $R(s,t) = \left(\frac{s}{s_0}\right)^{\alpha(t)} \xi(t)$, and $V_{ab}(t)$ the vertex functions. All processes can be described using 3 functions, V_{pp}, V_{DD} and $V_{pD} = V_{Dp}$. We take them as

$$V_{ab} = g_{ab} F_{ab}(t) \tag{4.25}$$

where a and b are either p or D, g_{ab} are the coupling strengths and $F_{ab}(t)$ is a form factor, with $F_{ab}(0) = 1$. The nature of form factors for the eigenstates $\Psi_{\{1,2\}}$ cannot be determined from experiments, therefore we invert the relations in Eq. (4.21) to express $\Psi_{\{1,2\}}$ in terms of $\Psi_{\{p,D\}}$. This allows us to work with the proton and diffractive state form factors; we assume the form factor for the latter is similar to that of the proton. The two GLM states

$$|\Psi_1\rangle = \cos\theta|p\rangle - \sin\theta|D\rangle \tag{4.26}$$
$$|\Psi_2\rangle = \sin\theta|p\rangle + \cos\theta|D\rangle, \tag{4.27}$$

correspond to amplitudes

$$a_{ij\to kl} = \langle ij|T|kl\rangle = V_{ik}(t)V_{jl}(t)R(s,t),\ i,j = 1,2 \tag{4.28}$$

which will be purely elastic if $V_{12} = V_{21} = 0$. This leads to

$$\tan(2\theta(t)) = \frac{2V_{pD}(t)}{V_{DD}(t) - V_{pp}(t)} \tag{4.29}$$

and

$$V_{11}(t) = V_{pp}(t)\cos^2(\theta) + V_{DD}(t)\sin^2(\theta) - V_{pD}(t)\sin(2\theta) \tag{4.30}$$
$$V_{22}(t) = V_{pp}(t)\sin^2(\theta) + V_{DD}(t)\cos^2(\theta) + V_{pD}(t)\sin(2\theta). \tag{4.31}$$

Hence at this point, we have traded three amplitudes V_{ab} for two amplitudes V_{ii} and an angle. We do not know, at the born level, how any of these should behave, except for $V_{pp}(t)$, for which the parameterisation (4.25) is a good representation at low energy [57]. One can assume the same functional form holds for V_{DD}, hence we keep these two parameterisations. Following GLM [87], we choose θ as a final input. Clearly, it depends on t. However, as we shall be considering integrated cross sections, and as the t dependencies of the various V_{ab} are not expected to be very different, it is reasonable to approximate

$$\tan(2\theta(t)) \approx \tan(2\theta(0)) = \frac{g_{pD} + g_{Dp}}{g_{DD} - g_{pp}} \tag{4.32}$$

and keep it as a parameter. To translate this into a specific expression for V_{11} and V_{22}, we eliminate V_{pD} using Eq. (4.29). This leads to

$$V_{11}(t) = \frac{\cos^2(\theta)V_{pp}(t) - \sin^2(\theta)V_{DD}(t)}{\cos(2\theta)} \tag{4.33}$$

$$V_{22}(t) = \frac{\cos^2(\theta)V_{DD}(t) - \sin^2(\theta)V_{pp}(t)}{\cos(2\theta)} \tag{4.34}$$

These can be used to build the amplitudes that will enter into the unitarisation schemes, using Eq. (4.28). One can thus obtain the elastic, single-diffractive and double-diffractive amplitudes from three purely elastic amplitudes [85, 86], given the fact that $a_{12\to12} = a_{21\to21}$:

$$a_{pp\to pp} = \cos^4(\theta)a_{11\to11} + 2\cos^2(\theta)\sin^2(\theta)a_{12\to12} + \sin^4(\theta)a_{22\to22} \tag{4.35a}$$

$$a_{pp\to pD} = \cos(\theta)\sin(\theta) \times (-\cos^2(\theta)a_{11\to11} + (\cos^2(\theta) - \sin^2(\theta))a_{12\to12} + \sin^2(\theta)a_{22\to22}) \tag{4.35b}$$

$$a_{pp\to DD} = \cos^2(\theta)\sin^2(\theta)(a_{11\to11} - 2a_{12\to12} + a_{22\to22}). \tag{4.35c}$$

At this point, it is easy to unitarise the amplitudes $a_{ij\to ij}(s,t)$, following what was done in Section 2 for elastic scattering. One goes into impact parameter space to obtain the corresponding $\chi_{ij\to ij}(s,\mathbf{b})$, replaces the amplitudes at the Born level by their unitarised version, as Eqs. (6.16) and (6.17):

$$X^{(E)}_{ij\to ij}(s,\boldsymbol{b}) = \frac{\mathrm{i}}{\omega}\left[1 - \mathrm{e}^{\mathrm{i}\omega\chi_{ij\to ij}(s,\boldsymbol{b})}\right] \tag{4.36a}$$

$$X^{(U)}_{ij\to ij}(s,\boldsymbol{b}) = \frac{\chi_{ij\to ij}(s,\boldsymbol{b})}{1 - \mathrm{i}\omega\chi_{ij\to ij}(s,\boldsymbol{b})}. \tag{4.36b}$$

and obtains the amplitudes of interest as in Eq. (4.35):

$$X_{el} = \cos^4(\theta)X_{11\to11} + 2\cos^2(\theta)\sin^2(\theta)X_{12\to12} + \sin^4(\theta)X_{22\to22} \tag{4.37a}$$

$$X_{sd} = \cos(\theta)\sin(\theta) \times (-\cos^2(\theta)X_{11\to11} + (\cos^2(\theta) - \sin^2(\theta))X_{12\to12} + \sin^2(\theta)X_{22\to22}) \tag{4.37b}$$

$$X_{dd} = \cos^2(\theta)\sin^2(\theta)(X_{11\to11} - 2X_{12\to12} + X_{22\to22}). \tag{4.37c}$$

The relevant $2 \to 2$ cross sections are then given by

$$\sigma_{tot} = 2 \int \mathrm{d}^2 b \; \mathfrak{Im} \{X_{el}\} \; ; \qquad \sigma_{el} = \int \mathrm{d}^2 b \; |X_{el}|^2 \, ; \tag{4.38a}$$

$$\sigma_{sd} = 2 \int \mathrm{d}^2 b \; \left(|X_{sd}|^2\right) \; ; \qquad \sigma_{dd} = \int \mathrm{d}^2 b \; |X_{dd}|^2 \, ; \tag{4.38b}$$

and the ρ parameter is defined by

$$\rho(s, t=0) = \frac{\mathfrak{Re} \{X_{el}(s, t=0)\}}{\mathfrak{Im} \{X_{el}(s, t=0)\}} \, . \tag{4.38c}$$

4.2.4 Fit parameters and data

Section 3 has introduced the basic ingredients and parameters of our model. First of all, one has of course the parameters of Section 2, i.e. ϵ and α', linked to the Pomeron trajectory $R(s,t)$, as well as g_{pp} and t_{pp}, linked to the $p\mathbb{P}p$ vertex $V_{pp}(t)$. To describe diffractive scattering in our scheme, one needs three more parameters: the $D\mathbb{P}D$ coupling g_{DD}, the scale t_{DD} in the form factor

$$F_{DD}(t) = \frac{1}{(1 - t/t_{DD})^2} \tag{4.39}$$

and the mixing angle θ. Finally, one can introduce the parameters ω and ω' corresponding to extended unitarisation schemes.

Several remarks are in order at this point. First of all, we have considered the minimal GLM scheme, where we mix the proton with one diffractive state. This corresponds to a 2-channel unitarisation scheme. In principle, one could consider an $N-$channel scheme, at the cost of multiplying the number of parameters $N(N+1)/2 + 8$. Given the paucity of diffractive data at high energy, going beyond $N = 2$ is not possible. Note that GLM considered the case $N-3$, and found that there is no significant improvement [85].

We can further limit the number of parameters by considering the two standard unitarisation schemes, i.e. fix $\omega = 1$ and $\omega' = 1/2$. We have checked that varying these parameters lead to an improvement of only 0.01 in the χ^2/d.o.f.

Nevertheless, even in the 2-channel scheme, one still has an over-parameterisation. The main problem comes from the fact that there is a strong correlation between the parameters of V_{pp} and those of V_{DD},

so that error bars are huge. As the pp parameters are determined by the fits of Section 2, we fix their values to their central values in that fit: $g_{pp} = 7.5$ (7.3) and $t_{pp} = 2.6$ (1.9) GeV^2 in the U-matrix (eikonal) schemes.

Since our focus is on high energy effects induced in $p^{(-)}\bar{p}$ cross sections, we use experimental data above 100 GeV. Together with the data set provided by the Particle Data Group [127], Table 4.2 includes the data from the following experiments:

- pp total and elastic cross sections from TOTEM [22, 25, 24, 23, 28], and ATLAS [5, 3];
- $p\bar{p}$ total and elastic cross sections from CDF [10], E710 [17, 18], and E811 [30, 31] experiments at the TeVatron; and UA4 at the Sp$\bar{\text{p}}$S [48];
- Direct measurements of inelastic cross sections, i.e. not derived from total and elastic measurements, from UA5 at the Sp$\bar{\text{p}}$S [15], ATLAS [4, 110], LHCb [6], ALICE [11], and TOTEM [26];
- Single diffractive $p\bar{p}$ cross sections from UA5 [15, 16] and E710 [19]; and
- pp single diffractive cross sections at various energies measured at ALICE [11].

A few caveats about our data selection are in order. We use measured data from experiments that quote both statistical and systematic errors, and combine them in quadrature. We omit pp cross-section measurements from cosmic-ray experiments because the reconstruction of these events uses Monte Carlo showering codes such as `SIBYLL` [73] and `QGSJET-II` [112] which use the eikonal unitarisation scheme.

As discussed in [42], there is considerable tension amongst the total and elastic cross sections at the same or similar energies from different experiments (see also [56, 46]). We quantify these inconsistencies by fitting each kind of cross section with a quadratic polynomial in $\log s$, the resulting χ^2 shown in Table 4.3.

We particularly note that at centre-of-mass energies of 7 and 8 TeV, total and elastic cross sections from TOTEM are consistently 1σ higher than those from ATLAS. The low statistics we have to work with prevents us from determining which experimental results are the outliers, so we shall continue to use all of the data points with the cognisance that the

Expt	$\sqrt{s}$	σ_{tot} [mb]	σ_{el} [mb]	σ_{in} [mb]	σ_{sd} [mb]
UA5	200 GeV				4.8 ± 0.9
	546 GeV				5.4 ± 1.1
	900 GeV			50.3 ± 1.1	7.8 ± 1.2
E710	1.02 TeV	61.1 ± 9.9			
	1.8 TeV	78.3 ± 5.9	19.6 ± 3.0		8.1 ± 1.7
ATLAS	7 TeV	95.4 ± 1.4	24.0 ± 0.6		
	7 TeV			69.4 ± 7.3	
	8 TeV	96.1 ± 0.9	24.3 ± 0.4		
	13 TeV			78.0 ± 3.0	
ALICE	2.76 TeV			62.8 ± 3.4	12.2 ± 4.6
	7 TeV			73.2 ± 4.3	14.9 ± 4.7
LHCb	7 TeV			68.7 ± 4.9	
	13 TeV			75.4 ± 5.4	
TOTEM	7 TeV			73.7 ± 3.4	
	13 TeV	110.6 ± 3.4	31.0 ± 1.7		

Table 4.2: High energy $p\overset{(-)}{p}$ experimental data set supplemented by data available in [127]

dataset	number of points	χ^2
σ_{tot}	18	21.7
σ_{el}	11	21.3
σ_{in}	8	4.1
σ_{sd}	6	2.6

Table 4.3: The values of χ^2 resulting from independent fits to quadratic polynomials in $\log(s)$, illustrating the tensions in some parts of the dataset.

resulting χ^2 will inevitably be high. When including single diffractive data, this enforces a baseline minimum of $\chi^2 = 49.6$ for 43 data points.

Furthermore, we do not include double diffractive cross-section measurements [21, 12, 11] in our fits since a proper description of these cross sections has so far eluded any theoretical description. We have checked that our models are not able to reproduce these, even if we free all possible parameters. We show the discrepancy in Fig. 4.4.

4.2.5 Results

We give the results of our fits in Fig. 4.4 and Table 4.4. We obtain equivalent fits for the U matrix and the eikonal, with respective values of the χ^2/d.o.f of 1.316 and 1.328. As discussed in Sec. 4.2.4, these high values are driven by disagreements in the elastic data at the high energies. With

Scheme	ϵ	α' (GeV^{-2})	g_{DD}	t_{DD} (GeV^2)	θ (rad)	χ^2/d.o.f
U-matrix	0.11 ± 0.08	0.35 ± 0.05	6.3 ± 1.3	2.2 ± 0.4	0.11 ± 0.02	1.316
Eikonal	0.12 ± 0.04	0.31 ± 0.10	8.81 ± 0.12	1.37 ± 0.05	0.20 ± 0.02	1.328

Table 4.4: χ^2/d.o.f and best-fit parameters obtained using the eikonal ($\omega = 1$) and U-matrix ($\omega' = 1/2$) unitarisation schemes with single diffractive data. The parameters of the pp vertex are fixed to the central values of Table 6.1.

this understanding, it is clear that the data allows for U-matrix unitarisation scheme. Either scheme describes the total and elastic cross sections equally well; however, the U-matrix scheme provides a slightly better fit to the high-energy single diffractive data than does the eikonal, as can be seen in Fig. 4.4.

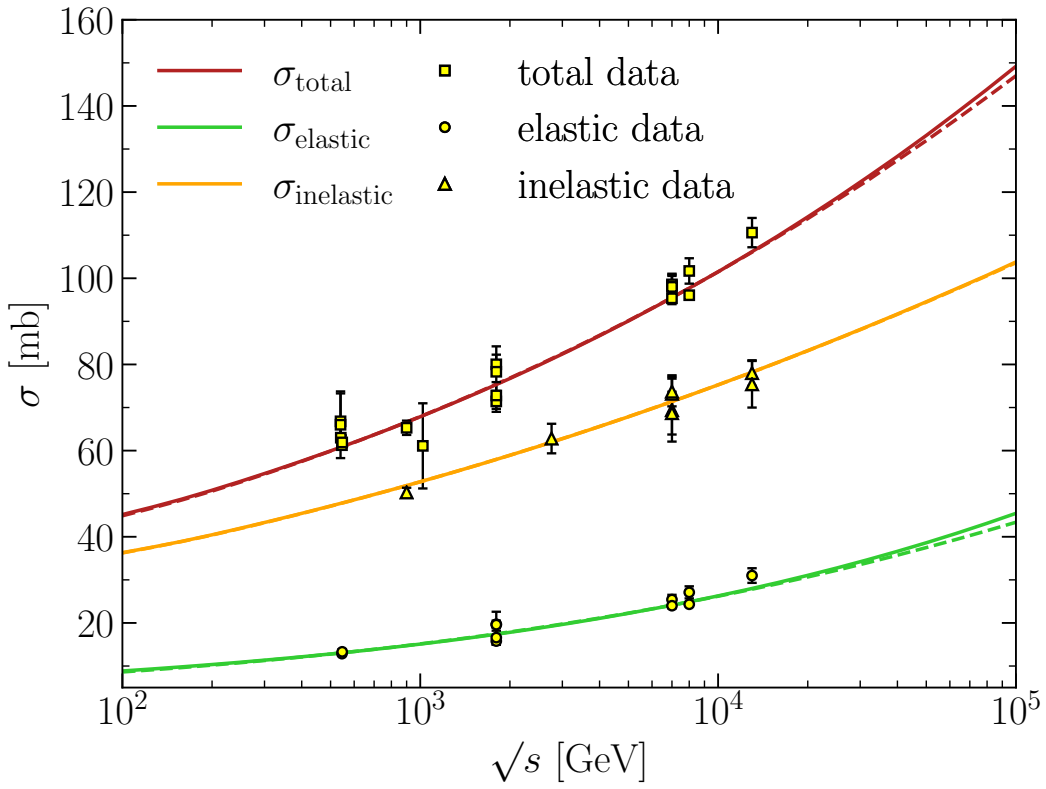

Figure 4.1: Top left: Total, elastic, and inelastic cross sections obtained with best-fit parameters for the U-matrix (solid curves) and the eikonal schemes (dashed curves) without using single-diffractive data. Top-right: Same as top-left but when single diffractive data is included in the fits. Bottom-left: Single diffractive cross-sections for best-fit values of the parameters when using the U-matrix (solid curves) and eikonal schemes (dashed curve). Bottom-right: Double diffractive cross-sections, which are not well fit by either scheme.

The parameters of the pomeron trajectory are not affected by the inclusion of the diffractive data, as they have a much lower weight than the elastic data. The parameters linked to the diffractive state are consistent with the physical picture underlying our model: the diffractive state is slightly bigger than the proton hence its scale t_{DD} is slightly lower than t_{pp}.

As noted previously, the double diffractive cross sections $p\overset{(-)}{p} \to 2\,X$ [21, 12, 11] are not fitted well by either of the unitarisation schemes. We show this in Fig. 4.4 (bottom-right panel).

Multiple experiments have investigated the ratio of the real part of the elastic scattering amplitude to its imaginary part at different centre-of-mass energies. Although we do not use ρ data in our fits, we can predict

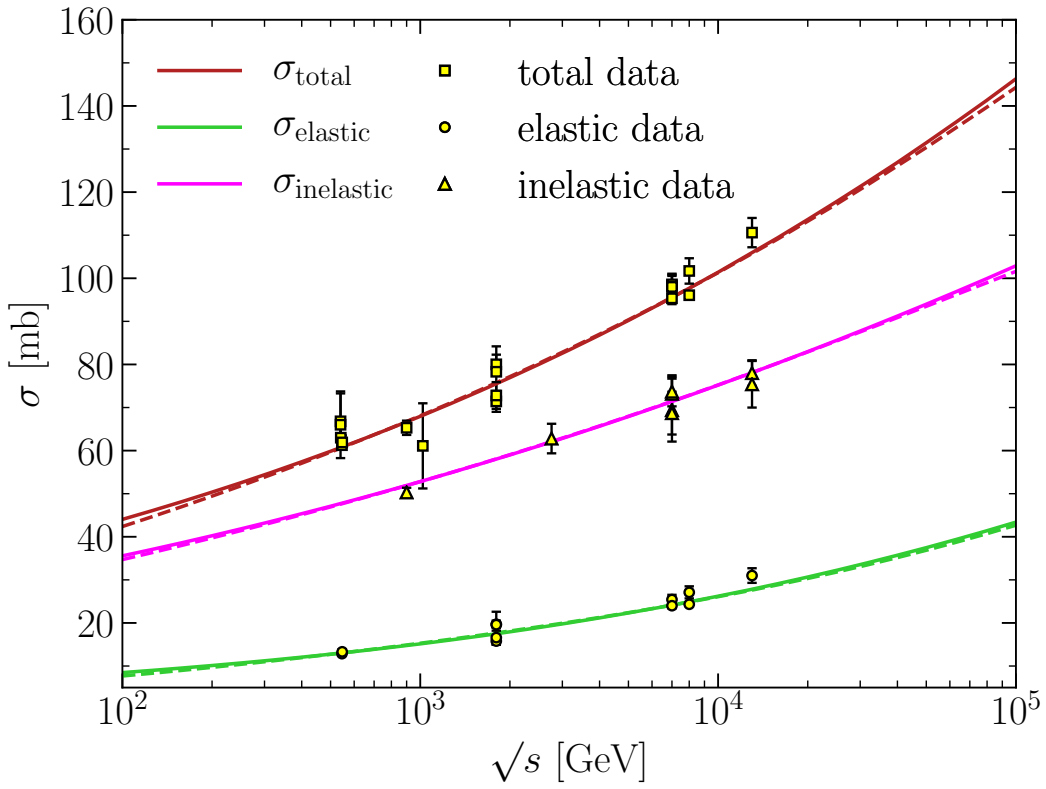

Figure 4.2: Top left: Total, elastic, and inelastic cross sections obtained with best-fit parameters for the U-matrix (solid curves) and the eikonal schemes (dashed curves) without using single-diffractive data. Top-right: Same as top-left but when single diffractive data is included in the fits. Bottom-left: Single diffractive cross-sections for best-fit values of the parameters when using the U-matrix (solid curves) and eikonal schemes (dashed curve). Bottom-right: Double diffractive cross-sections, which are not well fit by either scheme.

its values at different $\sqrt{s}$ using our best-fit parameters and compare these predictions against the experimental data. We find that the values of ρ and its slowly-falling shape as a function of $\sqrt{s}$ are largely consistent with experimental data between 100 GeV and 7 TeV (see e.g. [127]). We predict $\rho = 0.131 \pm 0.009$ for either unitarisation scheme at $\sqrt{s} = 13$ TeV. This agrees with the result $\rho = 0.14$ in [64]; however, it is in tension with the value of $\rho \approx 0.10$ obtained for the 13 TeV TOTEM data both by the collaboration itself [27] and in [61].

Despite their equivalence for existing data, the two schemes give significantly different predictions for the single-diffractive cross section at ultra-high energies. Unlike the total, elastic, and inelastic cross sections, the single diffractive cross section obtained using the eikonal scheme is

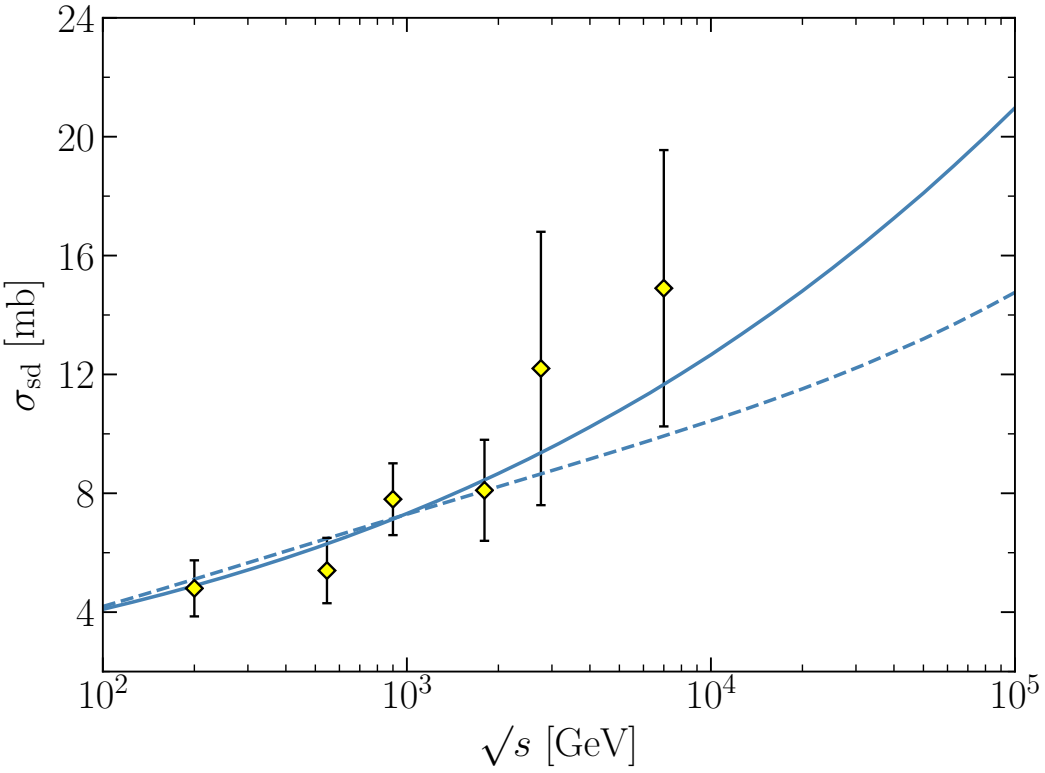

Figure 4.3: Top left: Total, elastic, and inelastic cross sections obtained with best-fit parameters for the U-matrix (solid curves) and the eikonal schemes (dashed curves) without using single-diffractive data. Top-right: Same as top-left but when single diffractive data is included in the fits. Bottom-left: Single diffractive cross-sections for best-fit values of the parameters when using the U-matrix (solid curves) and eikonal schemes (dashed curve). Bottom-right: Double diffractive cross-sections, which are not well fit by either scheme.

noticeably different from that obtained using the U-matrix, with the former exhibiting a slower growth with energies than the latter, as shown in Fig. 4.5. This difference is especially significant for ongoing cosmic-ray experiments measuring the pp cross-section at high energies from tens of TeV up to the GZK cut-off, $E_{\rm lab} \approx 5 \times 10^{10}$ GeV. As the single-diffraction is the parent process to forward pions, and hence to forward muons, it seems that considering different unitarisation schemes would lead to different muon multiplicities at ultra-high energies.

4.2.6 Conclusions

We have shown how the scheme proposed by Gotsman, Levin and Maor [85, 86] could be adapted to other unitarisation schemes. We have also

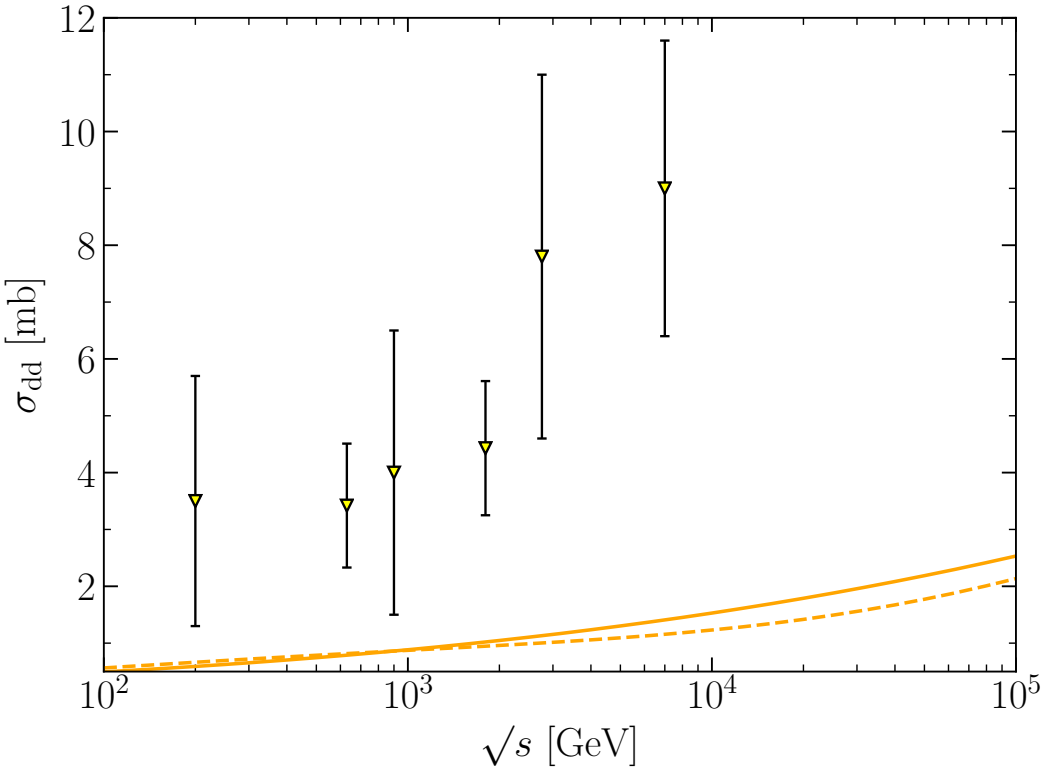

Figure 4.4: Bottom-left: Single diffractive cross-sections for best-fit values of the parameters when using the U-matrix (solid curves) and eikonal schemes (dashed curve). Bottom-right: Double diffractive cross-sections, which are not well fit by either scheme.

shown how the vertices of the mixed states could be deduced from those of the proton, allowing a more constrained parameterisation.

Using up-to-date collider data on $p^{(-)}\bar{p}$ total, elastic, and single diffractive cross sections, including 13 TeV data from recent LHC experiments, we have determined best fits to the parameters governing these cross sections in the context of different unitarisation schemes. Specifically, we have shown that the U-matrix scheme fits the data as well as the more ubiquitous eikonal scheme. In fact, the fits have a slight preference for the U Matrix. This difference is driven by the single diffractive cross section, especially at high energies, while the best-fit total and elastic cross sections are nearly identical up to energies of 13 TeV when using either of these schemes.

A consequence of the indifference of the elastic cross section to the choice of the unitarisation scheme up to tens of TeV is that values of the ρ parameter remain largely unaffected by the choice of the scheme too. We use our best-fit parameters to compute this parameter across different energies, and find that the corresponding values conform to existing data,

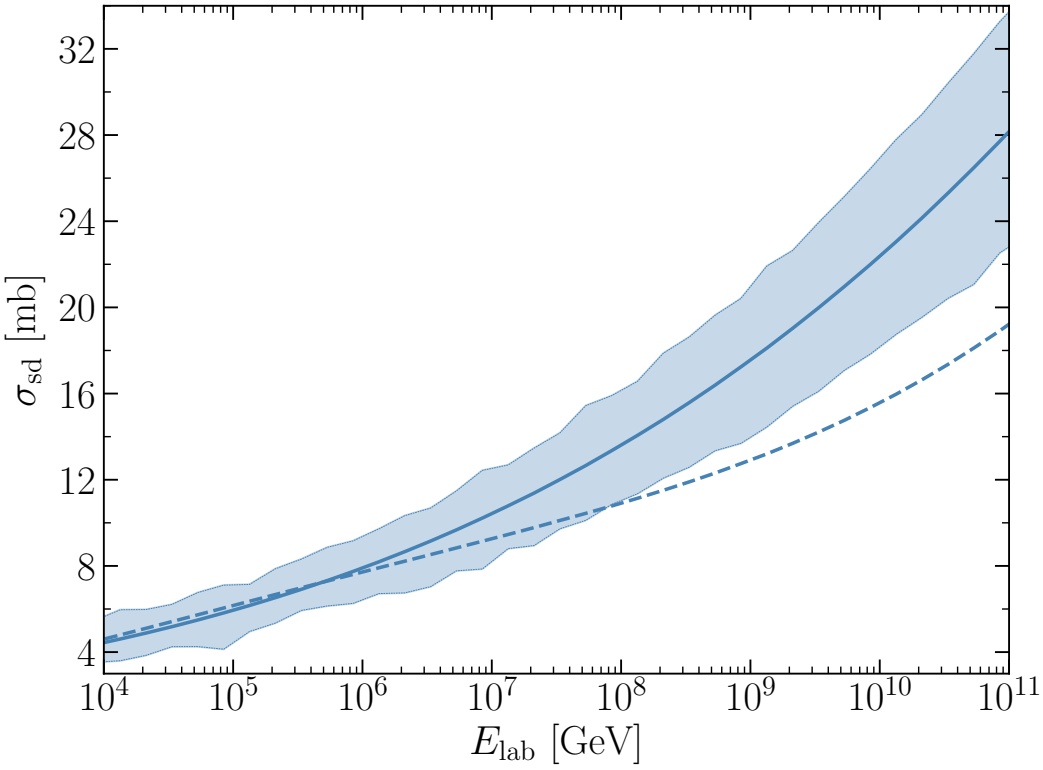

Figure 4.5: The growth of the single-diffractive cross section with *lab* energies up to $\sqrt{s} = 10^{11}$ GeV for both the U-matrix unitarisation scheme (solid curve) and the eikonal (dashed curve). We show a 1σ error band in the U-matrix case. The corresponding band is similar in the eikonal case, but we omit it for clarity.

to the exception of the TOTEM measurement at 13 TeV.

We have also analysed how the fits improve if one uses the generalised eikonal and U-matrix schemes and we find that these generalisations — at the cost of an additional free parameter (ω or ω') — do not improve the fits significantly.

The upshot of our analysis is that the overall best-fit cross section, in light of up-to-date collider data, is obtained using amplitudes unitarised via the U-matrix scheme. The resulting $p\overset{(-)}{p}$ single diffractive cross section shows a sharper growth at high energies than does the one obtained using the more commonly used eikonal scheme, and unitarisation could have an impact on the description of ultra-high-energy cosmic-ray showers.

Acknowledgments

AB is supported by the Fonds de la Recherche Scientifique-FNRS, Belgium, under grant No. 4.4503.19. AB is thankful to the computational resource provided by Consortium des Équipements de Calcul Intensif

(CÉCI), funded by the Fonds de la Recherche Scientifique de Belgique (F.R.S.-FNRS) under Grant No. 2.5020.11 where a part of the computational work was carried out. AV is supported by U.S. DOE Early Career Research Program under FWP100331.

5 Unitarity and Multi-Channel Diffraction

5.1 Context of the study

One of the striking results obtained from the previous study is related to the description of the total, elastic, and inelastic cross-sections, which were scheme-independent with the exception of the single-diffractive data that preferred the U-matrix scheme over the eikonal one, regardless of the data used.

Since hadron diffraction is closely tied to correlations arising from hadron fluctuations in various configurations, implementing a multi-channel model of high-energy hadronic interactions using the U-matrix scheme could enhance our understanding of these hadronic fluctuations. In light of this, we were spurred to undertake this study, in which we extend the two-channel model to a multi-channel one. It can be perceived as a continuation of the previous work, focusing on testing the hypothesis of considering an infinite parton configuration space and quantifying the uncertainties pertaining to the description of various hadronic observables, namely total, elastic, inelastic and single-diffractive cross-sections. In addition, it sought, based on our model, to predict the double diffractive cross-section, the ratio of the real part to the imaginary part of the elastic amplitude, i.e., the ρ parameter, and the elastic differential cross-section.

This study was conducted within the framework of the two-channel Good-Walker mechanism, which was extended to the multichannel case by considering the full range of parton configurations and mapping these configurations onto positive real numbers to facilitate the replacement of discrete sums with integrals, addressing the continuous nature of the problem.

5.2 ARTICLE 3

A Multi-Channel U-Matrix Model Of Hadron Interaction At High Energy

Rami Oueslati

Journal of High Energy Physics, 2023(08), 087
arXiv:2305.03424 [hep-ph]
doi: 10.1007/JHEP08(2023)087

Abstract: The present phenomenological study investigates a multi-channel model of high-energy hadron interactions by considering a full parton configurations space and the U-matrix unitarisation scheme of the elastic amplitude, comparing it to the two-channel model, and examining the consequences of up-to-date high-energy collider data on the best fits to various hadronic observables in pp and $p\bar{p}$ collisions. The findings of this study reveal that the data are well-fitted with the multi-channel model and that the difference compared to the two-channel one is negligible. Of particular significance is the observation that the U-matrix unitarisation is likely incompatible with uncorrelated pomeron exchange, as suggested by the equivalence between the U-matrix multi-channel and eikonal two-channel descriptions. Based on our best fit, predictions for the ρ parameter, the double diffractive cross-section, and the elastic differential cross-section are provided. We shed light on the effect of taking into account a multi-channel model on present and future cosmic ray data.

5.2.1 Introduction

When ultra-high energy cosmic ray particles first hit the Earth's atmosphere, several additional interactions take place. These interactions lead to particle multiplication and decay processes, which collectively result in a cascade of secondary particles known as an extensive air shower (EAS). In fact, observing these air showers is the only means of detecting high-energy cosmic ray particles. The development of air showers is dependent on hadronic cross sections and particle production characteristics in hadronic interactions.

However, it is worth noting that there is still much to be discovered about the evolution of the total and elastic cross sections in hadron-hadron collisions as functions of the center of mass energy as well as the characteristics of multiparticle production in these interactions. It is an interesting line of research given its phenomenological implications.

Indeed, estimating the features of hadronic interactions at LHC energies is crucial not only for modelling the background while looking for potential manifestations of new physics but also for the interpretation of the existing (and future) cosmic ray data, which relies on theoretical assumptions that describe these interactions.

As a matter of fact, despite being a well-known and experimentally supported theory of strong interactions, Quantum chromodynamics (QCD) can only currently predict processes involving large momentum transfer. Furthermore, the bulk properties of multiparticle production, which are required for air shower simulation, are still not calculable. Therefore, in order to create models for hadronic interactions that describe various particle generation processes, it is necessary to make further simplifying hypotheses in conjunction with phenomenological models that essentially consist of perturbative QCD (pQCD) predictions and phenomenological fits to experimental hadron spectra, which in turn are based on fundamental principles of quantum field theory – such as unitarity, analyticity and crossing, along with empirical parametrizations [68]. Certainly, it is crucial to validate these assumptions, constrain the parametrizations, and fine-tune the parameters using accelerator data comparisons.

For instance, in a prior study [135], the hypothesis of using two different unitarization schemes; the commonly employed eikonal as well as the U-Matrix, as unitarity constraint of the elastic amplitude was examined by looking into the effect of including recent collider data for total, elastic, inelastic and single diffractive cross sections in the framework of the two-channel model. The results showed nearly identical cross-sections, regardless of the unitarisation scheme adopted. Most importantly, it has been found that the single diffractive data are slightly better described with the U-matrix than with the eikonal one, in spite of the data used. Another hypothesis with regard to considering an infinite parton configurations space has been examined using the eikonal scheme [50]. We intend to investigate this hypothesis, but rather utilizing the U-matrix scheme.

It should be noted that the U-matrix scheme is not used as an alternative to phenomenologically studying hadronic interactions at high energy,

but rather for physical reasons. To start with, the choice of the U-matrix scheme is motivated by the aforementioned result [135]. Secondly, owing to the fact that correlations may emerge from the fluctuations of the hadrons in various configurations, which is a phenomenon closely connected to hadron diffraction [128], we then may infer that these hadron fluctuations might be increased through implementing a multi-channel model of high energy hadronic interactions using the U matrix scheme. We expect that it will produce a better description of the hadronic observables, compared with the eikonal scheme, within the multi-channel model. We also anticipate that it will provide better results within the multi-channel model than within the two-channel one.

This study has the following objectives. First of all, it will focus on testing the hypothesis of considering an infinite parton configuration space and compare it to the two-channel counterpart. Based on our model, it also seeks to predict the double diffractive cross-section, the ratio of the real part to the imaginary part of the elastic amplitude, i.e., the ρ parameter, and the elastic differential cross-section. Finally, the impact of considering a multi-channel model on present and future cosmic ray data will be discussed.

The present paper is organised as follows. In section 5.2.2 we will focus on the theoretical framework of the diffractive excitation in the context of the multi-channel Good-Walker approach. In section 5.2.3, an explicit model for the description of the elastic scattering amplitude as well as the treatment of the average number of interactions will be proposed. Moreover, the principal parameters of the model and data used will be highlighted. In section 6.2.4, the results of the study will be presented and discussed. In section 6.2.5, the conclusions will be given.

5.2.2 Diffraction and multi-channel Good-Walker approach

5.2.2.1 Theoretical framework

Hadrons are composite particles comprised of quarks and gluons which interact in a variety of ways during hadron collisions. It is possible to relate these interactions to the total and elastic cross sections using a suitable theoretical framework. But the specific way to achieve it is still an open question. In fact, "Mini-jet" models [67] are thought to be a viable option, with total and elastic cross sections calculated using an eikonal formalism in terms of the quantity $\langle n(b,s)\rangle$, representing the average number of ele-

mentary interactions at impact parameter b and c.m. energy $\sqrt{s}$.

It should be emphasized that predictions made using the simple eikonal scheme in these Mini-jet models are insufficient. The fact that this kind of elastic amplitude unitarization scheme is inappropriate for a collision of composite objects like hadrons is already supported by the findings of a number of studies [108, 130, 133] as well as certain (indirect) evidence. In fact, the eikonal unitarization scheme is a well-known technique for calculating the amplitude X, which meets some minimal s-channel unitarity constraints from the "non-unitary" amplitude χ, as

$$X = i(1 - \exp(i\chi)) \tag{5.1}$$

It is based on the assumption that the impact parameter (the perpendicular distance between the trajectories of colliding particles) is much larger than the characteristic size of the interacting particles. Regarding the statistical nature of this scheme, in collisions at a fixed impact parameter and c.m. energy, the fluctuations in the number of interactions are just Poissonian in nature [47]. The statistically independent and identically distributed interactions is equivalent that each exchange process is statistically equivalent and contributes equally to the overall scattering amplitude. This is equivalent to a sum of contributions derived from the multiple exchanges, emerging with even weights, which is described by the primary amplitude χ. While the assumption of equal weights is a useful simplification, it may not always accurately reflect the underlying physics. In reality, the individual exchange processes may have different strengths or probabilities, which could affect the overall scattering amplitude. Accounting for such differences would require a more detailed and sophisticated treatment beyond the eikonal approximation. Mathematically, the eikonal approximation allows us to factorize the overall scattering S-matrix associated with the interaction into a product of individual scattering matrices. This approach is sometimes connected with the image of a rapid particle travelling virtually straight ahead in target media, [81].

Furthermore, the eikonal approximation treats the hadrons as classical objects with fixed parton distributions. It assumes that during the interaction, the parton configurations remain frozen or unchanged. This approximation is valid when the timescale for the parton dynamics, such as radiation and absorption, is much longer than the timescale of the interaction itself [105]. The freezing of parton configurations in the eikonal approximation simplifies the calculations by considering the partons as

fixed distributions and focusing on the overall scattering process rather than the detailed internal dynamics. However, it is important to note that the freezing of parton configurations is an approximation and may not capture all aspects of the parton dynamics accurately. In reality, partons can undergo radiation and absorption processes, leading to changes in their energy and momentum distributions. Due to these limitations in the eikonal approximation, all such multiple exchanges may not occur simultaneously and may be dependent on each other. This challenges the assumption of equal weights and Poissonian behavior in the summation of exchanges. Furthermore, the need for multiple exchanges arises to account for phenomena such as screening effects and additional inelastic processes. The prevalence of the eikonal scheme in Monte Carlo event generators, such as SIBYLL [118] and QGSJET [114], prompts a reevaluation of its suitability for unitarizing the elastic amplitude in hadronic collisions. Continual assessment and refinement of theoretical frameworks and models are necessary to better capture the complexities of high-energy interactions.

The fluctuating structure of hadrons, which are composite particles made up of quarks and gluons bound together by the strong force, is thought to contribute to the process of diffractive excitation. The internal structure of hadrons is highly complex and dynamic, with quarks and gluons constantly interacting and creating temporary resonances within the hadron. During a high-energy collision between two hadrons, these resonances can be excited by the exchange of a pomeron, leading to diffractive excitation. The exact mechanism of this process is still an area of active research in particle physics. According to Good and Walker (GW) [82], inelastic diffraction occurs because an interacting hadron can be perceived as a superposition of several states that experience uneven absorptions. GW further depicted the diffractive excitation as the eigenstates of the scattering operator, which are utilized to describe the physical states.

In the same vein, Miettinen and Pumplin [109] postulated that these "transmission eigenstates" can be recognized as distinct "configurations" of the parton elements contained within a hadron. It is necessary to have a general grasp of the entirety of these parton configurations in order to estimate inelastic diffraction within this theoretical framework, which seems to be a challenging task. One possible method of doing so consists in lessening the space of parton configurations to a finite dimensional space and explicitly creating a matrix transition operator. As an illustration of this approach [135], we have taken into account the minimal scheme

initially proposed by Gotsman, Levin, and Maor (GLM) [84] and combined the proton with one diffractive state. This is equivalent to a two-channel unitarisation scheme. Another illustration can be found in [84], where GLM examined the case $N = 3$ in the eikonal scheme but discovered no appreciable improvement.

Therefore, in order to highlight the difference in the description of the hadronic observables between the models, the entirety of parton configurations as well as the scheme adopted should be taken into account. Practically speaking, an N channel scheme could be considered, but this would increase the number of parameters, which will affect the attainment of a reliable and realistic model in comparison with the physics that we aspire to describe.

An alternative approach assumed here is to map the space of the parton configurations into the real positive numbers. Various research papers in the field have already explored this approach [32, 76, 75, 77, 78, 90, 44, 50] but all of them with the eikonal scheme. However, since no single published study, to our knowledge, has estimated the inelastic diffraction within the GW approach by considering the entirety of parton configurations together with the U-matrix scheme, this study attempts to fill this gap, at least partially. The total cross-section and its various constituents (elastic, absorption, and diffraction) can be calculated as will be shown in the following section.

5.2.2.2 Formalism

We adopt the multichannel formalism presented in [50, 90], with a small modification to account for a full complex scattering amplitude. The starting point is the impact parameter space representation, where the hadronic observables, the total, elastic, single, and double diffractive scattering cross sections may be readily expressed as :

$$\sigma_{tot}(s) = 2\int \mathrm{d}^2b\ \mathfrak{Im}\left\{X_{el}(s,b)\right\}\ ; \qquad \sigma_{el}(s) = \int \mathrm{d}^2b\ \left|X_{el}(s,b)\right|^2 ; \tag{5.2a}$$

$$\sigma_{sd}(s) = 2\int \mathrm{d}^2b\ \left|X_{sd}(s,b)\right|^2 ; \qquad \sigma_{dd}(s) = \int \mathrm{d}^2b\ \left|X_{dd}(s,b)\right|^2 \tag{5.2b}$$

When a projectile P collides with a target T, represented by the physical states $|P\rangle$ and $|T\rangle$ respectively, we assume that both states can be diffracted onto various particle states $\{|A\rangle\}$ and $\{|B\rangle\}$ due to their sub-

structure. The GW approach states that the initial state can be expressed as a sum over the eigenstates $\{|\Psi_i\rangle\}$ of the scattering operator $\hat{T}$, forming a complete set of normalized states. This gives us the initial state $|I\rangle$ as:

$$|I\rangle = |P,T\rangle = \sum_{ij} C_i^P C_j^T |\psi_i \psi_j\rangle \tag{5.3}$$

where $\hat{T}|\psi_i\psi_j\rangle = t_{ij}|\psi_i\psi_j\rangle$, with the eigenvalues $t_{ij} = t_{ij}(b,s)$ depending implicitly on the projectile and target's specific configurations. The final state system can be described by

$$|F\rangle = \hat{T}|I\rangle = \sum_{i,j} C_i^P C_j^T t_{ij} |\psi_i \psi_j\rangle \tag{5.4}$$

leading to

$$\langle F|F\rangle = \sum_{i,j} |C_i^P|^2 |C_j^T|^2 |t_{ij}|^2 = \sum_{i,j} P_i^P P_j^T |t_{ij}|^2 = \langle |t|^2 \rangle_{P,T} \tag{5.5}$$

where we have identified $P_i^P = |C_i^P|^2$ and $P_j^T = |C_j^T|^2$ as configuration's probability distributions for projectile and target respectively, and $\langle ... \rangle_{P,T}$ refers to the mean value calculated across the different configurations present in both the projectile and the target.

The final state system can be expressed as a sum over the possible final states $\{|A,B\rangle\}$, which form a complete set of eigenstates, as:

$$|F\rangle = \sum_{A,B} |A,B\rangle = |P,T\rangle + \sum_{A\neq P} |A,T\rangle + \sum_{B\neq T} |P,B\rangle + \sum_{A\neq P, B\neq T} |A,B\rangle \tag{5.6}$$

As a result, we can deduce that:

$$\begin{aligned} \langle F|F\rangle &= \sum_{A,B} \langle F|A,B\rangle\langle A,B|F\rangle \\ &= |\langle P,T|F\rangle|^2 + \sum_{A\neq P} |\langle A,T|F\rangle|^2 + \sum_{B\neq T} |\langle P,B|F\rangle|^2 + \sum_{A\neq P;B\neq T} |\langle A,B|F\rangle|^2 \end{aligned} \tag{5.7}$$

Furthermore, by using the fact that

$$X_{el}(s,b) \equiv \langle P,T|F\rangle = \sum_{i,j} |C_i^P|^2 |C_j^T|^2 t_{ij} \equiv \langle t\rangle_{P,T} \ , \quad (5.8)$$

$$X_{sd}^P(s,b) \equiv \langle A,T|F\rangle|_{A\neq P} = \sum_{i,j} C_i^{*,A} C_i^P |C_j^T|^2 t_{ij} \ , \quad (5.9)$$

$$X_{sd}^T(s,b) \equiv \langle P,B|F\rangle|_{B\neq T} = \sum_{i,j} |C_i^P|^2 C_j^{*,B} C_j^T t_{ij} \ , \quad (5.10)$$

$$X_{dd}(s,b) \equiv \langle A,B|F\rangle|_{A\neq P;B\neq T} = \sum_{i,j} C_i^{*,A} C_i^P C_j^{*,B} C_j^T t_{ij}^* t_{ij} \ , \quad (5.11)$$

we can write by making use of the completeness of the states $\{|A\rangle\}(\sum_A C_i^{*,A} C_{i'}^A = \delta_{ii'})$:

$$\begin{aligned} |\langle P,T|F\rangle|^2 + \sum_{A\neq P} |\langle A,T|F\rangle|^2 &= \sum_A |\langle A,T|F\rangle|^2 = \sum_A \left| \sum_i C_i^{*,A} C_i^P \sum_j |C_j^T|^2 t_{ij} \right|^2 \\ &= \sum_A \left| \sum_i C_i^{*,A} C_i^P \langle t(j)\rangle_T \right|^2 = \sum_i C_i^{*,P} C_i^P |\langle t(j)\rangle_T|^2 \\ &= \langle |\langle t\rangle_T|^2 \rangle_P \end{aligned} \quad (5.12)$$

In a similar fashion, we can obtain the following result:

$$\begin{aligned} |\langle P,T|F\rangle|^2 + \sum_{B\neq T} |\langle P,B|F\rangle|^2 &= \sum_B |\langle P,B|F\rangle|^2 = \sum_B \left| \sum_j C_j^{*,B} C_j^T \sum_i |C_i^P|^2 t_{ij} \right|^2 \\ &= \sum_B \left| \sum_j C_j^{*,B} C_j^T \langle t(i)\rangle_P \right|^2 = \sum_j C_j^{*,T} C_j^T |\langle t(i)\rangle_P|^2 \\ &= \langle |\langle t\rangle_P|^2 \rangle_T \ , \end{aligned} \quad (5.13)$$

and

$$\begin{aligned} \sum_{A\neq P;B\neq T} |\langle A,B|F\rangle|^2 &= \langle F|F\rangle - |\langle P,T|F\rangle|^2 - \sum_{A\neq P} |\langle A,T|F\rangle|^2 - \sum_{B\neq T} |\langle P,B|F\rangle|^2 \\ &= \langle |t|^2\rangle_{P,T} - \langle |\langle t\rangle_T|^2\rangle_P - \langle |\langle t\rangle_P|^2\rangle_T + |\langle t\rangle_{P,T}|^2 \end{aligned} \quad (5.14)$$

Thus, based on the aforementioned relations, we can deduce the related cross-sections in the impact parameter space in the following manner:

- The elastic cross-section:

$$\frac{d^2\sigma_{el}}{d^2b} = |\langle P,T|F\rangle|^2 = |\langle t\rangle_{P,T}|^2 \ ; \tag{5.15}$$

- The projectile single diffractive cross-section :

$$\frac{d^2\sigma^P_{sd}}{d^2b} = \sum_{A\neq P} |\langle A,T|F\rangle|^2 = \langle|\langle t\rangle_T|^2\rangle_P - |\langle t\rangle_{P,T}|^2 \ ; \tag{5.16}$$

- The target single diffractive cross-section :

$$\frac{d^2\sigma^T_{sd}}{d^2b} = \sum_{B\neq T} |\langle P,B|F\rangle|^2 = \langle|\langle t\rangle_P|^2\rangle_T - |\langle t\rangle_{P,T}|^2 \ ; \tag{5.17}$$

- The double diffractive cross-section:

$$\begin{aligned}\frac{d^2\sigma_{dd}}{d^2b} &= \sum_{A\neq P;B\neq T} |\langle A,B|F\rangle|^2 \\ &= \langle|t|^2\rangle_{P,T} - \langle|\langle t\rangle_T|^2\rangle_P - \langle|\langle t\rangle_P|^2\rangle_T + |\langle t\rangle_{P,T}|^2 \ .\end{aligned} \tag{5.18}$$

- Moreover, the total single diffractive cross-section is expressed as :

$$\frac{d^2\sigma_{sd}}{d^2b} = \frac{d^2\sigma^P_{sd}}{d^2b} + \frac{d^2\sigma^T_{sd}}{d^2b} = \langle|\langle t\rangle_T|^2\rangle_P + \langle|\langle t\rangle_P|^2\rangle_T - 2|\langle t\rangle_{P,T}|^2 \ , \tag{5.19}$$

  and the total diffractive cross-section as :

$$\frac{d^2\sigma_{diff}}{d^2b} = \frac{d^2\sigma_{sd}}{d^2b} + \frac{d^2\sigma_{dd}}{d^2b} = \langle|t|^2\rangle_{P,T} - |\langle t\rangle_{P,T}|^2 \ . \tag{5.20}$$

- Finally, using the optical theorem, the total cross-section is given by

$$\frac{d^2\sigma_{tot}}{d^2b} = 2\,\mathfrak{Im}\left\{\langle t\rangle_{P,T}\right\} \ . \tag{5.21}$$

To compute the required average over the configurations in both the projectile and the target, necessary for obtaining these cross-sections and encompassing the entire space of parton configurations, we perform a mapping of this space onto the domain of real positive numbers. This mapping is established under the assumption that the distinct configurations $\mathbb{C}_i$ can be effectively represented by a continuous distribution, where each configuration is assigned a corresponding probability $P_{hi}(\mathbb{C}_i)$.

Accordingly, we can substitute a discrete summation with a continuous one, and this leads to the following correspondences :

$$\sum_i |C_i^P|^2 \to \int d\mathbb{C}_1 P_{h1}(\mathbb{C}_1) \text{ for the projectile,} \tag{5.22}$$

$$\sum_i |C_i^T|^2 \to \int d\mathbb{C}_2 P_{h2}(\mathbb{C}_2) \text{ for the target} \tag{5.23}$$

and

$$t_{ij}(b,s) \to t(b,s,\mathbb{C}_1,\mathbb{C}_2) \ , \tag{5.24}$$

where the different configurations are clearly displayed.

In order to reveal the role of taking into account a full parton configuration space based on this formalism, we need a model for the elastic scattering amplitude $t(b,s,\mathbb{C}_1,\mathbb{C}_2)$, and the probability distribution $P_{hi}(\mathbb{C}_i)$, which will explicitly be presented in the following section.

5.2.3 Explicit model and data

The elastic hadron scattering amplitude $t(b,s,\mathbb{C}_1,\mathbb{C}_2)$ is a complex function that describes the probability of two hadrons scattering off each other at a given energy and impact parameter. At high energies, this amplitude can become very large, which violates the unitarity condition that the probability of any physical process cannot exceed unity. To restore unitarity, we can use a process called unitarization. This involves modifying the amplitude in a way that satisfies unitarity while preserving its physical properties. As has been stated in the introduction, we will consider that $t(b,s,\mathbb{C}_1,\mathbb{C}_2)$ is given by the U-Matrix form [**?**], as the sum of all n-pomeron exchange contributions from the single-pomeron scattering amplitude which in turn is related to the expected number $\chi(b,s,\mathbb{C}_1,\mathbb{C}_2)$ of interactions between partons of the incident hadrons for a given combination of configurations $\mathbb{C}_1$ and $\mathbb{C}_2$:

$$t(b,s,\mathbb{C}_1,\mathbb{C}_2) = \frac{\chi(b,s,\mathbb{C}_1,\mathbb{C}_2)}{1 - \mathrm{i}\,\chi(b,s,\mathbb{C}_1,\mathbb{C}_2)/2} \tag{5.25}$$

In order to simplify the calculation of the elastic scattering amplitude, we suppose that the expected number of interactions between partons can be expressed as a product of the single-Pomeron scattering amplitude and some functions of impact parameter and configurations.

$$\chi(b, s, \mathbb{C}_1, \mathbb{C}_2) = f(b, \mathbb{C}_1, \mathbb{C}_2) \cdot \chi_P(s, b) \tag{5.26}$$

This factorization is based on the idea that the configurations dependence of $\chi(b, s, \mathbb{C}_1, \mathbb{C}_2)$ can be separated from the energy dependence, which is described by the single-Pomeron scattering amplitude. This assumption is based on the fact that the energy dependence of the elastic scattering amplitude is dominated by the exchange of a single Regge pole, the pomeron, which is independent of the specific hadronic configurations involved in the scattering process

In addition, if we assume that the distribution of parton configurations is independent of the impact parameter, which means that the parton density inside the hadron is the same at all points in space and that the hadron can be treated as a collection of independent partons, then we can write

$$\chi(b, s, \mathbb{C}_1, \mathbb{C}_2) = \chi_P(s, b) \cdot \alpha(\mathbb{C}_1)\alpha(\mathbb{C}_2) \tag{5.27}$$

where the functions $\alpha(\mathbb{C}_i)$ depend on the configurations of the incident hadrons. Therefore, we have

$$\int d\mathbb{C}_1 \int d\mathbb{C}_2 P_{h1}(\mathbb{C}_1) P_{h2}(\mathbb{C}_2) t(b, s, \mathbb{C}_1, \mathbb{C}_2) = \int_0^\infty d\alpha_1 \int_0^\infty d\alpha_2 p(\alpha_1) p(\alpha_2) t(b, s, \alpha_1, \alpha_2) \tag{5.28}$$

where the functions $p(\alpha_i)$ are defined by

$$p(\alpha_i) = \int d\mathbb{C}_i P_{hi}(\mathbb{C}_i) \delta[\alpha(\mathbb{C}_i) - \alpha_i], \tag{5.29}$$

which satisfy the following constraints:

$$\int_0^\infty d\alpha_i \, p(\alpha_i) = 1, \tag{5.30}$$

and

$$\int_0^\infty d\alpha_i \, \alpha_i \, p(\alpha_i) = 1 \quad (i = 1, 2) \, . \tag{5.31}$$

Accordingly, we can implicitly take into account of an infinite number of inelastic channels by using the function of a real positive variable, the probability distribution $p(\alpha)$ representing the fluctuations of the hadron configurations with some extension defined by its variance. This generalizes the GW approach to a multichannel framework, as demonstrated in [105], where the connection between the discrete and continuous multichannel GW was established.

Thus, The averaging over the configurations appearing in Eqs. (5.15) – (5.21) will be determined as follows:

- Mean value computed over the configurations of the projectile:

$$\langle t^n \rangle_P = \int_0^\infty d\alpha_1 \, p(\alpha_1) \, t^n(b, s, \alpha_1, \alpha_2); \tag{5.32}$$

- Mean value computed over the configurations of the target :

$$\langle t^n \rangle_T = \int_0^\infty d\alpha_2 \, p(\alpha_2) \, t^n(b, s, \alpha_1, \alpha_2); \tag{5.33}$$

- Mean value computed over the configurations of the projectile and the target :

$$\langle t^n \rangle_{PT} = \int_0^\infty d\alpha_1 \int_0^\infty d\alpha_2 \, p(\alpha_1) \, p(\alpha_2) \, t^n(b, s, \alpha_1, \alpha_2) \tag{5.34}$$

An advantage to the method disclosed here is that it considers the entirety of the parton configuration space. Nevertheless, it should be noted that the probability distribution $p(\alpha_i)$, remains unknown. We do anticipate, however, that this distribution will exhibit the following characteristics: it needs to be defined for positive values of its variable α and have the predicted limit, $p(\alpha) \to \delta(\alpha - 1)$, when its variance reaches zero, which is equivalent to no fluctuations and satisfies the above constraints 5.30 and 5.31. In order to satisfy these properties, we use for the probability distribution $p(\alpha_i)$, the gamma distribution, with variance w,

$$p(\alpha_i) = \frac{1}{w\Gamma(1/w)} \left(\frac{\alpha_i}{w}\right)^{-1+1/w} e^{-\alpha_i/w} \tag{5.35}$$

Since we are accounting for the collision of identical hadrons, we will suppose that the variance w of the distribution is independent of i. This assumption enables us to compute the average over configurations Eqs. (5.32), (5.33) and (5.34) needed to determine the various observables Eqs. (5.15)- (5.21).

To complete the description of our model, we parameterize the single-pomeron scattering amplitude, as the *Ansatz* put forth in [135] for comparison purposes :

$$a_P(s,t) = g_{pp}^2 \, F_{pp}(t)^2 \left(\frac{s}{s_0}\right)^{\alpha(t)} \xi(t), \tag{5.36}$$

where $\alpha(t)$ is the pomeron trajectory, $F_{pp}(t)$ is the proton elastic form factor, and g_{pp} is the coupling pomeron-proton-proton, with $\xi(t)$ the signature factor

$$\xi(t) = -e^{\frac{-i\pi\alpha(t)}{2}}, \tag{5.37}$$

where a full complex rather than a purely imaginary one was chosen in order to meet the elastic amplitude's analyticity constraint, which is essential to respecting causality. Regarding the proton elastic form factor, although the exact functional form is not very important as we want to make a comparison with the two-channel model, we shall consider here a dipole form factor :

$$F_{pp} = \frac{1}{(1 - t/t_{pp})^2} \tag{5.38}$$

Using an exponential form factor $\{F_1 = \exp(R_0 t)\}$, instead of the dipole form, leads to slightly poorer fits [43]. The pomeron trajectory is close to a straight line [60] and we take it to be

$$\alpha(t) = 1 + \epsilon + \alpha' t. \tag{5.39}$$

In the impact-parameter space representation, where the Fourier transform of the amplitude $a_P(s,t)$ rescaled by $2s$ is equivalent to a partial wave, we have :

$$\chi_P(s, \boldsymbol{b}) = \int \frac{\mathrm{d}^2\boldsymbol{q}}{(2\pi)^2} \frac{a_P(s,t)}{2s} \mathrm{e}^{\mathrm{i}\boldsymbol{q}\cdot\boldsymbol{b}}. \tag{5.40}$$

and by the unitarisation procedure we map the amplitude $\chi_P(s,b)$ to the physical amplitude $t(s,b)$, which in turn bears the same relation as Eq. (6.15), but this time to the physical amplitude :

$$t(s, \boldsymbol{b}) = \int \frac{\mathrm{d}^2\boldsymbol{q}}{(2\pi)^2} \frac{A(s,t)}{2s} \mathrm{e}^{\mathrm{i}\boldsymbol{q}\cdot\boldsymbol{b}}. \tag{5.41}$$

Thus, using the assumptions made in this model, we can make specific predictions and conclusions about the hadronic collisions at high energy and, at the same time, test the hypotheses that were adopted.

Before presenting our results in the subsequent section, we list here the model parameters that will be set by the data fit as well as the experimental data employed. The model parameters are the following: ϵ and α', which are associated with the Pomeron trajectory, as well as g_{pp} and t_{pp} linked

to the proton-pomeron $p\mathbb{P}p$ vertex, and the variance ω of the probability distribution. We employ experimental data above 100 GeV as we are concerned with high energy effects induced in $p\overset{(-)}{p}$ cross sections. And as we aim at looking into the impact of putting in place a multi-channel model in order to describe hadronic interactions and comparing it with the two-channel one, the same data set [1] as in [135], which involves statistical as well as systematic errors and combines them in quadrature, is used. The fitting process was conducted using the class Minuit2 from ROOT [91] and the MIGRAD algorithm. The fitting was performed by minimizing the χ^2 value, and the uncertainties in the free parameters were calculated with a 1σ confidence level, which was used to determine the error band.

5.2.4 Results and discussion

The results of our multi-channel model are provided in Fig. 4.4 and Table 5.1 using the formalism previously outlined. As can be seen from these findings, the multi-channel model describes well the total, elastic, inelastic, and single-diffractive cross-sections, with a χ^2 /d.o.f of 1.328. These outcomes are actually in line with those obtained using the U-matrix two-channel model with a χ^2 /d.o.f of 1.316 [135], which shows a difference of only 0.012 in the χ^2 /d.o.f.

The difference between the two χ^2 obtained in both models is marginal. As a matter of fact, it is somewhat surprising that there is no improvement with the multi-channel model given that the latter was expected to describe the diffractive phenomenon, in particular, better than the two-channel one. The reason for this similarity between the two models can be attributed to the unitarization process employed in both cases. Specifically, both models adhere to the same unitarity constraint, known as the U-matrix scheme. This can be observed in Fig. 5.5 (right panel), where the impact-parameter space representation showcases that the imaginary and real components of the elastic profile function at a specific energy, such as 13 TeV, are nearly identical in both models. Furthermore, it is evident that these components do not surpass the black disk limit, indicating consistency with the principles of unitarity. Most importantly, based on the similarity in the obtained $\chi^2/d.o.f.$ values between the U-matrix multi-channel model and the eikonal two-channel one [135], it seems likely that the factorization assumption adopted in the former case may not be

[1] see compilation in [135]

applicable. Specifically, if there is a correlation between the pomeron exchanges, then the impact parameter and configuration dependence of the scattering amplitude may not be separable from the energy dependence carried by the single-pomeron exchange. In this case, the distribution of parton configurations may depend on the impact parameter, and the average number of interactions at a fixed impact parameter and center of mass energy may not be separable from the configuration dependence of the incident hadrons.

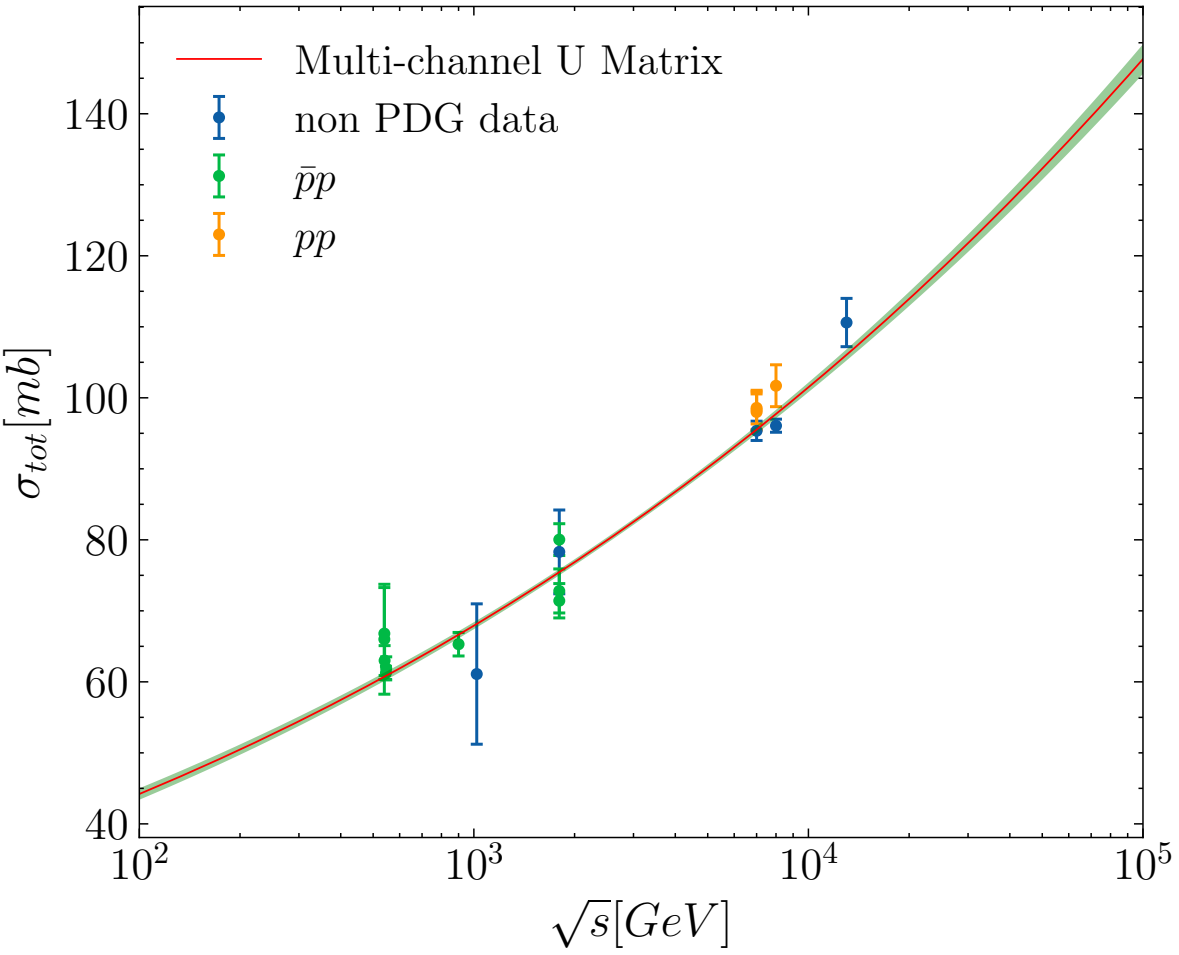

Figure 5.1: Total cross section with the Multi-channel model and the 1σ error bands around the fitted curve obtained with best-fit parameters.

Model	ϵ	α' (GeV^{-2})	g_{pp}	t_{pp} (GeV^2)	ω	χ^2/d.o.f
Multi-channel	0.11 ± 0.003	0.29 ± 0.04	8.25 ± 0.2	2.06 ± 0.75	0.59 ± 0.06	1.328

Table 5.1: χ^2/dof and best-fit parameters obtained with the U-matrix Multi-channel model.

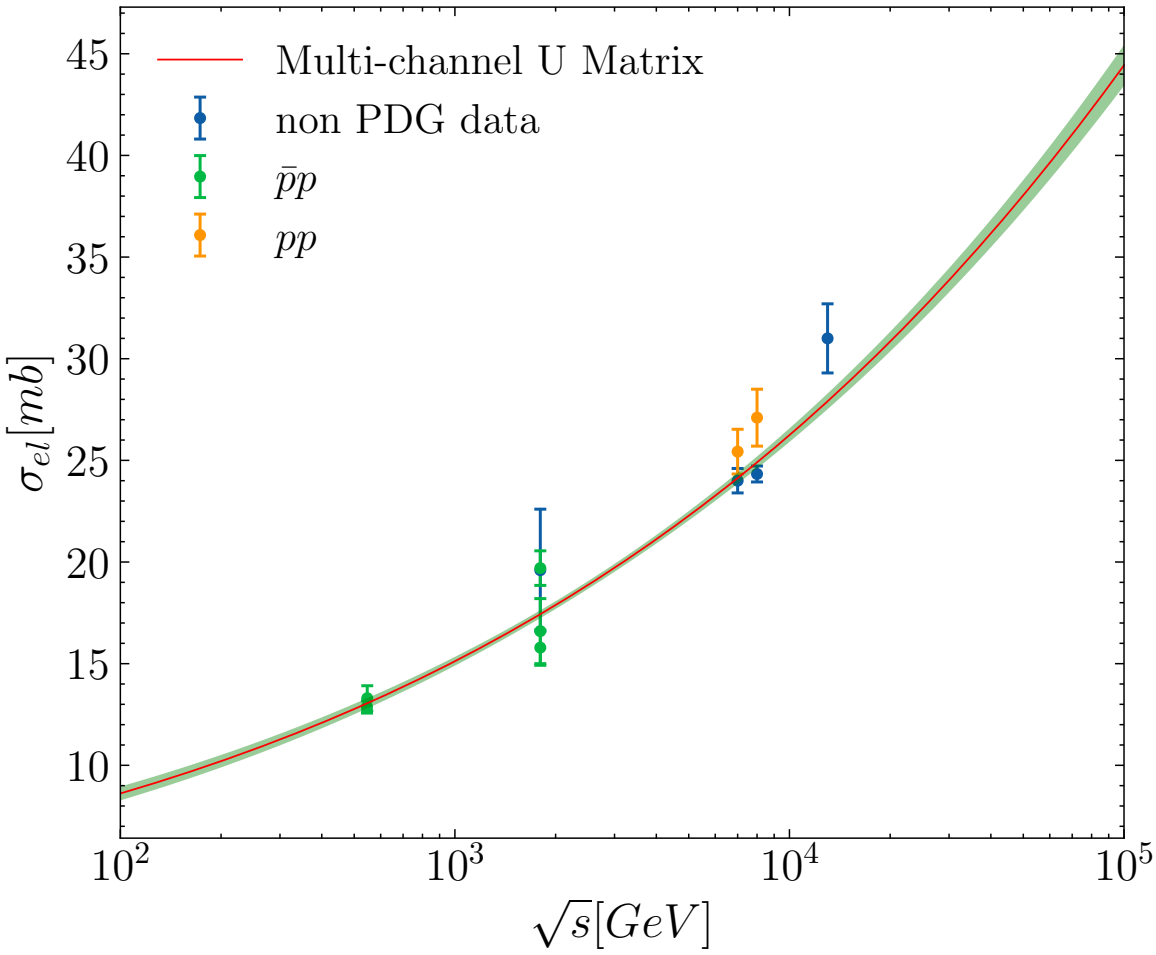

Figure 5.2: Elastic cross section with the Multi-channel model and the 1σ error bands around the fitted curve obtained with best-fit parameters.

Double diffractive cross-section measurements are not included in our fits and our prediction based on the model presented in this study doesn't reproduce these data in spite of considering an infinite parton configurations space, which corroborates the result reported in the context of a two-channel model [135], as illustrated in Fig. 5.5 (left panel). In fact, a proper description of this cross-section requires the introduction of an additional contribution due to the Pomeron-enhanced diagrams involving Pomeron-Pomeron interactions which is non GW. As the energy increases, more diagrams illustrating complicated topologies become involved. Consequently, the consistent treatment of these enhanced corrections proves to be a very challenging task [111].

Fig. **??** displays the predictions for the energy evolution of the cross sections in the impact parameter space from Tevatron to cosmic ray energies. The elastic, single-diffractive, and double-diffractive differential cross sections are shown in the top right, bottom left and right panels, respec-

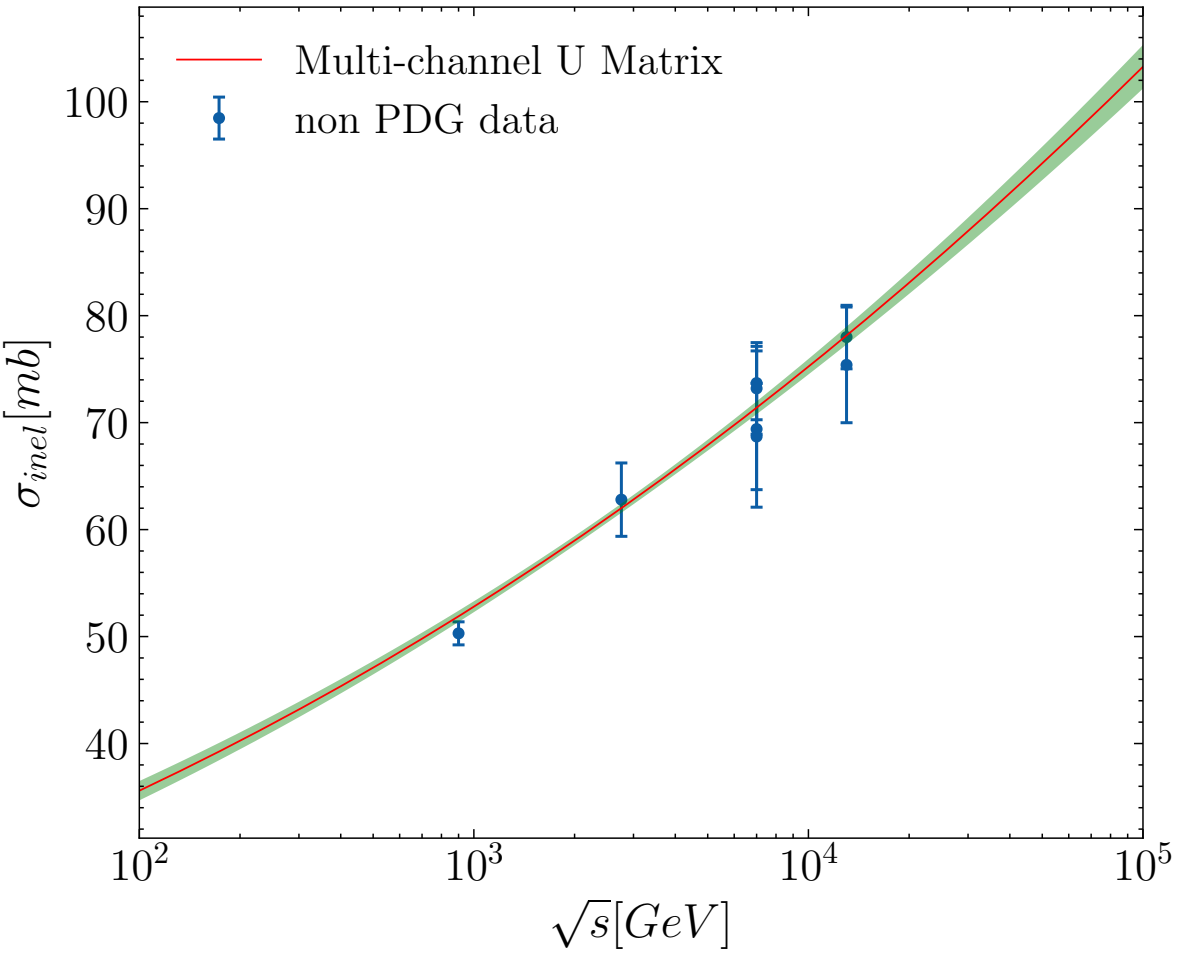

Figure 5.3: Inelastic cross-section with the Multi-channel model and the 1σ error bands around the fitted curve obtained with best-fit parameters.

tively. It can be seen that the elastic scattering is primarily central and increases with energy. This result is comparable to the one reported in [50]. In contrast, it gets much closer to the black disk limit at cosmic ray energies. The behaviour of the single diffractive differential cross-section is similar to that of the elastic scattering. At b = 0, it is mostly central and has a magnitude that grows with energy, but it is smaller than the one of the elastic scattering. It also declines more slowly than the elastic cross-section as b rises. Similar behaviours of the unintegrated profile for the single diffractive cross section at low mass are predicted by the Kolevatov and Boreskov model presented in [101]. This result contrasts with the one presented in [50], where the total single diffractive cross section becomes more peripheral, with a maximum moving to a higher impact parameter as the energy rises. Furthermore, as the c.m. energy increases, the magnitude of the SD cross-section at b = 0 decreases. This rather contradictory result might be attributed to the use of two different unitarization schemes.

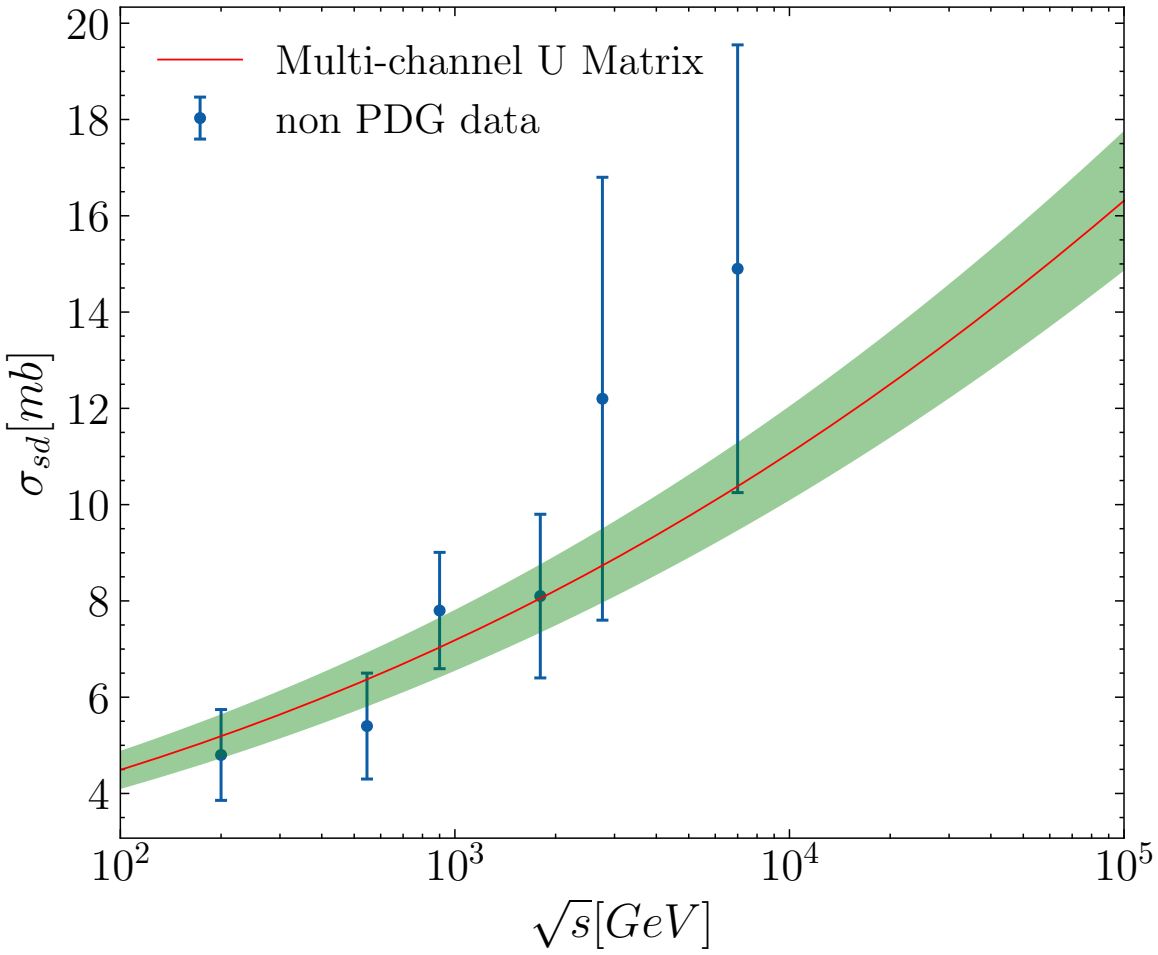

Figure 5.4: Single diffractive cross section with the Multi-channel model and the 1σ error bands around the fitted curve obtained with best-fit parameters.

The double diffractive cross-section becomes more peripheral when energy rises. Nevertheless, its magnitude at b = 0 diminishes as c.m. energy increases. This result is in line with that obtained in [50]. A note of caution with regard to the shape of the unintegrated profile for the double diffractive cross section is due here since it is not well described.

The ρ parameter, i.e., the ratio of the real part of the elastic scattering amplitude to its imaginary part has been studied in several experiments at different centre-of-mass energies. In spite of the fact that ρ data are not used in our fits, we can estimate its values at various $\sqrt{s}$ by using our best-fit parameters and then compare these predictions with the experimental data. Fig. 5.9 (left panel) illustrates our predicted values for this observable. As can be seen from this figure, while our model furnishes a reasonable description for this parameter at various high energies, it is unable to estimate the TOTEM data at 13 TeV since the 1σ error band of the model doesn't even reach the error bars of these data.

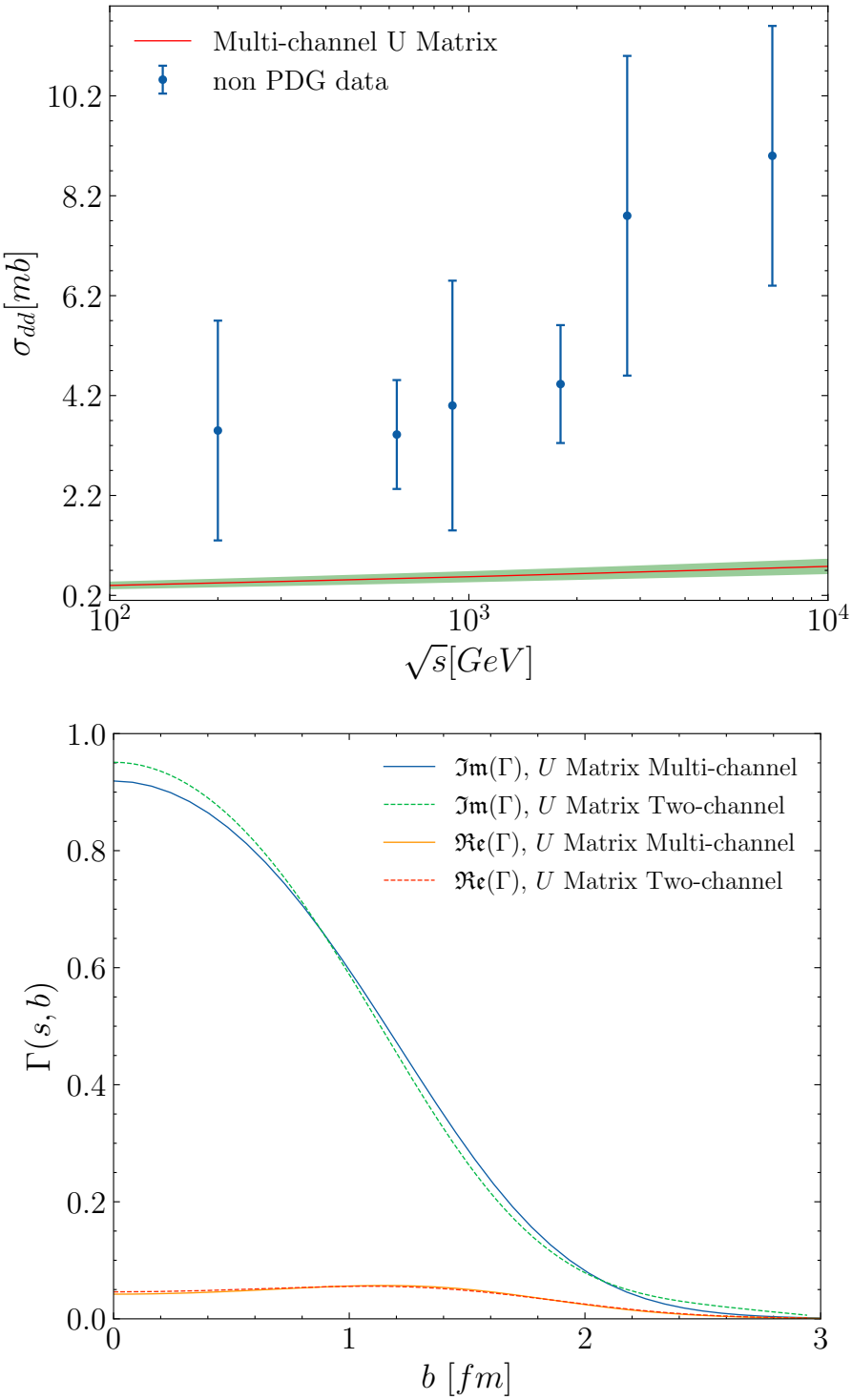

Figure 5.5: The double diffractive cross section with 1σ error bands around the predicted curve obtained with the Multi-channel model (left panel). The real and imaginary parts of the elastic profile function $\Gamma(s,b)$ at $\sqrt{s} = 13$ TeV with the U Matrix scheme for the two and multi-channel cases (right panel).

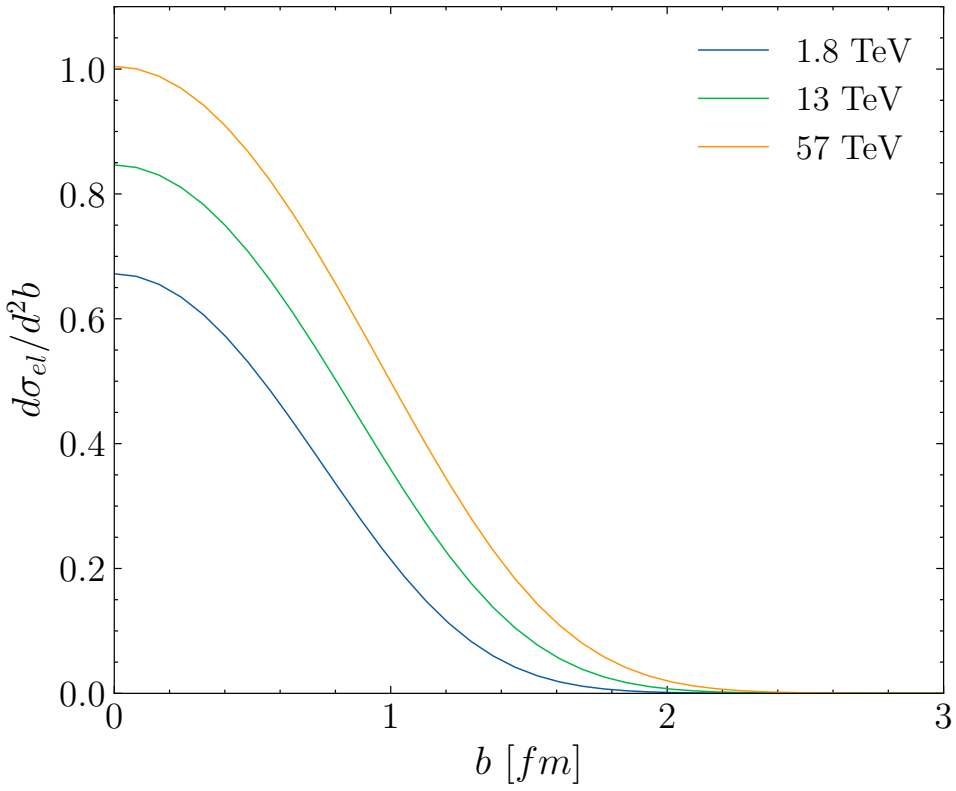

Figure 5.6: Multi-channel model prediction for the energy dependence of the elastic differential cross section in impact parameter space.

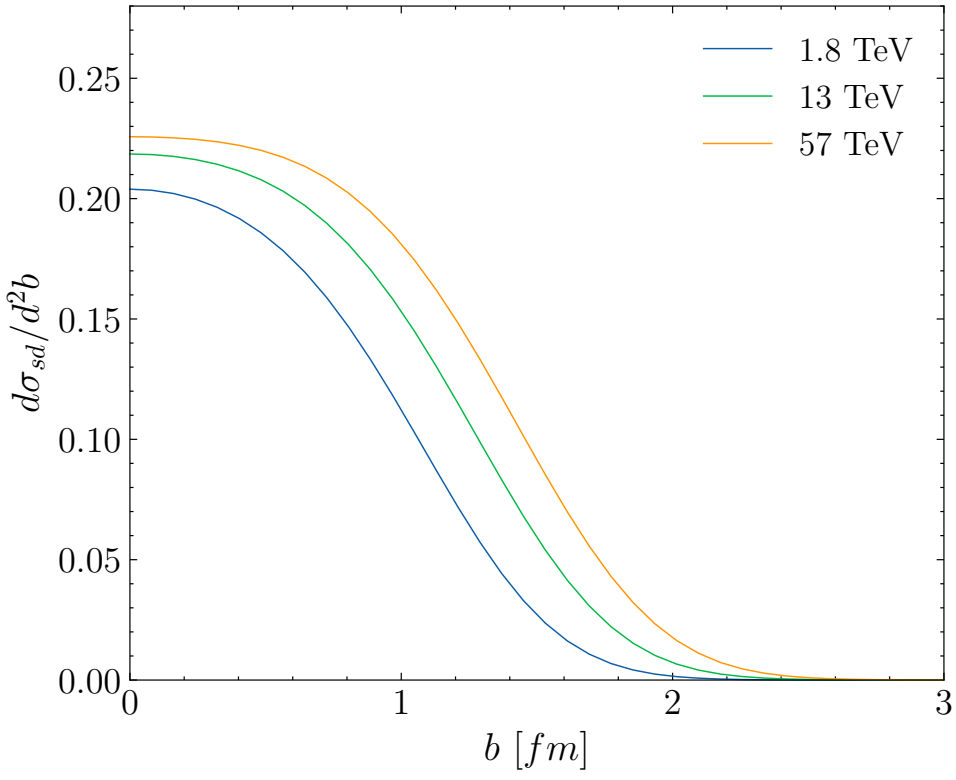

Figure 5.7: Multi-channel model prediction for the energy dependence of the single diffractive differential cross section in impact parameter space.

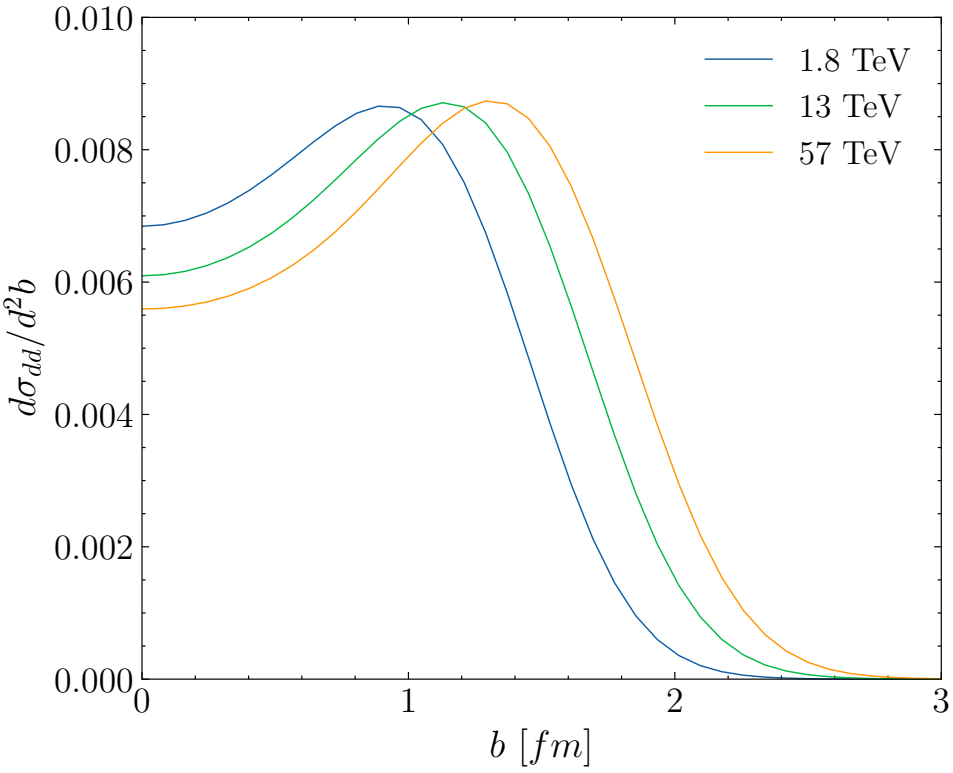

Figure 5.8: Multi-channel model prediction for the energy dependence of the double diffractive differential cross section in impact parameter space.

This finding can be explained by the fact that an odderon contribution, which emerged from the TOTEM and D0 experiments is required to be included, implying distinct energy dependencies of the pp and $p\bar{p}$ cross sections [7].

Fig. 5.9 (right panel) shows our prediction for the elastic differential cross-section in function of the transverse momentum in the context of a pp collision at 13 TeV. It is evident from the figure that while the model describes the experimental data for the elastic differential cross-section at small values of squared momentum transfer q^2, neither the position of the dip nor the behaviour at large q^2 is adequately described. Similar outcomes have already been reported in a number of previous studies [50, 75], which stresses the need for an improvement of the present model. Most importantly, this result points out that taking into account an entire parton configuration space doesn't have any impact on the description of the elastic differential cross section, as has been found in the two-channel case [98]. Our model can be enhanced by considering a complex hadron overlap function rather than a simple dipole form factor, which is a reasonable approximation, since it is known that the elastic differential cross-section depends on the description of the overlap function and, thus, on the inter-

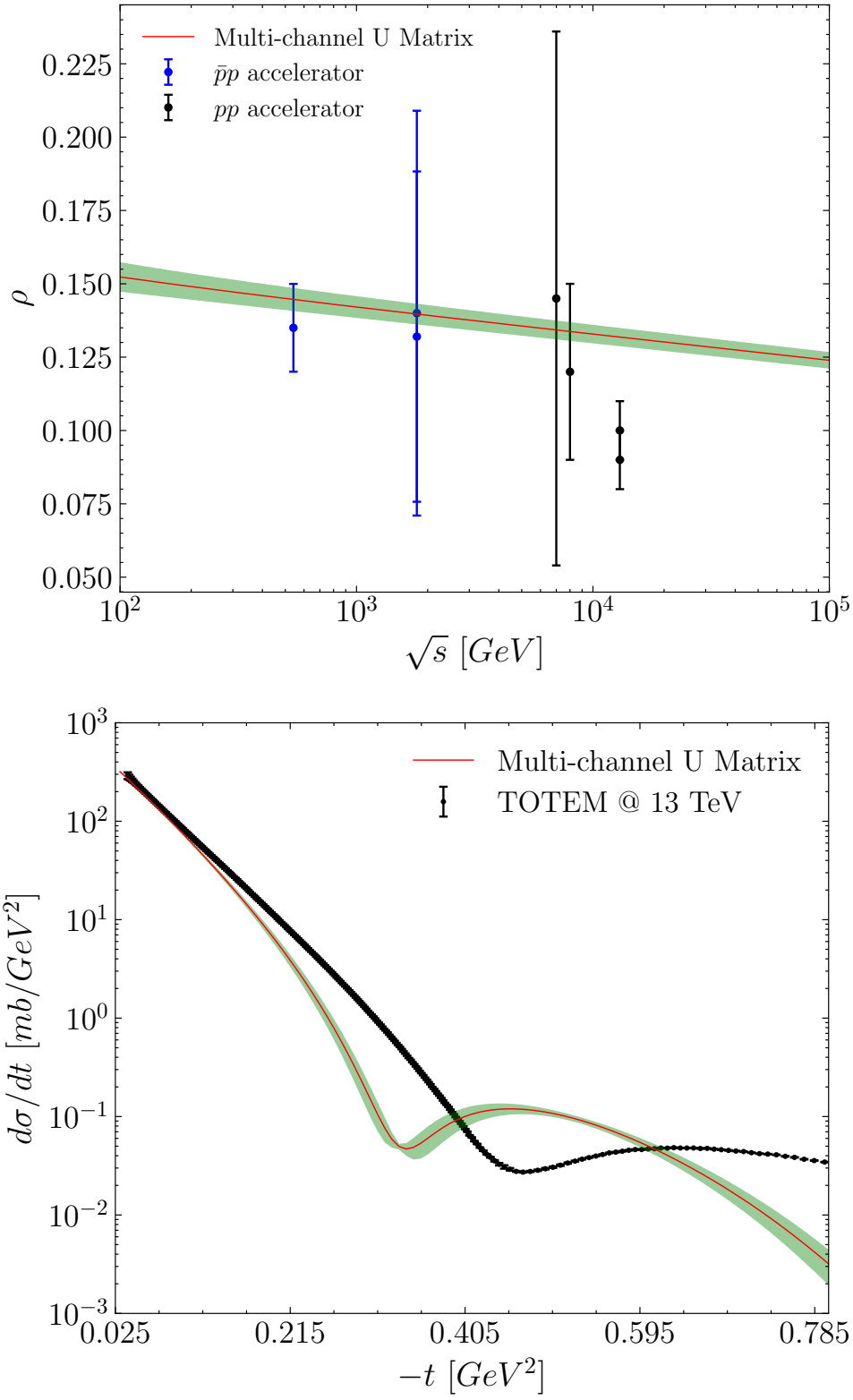

Figure 5.9: Multi-channel model predictions for the ρ parameter (left panel) and for the elastic differential cross-section at 13 TeV (right panel).

nal structure of the incident hadrons [98]. As regards the position of the dip, it has been reported in [98] that an Odderon contribution is required.

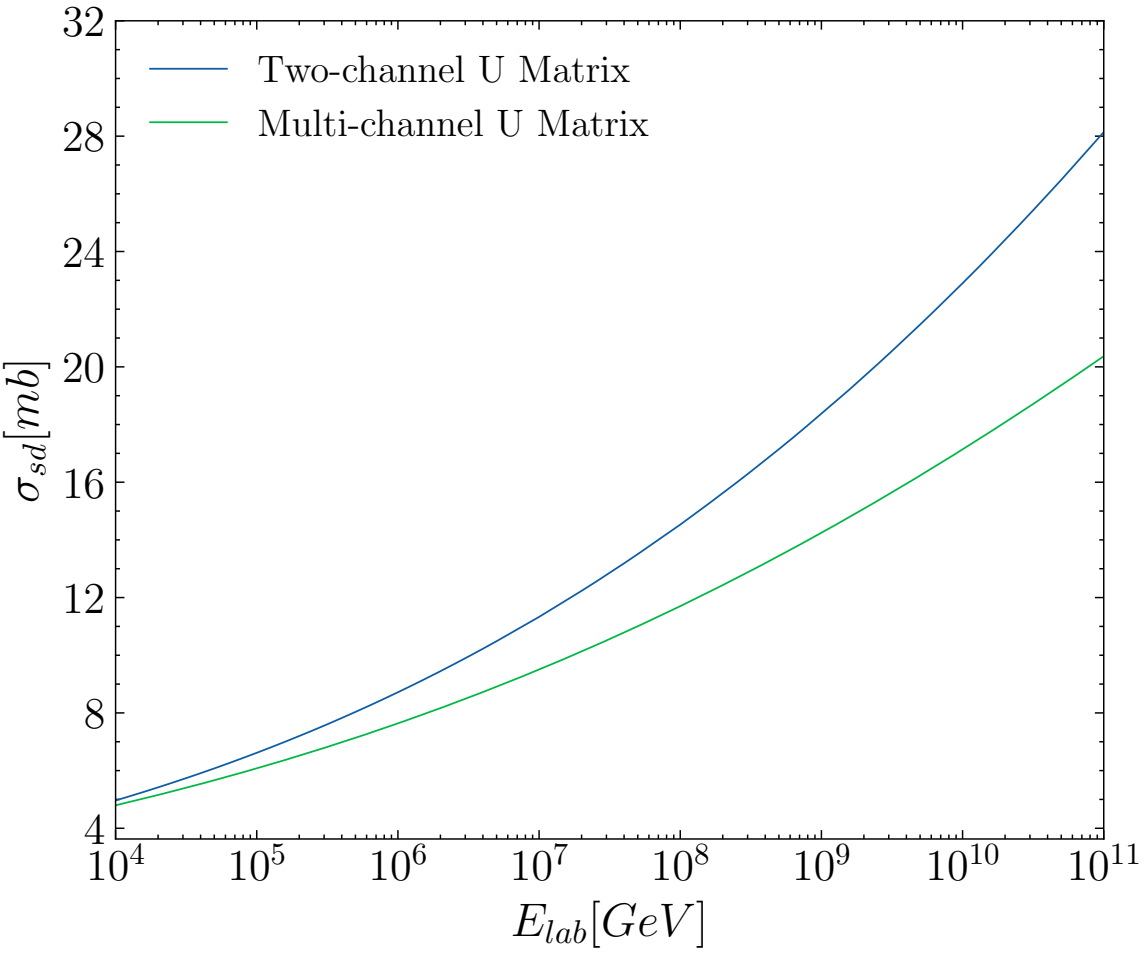

Figure 5.10: The growth of the single-diffractive cross-section with *lab* energies up to $\sqrt{s} = 10^{11}$ GeV for both the two and multi-channel models.

Although the two-channel and the multi-channel models are similar in describing the various hadronic observables in comparison to the currently available data, they provide differing predictions for the single-diffractive cross-section, in particular, at ultra-high energies, as shown in the right panel of Fig. 5.10, where the two-channel model exhibits a faster increase with energies than the multi-channel one, using the U matrix scheme.

This discrepancy may stem from the assumption of equal width for fluctuations in the parton configurations of colliding hadrons across different channels. This assumption simplifies the model by assuming uniform fluctuations across processes. However, in reality, fluctuations may vary between channels. To gain a deeper understanding, it would be valuable to investigate the potential for channel-dependent fluctuations. This would

entail allowing the width of fluctuations to vary for each channel, thereby encompassing the unique characteristics and dynamics of individual scattering processes.

5.2.5 Conclusions

The chief purpose of the study was to provide a phenomenological description of the hadronic interaction at high energy through extending the two-channel model into a multi-channel one using the U-matrix unitarization scheme of the elastic amplitude. It has been found that the multi-channel model accurately describes the total, elastic, inelastic, and single-diffractive cross-sections, with only a minor difference from the two-channel one.

In addition, in spite of considering an entire parton configuration space, the present model was not able to estimate the double-diffractive cross-section, which is in line with the results obtained with the two-channel model. In fact, a proper description of this cross-section requires the introduction of an additional contribution, i.e., pomeron interactions.

Moreover, the behaviour of the energy evolution of the various profile functions in the impact parameter space from Tevatron to cosmic ray energies was analysed.

The study has also found that the present model describes well the ρ parameter at different high energies, but it is unable to estimate the TOTEM data at 13 TeV. It has been suggested that an Odderon contribution is needed to be included in order to remedy this shortcoming.

Furthermore, the elastic differential cross-section at 13 TeV was predicted. It has been shown that the model describes the experimental data for this observable at small values of squared momentum transfer q^2, but it doesn't describe the position of the dip or the behaviour at large q^2. In this regard, it has been proposed that considering a complex hadron overlap function instead of a simple dipole form factor as well as an odderon contribution would be possible approaches to address this flaw.

Last but not least, despite similarities in the way the two models describe various hadronic observables, they provide distinct predictions for the single-diffractive cross-section, especially at ultra-high energies, which represents an interesting direction for future research on ultra-high energy cosmic rays.

The paper concludes by arguing that the U-matrix scheme is more likely to accounting for potential correlations between pomeron exchanges. Ad-

ditionally, it suggests that the two-channel model, as opposed to a multi-channel one, is adequate for modeling high-energy hadronic interactions, particularly single diffractive scattering, using the U-matrix scheme, even at ultra-high energies, provided that any potential pomeron correlations are disregarded.

In summary, the multi-channel model used in the paper has limitations because the probability distribution for hadron configurations is not unique, and that the impact parameter and configuration dependence of the scattering amplitude may not be separable from the energy dependence carried by the single-pomeron exchange. This would complicate the calculation of the total elastic scattering amplitude and may require a more advanced theoretical framework, which is beyond the scope of this work.

On the whole, the findings of this study can serve as a base for future improvements of the hadronic interaction models used in cosmic ray air shower simulations.

Acknowledgments

RO would like to thank Prof. Jean-René Cudell for his invaluable comments and fruitful discussions. Special thanks go to the computational resource provided by Consortium des Équipements de Calcul Intensif (CÉCI), funded by the Fonds de la Recherche Scientifique de Belgique (F.R.S.-FNRS) where a part of the computational work was carried out.

6 Unitarisation and Hadronic Multi-Particle Production

6.1 Context of the work

There is a growing interest in the study of multiple production of hadrons as it is perceived as the dominant phenomenon in high-energy particle and nuclear collisions. This interest is especially pronounced at ultra-high energies, as understanding this phenomenon is crucial for the accurate interpretation of air-shower cosmic ray observables. These interpretations are primarily achieved through Monte Carlo modelling of hadronic interactions.

However, modelling hadronic interactions is not devoid of uncertainties, which gives rise to model-dependent outcomes. For example, different Monte Carlo event generators such as EPOS, QGSJET, and SIBYLL can produce varying predictions for the same physical observables, complicating the interpretation of experimental data from cosmic ray detectors like the Pierre Auger Observatory. This discrepancy underscores the need for advances in the phenomenology and theory of modeling hadronic interactions, especially in the context of multi-particle production, to reduce uncertainties and achieve more reliable and consistent results.

Continuing from the previous chapters' work, the main focus of the present chapter is on the improved predictive ability of a hadronic interaction model based on the U-Matrix unitarisation scheme in explaining the dynamics of multi-particle production in high-energy hadronic collisions and its reliable prediction at ultra-high energies. More specifically, it carefully looks at some important aspects related to this phenomenon, in particular, multiplicity distributions, violation of scaling laws such as geometrical and KNO scaling, correlations, and fluctuations between the produced particles in the final state.

Scaling laws in hadronic multi-particle production are rules that describe how certain physical quantities remain invariant or follow predictable patterns as the energy of particle collisions changes. They

are crucial for simplifying the interpretation of high-energy collision data, validating theoretical models, and understanding the underlying dynamics of particle interactions.

Here we are concerned with two scaling laws, namely the geometrical scaling and the KNO scaling. They are both put forth by the ISR measurements of the proton-proton and proton-antiproton scattering. The first one stands for the invariability of the ratio between elastic and total cross-sections. One of the known scaling laws is the geometrical scaling. It is a regularity set forth by the ISR measurements of the proton-proton and proton-antiproton scattering. It stands for the invariability of the ratio between elastic and total cross-sections. According to experiments carried out at the CERN (SPS) collider, it is important to note that this regularity is violated when energy exceeds the ISR energy range, raising fundamental questions about the underlying mechanisms of hadronic interactions.

As for the second, it represents the energy independence of the shape of the multiplicity distribution, i.e. the distribution of the number of produced particles. Another example of scaling laws is the KNO scaling which is the energy independence of the shape of the multiplicity distribution, i.e. the distribution of the number of produced particles. The approximate KNO scaling is valid up to $\sqrt{s} = 20$ GeV. As the energy increases further, the distribution becomes wider than as expected from the scaling at lower energies. The violation of this scaling becomes significant as energy surpasses the ISR energy range.

Indeed, the violation of these scaling laws challenges our current understanding of hadronic interactions and motivates the refinement of existing theoretical frameworks to accommodate these discrepancies. These violations also highlight complex dynamics that traditional models may not fully capture, prompting further investigation into the underlying mechanisms governing particle production at high energies.

Several studies have been conducted on the description of the geometrical scaling and the KNO scaling violation, mainly using the eikonal scheme. However, some studies have revealed that this scheme is not without limitations. For example, in an eikonal model (ref), it has been demonstrated that strict KNO scaling is not valid as there exists a limited range of energy, where KNO scaling approximately holds. Besides, to date, no single study has examined the potential implications of using alternative schemes in the exploration of these phenomena or attempted to unravel the underlying physics behind the multi-particle production mechanism.

As shown in the previous chapters, the U-Matrix scheme has offered different and improved descriptions of certain hadronic cross-sections, which are associated with the geometrical and KNO scaling. Thus, it is believed that it may provide a good description of their violation as well and that it is poised to shed light on the underlying physics behind the multi-particle production mechanism.

As a matter of fact, the aforementioned reasons have prompted us to investigate these violations, using the U-matrix scheme. The investigation also extends to higher-order moments of multiplicity distributions, which provide critical insights into the correlations and collective behavior of particles produced in collisions. The U-Matrix framework allows for a detailed examination of these statistical properties and unveils the underlying physics behind using this scheme.

Based on the picture depicting the KNO scaling violation as an extension of the geometrical scaling violation, the present study presents a phenomenological model for multi-particle production in hadron collisions that is grounded in the geometrical approach and using the U-Matrix unitarization scheme of the scattering amplitude.

To highlight the connection between the multiplicity distribution $P_n(s)$ and the unitarisation scheme of the scattering amplitude, the overall multiplicity distribution is obtained by summing contributions from parton-parton collisions occurring at each impact parameter weighted by the inelastic overlap function, which dictates the unitarisation scheme.

We conducted a detailed analysis of the multiplicity distribution data in full phase space $p + p$ and $p + \bar{p}$ collisions across a broad spectrum of energies, specifically at $\sqrt{s}$ = 30.4, 44.5, 52.6, 62.2, 300, 546, 1000, and 1800 GeV. With regards to the fitting process, we utilized the Minuit2 class from ROOT and implemented the MIGRAD algorithm. The primary objective of the fitting procedure was to minimize the χ^2 value and the uncertainties associated with the free parameters were calculated using a 1σ confidence level.

After fine-tuning the model and deriving all parameters from optimal fits to the various hadronic multiplicity distributions data in $p + p(\bar{p})$ collisions over a wide energy range, we were able to predict the behaviour of the energy dependence of the hadron mean multiplicity. Additionally, we predicted the hadronic multiplicity distribution at new collision energy regimes, such as 14 TeV. We also examined the higher-order moments of the multiplicity distribution.

6.2 ARTICLE 4

The U-Matrix Geometrical Model For Multi-Particle Production In High-Energy Hadronic Collisions

Rami Oueslati, Adel Trabelsi

Journal of High Energy Physics, 2024(07), 100
arXiv:2403.02263 [hep-ph]
doi: 10.1007/JHEP07(2024)100

Abstract: Inspired by the picture portraying the KNO scaling violation as an extension of the geometrical scaling violation, the current study proposes a phenomenological model for multi-particle production in hadron collisions based on the geometrical approach and using the U-Matrix unitarization scheme of the scattering amplitude. The model has been fine-tuned and all parameters have been derived from optimal fits to various hadronic multiplicity distributions data in $p+p(\bar{p})$ collisions across a broad range of energies. The results have revealed that our model furnishes a reasonable description of diverse multiplicity distributions at various energies. Besides, they have demonstrated a pronounced violation of the geometrical scaling, which eventually resulted in a significant violation of the KNO scaling. The study has also analyzed the higher-order moments of the multiplicity distribution. We have observed an unexpected overestimation of the fluctuations and correlations between final state particles with increasing energy, particularly above LHC energy. It is claimed that this overestimation is due to statistical fluctuations embedded in the U-matrix scheme. The findings of this study have shed light on the key role of the U-matrix scheme in the impact of collision geometry on multi-particle production processes at high energy.

6.2.1 Introduction

Throughout the years, the study of multi-particle production in hadron collisions at high energies has sparked the interest of both theoretical physicists and experimentalists given its significance as it offers valuable

insights into the intricate mechanisms underlying the production of particles [134, 80, 106, 102, 65].

Similarly, the hadronic multi-particle production is primordial at ultra-high energies. Indeed, it is necessary to have a solid grasp of it so as to properly interpret air-shower cosmic ray observables, which are obtained through a simulation of a wide range of event generators based on Monte Carlo models. These models have been created and adjusted to describe hadronic multi-particle production in man-made accelerator experiments. Despite some minor differences in their fundamental assumptions, the majority of them employ the eikonal as the scheme of the unitarisation of the scattering amplitude. They must also be internally consistent as we depend on them for extrapolating to ultra-high energy scenarios. Nevertheless, modelling hadronic interactions is not devoid of uncertainties, which gives rise to model-dependent outcomes. Among them, one can cite the mass composition problem and the long-standing muon puzzle, which is regarded as one of the most significant issues in hadronic interaction physics [35].

Having said that, advances in the phenomenology and theory of multi-particle production may provide a solution to the aforementioned issues.

The study of multi-particle production may be carried out, particularly, through examining the multiplicity distributions of the produced particles. Their analysis is crucial since the patterns observed in them help reveal the complexity of the collision process, shedding light on the interactions involved in particle creation. In fact, this distribution has been thoroughly investigated by experimental collaborations at the LHC, including ALICE, ATLAS, CMS, and LHCb [89], to enhance our comprehension of the rudimentary characteristics of strong interactions and the behaviour of matter under extreme circumstances as well as to verify theoretical predictions.

Besides, the study of the higher-order moments of the multiplicity distribution is of paramount importance as they provide insight into particle features in high-energy collisions, such as correlation and collective behaviour. Indeed, the behaviour of these moments has been the subject of various experimental studies over a wide range of collision energies [126, 116], furnishing valuable data which are crucial in constraining theoretical models.

The multiplicity distribution $P_n(s)$ in hadron collisions refers to the distribution of the number of produced particles in a collision event. It is influenced by various factors, such as the colliding hadrons' energy, the

collision geometry, and the underlying dynamics of the interaction. More specifically, it is given by the ratio of the topological cross-section σ_n to the inelastic cross-section σ_{in}. The topological cross-section represents the probability or rate of observing a specific configuration of particles with a particular multiplicity value n. It is derived from the scattering amplitudes, which are influenced by the underlying scattering processes and dynamics. The inelastic cross-section, on the other hand, characterizes the probability of observing any final-state interaction or particle production, regardless of the specific configuration or multiplicity. It is closely related to the total cross-section and includes contributions from various interaction channels, including both diffractive and non-diffractive processes.

It is important to note that these cross-sections, and thus the multiplicity distribution P_n, cannot yet be calculated within the framework of quantum chromodynamics (QCD). Therefore, our current understanding of multi-particle production dynamics relies primarily on phenomenological approaches as well as certain underlying theoretical principles, which form the basis for a wide range of models [89]. Needless to say, the continuous enhancement of the theoretical models for particle production is critical so as to maintain consistency and coherence with the foundational principles of the Quantum Field Theory (QFT).

One of the key theoretical tenets in the construction of phenomenological models, such as those based on the geometrical or string approach, is the unitarity constraint [122, 40, 39, 41]. These models often utilize the eikonal scheme as a means to unitarize the scattering amplitude and describe inclusive multiplicity distributions. While this scheme provides a reasonable description of certain hadronic observables, there are compelling reasons to explore alternative schemes for unitarizing the scattering amplitude, namely the U-matrix one.

In a recent study [42], it was shown that despite unexpected agreement in the description of the inelastic pp and $p\bar{p}$ cross-sections with the eikonal and U-matrix schemes, a divergence in the individual order-by-order amplitudes can potentially impact the topological cross-section by influencing the relative probabilities of different multiplicity configurations and capturing specific physical processes.

By the same token, in another study [136], it has been found that the U-matrix scheme exhibits a slightly better fit to the single diffractive data at high-energies and a faster growth at ultra-high energies compared to the eikonal scheme. This result implies that the underlying physics and

dynamics of the single diffractive scattering are sensitive to the choice of scheme, especially at ultra-high energy, further reinforcing the significance of considering the U-matrix. Hence, it is worth noting that if the discrepancy in the single diffractive cross-section propagates to the topological cross-section, it can affect the relative probabilities or rates of observing different multiplicity configurations. Moreover, as the inelastic cross-section encompasses both diffractive and non-diffractive processes, the different behaviours in the single diffractive cross-section between unitarization schemes can contribute to variations in the overall inelastic cross-section.

It should be noted that the specific impact on the topological and inelastic cross-sections would depend on the detailed correlations and interplay between different interaction channels, including both diffractive and non-diffractive processes. In fact, when hadrons collide at high energies, several interactions and processes take place, leading to the formation of large numbers of particles with various species. Given the complex nature of these interactions, deciphering the contributions from individual channels and identifying the specific processes behind multi-particle production appears to be a daunting task [79].

On the whole, the inelastic and topological cross-sections are scheme-dependent, implying that the multiplicity distribution P_n is scheme-dependent as well. This will, therefore, impact the description of the multiplicity distribution in terms of its shape, magnitude, or other characteristic features.

An additional reason for considering an alternative to the eikonal unitarization scheme is related to the geometrical scaling, as supported by experimental observations. This scaling is a regularity established by the ISR measurements of the proton-proton and proton-antiproton scattering and refers to the invariability of the ratio between elastic and total cross-sections. Interestingly, experiments conducted at the CERN (SPS) collider have revealed that this regularity is violated when the energy surpasses the ISR energy range [70, 69]. Furthermore, from a theoretical perspective, it has been shown that the violation of the geometrical scaling is more pronounced with the U-matrix scheme than with the eikonal as energy increases [42]. It should be emphasized that this remarkable discrepancy has proved to occur mainly when we venture into the extremely high-energy region, roughly near the Grand Unification Scale. In this regard, one of the preliminary objectives of the present study is to examine this disparity

within an accessible energy range.

Another regularity put forth by the ISR measurements is the KNO scaling so named after its proponents Koba, Nielsen, and Olesen (KNO) [100]. It refers to the constancy of normalized moments in the distribution of multiplicities. Practically, the KNO function is often employed for the examination of multiplicity distributions in particle collisions. It is denoted as $\Phi(z)$, where $\langle n \rangle$ stands for the average of the multiplicity distribution, and $z = n/\langle n \rangle$ represents the normalized multiplicity. It is noteworthy that the KNO function $\Phi(z)$ tends to be independent of the collision energy $\sqrt{s}$ within the ISR energy range. However, considerable deviations from the KNO scaling start to occur at higher energies, such as those attained at FNAL and LHC.

As a matter of fact, several phenomenological studies have demonstrated the existence of a connection between the geometrical scaling of the profile function and the KNO scaling of the multiplicity distribution [92, 74, 104]. More precisely, these models have shown that the violation of the geometrical scaling, indicated by an increase in the ratio of elastic to total cross-sections (σ_{el}/σ_{tot}) between ISR and collider energies, is associated with the violation of the KNO scaling across these energy ranges within the eikonal scheme. This raises the question of potential consequences for the violation of the KNO scaling within the context of the U-matrix scheme. It is expected that the latter, with its modifications to the scattering amplitude, may introduce novel dynamics and fluctuations that influence the statistical behaviour of particle production. These effects can in turn influence the universal properties assumed in the KNO scaling and significantly lead to a violation or alteration of the constancy of normalized moments.

In view of all that has been mentioned so far, one can assume that considering an alternative adequate unitarization scheme can considerably change our understanding of the description of multi-particle production. In the present study, we propose a phenomenological model for multi-particle production in hadron-hadron collisions that hinges on both the geometrical approach and the picture depicting the KNO scaling violation as an extension of the geometrical scaling violation, using the U-Matrix scheme. The chief purposes of the study are to examine the geometrical scaling violation within an accessible energy range, describe the hadronic multiplicity distributions in full-phase space over a wide energy range in $p + p(\bar{p})$ collisions and to investigate the KNO scaling violation. It also

aims at probing the correlation between the final particles and revealing the physics that underlies it. In particular, it seeks to provide valuable insights into the relationship between the violation of both the geometrical and KNO scaling and the mechanism of particle production within the U-matrix scheme.

The remainder of the paper is organized as follows: In Section II, the theoretical background of the multi-particle production model will be outlined. Section III will focus on the explicit model and the data used. Section IV will present and discuss the results. Finally, Section V will summarize the findings and discuss the limitations and implications of this work so as to guide future research.

6.2.2 The theoretical framework of the Model

The multiplicity distribution $P_n(s)$, i.e., the probability of producing n charged particles in an inelastic $p + p(\bar{p})$ collision at the energy $\sqrt{s}$, is given by

$$P_n(s) = \frac{\sigma_n(s)}{\sigma_{in}(s)} \tag{6.1}$$

where $\sigma_n(s)$ and $\sigma_{in}(s)$ are the n-particle topological and inelastic cross-sections, respectively, with $\sum_n \sigma_n(s) = \sigma_{in}(s)$.

Great efforts have been devoted to explaining why the normalized moments in this multiplicity distribution remain constant in the ISR energy range but diverge from this pattern from the LHC energy range. A possible explanation for this phenomenon might be ascribed to the increasing importance of mini-jets production, resulting from both soft and semi-hard partonic processes, as energy increases. In fact, these mini-jets not only contribute to the rapid growth of hadron-hadron cross-sections, as demonstrated by several geometrical models [72, 42, 136, 115], but may also play a crucial role in the violation of the KNO scaling.

It goes without saying that the geometrical models based on the impact parameter space representation provide a good description of various aspects of hadron collisions at high energies. Technically speaking, by considering the impact parameter, which quantifies the distance between the colliding particles' centres, these models actually furnish a solid framework for understanding the initial stages of collisions, allowing a systematic exploration of the collision geometry, ranging from central (small impact

parameters) to peripheral (large impact parameters) collisions. Therefore, this geometrical approach links the collision geometry to the underlying physics processes, enabling us to infer certain properties. We particularly assume that this approach can also shed light on the intricate interplay between collision geometry and particle multiplicity distribution.

In addition, as has been mentioned in the previous section, the KNO scaling violation can be perceived as an extension of the geometrical scaling violation to the multi-particle production process. This extension highlights that the dynamics governing particle production become more complex and energy-dependent than what a purely geometrical approach can capture. It also suggests that additional physical processes, such as parton interactions, collective effects, or fluctuations, play a role in shaping the multiplicity distribution as collision energies increase. As a result, a more accurate description of the geometrical scaling violation is needed, which in turn will provide a better description of the violation extension to multi-particle production. In fact, the violation of geometrical scaling in impact parameter space occurs when the initial assumptions about simple geometrical overlap and scaling behaviour break down due to more intricate particle-particle interactions or energy-dependent effects. Consequently, this concept harmoniously aligns with the utilization of the impact parameter space representation, emphasizing the significance of collision geometry.

Overall, when combined with the geometrical scaling tenets, the geometrical models can be enhanced and thus provide a solid framework for describing the multiplicity distribution and uncovering the underpinning universal features of particle production in high-energy hadron collisions. They also furnish a reliable tool that serves to explain the impact of collision geometry on the multiplicity distribution and to analyze it across a broad range of collision energies and particle species, improving prediction and comparison accuracy in multiple collision systems.

To construct our model highlighting the intrinsic relationship between geometrical scaling and KNO scaling within a geometrical approach, we draw inspiration from [52, 33, 104, 103], where the essence of the approach lies in expressing the overall hadronic multiplicity distributions in the inelastic channel through a combination of an elementary distribution and the inelastic overlap function. Thus, this approach establishes a direct connection between the fluctuations in multiplicity and the fluctuations in the impact parameter, driven by the intuitive understanding that collisions

occurring at shorter distances tend to be more violent and yield a higher number of fragments, thereby leading to increased multiplicities. Therefore, in order to establish a reliable geometrical approach to calculate the multiplicity distribution in the impact parameter space representation, we rely on the unitarity condition of the S matrix. This involves examining the elastic scattering amplitude in the impact parameter b space, expressed by the equation:

$$2\,\mathrm{Im}[\Gamma(s,b)] = |\Gamma(s,b)|^2 + G_{in}(s,b), \tag{6.2}$$

where $\Gamma(s,b)$ denotes the profile function, i.e., the elastic hadron scattering amplitude, and $G_{in}(s,b)$ represents the inelastic overlap function. By employing the optical theorem, we can obtain

$$\sigma_{tot}(s) = 2\int d^2b\ \mathrm{Im}[\Gamma(s,b)], \tag{6.3}$$

and recognizing that the function $G_{in}(s,b)$ signifies the absorption probability associated with each b value, we can derive the total inelastic cross-section

$$\sigma_{in}(s) = \int d^2b\ G_{in}(s,b). \tag{6.4}$$

Thus, the unitarity condition (6.2) is equivalent to $\sigma_{tot}(s) = \sigma_{el}(s)+\sigma_{in}(s)$, where $\sigma_{el}(s) = \int d^2b\,|\Gamma(s,b)|^2$.

Various research papers in the field have already explored this phenomenological procedure based on the impact parameter space representation known as the geometrical or string approach [40, 39, 41, 38]. In this geometrical approach, wherein incident hadrons are treated as spatially extended objects and their collisions are represented as an ensemble of elementary interactions between quarks and/or gluons, the hadronic multiplicity distribution $P_n(s)$ is constructed based on elementary quantities associated with microscopic processes. It follows from this that the overall hadronic multiplicity distribution is estimated through summing contributions emerging from each impact parameter b of the incident hadronic system.

To do this, the topological cross-section σ_n is decomposed into contributions from each impact parameter b with weight $G_{in}(s,b)$ as follows:

$$\begin{aligned}\sigma_n(s) &\equiv \int d^2b\ \sigma_n(s,b) \\ &= \int d^2b\ G_{in}(s,b)\left[\frac{\sigma_n(s,b)}{\sigma_{in}(s,b)}\right],\end{aligned} \tag{6.5}$$

where $\sigma_{in}(s) \equiv \int d^2b\, \sigma_{in}(s,b) = \int d^2b\, G_{in}(s,b)$.

The quantity enclosed in brackets $\sigma_n(s,b)/\sigma_{in}(s,b) \equiv p_n(s,b)$ can be interpreted as the probability of producing n particles at impact parameter b. It accounts for interactions among the elementary components of the colliding hadrons. Keeping in mind that $p_n(s,b)$ should scale in KNO sense given its elementary structure, the multiplicity distribution $P_n(s)$ (6.1) can be reformulated as :

$$P_n(s) = \frac{1}{\sigma_{in}(s)} \int d^2b\, \frac{G_{in}(s,b)}{\langle n(s,b)\rangle} \left[\langle n(s,b)\rangle p_n(s,b)\right] \tag{6.6}$$

where $\langle n(s,b)\rangle$ represents the average number of particles produced at b and s.

Let $\Phi(s,z) = \langle n(s)\rangle P_n(s)$ be the overall multiplicity distribution in KNO form, where $z = n(s)/\langle n(s)\rangle$ is the corresponding KNO variable. A multiplicity distribution $\phi(s,\underline{z})$, associated with elementary processes occurring at b and s, can be written in the form $\phi(s,\underline{z}) = \langle n(s,b)\rangle p_n(s,b)$, where $\underline{z} = n(s)/\langle n(s,b)\rangle$. It is worth noting that both distributions adhere to the standard normalizations [104] :

$$\int_0^\infty dz\, \Phi(z) = \int_0^\infty d\underline{z}\, \phi(\underline{z}) = 2 \tag{6.7}$$

and

$$\int_0^\infty dz\, z\, \Phi(z) = \int_0^\infty d\underline{z}\, \underline{z}\, \phi(\underline{z}) = 2. \tag{6.8}$$

In this theoretical framework, the unknown function representing the average number of particles produced at a specific impact parameter b and energy s can be comprehended as the product of two factors: The first factor, $\langle n(s)\rangle$, representing the general behaviour depicts the average number of particles generated in a collision, regardless of the specific impact parameter. As for the second, it is denoted as $f(s,b)$ and perceived as a multiplicity function. It describes the variation of the average number of particles in accordance with the impact parameter b quantifying how collision geometry affects particle production. The mathematical expression for this factorization is:

$$\langle n(s,b)\rangle = \langle n(s)\rangle f(s,b) \tag{6.9}$$

and therefore the expression (6.6) can be rewritten in the KNO form as follows:

$$\Phi(s,z) = \langle n(s)\rangle P_n(s) = \frac{1}{\int d^2b\, G_{in}(s,b)} \int d^2b\, \frac{G_{in}(s,b)}{f(s,b)}\, \phi\left(\frac{z}{f(s,b)}\right) \quad (6.10)$$

and we also have

$$P_n(s) = \frac{1}{\langle n(s)\rangle \int d^2b\, G_{in}(s,b)} \int d^2b\, \frac{G_{in}(s,b)}{f(s,b)}\, \phi^{(1)}\left(\frac{z}{f(s,b)}\right), \quad (6.11)$$

The master formula eq. (6.11) highlights the connection between the multiplicity distribution $P_n(s)$ and the unitarisation scheme of the scattering amplitude which can ultimately be established within the inelastic overlap function, emphasizing that this multiplicity is scheme-dependent as stated in the introduction. The full phase space hadronic multiplicity distribution $P_n(s)$ is hence constructed by summing contributions from parton–parton collisions occurring at each value of b. These interactions give rise to the formation of string-like objects, similar to the string formation described by the Lund model [29]. These strings in turn fragment into hadrons. So, in order to stress the fundamental principle of the string approach, an index labelling the elementary multiplicity distribution $\phi^{(1)}$ has been introduced in the master formula (6.11). The essential elements in this formula eq. (6.11), namely the inelastic overlap function, the average number of particles produced at a specific impact parameter b and energy s, as well as the elementary multiplicity distribution function, will be explicitly presented in the following section, laying the groundwork for an in-depth analysis of the complex interactions between collision geometry and particle production.

6.2.3 Explicit model and data

The explicit model presented in this paper for describing High-energy hadronic scattering is theoretically grounded in the geometrical approach and is based on the Reggeon exchanges picture (see, e.g. [63] and references therein). In this picture, hypothetical exchange particles, known as pomerons, mediate interactions between hadrons and the procedure of obtaining the amplitude of a given hadronic process involves summing over all conceivable ways in which pomerons can be exchanged.

Diagrammatically, every pomeron exchange is represented by a line that connects the incoming and outgoing hadrons. Hence, by summing all possible topologies of these diagrams, the total amplitude is determined. Technically, the single-pomeron exchange amplitude, also known as, the Born term can be parameterized as follows:

$$a(s,t) = g_p^2 \, F_1(t)^2 \left(\frac{s}{s_0}\right)^{\alpha(t)} \xi(t), \tag{6.12}$$

where g_p is the pomeron-proton coupling, $F_1(t)$ denotes the proton elastic form factor, and $\xi(t)$ stands for the signature factor that is given by:

$$\xi(t) = -e^{-i\pi\alpha(t)/2}, \tag{6.13}$$

and the pomeron trajectory, represented by $\alpha(t)$, approximates a straight line:

$$\alpha(t) = 1 + \epsilon + \alpha' t. \tag{6.14}$$

In the impact-parameter space representation, where the Fourier transform of the amplitude $a(s,t)$ rescaled by $2s$ corresponds to a partial wave, we have:

$$\chi(s,\mathbf{b}) = \int \frac{\mathrm{d}^2\mathbf{q}}{(2\pi)^2} \frac{a(s,t)}{2s} \exp(\mathrm{i}\mathbf{q}\cdot\mathbf{b}). \tag{6.15}$$

When we venture into high energies, summing amplitudes may lead to a violation of unitarity, especially in the case of multi-pomeron exchanges. Therefore, in order to make the summed amplitudes comply with the unitarity constraint, unitarization techniques come into play by resuming infinite series or introducing additional terms to modify the amplitude's behaviour. As a matter of fact, there is a plethora of techniques in the literature [121, 58, 66] whose shared objective is to come up with a consistent approach to summing over various exchange contributions while making sure that the resulting amplitude $\Gamma(b,s)$, i.e., the hadronic profile function, satisfies the unitarity condition and may account for all features of interactions in the context of hadron collisions. Among them, we can cite the eikonal scheme, which is one of the most commonly used methods, positing that the profile function is provided by:

$$\Gamma_E(s,\boldsymbol{b}) = \mathrm{i}\left[1 - \mathrm{e}^{\mathrm{i}\chi(s,\boldsymbol{b})}\right], \tag{6.16}$$

Scheme	ϵ	α' (GeV^{-2})	g_p	t_0 (GeV^2)	χ^2/d.o.f
U-matrix	0.10 ± 0.01	0.37 ± 0.28	7.5 ± 0.8	2.5 ± 0.6	1.436
Eikonal	0.11 ± 0.01	0.31 ± 0.19	7.3 ± 0.9	1.9 ± 0.4	1.442

Table 6.1: χ^2/d.o.f and best-fit parameters obtained using the eikonal and U-matrix unitarisation schemes.

The U-matrix scheme is another illustration, which asserts that:

$$\Gamma_U(s, \boldsymbol{b}) = \frac{\chi(s, \boldsymbol{b})}{1 - \mathrm{i}\,\chi(s, \boldsymbol{b})/2}. \tag{6.17}$$

As previously mentioned in the introduction, we will consider that the hadronic profile function $\Gamma(b, s)$ is given by the U-Matrix form (6.17). This function represents the sum of all n-pomeron exchange contributions obtained from the single-pomeron exchange amplitude which is, in turn, related to the expected number $\chi(b, s)$ of interactions between partons of the incident hadrons.

Using both the eikonal and the U-matrix schemes as well as a dipole-like form factor for the proton, where $F_1(t) = 1/(1-t/t_0)^2$, the parameters ϵ and α' describing the pomeron trajectory, the coupling constant g_p, and the form-factor scale t_0 are adjusted based on a best fit to up-to-date hadron collider data on total, elastic, and inelastic cross-sections. The values of these parameters are provided in Table 6.1 [42]. Following this adequate description of the hadronic profile function, we can determine the inelastic overlap function $G_{in}(s, b)$, needed in our explicit model, by using the equation presented in (6.2).

Since the primary objective of this work is to examine the influence of geometrical collisions on multi-particle production processes, we shall propose two hypotheses concerning our choice of the elementary multiplicity distribution. First, it is sufficient for our study to consider that, on average, every string created in parton-parton interactions has the same likelihood of producing a certain number of charged hadrons, which is described by the elementary multiplicity distribution $\phi^{(1)}(z)$, even though the strings created may have different probabilities of turning into a pair of charged hadrons. Second, despite the fact that the parametrization of the elementary distribution $\phi^{(1)}(z)$ is key to capturing the overall shape of the multiplicity distribution, these two do not necessarily have similar shapes. This is mainly because the overall distribution is obtained

by summing contributions from elementary processes at different impact parameters, in the context of this superposition model eq. (6.11). That is to say, the peculiar combination of the individual contributions emerging from distinct impact parameters and which may be having differing shapes results in an overall distribution that reflects these contributions' combined effects and whose characteristics should be represented by their superposition. Hence, we will assume, as a first approximation, that the elementary distribution has the same shape as the overall distribution. More specifically, the choice of the functional form for this elementary distribution is motivated by phenomenological fits to data.

As a matter of fact, the Negative Binomial Distribution (NBD) has proved to provide a good description of the experimental data on the multiplicity distributions in the context of high-energy physics and hadron collisions [89]. Therefore, in the present study, the KNO form of the NBD, also known as the Gamma distribution, is adopted for the elementary multiplicity distribution and given by:

$$\phi^{(1)}(z) = 2\,\frac{K^K}{\Gamma(K)}\,z^{K-1}\,e^{-Kz}, \tag{6.18}$$

where K is a dimensionless parameter.

It should be pointed out that there exists a connection between the average number of particles generated at a specific impact parameter b and energy s, $\langle n(s,b)\rangle$, which determines the unknown multiplicity function $f(s,b)$ by the eq. (6.9), and the Born term in b space $\chi(s,b)$.

This link can be attributed to the various roles that the Born term plays. To begin with, the multiplicity of generated particles in b space and the Born term are interrelated given that the former can be impacted by the effective interaction of partons within the colliding hadrons and the latter provides a measure of this effective interaction since it represents the overlap of the colliding matter distributions. Not to mention, the Born term depends on the impact parameter. As such, it reflects how strong the interaction between colliding hadrons is at distinct impact parameters. Indeed, the impact-parameter-dependent strength of the interaction between hadrons may have an impact on the multiplicity of produced particles. Secondly, owing that the Born term is a crucial parameter in describing the energy dependence of the scattering amplitude and that particle generation is more likely to occur at higher energies, the Born term is inextricably connected to the average particle production. Thirdly, on the one hand, the imaginary part of the Born term is related

to inelastic processes in high-energy collisions and, on the other hand, multi-particle production is often associated with inelastic interactions, so relying on the imaginary part of the Born term will reflect the possibility of inelastic scattering and subsequent particle production. Therefore, the multiplicity function $f(s,b)$ is constructed to depend on the imaginary part of the Born term, denoted as $\chi_I(s,b)$.

Therefore, the connection between the multiplicity function $f(s,b)$ and the born term is formally defined as follows:

$$f(s,b) = \beta(s)\,[\chi_I(s,b)]^{2\lambda}, \tag{6.19}$$

where $\beta(s)$ is determined by the normalisation condition (6.8) :

$$\beta(s) = \frac{\int d^2b\, G_{in}(s,b)}{\int d^2b\, G_{in}(s,b)\,[\chi_I(s,b)]^{2\lambda}} \tag{6.20}$$

and the exponent 2λ in eq. (6.19) introduces a power-law dependence on $\chi_I(s,b)$, suggesting a non-linear relationship between the effective overlap and the particle production in the impact-parameter space.

It should be emphasized that according to the geometrical approach, the phenomenological portrayal of hadronic multiplicity distributions is considerably influenced by the values and behaviours of three key inputs: the inelastic overlap function G_{in}, the elementary multiplicity distribution $\phi(z)$, and the λ parameter determining the power-law dependence on the effective overlap $\chi_I(s,b)$. A previous study [40] has shown that changing one of these inputs, while keeping the other two fixed, produces different results across different parameterizations. For instance, if the inputs of the inelastic overlap function are different and λ, as well as $\phi(z)$, are kept constant, the obtained hadronic multiplicity distributions successfully replicate the experimental data. Interestingly, in all cases, the physical picture is that large multiplicities occur for small impact parameters while peripheral collisions (large b) lead to small multiplicities. It is worth noting that all these results, obtained for different inputs of the inelastic overlap function, are generated using the eikonal scheme. However, in the present study, we employ the U-matrix scheme for the reasons mentioned in the previous section. This will eventually allow us to fix our choice of the inelastic overlap function.

In order to present our findings in the following section, it is essential to provide an overview of the model parameters that were determined through data fitting, as well as the specific experimental data employed in

our analysis. Since the Born term $\chi_I(s,b)$ is completely determined from the best-fit, Table 6.1, we see from the master formula for the multiplicity distribution eq. (6.11) that the only free parameters are K, λ, and $\langle n(s,b)\rangle$. Further, for our purposes, it is sufficient to fix the value of K and assume λ and $\langle n(s,b)\rangle$ as the only fitting parameters. Indeed, in [40], it was shown that the choice of $K = 10.775$ by assuming a Gamma distribution gives a good description of the charged multiplicity distributions for e^+e^- annihilation data in a large energy interval. Based on the universality of multiplicities in e^+e^- and $p+p(\bar{p})$ collisions, we adopt this choice.

To determine the values of the parameters λ and $\langle n\rangle$, we fix the dimensionless parameter to $K = 10.775$ and conduct fits to full phase space P_n data in $p+p(\bar{p})$ collision across a wide range of energies, specifically at $\sqrt{s} = 30.4, 44.5, 52.6, 62.2, 300, 546, 1000$, and 1800 GeV [49, 14].

With regards to the fitting process, we utilized the Minuit2 class from ROOT [91] and implemented the MIGRAD algorithm. The primary objective of the fitting procedure was to minimize the χ^2 value and the uncertainties associated with the free parameters were calculated using a 1σ confidence level.

6.2.4 Results and discussion

6.2.4.1 Geometrical scaling violation

The preliminary objective of this study was to analyze the behaviour of the inelastic overlap function in the impact parameter space as well as the geometrical scaling violation using the U-matrix and the eikonal schemes, eqs. (6.16) and (6.17), in an attempt to offer valuable insights into the collision geometry and the interaction dynamics of colliding particles. Fig. 6.1 depicts the predictions for the energy evolution of the inelastic overlap function, eq. (6.2), in the impact parameter space at energies spanning from ISR to LHC levels using both schemes.

Looking at Fig. 6.1, it is apparent that this function exhibits a generally comparable pattern in impact parameter space across both schemes, with only minor differences. More specifically, it shows that it is predominantly central, indicating that it has a significant contribution at small impact parameters. This entails that most of the inelastic processes are more probably to take place when the colliding particles pass through one another within close proximity. Moreover, this function tends to decline more slowly with the impact parameter as energy rises. This points out that the

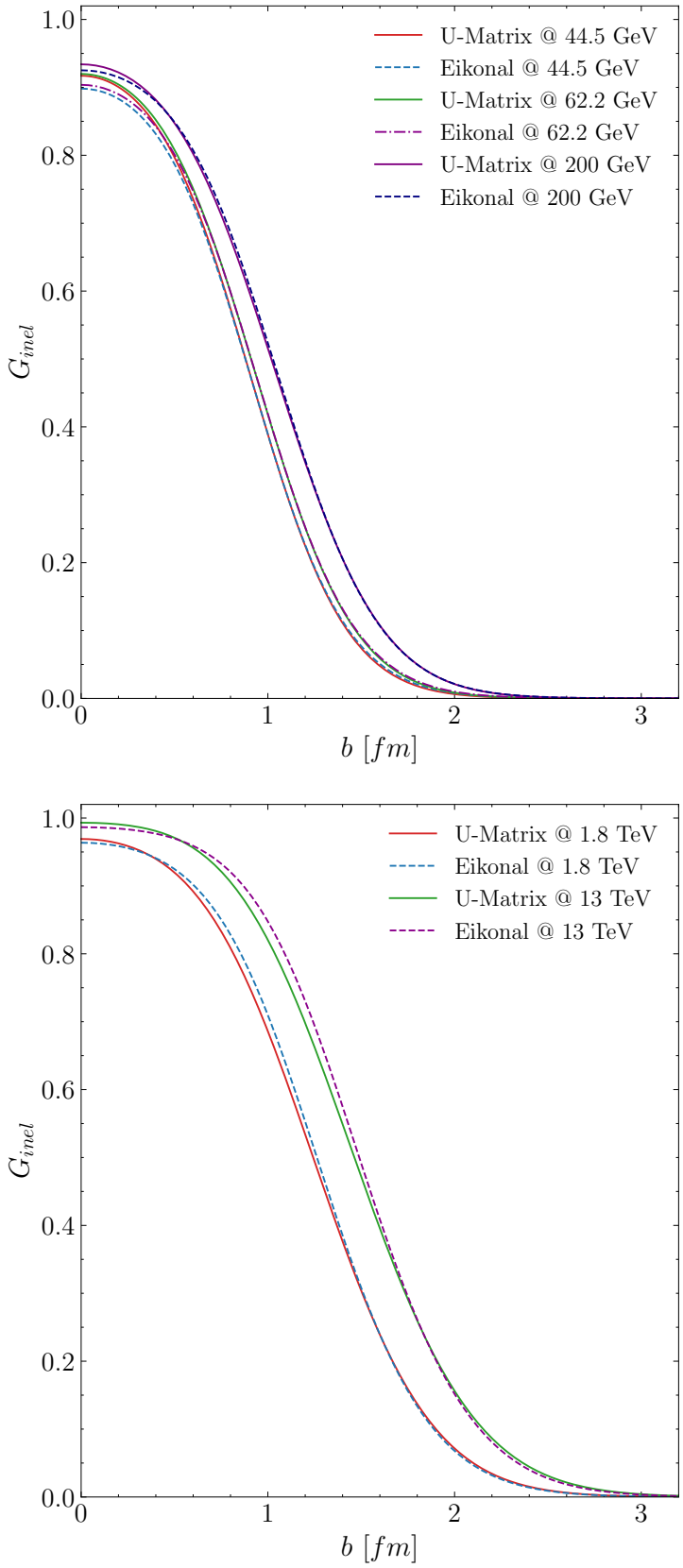

Figure 6.1: The energy evolution of the inelastic overlap function in the impact parameter space at energies spanning from ISR to LHC levels using both the U-matrix and the eikonal schemes.

inelastic processes become less dependent on the specific spatial distance between colliding particles and have a wider range of impact parameters at which they can happen at higher energies.

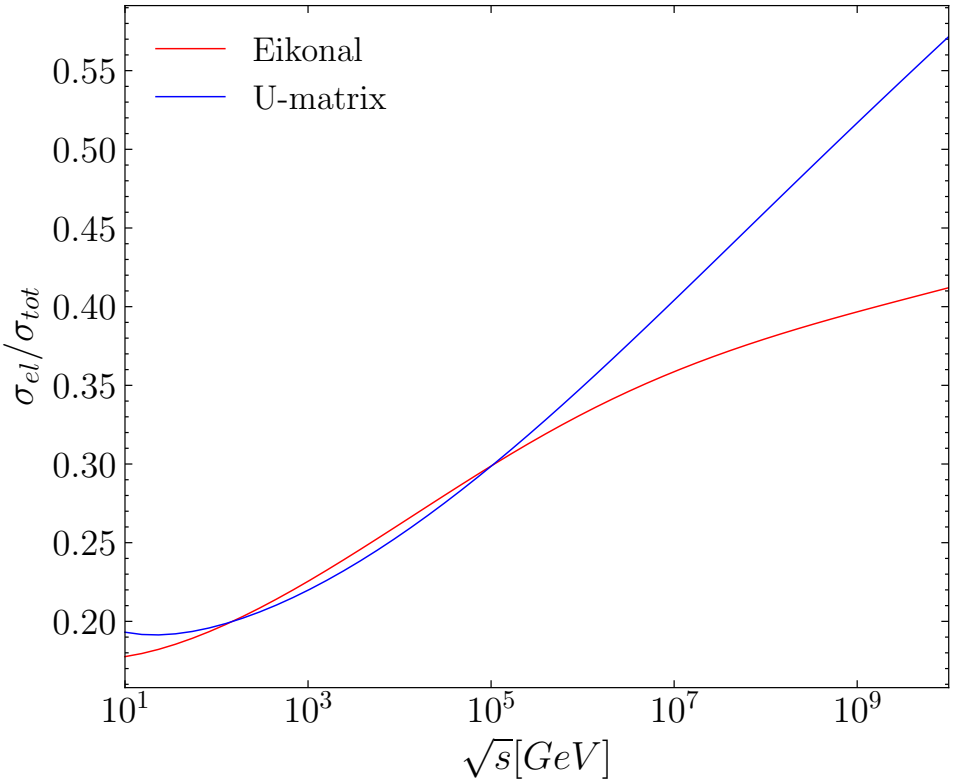

Figure 6.2: Energy evolution of the ratio elastic-to-total cross-section in both cases, the eikonal and U-matrix schemes

Furthermore, it can be seen from Fig. 6.1 that the magnitude of the inelastic overlap function grows with energy at the central impact parameter $b = 0$. This indicates that the higher the energy, the more likely it is that inelastic events will occur at the central impact parameter. Interestingly, as Fig. 6.1 shows, there is a significant divergence in the magnitude of the inelastic overlap function obtained from the U-matrix and the eikonal schemes. To be more specific, the former yields a greater magnitude than the latter at $b = 0$. It is clear from this difference that the chosen scheme has a profound impact on the inelastic processes, particularly on central collisions which will have distinct characteristics or probabilities.

In the same vein, Fig. 6.2 depicts the energy evolution of the ratio elastic-to-total cross-section using both schemes. As this Figure demonstrates, in both cases there is an overall increase of this ratio as energy rises from 10 GeV to 10 TeV, but does so in a non-linear manner, which is indicative of geometrical scaling violation. Interestingly, comparing the

behaviour of this ratio in both cases, it is clear that it increases more rapidly in the U-matrix case than in the eikonal one, as energy increases, demonstrating a stronger violation of the geometrical scaling and a more intricate behaviour in the former case.

It is possible to explain the divergence observed in the geometrical scaling violation between the two distinct schemes in terms of the behaviour of the inelastic overlap function in the impact parameter space with respect to energy. To be more precise, this difference lies in the behaviour of the inelastic overlap function at $b = 0$, where we can see from Fig. 6.1 that it has a magnitude that grows with energy in both cases. However, the U-matrix scheme yields a larger magnitude than the eikonal one. This implies that, in the former case, the inelastic interactions are more prominent, indicating that they have a remarkably and rapidly increasing strength at the central impact parameter with increasing energy, compared to the eikonal case.

It can be argued that the discrepancy found in the behavior of the inelastic overlap function as well as in the observed violation of the geometrical scaling between the two schemes can be ascribed to their differing approaches to the unitarization of the scattering amplitude. Indeed, based upon its thorough treatment of processes and its ability to take into account a wider range of interactions and collision dynamics compared to the Eikonal scheme, the U-matrix scheme is likely to be a more advanced mechanism for dealing with scattering processes and capturing the intricate dynamics of hadronic interactions, which is also supported by other results [115, 136, 42].

On the whole, this result validates the remarkable difference in the geometrical scaling violation between the U-matrix and eikonal schemes. Specifically, it supports the claim that this violation is more noticeable with the former scheme when energy levels rise. Notably, this outcome is in agreement with the theoretical prediction provided in [42] and further highlights that this discrepancy becomes apparent even before reaching the extremely high-energy region. Furthermore, it reinforces our motivation, as stated in the introductory section, for selecting the U-matrix scheme. In fact, the choice of this scheme, in particular, may contribute to answering the question posed in the introduction regarding its potential implications for KNO scaling violation and unravelling the underlying physics behind the multi-particle production mechanism, as will be elaborated in the forthcoming sections.

6.2.4.2 Hadronic Multiplicity Distributions

Using the master formula (6.11), the outcomes of the fitting procedure of the multiplicity distributions data across a wide range of energies are provided in Fig. 6.3, Fig. 6.4 and, Table 6.2, respectively, where the values of the parameters λ and $\langle n(s)\rangle$ obtained in each fitting procedure, along with the corresponding $\beta(s)$, are furnished, as well as the different χ^2/dof values.

$\sqrt{s}$ [GeV]	λ	$\beta(s)$	$\langle n(s)\rangle$	χ^2/DOF
30.4	0.2837 ± 0.0133	1.6014	9.0583 ± 0.1452	1.2714
44.5	0.2720 ± 0.0119	1.6308	10.5900 ± 0.1339	0.6170
52.6	0.2775 ± 0.0104	1.6430	11.2885 ± 0.1299	0.6443
62.2	0.2709 ± 0.0107	1.6547	12.0090 ± 0.1551	1.3303
300	0.3695 ± 0.0113	1.7327	23.4646 ± 0.2915	0.6046
546	0.4618 ± 0.0148	1.7420	27.7185 ± 0.4145	0.3406
1000	0.4230 ± 0.0110	1.7362	36.6360 ± 0.4042	1.5301
1800	0.4836 ± 0.0070	1.7132	42.7217 ± 0.3184	1.2004
7000	0.5936	1.5833	73.7117	–
14000	0.6597	1.4716	96.0705	–

Table 6.2: Values of the λ parameter and $\langle n(s)\rangle$ resulting from fits to the P_n data. The values of $\beta(s)$ were obtained from eq. (6.20).

According to Fig. 6.3, Fig. 6.4, and the different χ^2/dof values, our model gives a reasonable description of the different multiplicity distributions at each energy.

Moreover, it allows to predict the multiplicity distribution P_n at LHC energies by evaluating the energy dependence of the parameter λ using an appropriate function $\lambda(s)$.

As can be seen from Fig.6.5 (left panel), the behaviour of this parameter is energy-dependent and rapidly increases with increasing energy. This energy dependence can be aptly described by the following function:

$$\lambda(s) = a_0\ s^{a_1} \tag{6.21}$$

where the values $a_0 = 0.154$, $a_1 = 0.0762$ were determined by a careful χ^2 analysis. Thus, based on this function, the λ values at 7 and 14 TeV are retrieved and then displayed in Table 6.2.

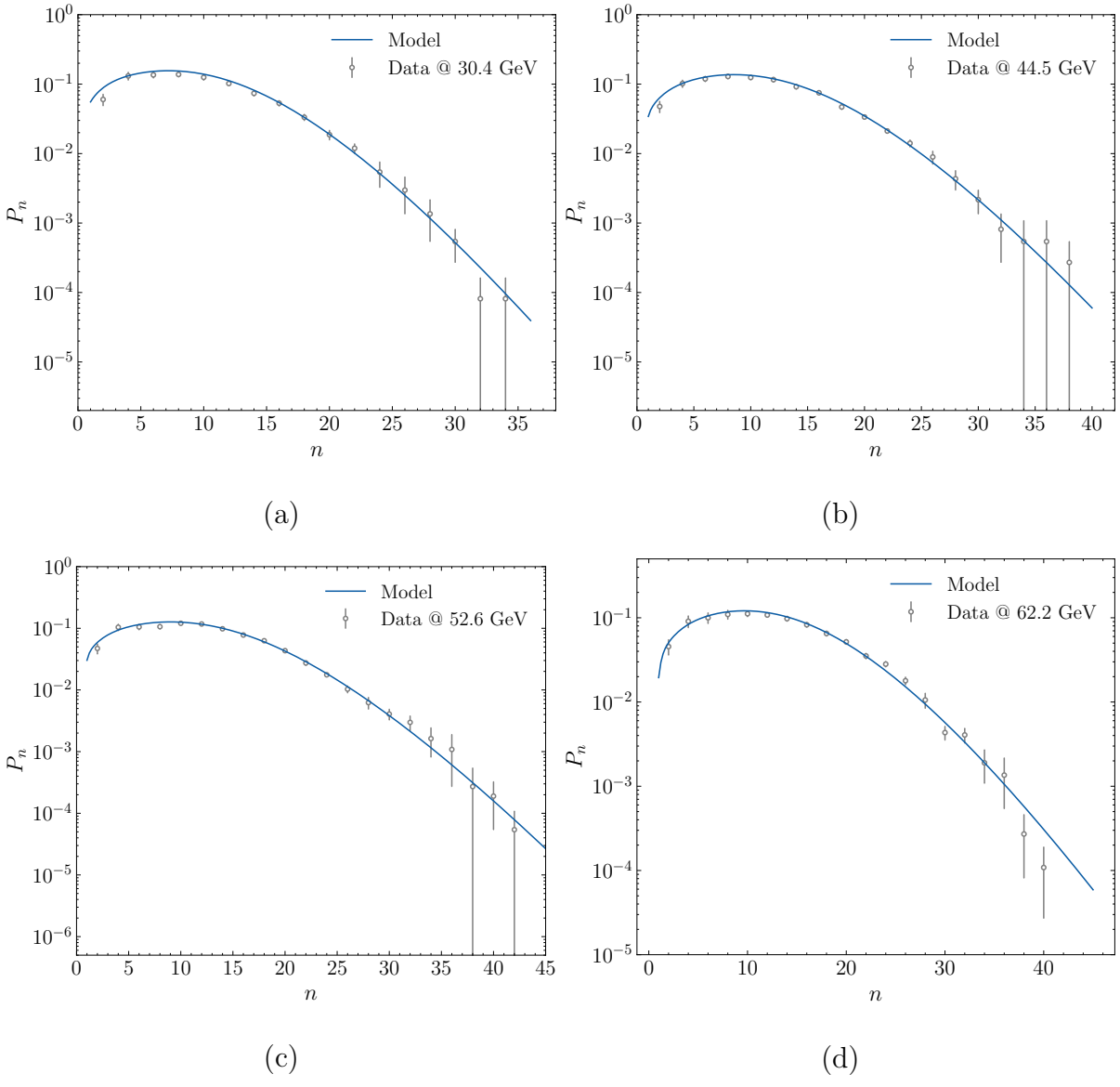

Figure 6.3: Multiplicity distributions for inelastic pp data at $\sqrt{s} = 30.4, 44.5, 52.6$ and 62.2 GeV compared with theoretical expectations.

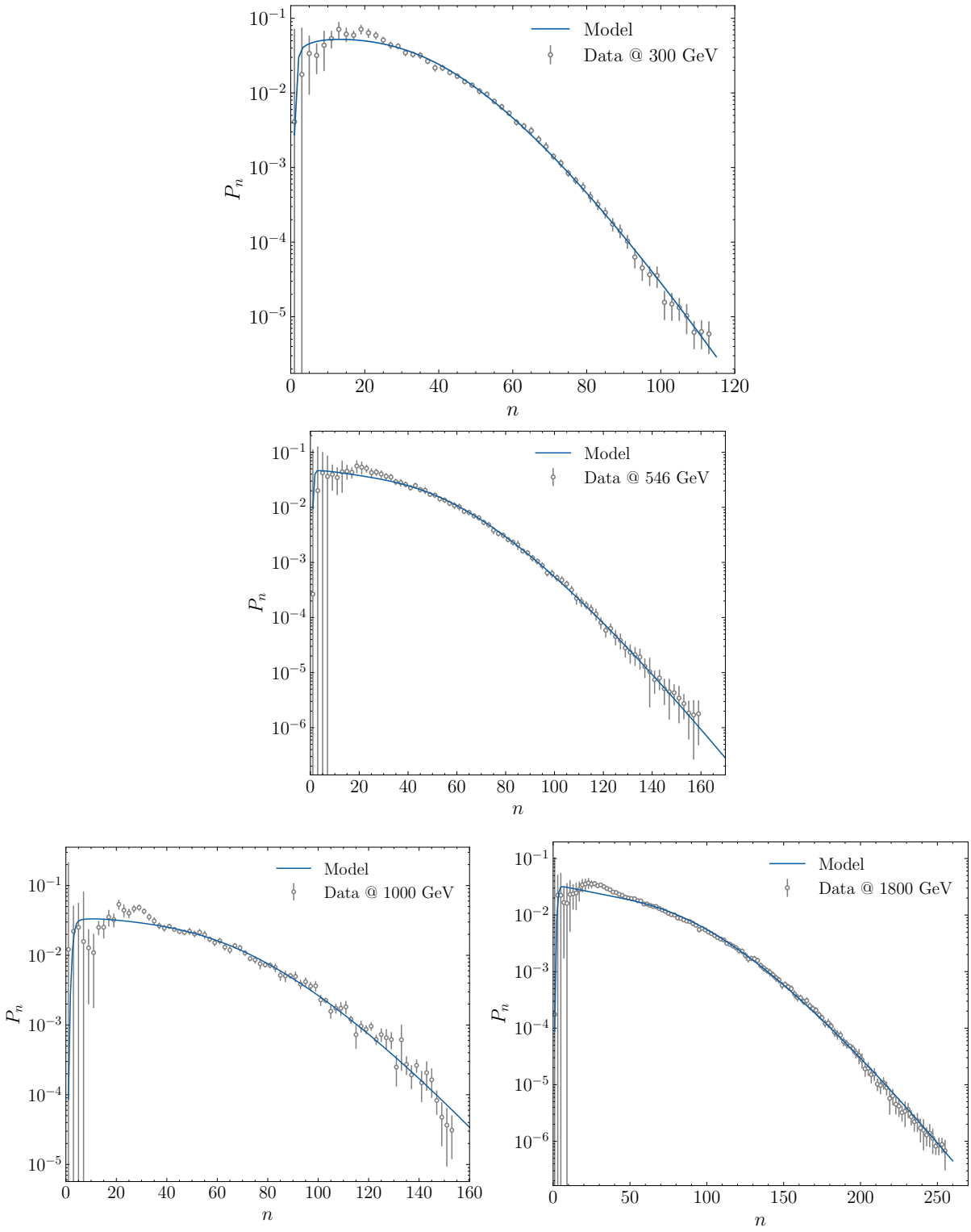

Figure 6.4: Multiplicity distributions for inelastic $\bar{p}p$ data at $\sqrt{s} = 300, 546, 1000$ and 1800 GeV compared with theoretical expectations.

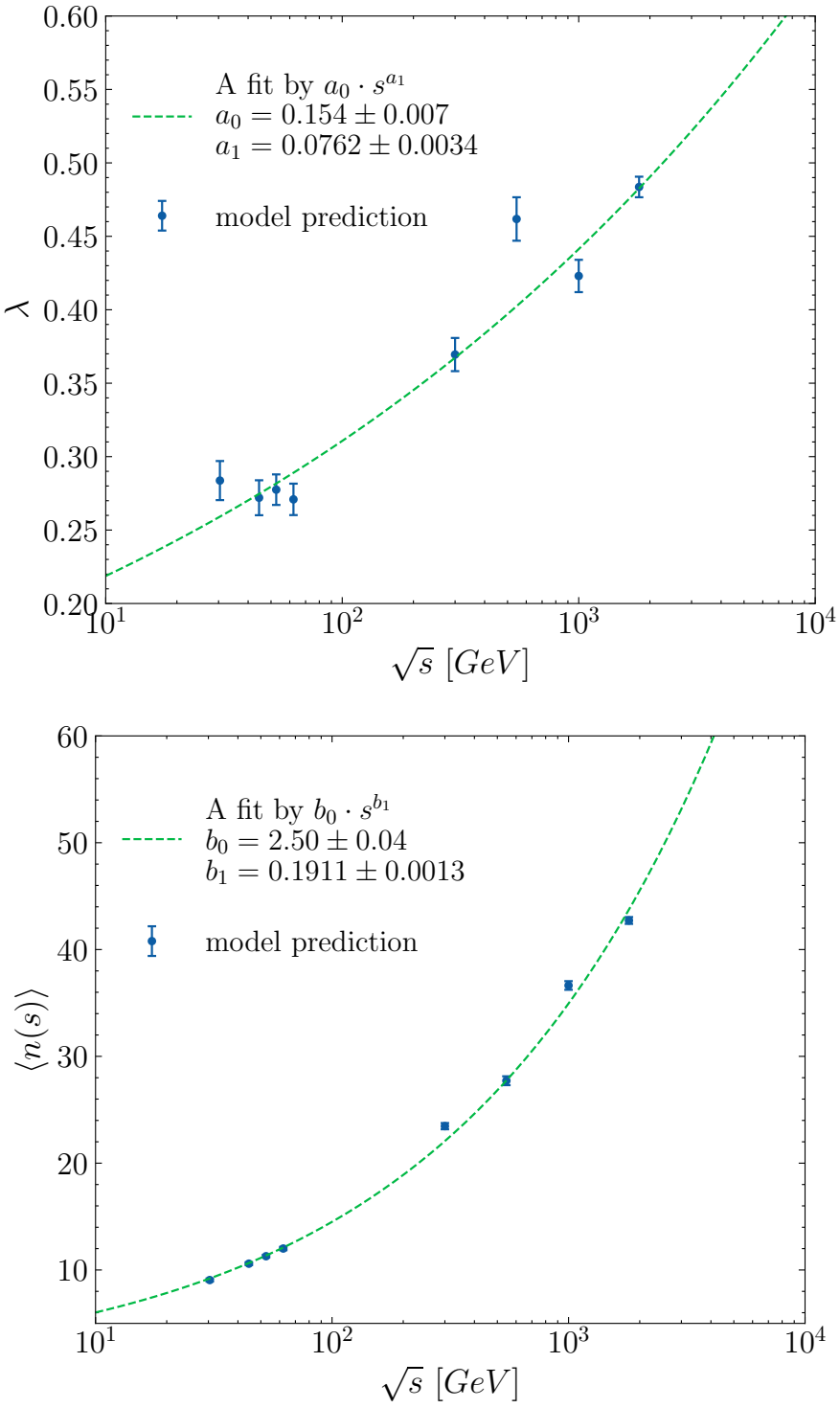

Figure 6.5: The energy dependence of the parameter λ (left panel) and the mean multiplicity (right panel)

Similarly, the estimates for the average multiplicity of hadrons at LHC energies can be derived. As depicted in Figure 6.5 (right panel), this parameter exhibits a rapid increase with the energy s, and its energy dependence can be consistently described using this function:

$$\langle n(s)\rangle = b_0\ s^{b_1}, \tag{6.22}$$

where the values of b_0 and b_1 are 2.5 and 0.1911, respectively. These coefficients were determined through a rigorous χ^2 analysis. Hence, by using this dependence, one can determine the values of $\langle n(s)\rangle$ at 7 and 14 TeV, as illustrated in Table 6.2.

An intriguing aspect of our findings lies in the remarkable accord between our result concerning the energy dependence of the hadron mean multiplicity and that obtained by Troshin and Tyurin with their model for multi-particle production with antishadowing [129], adding to the growing body of evidence that supports the fundamental principles underlying the U-Matrix approach. This alignment is highlighted by the following equation [129] :

$$\langle n(s)\rangle = 2.328\ s^{0.201}, \tag{6.23}$$

This also implies that this approach is highly predictive and can accurately describe and interpret multi-particle production in different energy regimes. Besides, we should emphasize that the power-law energy dependence of the hadron mean multiplicity is often regarded as a prominent feature observed in different models and consistent with experimental data from heavy ion collisions [34, 124] and this alignment in results further reinforces this assumption.

Having tuned our model with all parameters obtained from the best fits, we can now rely on its potential extrapolations to novel collision energy regimes and investigate various phenomena, such as the KNO scaling violation and the correlation of final state particles, as will be presented in the subsequent sections.

6.2.4.3 KNO scaling violation

Using our model, the KNO scaling violation was also examined. The predictions for the full-phase space multiplicity distribution in $p + p(\bar{p})$ collision, in KNO form at various energies, spanning from ISR to LHC ones, are displayed in Fig. 6.6 and Fig. 6.7.

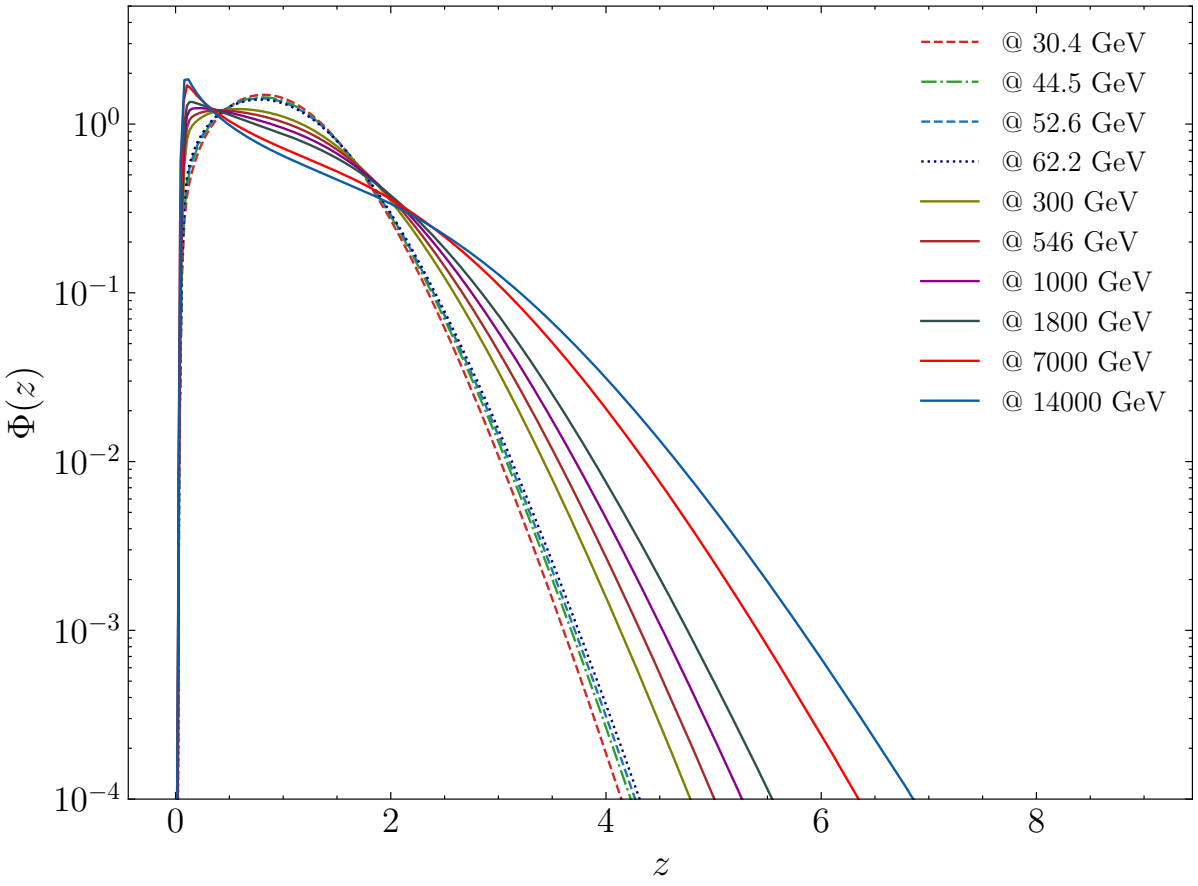

Figure 6.6: Logarithmic view of the multiplicity distributions from ISR to LHC energies in full-phase space.

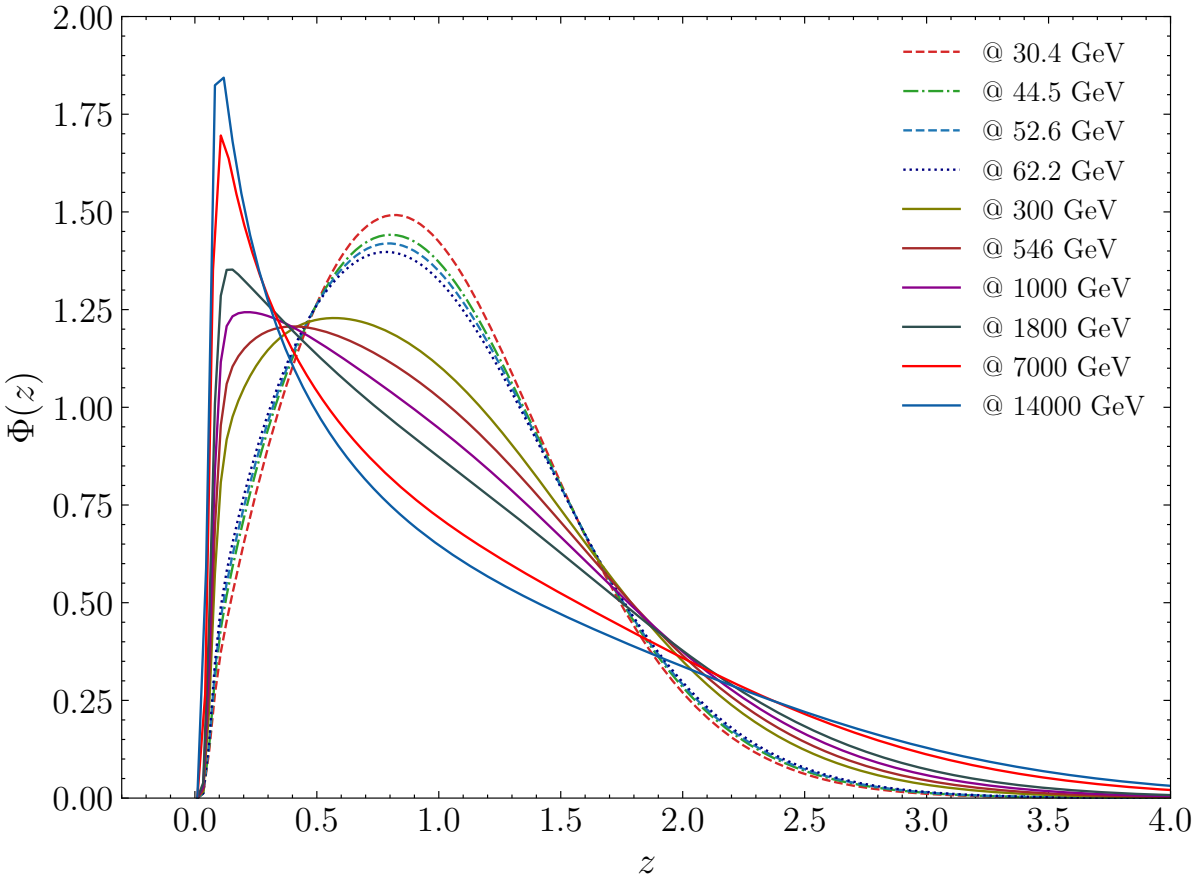

Figure 6.7: The multiplicity distributions from ISR to LHC energies in full-phase space in a linear scale

Fig. 6.6 with a logarithmic scale shows that the high-multiplicity tail rises with increasing energy. At the same time, by looking at the Fig. 6.7 with a linear scale along with a zoom into the low-multiplicity region we can see that the maximum of the distribution shifts towards smaller values of z.

This interpretation demonstrates the dynamic behaviour of the system, especially as the energy level rises, and further validates the violation of the KNO scaling. Interestingly, we can also see that beyond the ISR energy range, the width of the distribution gets larger with increasing energy, which underscores the strong violation of the KNO scaling. It is worth noting that this finding resonates with experimental observations [89].

Most importantly, based on the picture that KNO scaling violation is an extension of geometrical scaling violation, we can also claim that the strong violation of the former stems from the strong violation of the latter, emphasizing the interconnected nature of these phenomena within the U-matrix representation and stressing the latter's pivotal role in describing collision geometry and the processes of multi-particle production in hadron collisions.

To further illustrate the role of the U-matrix scheme, we examined the average number of particles $\langle n(b,s)\rangle$ as a function of impact parameter b for various collision energies, as its pattern offers insights into the collision geometry and the distribution of particles in the transverse plane. The result is illustrated in Fig. 6.8. Based on this figure, it is clear that, at central collision, $(b = 0)$, the magnitude of the average number of particles increases with increasing energy. This is quite anticipated since central collisions yield more produced particles than peripheral collisions [137]. This trend causes the tail of the multiplicity distribution to extend to higher values and eventually to a broader distribution as energy increases, indicating the possibility of rare high-multiplicity events.

A possible explanation for the broadening of the multiplicity distribution might be related to the effect of using the U-matrix scheme. Indeed, as previously illustrated in Fig. 6.1, the disparity found between the eikonal and U-matrix schemes is noticeable at the central impact parameter, where the overlap of hadronic matter distributions is greater with the latter scheme. This discrepancy not only influences the inelastic overlap function, and hence the overall magnitude of multiplicity, but it also has a significant impact on the tail of the multiplicity distribution.

In addition, irrespective of the energy level, the average number of

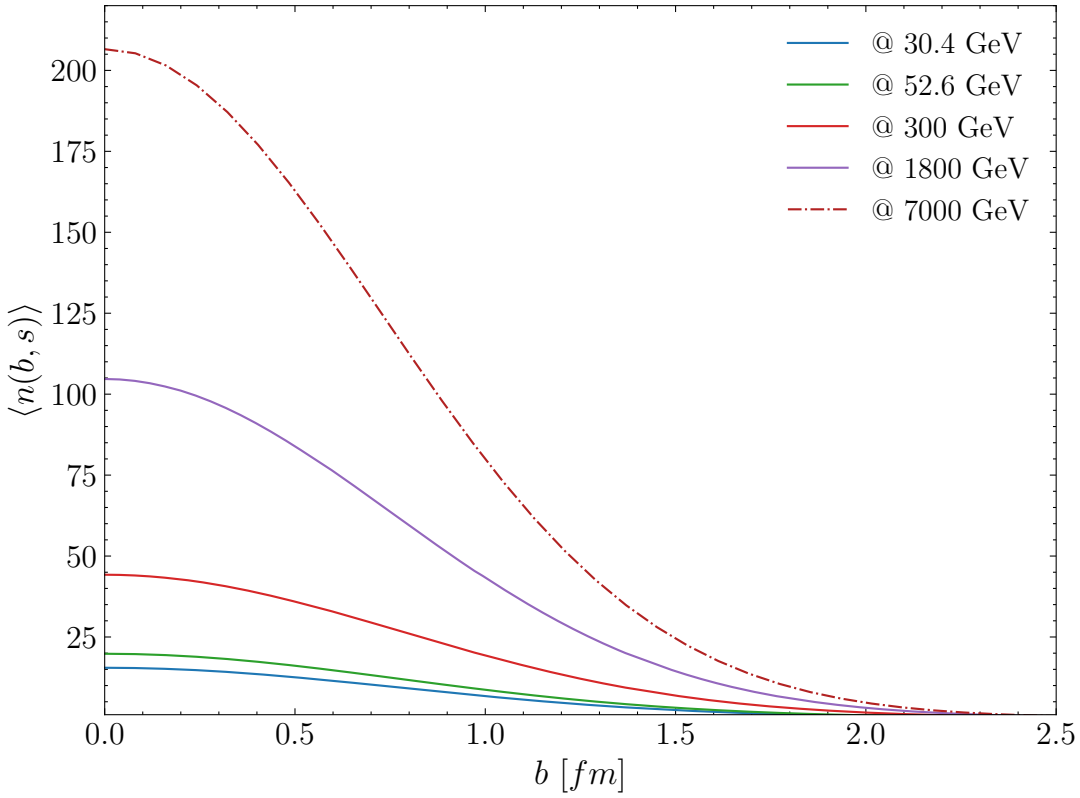

Figure 6.8: The energy dependence of the average multiplicity in the impact parameter space.

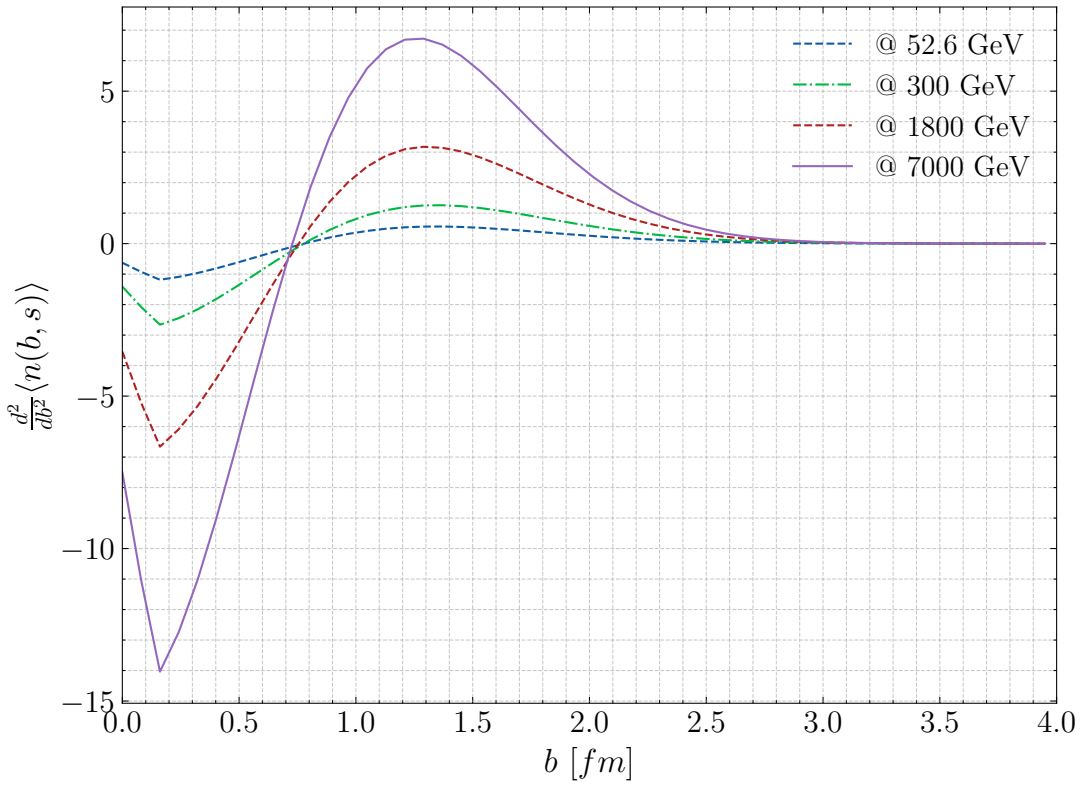

Figure 6.9: Second derivative of the average multiplicity in the impact parameter space

particles generally decreases as the impact parameter b increases, which eventually leads to a decrease in the magnitude of the multiplicity distribution. This phenomenon aligns with the notion that larger impact parameters lead to less violent collisions, resulting in events with smaller multiplicities [137].

Furthermore, as Fig. 6.8 manifests, the average number of particles is energy-dependent, increasing with higher collision energies at each impact parameter. This behaviour is also expected in high-energy physics experiments, where higher energies often result in increased particle production [89].

Fig. 6.8 shows that the curvature of the average number of particles changes, at a specific impact parameter, regardless of the energy level. More quantitatively, we show the second derivative of the average number of particles as a function of the impact parameter in Fig. 6.9, illustrating a change of sign of this function which demonstrates the existence of an inflection point at exactly 0.7 fm. This change in the curvature could signify a shift in the particle production behaviour. For instance, at this specific impact parameter value, there might be a change in the interaction dynamics or the nature of the collision process. It should be noted that this result is in line with what has been reported in [36], where the inflection point was roughly estimated to be at around 1fm. The fact that the inflection point is specifically at around 1 fm suggests that there is something unique or significant about collisions occurring at this distance. This could be related to the characteristics of the colliding particles or the structure of the hadrons involved. This common behaviour underscores the notion of the critical phenomenon in hadronic interactions [93].

On the whole, the shape of the multiplicity distribution is influenced not only by the impact parameter and collision energy but also by the unitarisation scheme, particularly the U-matrix, which reinforces our claim that this distribution is scheme-dependent, as outlined in the introductory section. Besides, the tail of the multiplicity distribution gives insights into the rare but significant events that constitute the overall dynamics of high-energy collisions and hence highlights the importance of this scheme in multi-particle production processes.

In light of this result, the U-matrix scheme may prove to be a significant alternative for addressing multi-particle production challenges at ultra-high energies, including the muon puzzle in cosmic ray interactions at this energy level. In situations such as these, where extreme conditions and

rare events are likely to play a significant role, scheme-dependent effects on multiplicity distribution become relevant.

Having said that, it is vital to consider this scheme in enhancing the existing hadronic interaction models to tackle several lingering issues in high and ultra-high energy physics. However, this is beyond the remit of this study.

6.2.4.4 Hadronic multi-particle correlations

Now that we have estimated the multiplicity distribution P_n across various energies, it seems appropriate to characterize it in an attempt to obtain a better understanding of the dynamics of the particle production process in hadron collisions. In order to fulfil this purpose, the normalized ordinary higher-order moments ($q > 2$) of this distribution are analyzed. Technically speaking, P_n's moments of order q are defined as follows:

$$C_q = M_q/M_1^q, \tag{6.24}$$

and

$$M_q = \sum_{n=0}^{\infty} n^q P_n, \tag{6.25}$$

Our results, along with their comparison with the experimental data [1], are given in Table 6.3 and illustrated in Fig. 6.10 and Fig. 6.11.

Based on Fig. 6.10 and Fig. 6.11, we can see that, as energy levels rise, our proposed model predicts a gradual increase in the ordinary higher-order moments, represented by C_2, C_3, C_4, and C_5. Surprisingly, while our predictions match with the data points within the ISR energy range, it is clear that the model overestimates the fluctuations and correlations in the multiplicity distribution with rising energy, notably above LHC energy. In order to further illustrate this overestimation, we computed the f_2 moment (or the two-particle correlation parameter), as a means of examining the correlation between pairs of particles during a collision event, which is defined by the following formula :

$$f_2 =< n(n-1) > - < n >^2 \tag{6.26}$$

Interestingly, as illustrated in Fig. 6.12, there is a noteworthy and sudden increase in the two-particle correlation parameter versus the average

[1] see compilation in [37]

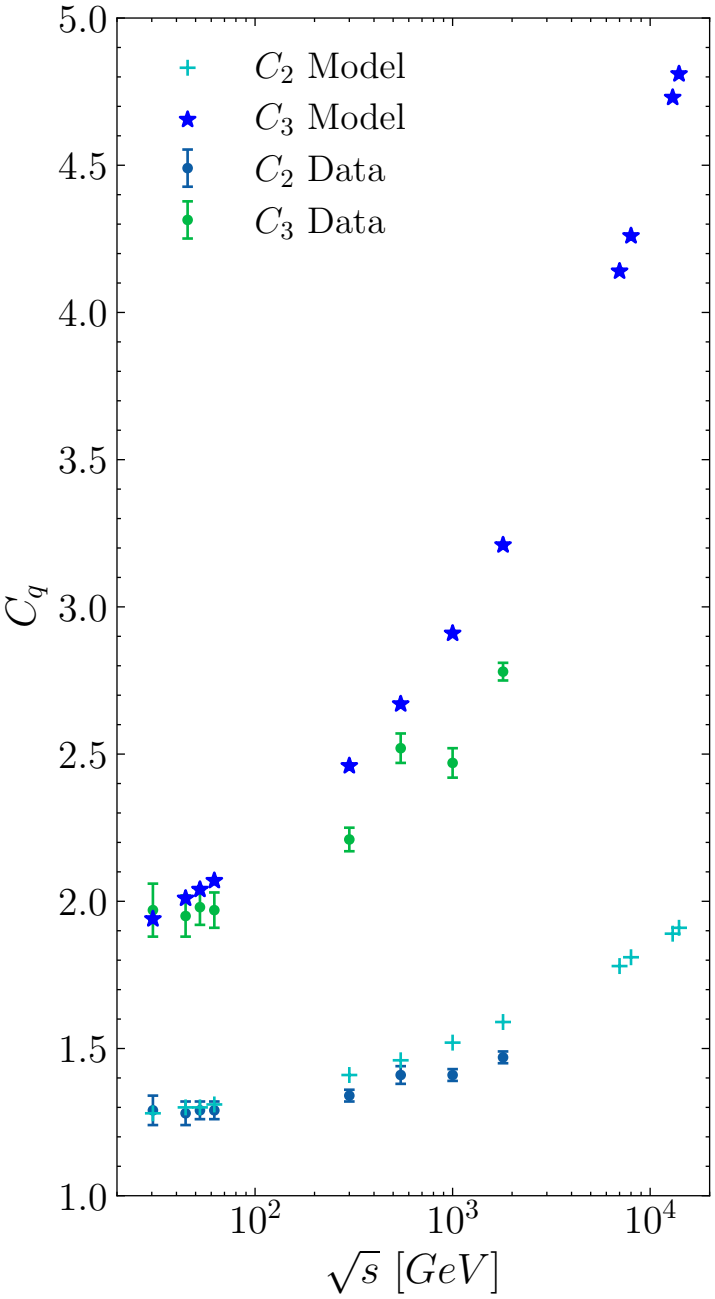

Figure 6.10: Experimental and Theoretical C_q moments, q = 2, 3.

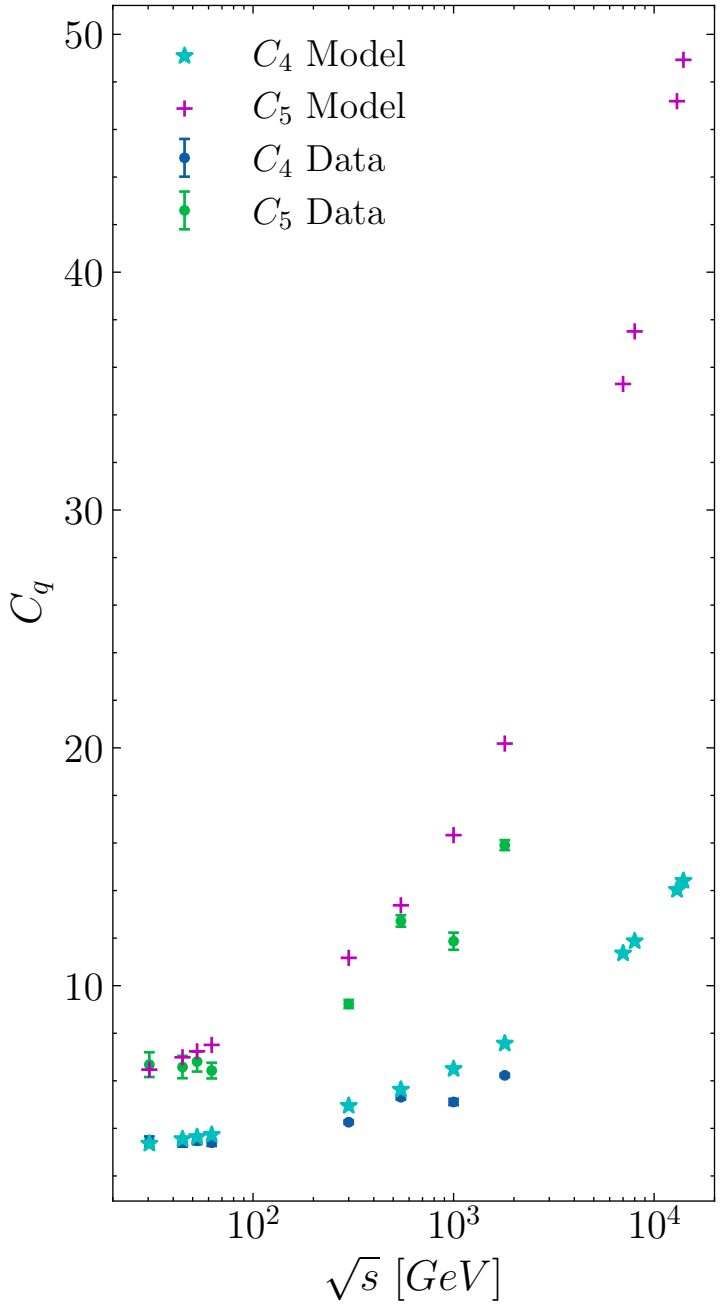

Figure 6.11: Experimental and Theoretical C_q moments, q = 4, 5.

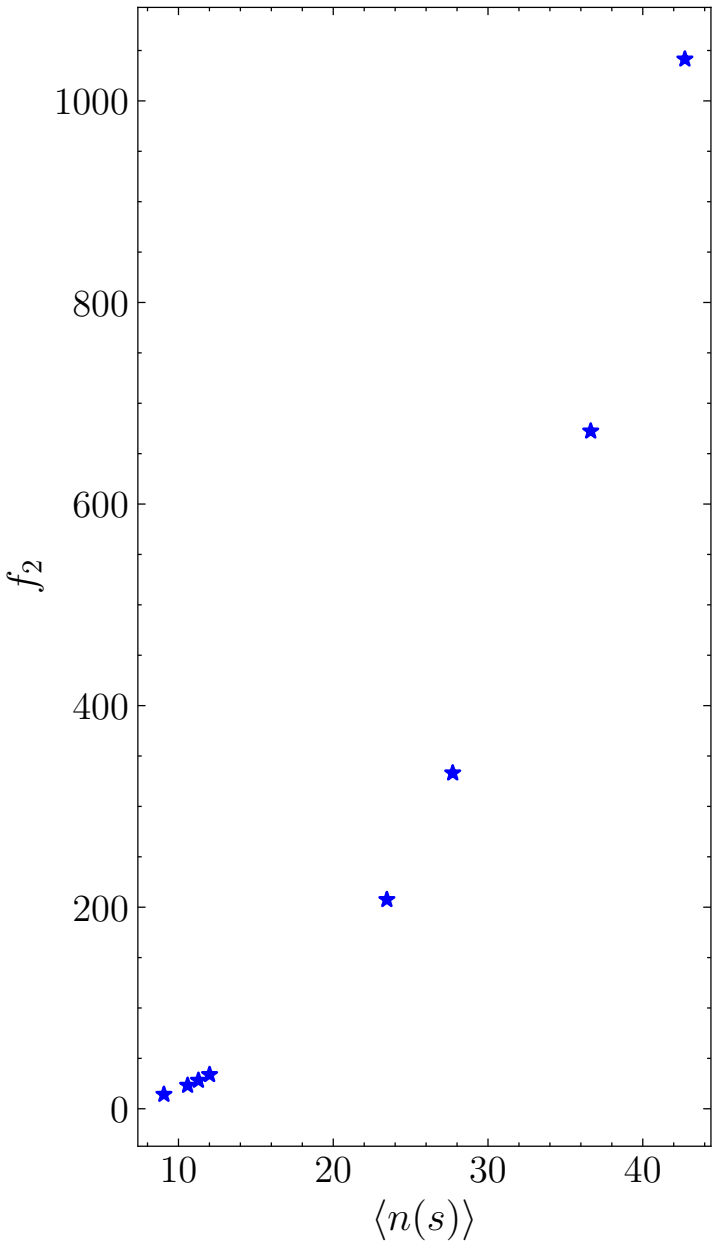

Figure 6.12: f_2 moment versus the average number of produced particles.

$\sqrt{s}$ $[GeV]$	C_2	C_3	C_4	C_5
30.4	1.29 ± 0.05	1.97± 0.09	3.45 ± 0.21	6.68 ± 0.52
	1.28	1.94	3.36	6.47
44.5	1.28 ± 0.04	1.95± 0.07	3.40 ± 0.17	6.58 ± 0.47
	1.3	2.01	3.55	6.99
52.6	1.29 ± 0.03	1.98± 0.06	3.48 ± 0.15	6.81 ± 0.42
	1.3	2.04	3.64	7.24
62.2	1.29 ± 0.03	1.97± 0.06	3.40 ± 0.14	6.43 ± 0.33
	1.31	2.07	3.73	7.51
300	1.34 ± 0.02	2.21± 0.04	4.26 ± 0.07	9.23 ± 0.17
	1.41	2.46	4.95	11.17
546	1.41 ± 0.03	2.52± 0.05	5.31 ± 0.10	12.72 ± 0.24
	1.46	2.67	5.63	13.38
1000	1.41 ± 0.02	2.47± 0.05	5.11 ± 0.13	11.87 ± 0.36
	1.52	2.91	6.5	16.33
1800	1.47 ± 0.02	2.78± 0.03	6.23 ± 0.07	15.91 ± 0.21
	1.59	3.21	7.57	20.18
7000	1.78	4.14	11.36	35.3
8000	1.81	4.26	11.87	37.51
13000	1.89	4.73	14.03	47.19
14000	1.91	4.81	14.41	48.93

Table 6.3: C_q Moments: experimental data with error bar and theoretical predictions. Data points are from [37]

number of produced particles, indicating the existence of strong correlations among the charged particles. Consequently, we can infer that the model incorporates correlations in the final state, despite being constructed on the basis of independent particle production. So the question that arises is where this correlation emerges from. As the overall hadronic multiplicity distribution is constructed by summing contributions from parton–parton collisions occurring at each impact parameter weighted by the inelastic overlap function, this overestimation of correlation is linked to the weight in this superposition model, and hence to the unitarisation scheme, in

comparison with the predictions provided by an eikonal geometrical independent string model [37].

Our model's outcomes of a pronounced KNO scaling violation, together with the unexpected overestimation of the fluctuations and correlations with increasing energy, can potentially be attributed to statistical fluctuations. Hence, we may claim that in this U-matrix representation, pomeron exchange may involve more intricate dynamics, such as collective effects, non-perturbative QCD dynamics, or other interactions, leading to different statistical fluctuations beyond a simple Poissonian eikonal summation [47].

6.2.5 Conclusions

The first part of the results' section was concerned with the description of the geometrical scaling violation. In fact, the energy evolution of the elastic-to-total cross-section ratio was investigated using both the eikonal and U-matrix schemes. The results have revealed that when energy rises, this ratio increases non-linearly and more rapidly with the U-matrix scheme than with the eikonal, implying a stronger violation of the geometrical scaling. This pronounced violation was understood in terms of the divergence in the behaviour of the inelastic overlap function, particularly at the central impact parameter, where the magnitude of this function is greater with the U-matrix scheme than the eikonal, regardless of the energy level.

The second part of the results' section was devoted to the hadronic multiplicity distributions. Our model was tuned and all parameters were obtained from the best fits to various hadronic multiplicity distributions data over a wide range of energies. It has been found that the present model provides a reasonable description of the different multiplicity distributions at each energy. Interestingly, our findings about the energy dependence of the hadron mean multiplicity agree well with Troshin and Tyurin's analyses of the multiparticle production in the antishadowing model [129]. This agreement adds to the growing body of evidence supporting the fundamental principles underlying the U-Matrix approach, which ensures reliable extrapolations to novel collision energy regimes.

Based on our model, the KNO scaling violation was investigated as well. Our results, related to the behaviour of the tail, as well as the maximum of the multiplicity distribution, and especially to the strong KNO scaling violation, are in line with the experimental findings [89].

The broadening of the multiplicity distribution has been also confirmed with the behaviour of the particles' distribution in the transverse plane at various collision energies. Besides, the interesting finding of an inflection point in the average number of particles' curve irrespective of the energy level, corroborates with another finding (ref) and highlights the concept of a critical phenomenon in hadronic interactions.

Besides, the normalized ordinary higher-order moments ($q > 2$) of the multiplicity distribution were analyzed. Another surprising result was related to our model's overestimation of the fluctuations and correlations in the multiplicity distribution as energy rises, notably above LHC energy. It is argued that this overestimation, is linked to the weight in this superposition model, and hence to the unitarisation scheme. It should be noted that the shape of the hadron multiplicity distribution is influenced not only by the impact parameter and collision energy but also by the unitarisation scheme, particularly the U-matrix.

On the whole, the results of this study, such as those related to the strong geometrical scaling violation and its resultant pronounced KNO scaling violation, coupled with the overestimation of the charged particles' correlation, can potentially be attributed to statistical fluctuations inherent in the U-matrix scheme. Hence, we may argue that in this U-matrix representation, pomeron exchange may involve more intricate dynamics, leading to different statistical fluctuations beyond a simple Poissonian eikonal summation.

As any research, this study is not without limitations. For instance, the assumption that each created string has an equal probability of turning into a pair of charged hadrons is acceptable but only as a first approximation. To refine the present model for a more reliable description, we can consider the introduction of charged particle correlations in the final state by incorporating, for example, string fusion, overlapping processes, or other interactions leading to correlated string dynamics as evidenced by theoretical predictions [39] and experimental observations [126]. Additionally, it is important to investigate the impact of the implicit different statistical fluctuations in pomeron exchanges within the U-matrix representation, along with the correlation and/or collective behaviour in the production of final state particles.

The study concludes by proposing the U-matrix scheme as a noteworthy alternative for tackling challenges related to multi-particle production in hadron collisions, especially in scenarios where extreme conditions and rare

events play a significant role in high and ultra-high energy physics. It also prompts an inquiry into the fundamental nature of pomeron exchange within the U-matrix scheme in comparison to the eikonal, despite that both schemes verify the unitarity constraint principle.

RO would like to thank Jean-René Cudell for his invaluable comments. RO also appreciates the insightful discussions with Paulo Cesar Beggio and Emerson Luna. Special thanks go to the computational resource provided by Consortium des Équipements de Calcul Intensif (CÉCI), funded by the Fonds de la Recherche Scientifique de Belgique (F.R.S.-FNRS) where a part of the computational work was carried out.

6.3 Further results

In this section, we present additional insights into the behavior of the normalized moments C_q at different LHC energies. We observe that the moments at higher energies, specifically at 13 TeV, are notably larger compared to those at lower energies such as 7000 GeV. This increase may be explained by the enhanced contribution of mini-jets, as well as the onset of saturation effects, which are expected to become more significant at higher energies. These phenomena are anticipated to be particularly pronounced in heavy ion collisions, where the larger number of parton interactions could play a key role. While our current model focuses on proton-proton collisions, future studies will extend this analysis to heavy ion collisions.

From Table 6.3, we have the following normalized moments C_q:

Comparison from Lower LHC Energies (example: 7000 GeV) to higher LHC energies (example: 13 TeV):

- C_2 increases from 1.78 to 1.89
- C_3 increases from 4.14 to 4.73
- C_4 increases from 11.36 to 14.03
- C_5 increases significantly from 35.3 to 47.19.

In addition, one might wonder about the value of the K parameter if it were left free in the fit and how this would affect the predictions at LHC energies. To address this, we analyze the results of the fits with the K parameter released. As can be seen from the Fig. 6.14, the shape parameter k of the elementary multiplicity distribution generally shows

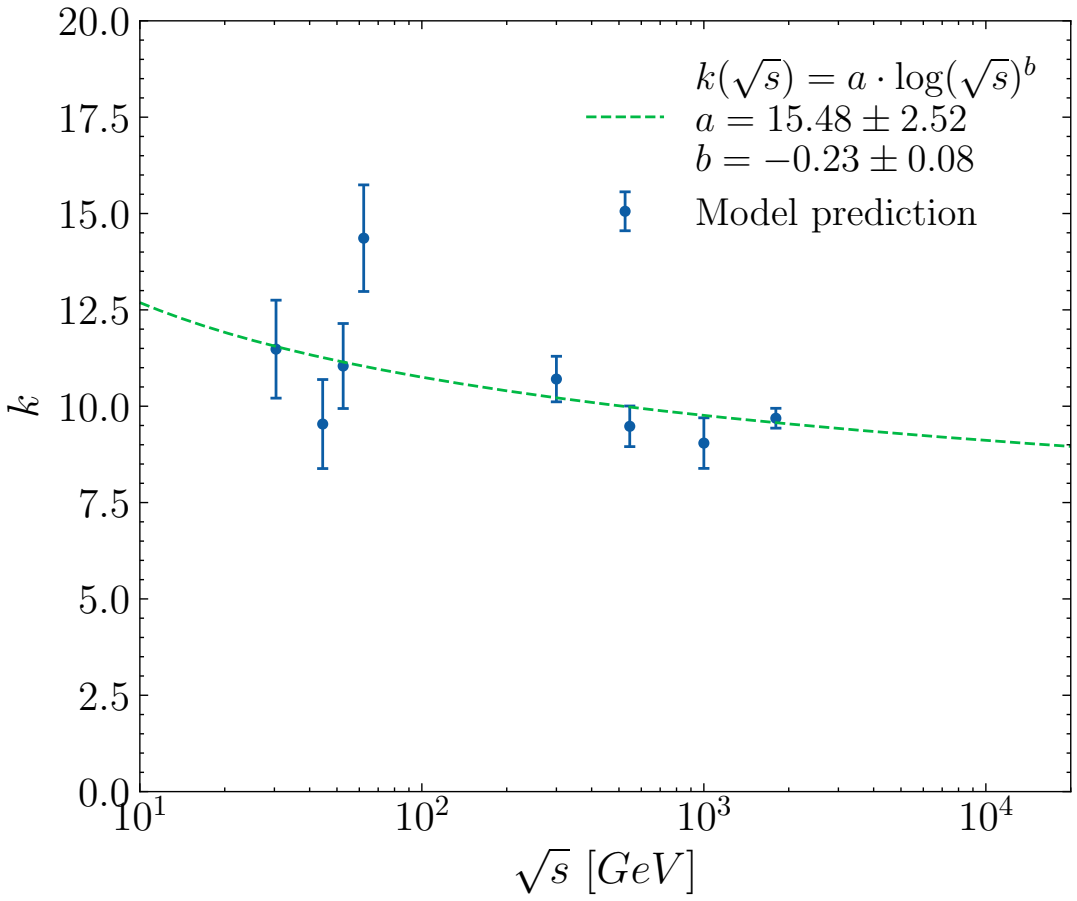

Figure 6.14

a trend of decreasing with increasing energy, particularly noticeable from lower to higher energy ranges. This decrease in k can be described by the following function, which was obtained by a chi-squared fitting to the k values derived from the model fitting:

$$k(\sqrt{s}) = a \cdot \ln(\sqrt{s})^b \tag{6.27}$$

where $a = 15.48 \pm 2.52$ and $b = -0.23 \pm 0.08$.

Note that the two other parameters of the model, namely the hadron mean multiplicity and the λ parameter, are almost insensitive to this change, as shown in the Fig. 6.16 and Fig. 6.18 with their best-fit functions, and Fig. 6.20 illustrates the predictions of the fits at LHC energy in this case.

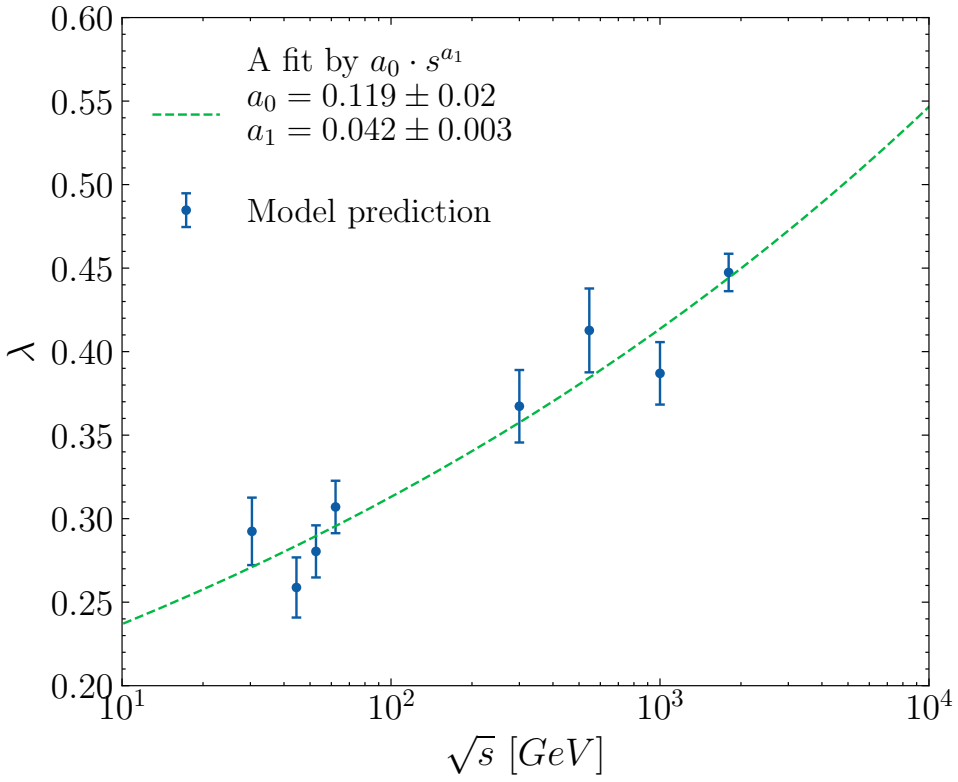

Figure 6.16

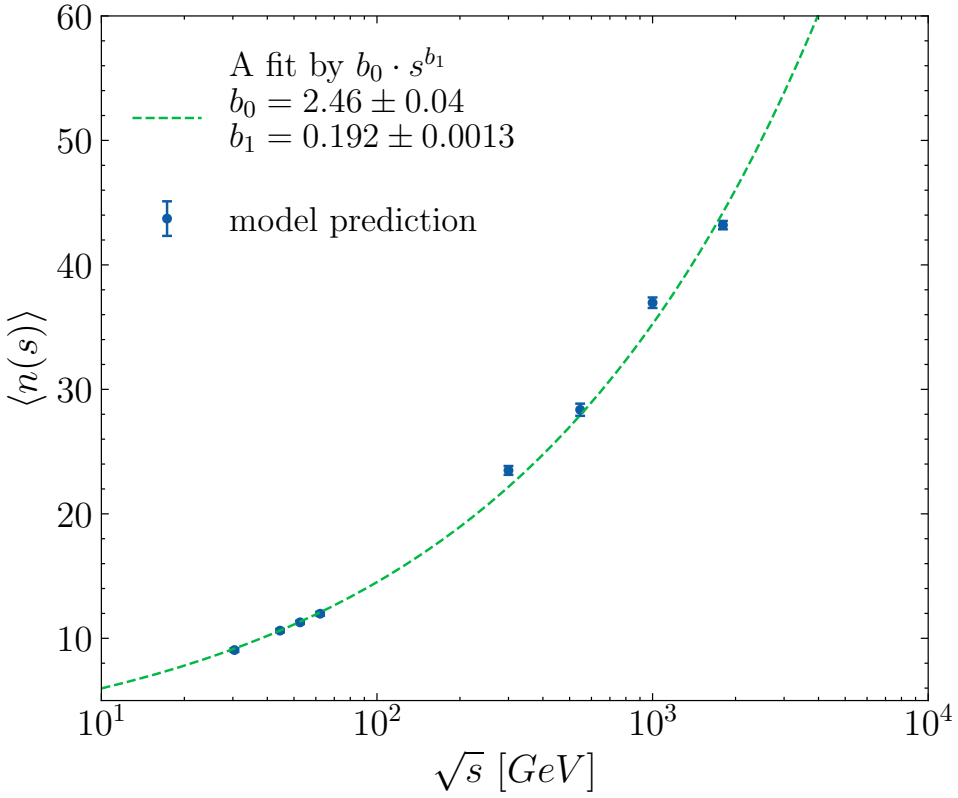

Figure 6.18

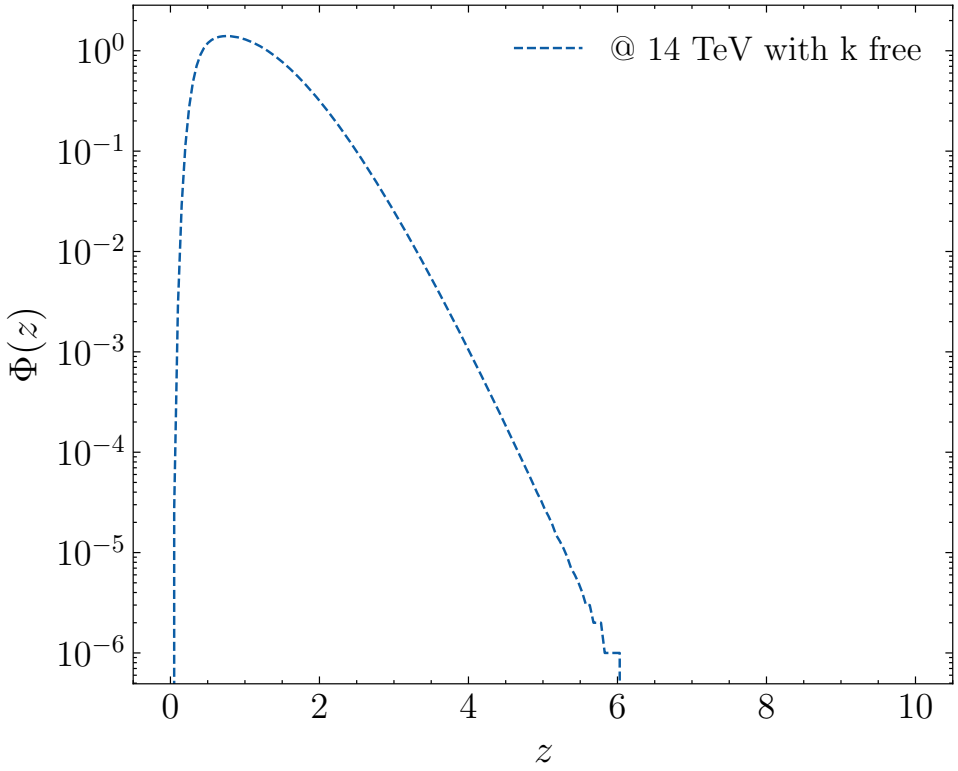

Figure 6.20

It is worth noting that the differences observed at different $\sqrt{(}s)$ indeed have implications for cosmic ray data, particularly concerning particle production rates and energy distribution. Specifically, the observed increase in the ratio of elastic-to-total cross-section with energy, notably more pronounced in the U-matrix case compared to the eikonal case, signifies a heightened contribution from inelastic scattering processes. This observation aligns with studies, such as [88], which explore the influence of increasing effective cross-sections for hadron inelastic interactions with rising energy, especially regarding high-energy cosmic ray hadron energy spectrum shape. Fig. 6.22 illustrates the predictions at 13 TeV

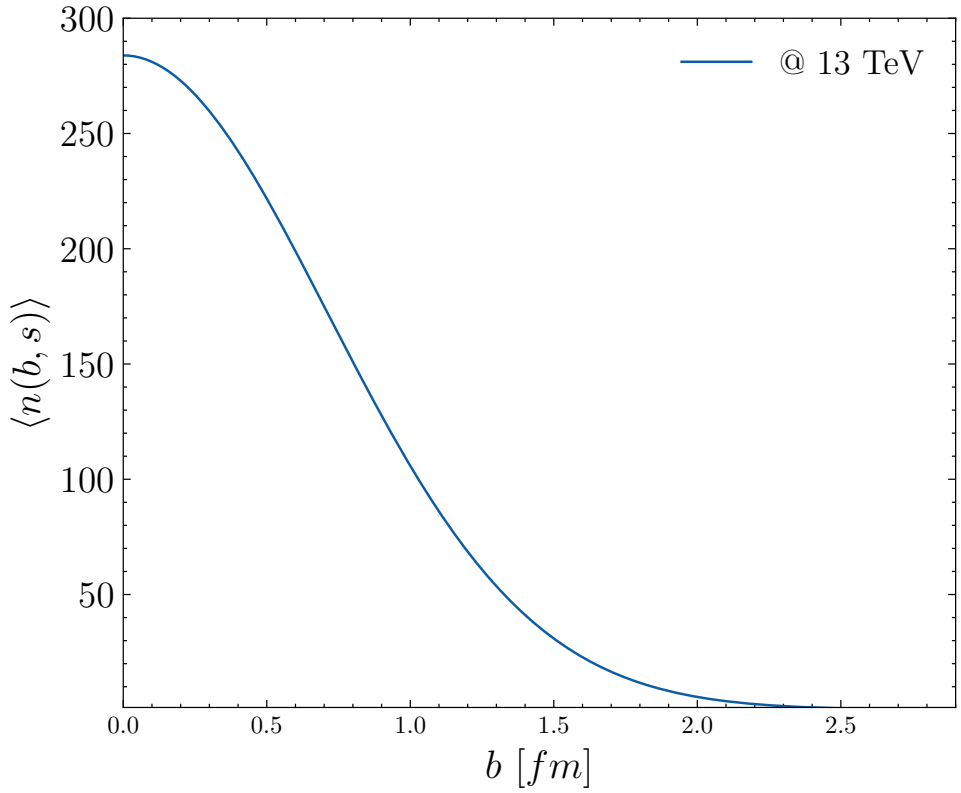

Figure 6.24

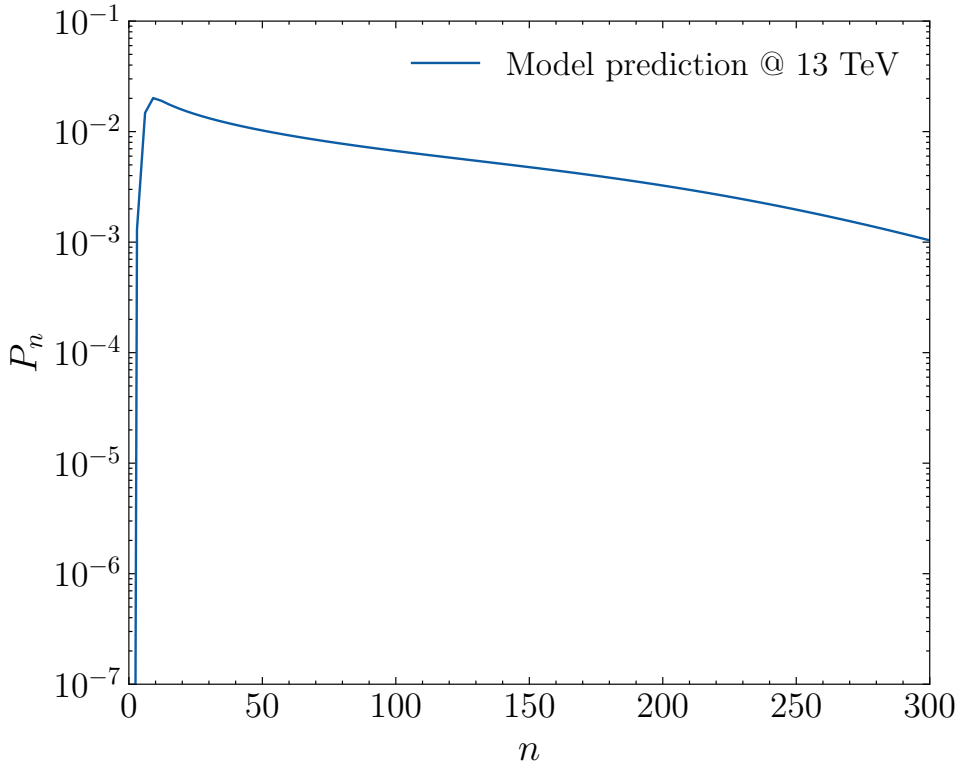

Figure 6.22

The Fig. 6.24 shows a continuous growth of $\langle n(b,s)\rangle$ with energy, partic-

ularly in central collisions, and there are no signs of saturation behavior, such as a slowing down or plateauing of the growth rate of $\langle n(b,s)\rangle$ at higher energies. Based on this observation, we may infer that this trend is more closely related to mini-jet production.

Finally, the physical reason for the inflection point at 0.7 fm could be related to the typical size of the proton. For Pb ions, we anticipate that the inflection point would shift due to their larger size and different internal structure.

7 Multi-pomeron exchange nature

7.1 Context of the work

The findings presented in the previous chapters, especially those showing that, when compared to the eikonal scheme, the U-matrix offers a better description of certain hadronic observables, raise the question about the fundamental nature of pomeron-exchange within the latter scheme, despite that both schemes satisfy the unitarity condition. This has sparked our interest and motivated us to delve deeper into the study of the U-matrix scheme in the context of the Soft QCD processes.

As a matter of fact, the description of the Soft QCD processes, occurring at low momentum transfer which is governed by non-perturbative effects, is not an easy task. This is simply because perturbative QCD strategies are not applicable in this case.

To remedy this, we are compelled to use phenomenological models that hinge on fundamental principles of quantum field theory, such as unitarity, analyticity and crossing, in conjunction with empirical parametrizations.

Hadronization, the process by which the quarks and gluons generated in high-energy collisions turn into hadrons in the final state, is viewed as one of the most significant QCD processes. In fact, several phenomenological models have been used to describe this process; for example, we can cite the string models which have been employed together with the Gribov-Regge theory, like in Sibyll and QGSJET.

In fact, multi-pomeron exchange is crucial to the hadronization process in these string models. More specifically, the color strings are stretched between the projectile and target partons during the first stage. According to the Gribov-Regge theory, the pair of strings' construction corresponds to the cut pomeron. The strings are then hadronized, yielding the observed hadrons.

The Gribov-Regge theory states that the unitarization of the elastic scattering amplitude is the technique by which multi-pomeron exchange is accomplished in order to satisfy the unitarity principle.

One example of satisfying the unitarity principle into these models while

addressing multi-pomeron exchanges is the widely utilized eikonal approximation. Direct and indirect evidence, however, has shown that the eikonal or its extended quasi-eikonal schemes used in these models, while describing some hadronic observables reasonably well, are not sufficient for a comprehensive description of the physics in question, especially in hadron collisions at (ultra-) high energies. Fundamentally, there is no good reason for pomerons to be independent as they are exchanged between composite particles consisting of bound quarks and gluons. As a result, it is theorized that interactions between quarks and gluons may cause pomeron exchanges to be correlated and interdependent.

There are fundamental problems with string models that need to be addressed. The generated particles in these models are thought to originate from the exchanged Pomerons-each composed of two strings. In this approach, the probability of configurations including n string pairs is equal to the probability of exchanging a specific number of these n pomerons, which is Poissonian according to the eikonal scheme.

But for the reasons listed below, this approach is erratic. While all of the pomerons in the Gribov-Regge model are the same, the first and subsequent pairs in the string picture are of distinct nature. Another reason behind the inconsistency is related to the energy sharing between the strings. In fact, energy is properly shared in the string (chain) model, while it is completely overlooked in the Gribov-Regge theory.

Actually, we can claim that the mismatch resulting from the aforementioned inconsistencies is associated with the eikonal scheme since the Gribov-Regge probability is Poisonian.

Indeed, the problems indicated above could be resolved, for instance, by developing a consistent approach that distinguishes between the first string pair and subsequent pairs. To do so, it could be necessary to modify the Gribov-Regge theory in order to differentiate between initial and subsequent Pomerons or to adjust the string model to better fit the uniform treatment in Gribov-Regge theory.

They can also be dealt with by devising a method to include detailed energy sharing among the strings in the Gribov-Regge theory. This could entail mapping the Gribov-Regge probability onto a framework that incorporates energy sharing, or expanding the Gribov-Regge model to include energy distribution among the Pomerons.

In addition, considering an alternative scheme which may provide another probability of the pomerons exchanged, namely the U matrix, could

be another solution to the aforementioned issues.

By taking these possible solutions into consideration , we believe that a more consistent and accurate predictive model for soft QCD processes may be developed.

In this study, we attempted to give a probabilistic interpretation of Pomeron exchange within the U-matrix scheme. In order to achieve this, we employed a spectral representation of Pomeron exchange in perturbative Reggeon field theory, derived from the Kancheli formalism. This allowed us to determine both the Pomeron topological cross-section and the Pomeron multiplicity distribution, irrespective of the unitarization scheme employed. After that, we looked at the pomeron multiplicity distributions' statistical characteristics, especially their moments, to learn more about the correlation between the Pomerons that were exchanged in each scheme. Additionally, we investigated how these Pomeron weights affected the multiplicities in pp collisions and explained how the mismatch between Gribov-Regge theory and string models might be resolved by using the U-matrix technique.

7.2 ARTICLE 5

Pomeron Weights in QCD Processes at High Energy and the S-Matrix Unitarity Constraint

Rami Oueslati

Prepared for submission to PRD

Pomeron Weights in QCD Processes at High Energy and the S-Matrix Unitarity Constraint

Rami Oueslati *
Space sciences, Technologies and Astrophysics Research (STAR) Institute, Université de Liège, Bât. B5a, 4000 Liège, Belgium
(Dated: December 24, 2024)

The pomeron topological cross-section is derived for the eikonal and the U-matrix unitarization schemes using a generalized expansion of the unitarized elastic amplitude in an effort to examine pomeron characteristics, namely the multiplicity distribution, fluctuation, and correlation, and to reveal the impact of pomeron weights on the pp multiplicity distribution. The results demonstrate that the U-matrix inherently incorporates a larger amount of diffraction production into the multi-pomeron vertices, yielding a larger pomerons' variability regardless of the energy range, while such fluctuations become significant only beyond a specific high-energy threshold in the eikonal and quasi-eikonal schemes. Most importantly, our findings indicate that within the U-matrix scheme, an increase in exchanged pomerons results in more pronounced higher-order pomeron correlations, which are affected by the energy and the impact parameter. Interestingly, our outcomes also highlight that the correlated pomeron exchanges within the U-matrix summation play a key role in enhancing multi-parton collisions. In light of these results, we can argue that the U-matrix is fundamentally more valid for theories with growing cross-sections with energy, such as QCD at high energies.

I. INTRODUCTION

In the study of hadronic interactions at high energy, understanding soft QCD processes that occur at low momentum transfer is a daunting task since perturbative QCD techniques are inapplicable and, to date, there is no fundamental theory that underlies these processes. That being said, we can approach them through phenomenological models that are based on fundamental principles of quantum field theory – such as unitarity, analyticity and crossing symmetry, along with empirical parametrizations. In order to improve these models, extensive data comparisons from collider experiments and cosmic-ray air showers are necessary to validate their underlying assumptions and fine-tune their parameterizations.

One of the most important soft QCD processes is Hadronization, which involves the transformation of quarks and gluons produced in high-energy collisions into the observed hadrons. Indeed, this process has been described by a number of phenomenological models implemented in Monte Carlo event generators. For instance, we can cite the Lund string model [1] in conjunction with the Gribov-Regge theory [2], in Sibyll [3] and QGSJET [4]. In these models, multi-pomeron exchanges play a crucial role in the hadronization process. The unitarization of the elastic scattering amplitude allows for their inclusion, with the eikonal approximation being the most commonly used method satisfying the unitarity principle in this context.

In these models, multi-pomeron exchanges play a crucial role in the hadronization process. The unitarization of the elastic scattering amplitude allows for their inclusion, with an eikonal-like unitarisation scheme being the most commonly used method satisfying the unitarity principle in this context. Indeed, the formation of string pairs, which corresponds to cut pomerons in the Gribov-Regge framework, is influenced by the weights of the pomerons. These strings, stretched between projectile and target partons, undergo hadronization, leading to the production of observed hadrons. However, despite the reasonable description of some hadronic observables provided by the eikonal or its extended version the quasi-eikonal, both direct and indirect evidence indicate that these approaches are inadequate for a complete understanding of the physics in question, particularly in hadron collisions at (ultra-) high energies. As such, a more comprehensive approach is necessary to accurately describe the complex dynamics involved in these processes.

In [5], it has been shown that pomeron exchange in an eikonal-like scheme is a Poisson-distributed variable, where the number of exchanged pomerons is statistically independent. From a fundamental standpoint, since pomerons are exchanged between composite particles consisting of bound quarks and gluons, there is no sound reason why they should be independent. Hence, it is hypothesized that pomeron exchanges may be correlated and interdependent as a result of interactions between the quarks and gluons. This raises the question of identifying the appropriate unitarization scheme for such dependent exchanges.

From a phenomenological point of view, modelling problems caused by an eikonal-like unitarization technique are numerous. For instance, it has been demonstrated in [6] that shadow corrections to the rapidly rising contribution of the input supercritical pomeron, which arise from pomeron rescatterings or, equivalently, from considering the survival probability factor, do not resolve

* rami.oueslati@uliege.be

the Finkelstein-Kajantie problem. Consequently, it has been argued that an alternative method for unitarization is necessary.

Another fundamental issue that needs to be addressed relates to string models for hadronization [7]. In these models, the probability of configurations with n string pairs is given by the probability of having n exchanged pomerons, which is a Poisson distribution through the eikonal scheme. Nevertheless, this approach is inconsistent for the following reasons.

To begin with, in the string model, the first pair of quark-antiquark strings and the subsequent pairs are fundamentally different. This distinction arises because the first string pair is formed from the initial quarks of the colliding protons, while the subsequent pairs are typically generated from secondary interactions. These secondary interactions involve different quark content and a different distribution of energy among the strings, with the first string pair generally receiving a larger share of the available energy compared to the subsequent pairs. Conversely, in the Gribov-Regge theory, all elementary interactions -pomerons- are treated as identical. Thus there is no distinction between the initial and subsequent interactions and all pomerons are dealt with statistically uniformly. Additionally, in the Gribov-Regge framework, the energy sharing among the different pomerons is not considered. These inconsistencies result in a mismatch when using the Gribov-Regge pomeron probability distribution for configurations with different numbers of string pairs. Therefore, we can argue that this mismatch is attributed to the eikonal scheme given that the Gribov-Regge pomeron probability is essentially Poisonian and basically defined from the eikonal scheme. Consequently, considering an alternative unitarisation scheme, namely the U-matrix, could be a solution to the aforementioned issues. In fact, throughout the years, various arguments have been furnished in favor of the U-matrix scheme.

For instance, in [8], a phenomenological model based on the picture depicting the KNO scaling violation as an extension of the geometrical scaling violation and using the U-matrix unitarization scheme has been presented within the framework of the geometrical approach in an attempt to describe multi-particle production. In this study, it has been suggested that the U-matrix scheme may serve as a noteworthy alternative for tackling challenges related to multi-particle production in hadron collisions, especially in scenarios where extreme conditions and rare events play a significant role in high and ultra-high energy physics. It also prompts an inquiry into the fundamental nature of pomeron exchange within the U-matrix scheme in comparison to the eikonal, despite that both schemes verify the unitarity constraint principle.

In another study [9], owing to the fact that correlations could arise from hadron fluctuations in various diffractive configurations, a multi-channel model was introduced to better describe diffractive cross-sections by enhancing these hadron fluctuations. This model has shown that U-matrix unitarization is likely incompatible with the assumption of uncorrelated pomeron exchange, primarily because the findings are independent of the details of the diffractive states.

In addition, the rational form of unitarization (e.g., the U-matrix) has long been supported by arguments based on the analytical features of the scattering amplitude. It has been demonstrated that, in contrast to the exponential form of unitarization (e.g., the eikonal), this type of unitarization far more easily replicates correct analytical characteristics of the amplitude in the complex energy plane [10]. Moreover, much research (e.g., [8, 11]) has highlighted the efficacy of the rational form in offering a more accurate description of the underlying physics in hadronic collisions at high energy.

At ultra-high energy, it has been shown that the eikonal causes problems in describing the data obtained from cosmic-ray air showers. Indeed, the development of air showers can be significantly affected by diffractive collisions [12]. For example, based on the predictions of MC simulations, it has been revealed that diffractive collisions have an impact on the prediction of observables in ultra-high energy cosmic ray experiments, such as the depth of the maximum of the shower development X_{max} and the depth of the maximum of the muon productions in an air shower X^{μ}_{max}. As it has been revealed in [13] the single diffractive data preferred the U-matrix scheme over the eikonal, particularly at ultra-high energy. Switching from the commonly used eikonal in these MC simulations could hence reshape our understanding of cosmic-ray physics.

Overall, selecting the appropriate elastic scattering amplitude unitarisation is primordial in high-energy hadron scattering, particularly for various phenomenological models and generators. Indeed, multi-pomeron exchange weights considerably impact high-energy hadron amplitudes, thereby directly affecting hadron process cross-sections. This includes the energy-dependent growth pattern of inclusive cross-sections and the shape of produced particle multiplicity distributions [14, 15].

The study set out to understand the nature and role of pomeron exchanges in the U-matrix scheme in comparison to an eikonal-like one. It also aims to shed light on the impact of the pomeron weights for QCD processes.

This work is organized as follows. In the next section, we will outline the theoretical framework of the pomeron vertices in Gribov-Regge theory, along with a detailed review of the generalized representation of the unitarized elastic scattering amplitude, as proposed by Kancheli. Section III will present and thoroughly discuss the results. Section IV will summarize the main findings and implications of the study.

II. POMERONS VERTICES IN GRIBOV-REGGE THEORY

Unitarization in the Gribov-Regge theory [2] is accomplished by summing the contributions from all multi-reggeon exchanges. Using this method, the Reggeon vertices, referring to the coupling between the exchanged Reggeons and the external particle, are used to calculate the amplitudes for multi-Reggeon exchanges and their values determine the weights of the n-reggeon exchange. It is worth noting that it is difficult to compute the values of these vertices from first principles. In fact, from a phenomenological procedure, they are parameters determined by fitting to experimental data using some functional form. However, as previously stated in the first section, there is no specific reason to assume that these weights should adhere to the simple Glauber-eikonal form. Therefore, a more thorough treatment of them is needed. In [16], the structure of these multi-pomeron vertices has been analyzed and generalized to take into account more complex interactions, specifically the contribution from diffraction production in the weights of multi-reggeon exchange. In this section, the formalism put forth in [16] will be thoroughly reviewed as it lies the theoretical foundations for our objectives.

We begin with the expression of the unitarized elastic hadronic amplitude represented as follows :

$$F(s,t) = \sum_{n=1}^{\infty} F_n(s,t), \tag{1}$$

with the n Reggeon exchange amplitude given by :

$$F_n(s, t \simeq -k_\perp^2) = \frac{-i}{nn!} \int N_n^2(k_{\perp i}) \cdot \prod_{i=1}^{n} \frac{d^2 k_{\perp i}}{(2\pi)^2} \cdot D(s, k_{\perp i}) \delta^2 \left(k_\perp - \sum k_{\perp i} \right), \tag{2}$$

where at high energy, the primary amplitude $F_1(s,t)$ can be represented either as a pomeron exchange or as a more intricate set of reggeon diagrams and its factorized form is given by

$$F_1(s,t) = G(k_\perp) D(s, k_\perp) G(k_\perp), \tag{3}$$

where $D(s, k_\perp)$ refers to the Green function of the Pomeron. As stated in [17], the vertex function $N_n(k_{\perp i})$ in (2), representing the emission of n pomerons with transverse momenta $k_{\perp i}$ by the external hadron particle, can be expressed through integrals of the product of G vertices. Likewise, the vertices can be expanded over on mass shell states of diffractive-like beams [18], thereby accounting for the contribution from diffractive production in the multi-reggeon exchange weights :

$$N_n(k_i) = \sum_{\nu_1, \nu_2, .. \nu_n} \int G_{1\ \nu_1}(P_{in}, p_i^{(1)}) G_{\nu_1 \nu_2}(p_i^{(1)}, p_j^{(2)}) \cdots \cdots G_{\nu_{n-1} 1}(p_i^{(n-1)}, P_{out}) \prod_{i=1}^{n-1} d\Omega_{\nu_i}(p_i^{(1)}), \tag{4}$$

where $G_{\nu_1 \nu_2}(p_i^{(1)}, p_j^{(2)}, k_\perp)$ is the transition amplitude for a beam of ν_1 particles with momenta $p_i^{(1)}$ into a beam of ν_2 particles with momenta $p_j^{(2)}$, and with the emission of a pomeron with the transverse momentum $k_\perp$. In (4), the $d\Omega_\nu(p_i)$ represents the element of the ν particles phase-space volume. The Eq. (4) incorporates both the summation and integration over all conceivable physical states of the particles in the beams and thus accounts for their full masses. It is important to note that the multi-particle amplitudes $G_{\nu_1 \nu_2}$ are complex and may contain unrelated contributions, whereas the vertex functions $N_n(k_i)$ are real.

Considering a non-local field operator $\hat{G}(k)$ describing the pomeron emission vertices $G_{\nu_1 \nu_2}(k)$ between the initial and final states of the external particle, the expression (4) for the vertex functions $N_n(k_i)$ can be written in a symbolic operator form as the average of the product of this field operator $\hat{G}(k)$:

$$N_n(k_i) = \langle P_{in} | \hat{G}(k_1) \hat{G}(k_2) \cdots \hat{G}(k_n) | P_{out} \rangle \tag{5}$$

This product can further be decomposed over the complete set of physical states of the beams $|\nu\rangle$ as follows

$$N_n(k_i) = \sum_{\nu_1, \ldots, \nu_{n-1}} \langle P_{in} | \hat{G}(k_1) | \nu_1 \rangle \langle \nu_1 | \hat{G}(k_2) | \nu_2 \rangle \langle \nu_2 | \hat{G}(k_3) | \nu_3 \rangle \cdots \langle \nu_{n-2} | \hat{G}(k_{n-1}) | \nu_{n-1} \rangle \langle \nu_{n-1} | \hat{G}(k_n) | P_{out} \rangle \tag{6}$$

One can simplify the handling of the vertex operators $\hat{G}(k)$ by redefining the basis for the beam states $|\nu\rangle$ where $\hat{G}(k)$ has a simple diagonal form :

$$\hat{G}(k) |\nu\rangle = g_\nu(k) |\nu\rangle, \tag{7}$$

with $g_\nu(k)$ acting as eigenvalues. Then the expression Eq. (6) is simplified as the summation over all possible beam states, with the contribution from each state weighted by a function $w(\nu)$ and the product of its associated vertex functions for the different momentum com-

ponents k_i :

$$N_n(k_i) \ = \sum_{\nu} w(\nu) \ \prod_{1}^{n} g_\nu(k_i) \tag{8}$$

where $w(\nu)$ can be interpreted as the probability of finding the fast hadron in the state $\mid \nu\rangle$ and is given by:

$$w(\nu) = \langle P_{in}|\nu\rangle \ \langle \nu|P_{out}\rangle \tag{9}$$

Following this simplification, the S-matrix in the impact parameter representation can be written as follows:

$$\begin{aligned} S(s,b) \ &= \ \sum_{\nu_1\nu_2} w(\nu_1)w(\nu_2) \ \sum_{n=0}^{\infty} \frac{(\ i\ \chi_{\nu_1\nu_2}(s,b))^n}{n!} \\ &= \ \sum_{\nu_1\nu_2} w(\nu_1)w(\nu_2) e^{i\chi_{\nu_1\nu_2}(s,b)} \end{aligned} \tag{10}$$

where

$$\chi_{\nu_1\nu_2}(s,b) = \int d^2k_\perp e^{ibk_\perp} g_{\nu_1}(k_\perp) D(s,k_\perp) g_{\nu_2}(k_\perp) \tag{11}$$

One can further simplify the expression for the vertices by factorizing the vertex function $g_\nu(k)$ into a universal term $g(k)$ and a state-dependent coefficient $\lambda(\nu)$, with a small non-factorizable correction $\tilde{g}(\nu,k)$:

$$g_\nu(k) \ = \ g(k)\lambda(\nu) + \tilde{g}(\nu,k) \tag{12}$$

then the vertices can be represented as :

$$N_n(k_i) \ \simeq \ \beta_n \ \prod_{1}^{n} g(k_i), \tag{13}$$

where

$$\beta_n \ = \ \sum_{\nu} w(\nu) \ (\lambda(\nu))^n \tag{14}$$

Under this assumption of factorization, the vertices simplify to a product of universal functions $g(k_i)$, weighted by β_n, which encapsulates the sum over the probabilities $w(\nu)$ and the coefficients $(\lambda(\nu))^n$.

All in all we obtain the following expression for the S-Matrix in the impact parameter representation :

$$S(s,b) = \sum_{n=0}^{\infty} \frac{\beta_n^2}{n!} \left(i\,\chi(s,b)\right)^n \tag{15}$$

where the real coefficients $\beta_n \geq 1$ are largely arbitrary. Yet, their expressions will be determined depending on the unitarisation scheme chosen for the elastic amplitude, which will be illustrated in the forthcoming section.

The above equation provides a generalized expansion of the S-matrix whereby the coefficients govern the contributions of different orders of the interaction between the particles. Technically, the expansion is developed as a power series increasingly summing over complex interaction terms dictated by the function $\chi(s,b)$ which incorporates the scattering dynamics. Each term's weight is controlled by the coefficient β_n, reflecting the relative probability of different interaction strengths leading to the scattering process.

It is often not feasible to work directly with an infinite series due to the computational cost of calculating each term and the potential difficulty of evaluating the convergence characteristics. Yet, it might be possible to gain a better understanding of the series' structure in (38) by constructing a more compact and manageable formulation. This can be accomplished in a few different ways, for instance by mapping the series into an integral. By using spectral theory, for example, hidden spectral properties may be uncovered. To do so, we replace the coefficients β_n in (38) with the following expression :

$$\beta_n = \int_0^\infty d\tau\, \tau^n\, \varphi(\tau) \ , \tag{16}$$

then the $S[\chi]$ matrix can be rewritten as a combination of Glauber-type eikonal terms:

$$S(s,b) \equiv S[\chi] = \int_0^\infty d\tau\, \rho(\tau)\, e^{i\tau\chi(s,b)} \tag{17}$$

$$\rho(\tau) = \int_0^\infty \frac{d\tau_1}{\tau_1}\, \varphi(\tau_1)\, \varphi(\tau/\tau_1) \tag{18}$$

where $\rho(\tau)$ functions as a weight. The constraints $\beta_0 = \beta_1 = 1$ are imposed by the normalization condition for $S[\chi]$ and $w(\nu)$. This results in the following relations:

$$\int_0^\infty d\tau\, \rho(\tau) = \int_0^\infty d\tau\, \tau\rho(\tau) = 1 \tag{19}$$

It is worth noting that, in the Glauber eikonal case, the single-particle state in beams contributes very little to $N_n(k_i)$. When this occurs, the integrals in (4) disappear and the expression for $N_n(k_i)$ becomes a simple product of n elastic pomeron vertices as :

$$N_n(k_i) = \prod_{i=1}^{n} g(k_i), \tag{20}$$

where $g(k) = G_{11}(p, p+k)$.

Using the generalised S matrix representation, we can write some general relationships for cross-sections at a given impact parameter, which are expressed using the function $S[\chi(s,b)]$, and are valid for any spectral density $\rho(\tau)$.

- The total cross-section :

$$\sigma_{tot}(s,b) = 2(1 - Re(S[\chi])), \tag{21}$$

- The elastic cross-section

$$\sigma_{el}(s,b) = \mid 1 - S[\chi] \mid^2, \tag{22}$$

- The total inelastic cross-section

$$\sigma_{in}(s,b) = \sigma_{tot} - \sigma_{el} = 1 - |S[\chi]|^2 \tag{23}$$

- The total cross-section of diffraction generation : single σ_{sd} and double σ_{dd}

$$\begin{aligned}\sigma_{dif}(s,b) &= \sigma_{in} - \sigma_{\text{in, cut}} = 2\sigma_{sd} + \sigma_{dd} \\ &= S[2iIm(\chi)] - \mid S[\chi] \mid^2\end{aligned} \tag{24}$$

- The cross-section corresponding to processes when at least one pomeron is s-cut : when we cut a single pomeron from the elastic amplitude, this corresponds to taking the imaginary part of the corresponding partial-wave amplitude. From the optical theorem, we know that this is related to the cross-section for cutting a single pomeron. Therefore

$$\sigma_{\text{in, cut}}(s,b) = 1 - S[2i\ Im(\chi)] \tag{25}$$

and so the pomeron topological cross-section: these are the contributions of diagrams with n cut pomerons and of the arbitrary number of uncut pomeron lines

$$\sigma_n(s,b) = \int_0^\infty d\tau\rho(\tau)\ \frac{(2\tau Im(\chi))^n}{n!}\ e^{-2\tau Im(\chi)} \tag{26}$$

where $\rho(\tau)$ is a spectral density. The pomeron topological cross-section resembles a superposition of Poisson distributions, where each term represents the contribution of a Poisson distribution with mean $(2\tau\text{Im}(\chi))$ weighted by the spectral density $\rho(\tau)$.

III. RESULTS

A. Pomeron topological cross-section

This section is concerned with the investigation of the pomeron dynamics by utilizing the general representation of the S-Matrix. First of all, we start with highlighting the link between this general representation and the unitarization scheme and then with the pomeron weights. Let's examine two prominent unitarization schemes: the eikonal and the U-matrix. They are distinguished by their respective spectral functions $\rho(\tau)$, i.e. the β_n coefficients. For instance, if we consider a simple spectral function as a delta function,

$$\rho(\tau) \ = \ \delta(\tau - 1)\ , \tag{27}$$

then we obtain for the unitarised elastic scattering amplitude, the following expression :

$$A(s,b) = \mathrm{i}\left[1 - \mathrm{e}^{\mathrm{i}\chi(s,b)}\right] \tag{28}$$

which is the eikonal form of the unitarisation scheme [19]. In this case, using Eq. 26 , the pomeron topological cross-section is given by

$$\sigma_n(s,b) = \frac{(2\text{Im}(\chi))^n}{n!} e^{-2\text{Im}(\chi)} \tag{29}$$

While if we take for the spectral function, the expression :

$$\rho(\tau) = \frac{\mathrm{e}^{-\tau/c}}{c} \tag{30}$$

[20] and with $c = \frac{1}{2}$ then we get for the unitarised elastic scattering amplitude, this form :

$$A(s,b) = \frac{\chi(s,b)}{1 - \mathrm{i}\chi(s,b)/2} \tag{31}$$

which is the U-Matrix form of the unitarisation scheme [19], and for the pomeron topological cross-section, Eq. 26 gives :

$$\sigma_n(s,b) = \frac{(\text{Im}(\chi))^n}{(1 + \text{Im}(\chi))^{1+n}} \tag{32}$$

It is worth noting that different schemes for unitarizing the elastic amplitude, and hence various approaches to ensure the unitarity constraint, arise from the generalized S matrix form, which depends on the choice of the spectral function. Owing to the ambiguity of selecting the appropriate unitarisation scheme, particularly for hadron scattering at high energy, in spite of satisfying the unitarity constraint, one can resort to some general procedure. Indeed, it is significant to note that the optimization of a phenomenological model from the general expansion of the S-matrix may facilitate the identification of the suitable scheme. This can be achieved by fitting experimental data to some observables, such as total, elastic and inelastic cross-sections, among others. Then, the adequate scheme can be determined by deriving the appropriate spectral function from the best fits.

In the eikonal case, the number of pomerons is a random variable Poisson distributed [5]. Therefore, one may inquire about the nature of the probability distribution for the number of pomeron exchanged in alternative approaches, mainly the U-matrix scheme. As a matter of

fact, the expression 26 of the pomeron topological cross-section $\sigma_n(s,b)$, as a superposition of Poisson distribution, can be understood as a mixed Poisson distribution, in which the conditional distribution of the number of pomeron exchanged, given a certain rate parameter, is a Poisson distribution. Nevertheless, the rate parameter itself, in the mixed poisson framework, is handled as a random variable with its own distribution [21]. Thus, one can query what kind of features can be obtained with this random rate parameter rather than with a fixed Poisson rate parameter for all events. To achieve this, let a random variable X satisfies a mixed Poisson distribution with density $\pi(\lambda)$, then the probability distribution has this form :

$$Pr(X=n) = \int_0^\infty \frac{\lambda^n}{n!} e^{-\lambda}\ \pi(\lambda)\,\mathrm{d}\lambda. \tag{33}$$

If we consider that the Poisson rate parameter is distributed according to an exponential distribution, $\pi(\lambda) = \frac{1}{\gamma} e^{-\frac{\lambda}{\gamma}}$ and using integration by parts n times yields:

$$Pr(X=n) = \frac{1}{n!}\int_0^\infty \lambda^n\ e^{-\lambda}\ \frac{1}{\gamma} e^{-\frac{\lambda}{\gamma}}\,\mathrm{d}\lambda = \left(\frac{\gamma}{1+\gamma}\right)^n \left(\frac{1}{1+\gamma}\right) \tag{34}$$

we get $X \sim \text{Geo}\left(\frac{1}{1+\gamma}\right)$. And so the pomeron probability distribution in case of the U-matrix scheme gives the probability distribution of the number of failures until the first success of the exchanged pomerons.

$$Pr(X=n) = (1-p)^n\ \ p \tag{35}$$

for $n = 0, 1, 2, 3, ...$, where

$$p = \frac{1}{1+\gamma} \tag{36}$$

Thus, when compounding a Poisson distribution with rate parameter distributed according to an exponential distribution yields a geometric distribution. Or according to (32), for the pomeron topological cross-section in the U-Matrix case, we have :

$$P(X=n) = \left(\frac{\gamma}{1+\gamma}\right)^n \left(\frac{1}{1+\gamma}\right) = \sigma_n(s,b) = \frac{(\mathrm{Im}(\chi(s,b))^n}{(1+\mathrm{Im}(\chi(s,b))^{1+n}}, \tag{37}$$

with $\gamma = Im(\chi(s,b))$. Consequently, within the U-matrix scheme, the number of pomerons is a random variable that follows a geometric distribution, and hence pomeron exchanges are no longer independent, and this dependency implies collective phenomena such as correlation among the exchanged pomerons. This outcome distinguishes the U-matrix scheme from others, particularly the eikonal, which lacks these properties.

Another approach in [22] involves deriving the pomeron topological cross-section by applying the AGK cutting rules and using the coefficients obtained in each scheme by expanding the elastic scattering amplitude in impact parameter space as a power series of the Born term. The resulting expression is very similar to our result 32, with the main difference being an additional multiplicative factor of 2. Moreover, it was shown that the U-matrix unitarization is inconsistent with the AGK rules and in turn that the U-matrix scheme cannot be used for the unitarization of the pomeron with intercept greater than 1. Nevertheless, using the generalized representation of the S matrix 38, and the constraints $\beta_0 = 1$ imposed by the normalization condition for $S[\chi]$ and $w(\nu)$:

$$S(s,b) = \beta_0^2 + \sum_{n=1}^{\infty} \frac{\beta_n^2}{n!}\,(i\,\chi(s,b))^n = 1 + i\ A(s,b) \tag{38}$$

we obtain a generalized expansion of the unitarized elastic amplitude in impact parameter space :

$$A(s,b) = -i\ \sum_{n=1}^{\infty} \frac{\beta_n^2}{n!}\,(i\,\chi(s,b))^n \tag{39}$$

To obtain the expression of the unitarized elastic amplitude in each scheme, fixing in 39, the weight's coefficient β_n^2, reflecting the relative probability of different interaction strengths.

For the eikonal, case, let $\beta_n^2 = 1$ and so (39) implies

$$A(s,b) \;=\; i[1-e^{i\chi(s,b)}] = -i\sum_{n=1}^{\infty}\frac{[i\chi(s,b)]^n}{n!} = i\sum_{n=1}^{\infty} C_n^{eik}\cdot(-1)^{n-1}[\Omega(s,b)]^n, \tag{40}$$

where $\Omega(s,b) \equiv -2i\chi(s,b)$ is the opacity of pp interaction, and the coefficients of the power series are as in [22]:

$$C_n^{eik} = 2^{-n}/n!, \tag{41}$$

and for the U-matrix case, let $\beta_n^2 = c^n\ n!$ [23] with $c = \frac{1}{2}$, then (39) gives

$$\mathcal{A}(s,b) \;=\; \frac{\hat{\chi}(s,b)}{1-i\hat{\chi}(s,b)/2} = -2i\sum_{n=1}^{\infty}\frac{[i\hat{\chi}(s,b)]^n}{2^n} = i\sum_{n=1}^{\infty} C_n^U\cdot(-1)^{n-1}[\hat{\Omega}(s,b)]^n, \tag{42}$$

where $\hat{\Omega}(s,b) \equiv -2i\hat{\chi}(s,b)$ is the respective opacity, and the coefficients of the power series are :

$$C_n^U = 1/4^n \tag{43}$$

Note that, as opposed to [22], the first two terms of the pomeron exchange in the eikonal (40) and the U-matrix (42) schemes (with $\Omega = \mathbb{P} = \hat{\Omega}$) are not the same. Using the expression from [22] of the pomeron topological cross-section derived by applying the AGK cutting rules :

$$\sigma^k(s,b) = 2\sum_n C_n\cdot(-1)^{n-k}2^{n-1}\frac{n![\mathbb{P}(s,b)]^n}{k!(n-k)!}. \tag{44}$$

and replacing in (44) the coefficients C_n by C_n^U in the U matrix case, we get

$$\sigma_U^k(s,b) = \left[\frac{\mathrm{Im}\hat{\chi}(s,b)}{1+\mathrm{Im}\hat{\chi}(s,b)}\right]^k\frac{1}{1+\mathrm{Im}\hat{\chi}(s,b)} \tag{45}$$

exactly the same as our result (32). Regarding the problem of the inconsistency of the U-matrix unitarization with the AGK rules, we have from the unitarity equation in impact parameter space and (42) that:

$$\begin{aligned} G_{inel}(s,b) \;&=\; 2\mathrm{Im}\mathcal{A}(s,b) - |\mathcal{A}(s,b)|^2 \\ &=\; \frac{2\mathrm{Im}\hat{\chi}(s,b)}{(1-i\hat{\chi}(s,b)/2)(1+i\hat{\chi}^*(s,b)/2)}, \end{aligned} \tag{46}$$

and from (45) we get

$$G_{inel}(s,b) = \sum_k \sigma_U^k(s,b) = \frac{\mathrm{Im}\hat{\chi}(s,b)}{1+\mathrm{Im}\hat{\chi}(s,b)}\ . \tag{47}$$

In particular, at very large $s\to\infty$ according to (46) $G_{inel}\to 0$ whereas from (47) $G_{inel}\to 1$ .It is worth noting that the limit $G_{inel}\to 1$ provides a more physically consistent approximation of inelastic scattering at large $\hat{\chi}$, as it better reflects the suppression of contributions compared to the unphysical saturation implied by $G_{inel}\to 2$ in [22], bringing it closer to the expected asymptotic behavior of $G_{inel}\to 0$. Moreover, the discrepancy between the limit of convergence of G_{inel} in our result and the physical limit of convergence arises from the fact that, in the application of the AGK cutting rules in [22], the cut amplitude does not include contributions from the cross-section of the diffractive states, which corresponds to the production of states accompanied by a rapidity gap. Indeed, the AGK cutting rules relate different cuts of the same diagram, potentially leading to subtle connections or cancellations.

B. Pomeron multiplicity distribution

Let us quantify the implications of this finding in an explicit model. The starting point is the single pomeron scattering amplitude, i.e. the Born term. We parameterise it as

$$a(s,t) = g_p^2\,F_1(t)^2\left(\frac{s}{s_0}\right)^{\alpha(t)}\xi(t)\,, \tag{48}$$

using the pomeron trajectory $\alpha(t)$, the proton elastic form factor $F_1(t)$ and the coupling pomeron-proton g_p, with $\xi(t)$ the signature factor

$$\xi(t) = -e^{\frac{-i\pi\alpha(t)}{2}}\,. \tag{49}$$

and the pomeron trajectory close to a straight line

$$\alpha(t) = 1+\epsilon+\alpha' t. \tag{50}$$

In the impact-parameter representation, where the Fourier transform of the amplitude $a\,(s,t)$ rescaled by $2s$ is equivalent to a partial wave

$$\chi(s,\boldsymbol{b}) = \int\frac{\mathrm{d}^2\boldsymbol{q}}{(2\pi)^2}\frac{a(s,t)}{2s}\mathrm{e}^{\mathrm{i}\boldsymbol{q}\cdot\boldsymbol{b}}. \tag{51}$$

We used a dipole-like form factor for the proton $F_1 = 1/(1 - t/t_0)^2$. The parameters ϵ and α' describing the pomeron trajectory, the coupling constant g_p and t_0 the form-factor scale, are adjusted from a fit to up-to-date hadron collider data on total, elastic and inelastic cross-sections both for the eikonal and U-matrix unitarisation schemes [24] and are provided in table I.

In order to understand the hadronic dynamics at high and ultra-high energies, particularly in terms of the spatial distribution of the interactions and their implications for particle production, we examined the behaviour of the pomeron topological cross-section in the impact parameter space with energy and the number of pomerons exchanged, in both the eikonal and U-matrix cases, as shown in Fig. 1 and Fig. 2.

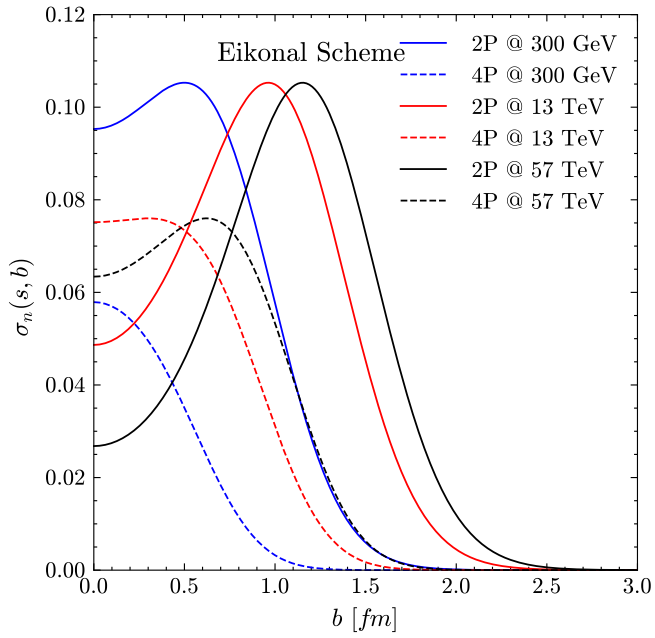

FIG. 1. Impact parameter evolution of the Pomeron Topological cross-section in the Eikonal case.

As can be seen from both figures, this function exhibits a distinct pattern in impact parameter space regardless of the scheme used. Nevertheless in each scheme, it has a broadly similar shape irrespective of both the energy level and the number of the pomerons exchanged. More specifically, as shown in the eikonal case, this function is predominantly peripheral, indicating a substantial contribution at large impact parameters. This implies that the majority of pomeron interactions are more likely to occur when the colliding hadrons pass through each other at large distances, reflecting that the interactions are "softer" in nature, meaning they involve long-range processes, likely mediated by soft pomeron exchanges. On the other hand, in the U matrix case, we can clearly see that this function is primarily central, suggesting that pomeron interactions tend to happen when the colliding hadrons pass through each other in close proximity, entailing that the collisions tend to involve higher energy densities, leading to more intense interactions in the core of the colliding hadrons.

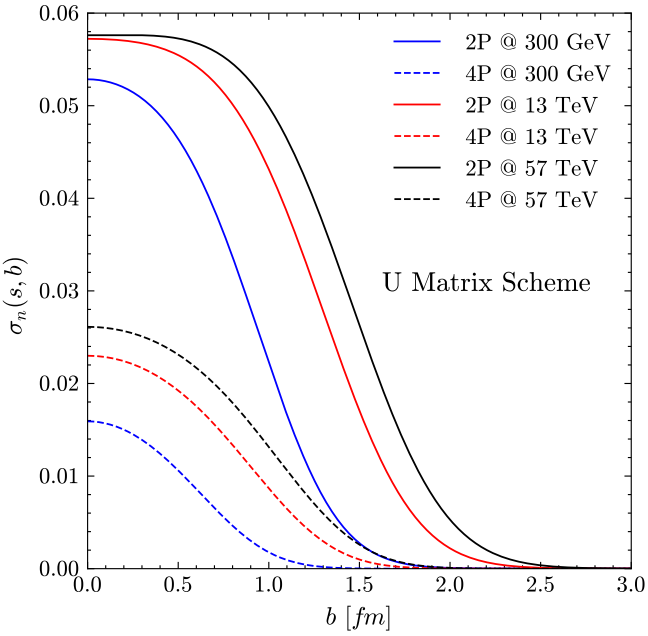

FIG. 2. Impact parameter evolution of the Pomeron Topological cross-section in the U-Matrix case.

Furthermore, another aspect observed from these figures is that, with the exponential scheme, this function tends to decline in the same manner with respect to the impact parameter as energy increases. Notably, for a given n, the peak of this function shifts toward larger values of b with increasing energy, while the magnitude of the peak remains approximately constant. This suggests that the spatial region, where the interactions take place, expands with increasing energy, making peripheral collisions even more dominant at ultra-high energy. Most importantly, this peripheral behaviour and constancy of the peak's magnitude are indicative of reaching a saturation effect where the available parton density limits the increase in the interaction strength even with increasing energy.

Whereas, with the rational scheme, this cross-section typically shows a more gradual decrease with increasing impact parameter as energy rises. More interestingly, for a given n, the maximum remains near the centre of the collision, and its value increases with energy. This indicates that the strength of the pomeron interactions grows at the core of the collision and we can understand that more partons are involved in the interaction in the central region. This reflects a regime where the interactions are still increasing, indicating that saturation has not yet been reached in the central collision region.

Additionally, according to these figures, it is clear that, for a fixed energy, with two and four pomerons exchanged the magnitude of this function decreases as n increases

Scheme	ϵ	α'	g_p	t_0	$\frac{\chi^2}{\text{d.o.f}}$
Eikonal	0.11 ± 0.01	0.31 ± 0.19	7.3 ± 0.9	1.9 ± 0.4	1.442
U-matrix	0.10 ± 0.01	0.37 ± 0.28	7.5 ± 0.8	2.5 ± 0.6	1.436

TABLE I. χ^2/d.o.f and best-fit parameters obtained using the eikonal and U-matrix unitarisation schemes.

for both schemes. We may suggest that higher-order pomeron exchanges become less significant at higher energies depending on their nature.

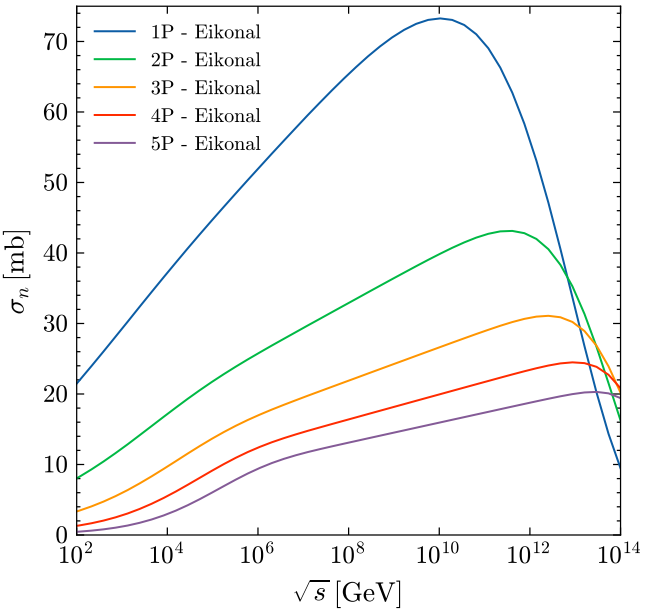

FIG. 3. Energy evolution of the Pomeron topological cross-section in the Eikonal case.

The energy evolution of the pomeron topological cross-sections for $1, 2, 3, 4$ and 5-pomerons exchanged has also been examined in both the eikonal and U-matrix cases. By looking at Fig. 3 and Fig. 4, we can generally see that these cross-sections roughly exhibit the same behavior in both schemes. To be more specific, for each pomeron exchanged, the cross-sections increase as energy rises, with the contribution of 1-pomeron exchanged showing the highest value across all energy ranges. This suggests that the interactions are primarily governed by the simplest diagrams in the pomeron exchange framework, especially at lower energies. As for the higher-order pomeron exchanges σ_{2pom}, σ_{3pom}, etc.), they contribute gradually less. It also shows that all cross-sections tend to reach a maximum then decline abruptly at extreme energies, indicating a signature of the unitarity constraint. It is significant to note that in comparison with the eikonal case, this unitarity constraint signature is hit at a slightly higher energy for each pomeron exchanged in the U-matrix case. Indeed, this demonstrates the different energy levels at which unitarity effects take

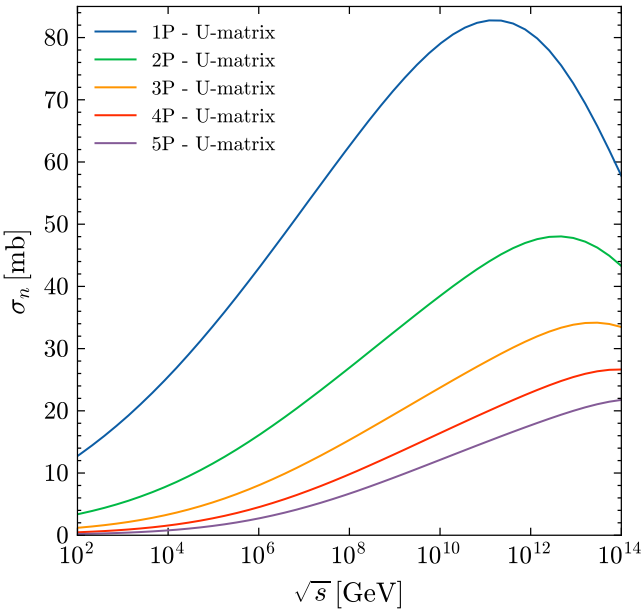

FIG. 4. Energy evolution of the Pomeron topological cross-section in the U Matrix case.

over for each pomeron contribution in these two schemes.

Furthermore, before reaching the energy threshold of the unitarity signature, it is evident that all cross-sections' curvatures, starting from 2 pomerons exchanged, significantly change at energies beyond 10^4 GeV in the eikonal case. It should be noted that with more pomerons being exchanged, this effect intensifies. Conversely, in the U-matrix case, despite taking into consideration several pomeron exchanges, the cross-sections show a more constant and progressive behaviour without any change in curvature.

The pomeron multiplicity distribution $W_n(s)$, i.e., the probability of n pomerons exchanged in an inelastic collision at the energy s, is given by

$$W_n = \frac{\sigma_n}{\sum_{n'} \sigma_{n'}} \tag{52}$$

Using the ansatz for the single pomeron exchange amplitude in the eikonal and U-Matrix cases, we compute W_n. The results are plotted in Fig. 5 for three collision energy scales.

Fig. 5 clearly shows that in the eikonal case, the exchange of a large number of pomerons is significantly suppressed compared to the U-matrix case. In the latter

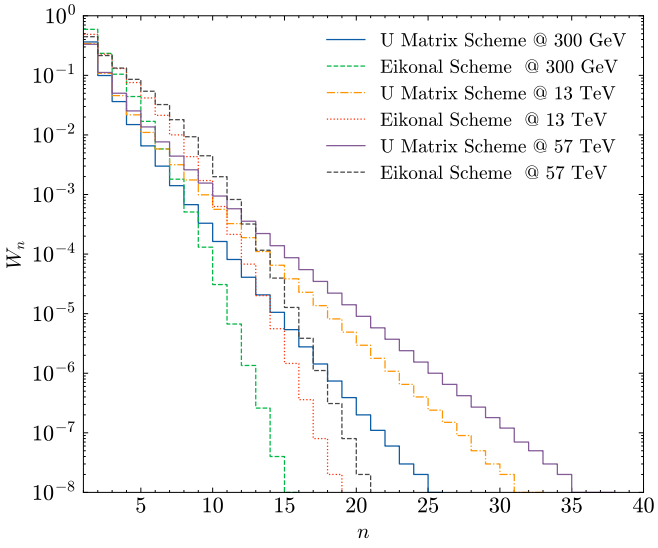

FIG. 5. Pomeron multiplicity distribution in both cases, eikonal and U-matrix.

scheme, the exchange of one pomeron enhances the probability of exchanging additional pomerons, and then the pomeron multiplicity distribution would deviate from a Poissonian one. This remarkable difference entails that multi-pomeron exchange is different in the two schemes. In particular, it may result from the presence of collective phenomena, such as correlations between the exchanged pomerons in contrast to what would be expected from an independent exchange.

It goes without saying that the role of the multi-pomeron exchange becomes more significant as energy grows. In the case of a Poisson distribution, the mean and the variance are equal. In hadronic interactions, however, their relationship tends to vary depending on a number of factors, such as the energy of the interaction. As a matter of fact, in order to highlight the role of the multi-pomeron exchange, particularly at high energy, we investigated the energy evolution of the mean and the variance of the number of pomerons exchanged. Using the probabilities in each scheme, we can calculate the mean and variance of the number of cut-pomerons as a function of the energy:

$$\langle n \rangle = \sum_{n'=0}^{\infty} n' W_{n'} \tag{53}$$

and

$$\mathrm{Var}(n) = \sum_{n'=0}^{\infty} n'^2 W_{n'} - \langle n \rangle^2. \tag{54}$$

By looking at Fig. 6, we can clearly see that in the eikonal case both the mean and the variance of the exchanged pomerons increase more considerably with energy. In addition, it is evident that the mean-variance relationship shows a noticeable shift around 10^4 GeV. More precisely, at energies below 10^4 GeV, we can notice that the variance is steadily smaller than the mean. This suggests that the fluctuations of the exchanged pomerons are not as severe as they are in the average behavior. This also points to a more consistent and stable interaction dynamics at lower energy, where more predictable contributions govern the pomeron exchanges. Nevertheless, at energies above 10^4 GeV, the variance exceeds the mean with a disproportionate growth.

It is significant to note that the result regarding the energy evolution of both the mean and the variance of the pomerons exchanged aligns with that reported in the quasi-eikonal framework [25]. Most importantly, they uncover a significant distinction in the energy shift of the mean-variance relationship. Indeed, the transition in the quasi-eikonal case, where the variance exceeds the mean, takes place at a lower energy scale, around 200 GeV. In contrast, this transition is seen at a greater energy, roughly 10^4 GeV, in the eikonal case. One of the possible explanations for this discrepancy is linked to the fact that the quasi-eikonal unitarization is an extended eikonal-like scheme, with an extra factor c in the expression of this unitarisation scheme accounting for the modification of the simple eikonal due to inelastic diffractive states. For instance, a value of $c = 1.5$ is utilized, corresponding to a 50% contribution of low-mass diffractive states, in comparison to the elastic ones. Hence, the additional dynamics from the diffractive process in the quasi-eikonal scheme make the number of exchanged pomerons more variable, which lowers the energy threshold for the transition regime in which the variance is greater than the mean.

Fig. 7 demonstrates the evolution of both the mean and the variance with energy in the U-matrix scheme. As can be seen, the mean number of pomerons exchanged progressively rises as energy grows and it keeps increasing at higher energies.

As far as the variance is concerned, it exhibits a similar increase. However, surprisingly enough, it is constantly greater than the mean throughout the whole energy range. This suggests that the number of pomerons exchanged shows greater fluctuations than the average at each energy level, and this deviation becomes more significant as energy rises. As a matter of fact, this striking result can be explained in terms of the vertices, i.e., the pomeron weights, pertaining to hadronic interactions at high energy. More precisely, on the one hand, we can infer that the U-matrix scheme intrinsically incorporates diffraction production into the multi-pomeron vertices, as they are weighted by the probabilities of the fast hadron being in various diffractive states (13), reflecting a wider range of interaction possibilities. The eikonal scheme, on the other hand, having a simpler vertex structure (20) has restricted variability at lower energies and exhibits fluctuations that only exceed the mean at higher energies, where the role of the multi-pomeron exchanges becomes substantial.

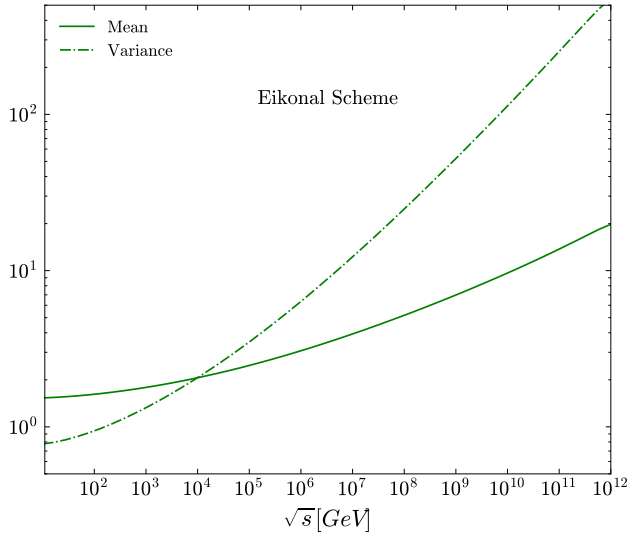

FIG. 6. Mean and variance of the number of pomerons in the eikonal and U Matrix case

Due to the fact that the U-matrix scheme yields larger fluctuations of the number of pomerons exchanged irrespective of the energy range in comparison to the simpler eikonal and the quasi-eikonal schemes, we can argue that it accounts for more complex interaction dynamics and for a larger amount of diffraction production. Interestingly, this resonates with a result obtained in [13] and most importantly helps explain why the U-matrix scheme describes the single diffractive data slightly better than the eikonal regardless of the data employed.

The disparity between the U-matrix and eikonal frameworks, with respect to the fluctuations in the number of pomerons exchanged, is most likely due to the diffractive states' overlap. It is significant to note that, the difference between the two schemes with regards to the parametrized hadronic overlap function is marginal (48). However, in the U-matrix scheme, there is a considerable diffractive states' overlap, which increases pomerons' variability and gives rise to more pronounced fluctuations. Conversely, since the eikonal scheme does not take into consideration such overlap, it shows simpler dynamics with suppressed fluctuations at lower energies. This comparison sheds light on the role that the U-matrix scheme plays in accounting for more intricate dynamics, particularly, when considering scattering processes with significant diffractive contributions.

Overall, despite the marginal difference in the functional form of the pomeron input in both schemes, we can deduce that the mechanism of unitarization significantly affects the fluctuations in the number of pomerons exchanged, and claim that the U-matrix scheme offers an efficient phenomenological approach to consider pomerons' variability regardless of the energy range, while such fluctuations become significant only beyond specific high-energy thresholds in the other schemes, namely the eikonal and quasi-eikonal.

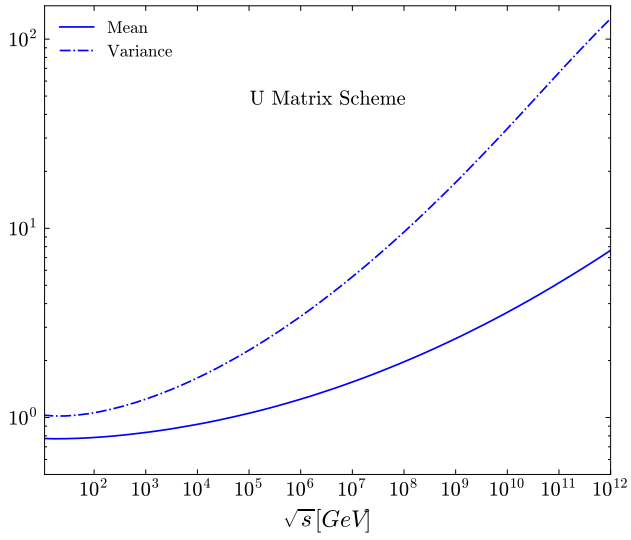

FIG. 7. Mean and variance of the number of pomerons in the eikonal and U Matrix case

The intriguing energy shift with regards to the mean-variance relationship hints at a transition in the underlying dynamics of the hadronic scattering process with respect to the energy regime. Thus, in order to better comprehend this energy transition, we will examine the f_2 moment of the pomeron multiplicity distribution, i.e., the two-particle correlation parameter, measuring the correlation between pairs of pomerons, across various energies within both the eikonal and U-matrix frameworks. This parameter is defined as follows :

$$f_2 =< n(n-1) > - < n >^2 = D_2^2 - < n > \qquad (55)$$

where D_2 is the dispersion: $D_2^2 =< n^2 > - < n >^2$. The two-particle correlation parameter has three possible values: negative, zero, and positive, in accordance with the multiplicity distributions that are narrower, equal to, or broader than a Poisson distribution.

By looking at Fig. 8, we can vividly see in the eikonal case that the f_2 moment displays a changing behavior in variation with energy. Indeed, at energies below 10^4 GeV, the f_2 moment is negative. This suggests that the pomeron multiplicity distribution is narrower than the Poisson distribution. This also implies that the particle production fluctuations are suppressed and the number of pomeron exchanges is distributed uniformly. At 10^4 GeV, the value of the f_2 moment is zero, which is indicative of the alignment of both the pomeron multiplicity and the Poisson distributions. This entails independent and randomly occurring events. At energies above 10^4 GeV, the f_2 moment becomes positive. This demonstrates that the pomeron multiplicity distribution is broader than the Poisson distribution, indicating an enhancement of pomeron fluctuations.

Turning now to the U-matrix case, Fig. 8 strikingly shows that the f_2 moment remains positive throughout various energy ranges, suggesting that the pomeron multiplicity distribution is constantly broader than the Poisson distribution and hence indicating an enhancement of pomeron fluctuations. These fluctuations become more noticeable with increasing energy and are remarkably constantly larger than those yielded in the eikonal case.

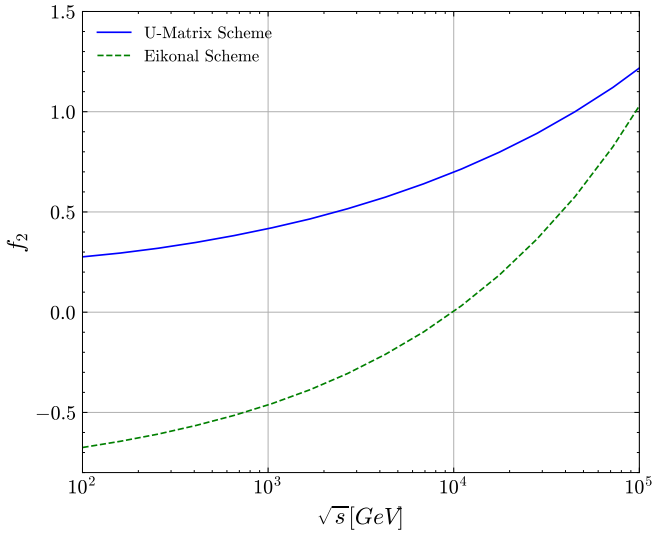

FIG. 8. The two-particle correlation parameter versus the interaction energy in the eikonal and U Matrix case

Fig. 9 displays the behavior of the f_2 parameter with respect to the mean number of pomerons in the eikonal and U-matrix cases, specifically for energies exceeding 10^4 GeV, where both schemes manifest pomeron fluctuations. It is apparent from this figure that both schemes yield amplified fluctuations. It also shows that the increasing mean number of pomerons with energy results in a rise in the correlation between pairs of pomerons. Nevertheless, it is worth noting that when comparing the two schemes, the correlation between pairs of pomerons rises considerably faster as the number of exchanged pomerons increases in the U-matrix scheme. This signifies that this latter incorporates enhanced correlations, indicating strong multi-pomeron dynamics.

It is evident from the sharper increase in f_2 in the U-matrix case that the two approaches handle high-energy hadronic interactions differently, with the U-matrix revealing more noticeable pomeron collective effects and non-linear pomeron exchanges.

These results strongly confirm our previous assertion that the U-matrix scheme naturally comprises pomeron statistical fluctuations that are distinct from those in eikonal-like schemes and further explain their impact on the properties of hadronic multi-particle production, in particular the unexpected overestimation of the fluctuations and correlations between final state particles with increasing energy in pp collisions, as shown in [8].

In view of the aforementioned results, we understand that the energy transition in the underpinning dynamics of the scattering process, which is only present in eikonal-like schemes, stems from a movement from a regime of suppressed pomeron fluctuations to a regime of enhanced fluctuations with increasing energy.

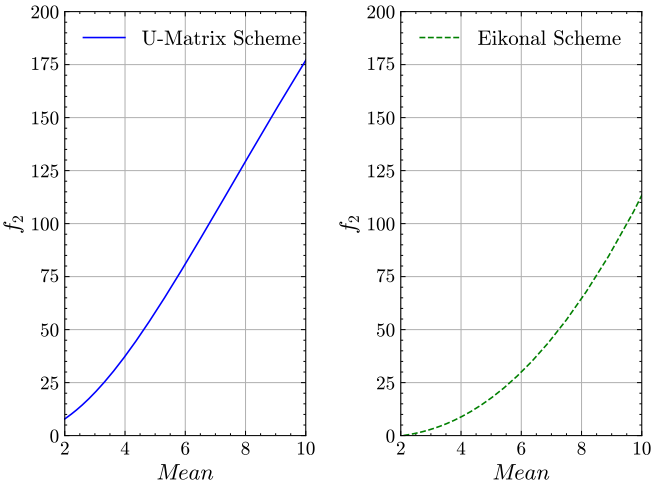

FIG. 9. The two-pomeron correlation parameter versus the average pomeron in the eikonal and U Matrix case

In light of the presence of enhanced pomeron fluctuations and a broader distribution within the U-matrix scheme, it is argued that the exchanged pomerons exhibit correlations which could be the result of collective effects, such as those stemming from the overlap of diffractive states that are in turn, emerging from the pomeron weights.

In an attempt to better comprehend these correlations, the higher-order moments of the pomeron multiplicity distribution were analyzed, as will be seen in the forthcoming subsection.

C. Pomeron correlations

In order to elucidate the nature of correlations among the pomerons exchanged in hadronic collisions, we examine the normalized factorial moments F_q of the pomeron multiplicity distribution. In fact, the moment F_q equals unity for all rank q in the case of an independent exchange of pomerons. Nevertheless, F_q is greater (less) than unity depending on whether the exchanged pomerons are correlated (anti-correlated) [26]. These moments are provided by

$$F_q = \frac{1}{\langle n \rangle^q} \sum_{n=q}^{\infty} n(n-1)...(n-q+1)\, P_n\,, \qquad (56)$$

where $\langle n \rangle = \sum_n n W_n$ is the average multiplicity and q is the rank of the moment. In the eikonal case, regard-

less of the energy scale, the normalized factorial moment remains equal to 1 for all ranks q, reflecting a Poisson distribution of the exchanged pomerons and indicating an uncorrelated distribution of events. In case of the U-matrix scheme, the moments are given by :

$$E(X^q) = p\ \mathrm{Li}_{-q}(1-p) \tag{57}$$

where $\mathrm{Li}_{-q}(1-p)$ is the polylogarithm function. So the normalized factorial moment of rank q is given by :

$$\mathrm{F}_q(s) = \frac{p\ \mathrm{Li}_{-q}(1-p)}{(\frac{1-p}{p})^q} \tag{58}$$

and p defined by 36.

Fig. 10 illustrates the behavior of the normalized factorial moments of pomerons exchanged in function of the rank q of pomerons and across various impact parameter b values within the framework of the U-matrix scheme, specifically at 13 GeV and 57 GeV. According to this figure, we can see that the normalized factorial moments F_q exhibit a considerably increasing pattern with q at both energies, indicating stronger higher-order correlations, where pomeron correlations emerge from $q = 3$ at 13 GeV, with two pomerons showing anti-correlation. However, they appear starting from $q = 2$ at 57 GeV, with all pomerons being positively correlated.

In both energies, when $b = 0$ fm, F_q is the highest suggesting that the strongest correlations occur in central collisions. Nevertheless, when b rises, we observe a decrease in F_q, indicating weaker correlations in less-central collisions because of a reduced interaction overlap. When comparing the two energies, F_q values are consistently greater at 57 GeV than at 13 GeV for all pomerons exchanged and impact parameter b, showing that pomeron correlations become more intense as center-of-mass energy increases. In addition, at both energies, F_q remains dependent on b, with correlations decreasing as b rises. Yet, it is significant to note that at 57 GeV we have stronger correlations even at larger b. This highlights that increasing collision energy mediates the influence of the impact parameter on the correlation strength while simultaneously strengthening correlations and reducing the prevalence of anti-correlation effects.

On the whole, both the energy and the impact parameter b have a combined impact on the correlation between pomerons exchanged, indicating that these two parameters are not entirely independent when it comes to influencing the number of elementary interactions.

To delve deeper in the interdependence between these two factors, we demonstrate in Fig. 11, 12, 13 and 14 the impact parameter evolution of the normalised factorial moment for various energy scales and different pomerons exchanged. One intriguing trend revealed by this evolution is that for each energy, F_q shows an inflection point at a specific value of b at which the correlation strength changes noticeably. Moreover, we can see that as energy increases, this inflection point moves to larger impact parameters, implying that the correlations between exchanged pomerons spread out more in transverse space. And, at extremely high energies, it reaches a value of about 1 fm, where correlations are roughly zero. In this regard, we suggest that as energy grows, the spatial scope of the interactions becomes more significant, reflecting an interdependence between the energy scale and the transverse position of pomerons.

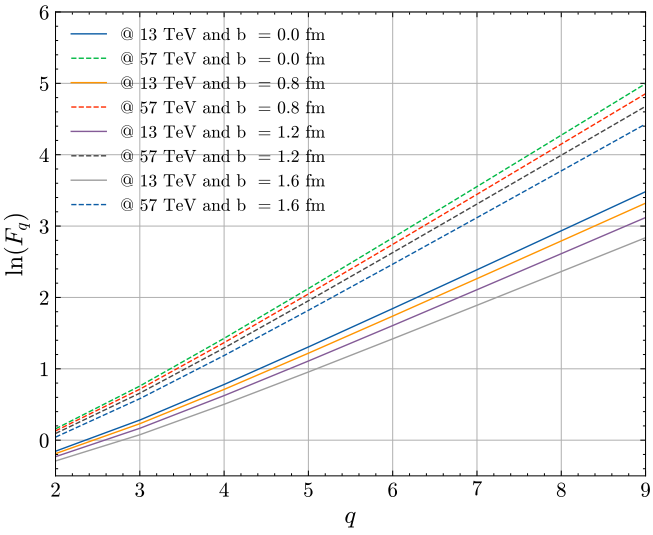

FIG. 10. Normalized factorial moment of pomeron exchanges as a function of the rank q and for different impact parameter b values with the U Matrix scheme

As a matter of fact, the aforementioned findings come in support of a previous suggestion that the U-matrix unitarization is probably incompatible with uncorrelated pomeron exchanges as there was no improvement in the description of the single diffractive data with a multi-channel model compared to a two-channel one [9]. To be more specific, [9] a multi-channel model of high-energy hadron interactions was created by considering a full parton configuration space and using the U-matrix unitarization scheme. Moreover, the mean number of interactions between partons was assumed to be expressed as a product of the single-pomeron scattering amplitude, together with functions of the impact parameter and configurations. Furthermore, we assumed that the impact parameter had no effect on the distribution of parton configurations. Nevertheless, in the present study, the interdependence effect observed between s and b on the number of pomerons exchanged breaks down the rigorous validity of such factorization within the U-matrix scheme. Furthermore, aside from its ease of use as a workable framework, as with the eikonal approach, this factorization assumption is short of a compelling theoretical foundation. As a result, the parton distribution functions cannot be efficiently separated into longitudinal and transverse components.

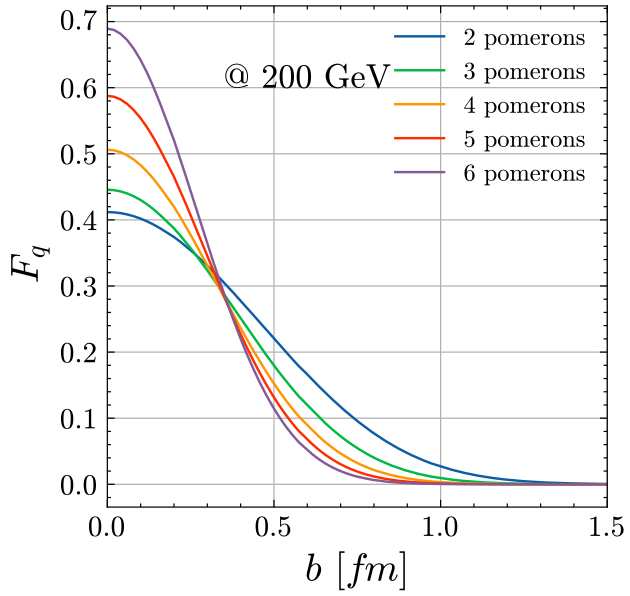

FIG. 11. Impact parameter evolution of the normalized factorial moment at 200 GeV

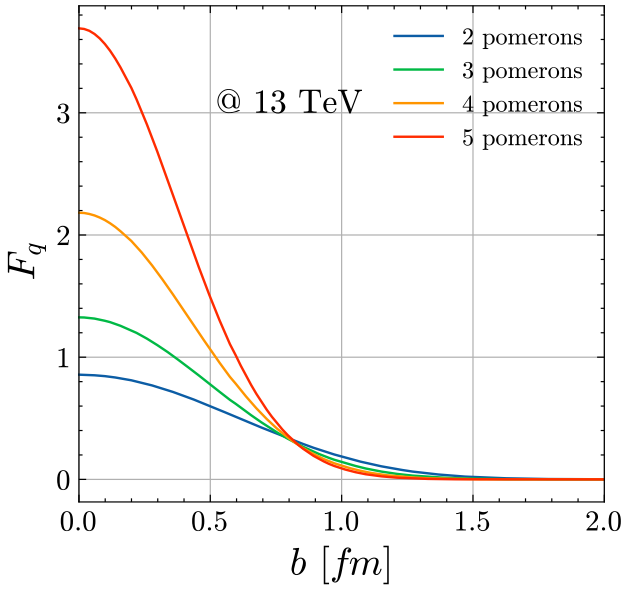

FIG. 13. Impact parameter evolution of the normalized factorial moment at 13 TeV

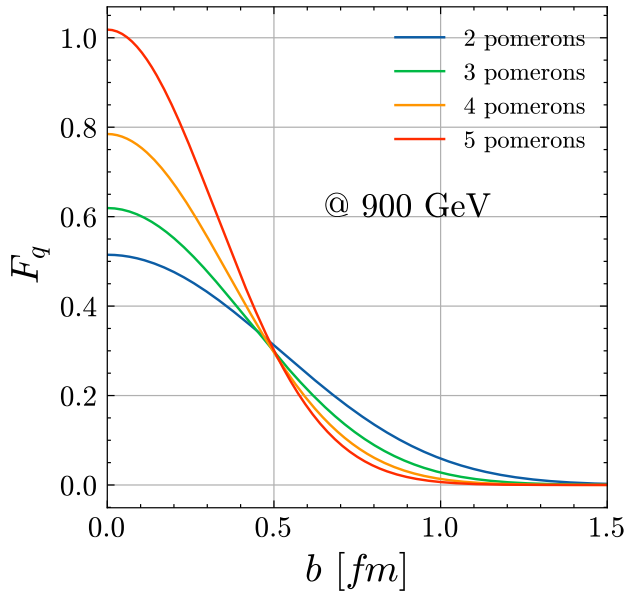

FIG. 12. Impact parameter evolution of the normalized factorial moment at 900 GeV

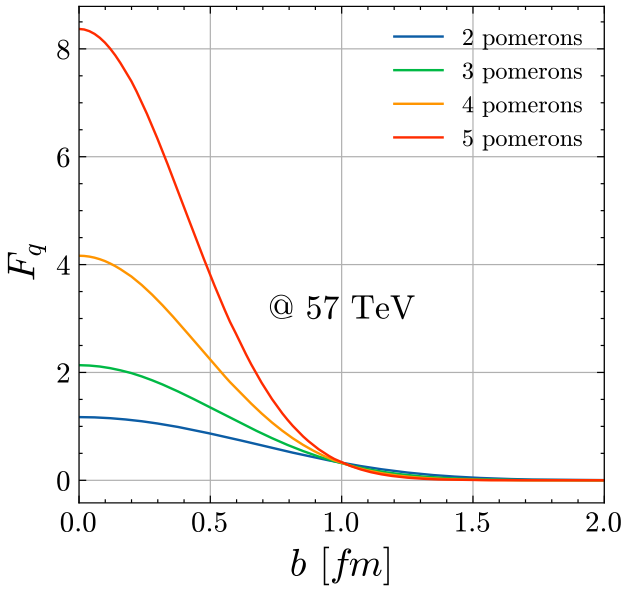

FIG. 14. Impact parameter evolution of the normalized factorial moment at 57 TeV

We can contend that the U-matrix approach offers a more suitable framework, as it provides a more accurate representation of the underlying elementary interactions, by taking into account the interdependence on all hadronic degrees of freedom. Moreover, correlations between pomerons allow the hadron's internal partonic structure to evolve dynamically during the scattering process. Thus, the U-matrix scheme does not require the hadrons to be frozen in their internal partonic configurations during the interaction, unlike the eikonal. Furthermore, by allowing for correlation between the exchanged pomerons, one can take into account the fact that the first pair of quark-antiquark strings is different from subsequent pairs, as the pomeron weights influence the dynamics of string pair formation. Consequently, the inconsistencies between the string model and the Gribov-Regge theory in hadronization models could be partially resolved within the U-matrix scheme.

D. Multiplicities in pp collisions

Correlations between partons are known to occur as a result of the fundamental dynamics of partonic interactions as well as the spatial and momentum structure of the hadron. In fact, these correlations are critical in identifying the topological cross-sections for processes, such as double and triple parton scattering, which in turn influence the observed multiplicity patterns and cross-sections in hadronic collisions.

This subsection elucidates the role of the correlated multi-pomeron exchange in hadronic collisions by analyzing the multiplicity distribution of pp and $\bar{p}p$ collisions from the point of view of multi-parton interactions, as described by string models along with the Regge Phenomenology (see the introduction section). According to this conjunction, a cut in the multi-pomeron exchange diagram is responsible for the hadrons yielded in the final state. More precisely, a cut of n pomerons results in $2n$ chains that connect to the partons of the initial hadrons. The number n, representing the pairs of simultaneously colliding partons from the different hadrons involved in the interaction, corresponds to the number of resulting showers. For instance, $n = 1$ translates into a single collision of one pair of partons emerging from the two colliding hadrons, which is ascribed to the Regge pole. $n = 2$ corresponds to a double collision of two pairs of partons from the different hadrons, which refers to the exchange of two pomerons, and so on.

In our analysis of the cross-section corresponding to the production of N secondary hadrons, $\sigma_N(s)$, diffraction processes were not considered so as to overlook long-distance correlations among particles within the same shower and the picture of the hadronic multi-particle production based on the Dual Parton Model (DPM) presented in [27] was followed mainly for comparison purposes.

In fact, in order to simplify our analysis, we assumed that the multiplicity distribution maintains its Poissonian character regardless of the energy scale, in spite of the known phenomenon of the violation of the KNO scaling [28] which entails that as energy increases, the hadronic multiplicity distribution broadens and deviates from a purely Poissonian nature :

$$P_n(N) = \frac{\langle N_n \rangle^N}{N!}\, e^{-\langle N_n \rangle} \tag{59}$$

where $\langle N_n \rangle$ represents the mean number of particles produced in n showers and is taken proportional to the mean multiplicity for a single shower :

$$\langle N_n \rangle = n \langle N_1 \rangle \tag{60}$$

and the mean multiplicity for a single shower is modelled as :

$$\langle N_1 \rangle = a + b\ \ln(s/s_0) \tag{61}$$

representing a logarithmic growth with centre-of-mass energy s, in agreement with experimental observations at low energy, with $a = -7.3$ and $b = 2.56$ from [27]. Thus, the total inelastic cross-section is constructed as a sum over contributions from n-shower events:

$$\sigma_{in}(N,s) = \sigma_1 P_1(N) + \sigma_2(P_2(N) + \sigma_3 P_3(N) + \ldots, \tag{62}$$

where the pomerons weights $\sigma_n(\xi_n)$ are given after impact parameter integration of the cross-section for the production of n showers in both schemes (32), (29) and $\xi_n = \ln\left(\frac{s}{s_0 n^2}\right)$. We retain three terms in 62 since the quadruple (or four-parton pair) collision has a small effect.

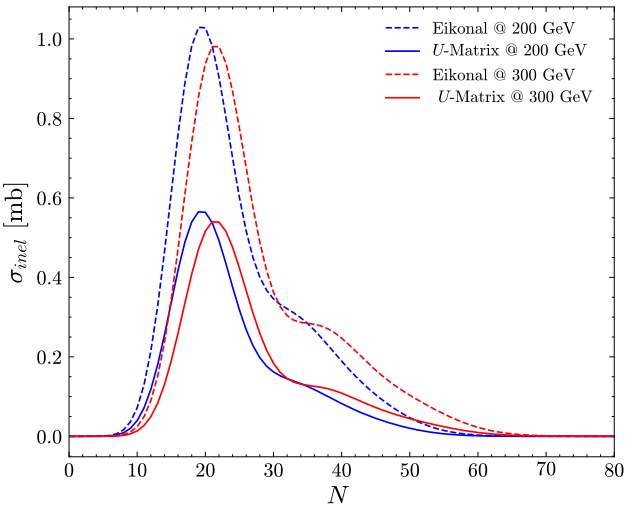

FIG. 15. Topological cross sections σ_N in the eikonal and U Matrix approximation with exchanges of three effective soft Pomerons.

By looking at Fig. 15 and Fig. 16, the shoulder, associated with the double collision, is clearly visible at low energies in the eikonal case, which is in concordance with the quasi-eikonal case [27]. Interestingly enough, in the U-matrix case, this second peak of $\sigma_N(s)$ is rather slightly resolved and tends to become broader and lower with increasing energy as opposed to the eikonal case. This behavior can be explained by the impact of correlated pomeron exchanges given that parton correlations enhance the probability of multi-parton collisions and hence re-distribute the contributions throughout the topological cross-sections. Thus, in the U-matrix scheme, correlated pomeron exchanges play a key role in enhancing multi-parton collisions, particularly double parton collisions.

These outcomes suggest that pomeron exchanges in the U-matrix framework embed a probability of concurrently finding partons with momentum fractions x_1 and x_2 within the hadron, which is represented by a non-zero correlation function $F(x_1, x_2)$, emphasizing the deviation

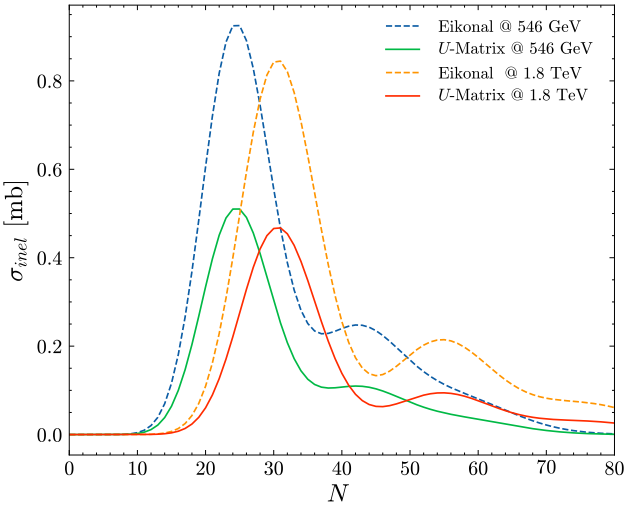

FIG. 16. Topological cross sections σ_N in the eikonal and U Matrix approximation with exchanges of three effective soft Pomerons.

from independent multi-parton interactions. In this regard, one may wonder how the U-matrix approach could allow disentangling correlations in multiple parton interactions, specifically separating the effects of fractional momentum correlations from those of transverse coordinate correlations, which is beyond the remit of this paper.

It is worth noting that in [27], the Dual Parton Model (DPM) was used to describe the double-parton collision, while solely taking the soft pomeron as the main component mediating the interactions between partons and comparing it to its hard counterpart. It has been argued that soft interactions are also responsible for the double inelastic parton collisions, which is confirmed by our result.

Moreover, given that the DPM is based on the quasi-eikonal scheme, we can infer that the incorporation of higher levels of diffractive production, resulting in an enhanced parton correlation, makes the U-matrix scheme a more reliable approach to the description of multi-parton collisions, compared to both the eikonal and quasi-eikonal schemes.

Owing that the soft interactions are also responsible for the double parton collisions, while a cut pomeron comprises contributions from both hard and soft processes, this makes us wonder about its nature, particularly in relation to the hard-soft hadronic physics transition, and may pave the way for a unified description of high-energy hadronic collisions in the context of the U-matrix.

IV. CONCLUSION

The chief purpose of the present paper was to understand the nature of the pomeron exchanges in hadronic interaction. Using a generalized representation of the unitarized hadronic elastic amplitude, the pomeron topological cross section was derived for both the U-matrix and eikonal schemes. Our results have demonstrated that the mechanism of the multi-pomeron exchange summation is distinct in each scheme at many levels. To be more specific, it has been found that in the impact parameter space, the elementary interactions tend to occur at the core of the collision in the U- matrix case as opposed to the eikonal case.

In addition, in both schemes, it has been shown that the pomeron topological cross-section for each higher-order exchanged pomeron increases with increasing energy and tends to reach a maximum then suddenly decreases at extreme energies, which marks the unitarity constraint. However, this unitarity constraint mark is reached at a somewhat higher energy for each pomeron exchanged in the U-matrix case. The disparity between the two schemes has also been shown concerning the curvature of this cross-section. More specifically, in the eikonal case, it considerably changed at energies beyond 10^4 GeV. In the U-matrix case, no change was observed.

Furthermore, the pomeron multiplicity distribution has been computed. In the U-matrix case, the pomeron exchange is a random variable geometrically distributed, and the exchange of one pomeron has been demonstrated to enhance the probability of exchanging additional pomerons.

Moreover, in the U-matrix case, the number of pomerons exchanged has shown greater fluctuations than the average at each energy level, and this deviation becomes more significant as energy rises. It has been deduced that the U-matrix scheme intrinsically incorporates diffraction production into the multi-pomeron vertices, reflecting a larger pomerons' variability regardless of the energy range, while such fluctuations become significant only beyond a specific high-energy threshold in the eikonal and quasi-eikonal schemes.

Furthermore, the pomeron exchange in the U-matrix scheme exhibits collective effects, as an increase in the number of exchanged pomerons leads to more pronounced higher-order pomeron correlations, which depend on both the energy and the impact parameter. This behavior contrasts with the independent pomeron exchange characteristic of the eikonal scheme.

Last but not least, the impact of pomeron weights on the proton-proton multiplicity distribution has been examined from the point of view of multi-parton interactions. The results have revealed that, in the U-matrix scheme, correlated pomeron exchanges play a key role in enhancing multi-parton collisions, particularly double parton collisions.

We understand from the findings of this study that the pomeron distribution is fixed by the unitarization scheme chosen to satisfy the unitarity constraint, and that this choice cannot be arbitrary.

In light of these results, although there is no fundamental theory to compute the vertices in hadronic interactions at high energy, we can claim that the U-matrix

scheme may incorporate the proper vertices for such phenomena. We also argue that the distribution of the number of elementary interactions pertaining to the U-matrix scheme should be implemented in Monte Carlo event generator in order to have more realistic predictions for high and ultra-high energy hadronic observables.

ACKNOWLEDGMENTS

RO would like to thank Jean-René Cudell for his invaluable comments. RO also appreciates the insightful discussions with Sergey Troshin. Special thanks go to the computational resource provided by Consortium des Équipements de Calcul Intensif (CÉCI), funded by the Fonds de la Recherche Scientifique de Belgique (F.R.S.-FNRS) where a part of the computational work was carried out.

[1] B. Andersson, G. Gustafson, G. Ingelman, and T. Sjöstrand, Physics Reports **97**, 31 (1983).
[2] V. N. Gribov, Zh. Eksp. Teor. Fiz. **53**, 654 (1967).
[3] F. Riehn, R. Engel, A. Fedynitch, T. K. Gaisser, and T. Stanev, Phys. Rev. D **102**, 063002 (2020).
[4] S. Ostapchenko, EPJ Web Conf. **208**, 11001 (2019).
[5] K. G. Boreskov, A. B. Kaidalov, V. A. Khoze, A. D. Martin, and M. G. Ryskin, The European Physical Journal C **44**, 523–531 (2005).
[6] E. Martynov and G. Tersimonov, Phys. Rev. D **101**, 114003 (2020).
[7] F. M. Liu, J. Aichelin, M. Bleicher, H. J. Drescher, S. Ostapchenko, T. Pierog, and K. Werner, Phys. Rev. D **67**, 034011 (2003).
[8] R. Oueslati and A. Trabelsi, JHEP **07**, 100, arXiv:2403.02263 [hep-ph].
[9] R. Oueslati, JHEP **08**, 087, arXiv:2305.03424 [hep-ph].
[10] R. Blankenbecler and M. L. Goldberger, Phys. Rev. **126**, 766 (1962).
[11] S. M. Troshin and N. E. Tyurin, Journal of Physics G: Nuclear and Particle Physics **29**, 1061 (2003).
[12] K. Ohashi, H. Menjo, Y. Itow, T. Sako, and K. Kasahara, Progress of Theoretical and Experimental Physics **2021**, 033F01 (2021), https://academic.oup.com/ptep/article-pdf/2021/3/033F01/36647718/ptab013.pdf.
[13] A. Vanthieghem, A. Bhattacharya, R. Oueslati, and J.-R. Cudell, JHEP **09**, 005, arXiv:2104.12923 [hep-ph].
[14] G. Feofilov, V. Kovalenko, and A. Puchkov, EPJ Web Conf. **171**, 18003 (2018), arXiv:1711.00842 [nucl-th].
[15] J. Bleibel, L. V. Bravina, A. B. Kaidalov, and E. E. Zabrodin, Phys. Rev. D **93**, 114012 (2016), arXiv:1011.2703 [hep-ph].
[16] O. V. Kancheli, (2013), arXiv:1309.5860 [hep-ph].
[17] V. N. Gribov, Soviet Physics JETP **100** (1983).
[18] V. N. Gribov and A. A. Migdal, Sov. J. Nucl. Phys. **8**, 1002 (1968).
[19] J.-R. Cudell, E. Predazzi, and O. V. Selyugin, Phys. Rev. **D79**, 034033 (2009), arXiv:0812.0735 [hep-ph].
[20] There appears to be a typo in the formula in [16].
[21] N. L. Johnson, S. Kotz, and A. W. Kemp, *Univariate Discrete Distributions*, 2nd ed. (John Wiley & Sons, New York, 1992).
[22] E. G. S. Luna and M. G. Ryskin, Phys. Rev. D **110**, 094007 (2024), arXiv:2408.00194 [hep-ph].
[23] There appears to be a typo in the formula in [16].
[24] A. Bhattacharya, J.-R. Cudell, R. Oueslati, and A. Vanthieghem, Phys. Rev. D **103**, L051502 (2021), arXiv:2012.07970 [hep-ph].
[25] E. Bodnia, D. Derkach, G. Feofilov, V. Kovalenko, and A. Puchkov, PoS **QFTHEP2013**, 060 (2013), arXiv:1310.1627 [hep-ph].
[26] I. M. Dremin, Phys. Usp. **37**, 715 (1994), arXiv:hep-ph/9406231.
[27] S. G. Matinyan and W. D. Walker, Phys. Rev. D **59**, 034022 (1999), arXiv:hep-ph/9801219.
[28] Z. Koba, H. Nielsen, and P. Olesen, Nuclear Physics B **40**, 317 (1972).

8 Conclusion

The chief goal of this thesis was to improve the modelling of hadronic interactions at high and ultra-high energies. To do so, the intricate dynamics of hadronic interactions were investigated at high energies, utilizing a combination of theoretical modelling and empirical data analysis in order to get a deeper understanding of proton-proton pp and proton-antiproton $p\bar{p}$ scattering. The problem of the S-matrix's unitarity lies at the core of this research, attempting to select the most accurate unitarity condition for composite particle interactions, such as hadrons, at high energies.

Practically, we focused on two unitarization schemes, namely the commonly used eikonal and the U-matrix, both of which were rigorously tested for their efficiency in predicting various key hadronic observables, such as the total, elastic, inelastic and diffractive cross-sections, as well as the multiplicity distributions, which are essential for both high-energy particle physics and astrophysical applications.

A brief review of what has been accomplished in the preceding pages will show to what degree this goal has been reached.

In the first study, the implications of high-energy collider data up to $\sqrt{s} = 13$ TeV on the best fits to total, elastic, and non-diffractive inelastic cross-sections for pp and $p\bar{p}$ scattering were examined using the two schemes. The findings demonstrated that, in comparison to the eikonal scheme, the U-matrix produces cross-sections that also fit the data, with marginal differences at energies relevant to present and near-future colliders. Although the overall inelastic cross-sections align, there are considerable differences in the amplitudes at each order in the series expansions, which could have implications for Monte Carlo showering codes.

In order to gain a more comprehensive understanding of high-energy hadronic interactions, the second study builds on the prior analysis by including diffractive interactions and using the two schemes in the context of a two-channel model. Best fits to the parameters governing the p p and pbar p total, elastic, inelastic and single diffractive cross sections we identified using up-to-date collider data, including 13 TeV from recent LHC experiments. The results have shown that both schemes generally fit the

data, with a minor preference for the U-matrix. While the best-fit total, elastic, and inelastic cross-sections are almost equal up to energies of 13 TeV when employing either of them, this difference is ascribed, particularly at high energies, to the single diffractive cross-section. It should be noted that, at the cost of an additional parameter, the extended version of these two schemes has yielded a marginal improvement in the fits.

Moving on to the third study, it aimed to provide a phenomenological description of the hadronic interaction at high energy through expanding the two-channel model into a multi-channel one, mainly using the U-matrix scheme. The results have indicated that the multi-channel model accurately describes the total, elastic, inelastic, and single-diffractive cross-sections, with only a minor difference from the two-channel one. Furthermore, it has been found that the model used fell short in estimating the double-diffractive cross-section, which further corroborates the results of the previous study. To remedy this, it has been proposed that an additional contribution, i.e., pomeron interaction can be introduced as a way to provide an adequate description of this cross-section.

In addition, the results have demonstrated that the present model describes well the ρ parameter at different high energies, but it is unable to estimate the TOTEM data at 13 TeV. In order to overcome this flaw, it has been suggested that an Odderon contribution is needed to be included. Moreover, despite similarities in the way the two models describe various hadronic observables, it has been shown that both furnish different predictions for the single-diffractive cross-sections, particularly at ultra-high energies, which represents an interesting direction for future research on ultra-high energy cosmic rays. Most importantly, the study has concluded by assuming that the U-matrix scheme is more likely to account for potential correlations between pomeron exchanges. Additionally, it has suggested that the two-channel model, as opposed to the multi-channel one, is adequate for modelling high-energy hadronic interactions, particularly single diffractive scattering, using the U-matrix scheme, even at ultra-high energies, provided that any potential pomeron correlations are disregarded.

In the fourth study, a phenomenological model for multi-particle production in hadron collisions based on the geometrical approach and using the U-Matrix scheme has been introduced. The model has been fine-tuned and all parameters have been derived from optimal fits to various hadronic full phase space multiplicity distributions data in $p+p(\bar{p})$ collisions across a broad range of energies. Broadly speaking, the results have revealed that

our model furnishes a reasonable description of these multiplicity distributions at various energies. Besides, they have demonstrated a pronounced violation of the geometrical scaling, which eventually resulted in a significant violation of the KNO scaling. The study has also analyzed the higher-order moments of the multiplicity distribution. We have observed an unexpected overestimation of the fluctuations and correlations between final state particles with increasing energy, particularly above LHC energy. It is claimed that this overestimation is due to statistical fluctuations embedded in the U-matrix scheme. Furthermore, the findings of this study have shed light on the key role of the U-matrix scheme in the impact of collision geometry on multi-particle production processes at high energy.

Lastly, in the fifth study, irrespective of the unitarization scheme employed, both the Pomeron topological cross-section and the Pomeron multiplicity distribution have been determined based on the Kancheli formalism. Interestingly, it has been found that compared to the eikonal scheme, in the U-matrix, pomerons are geometrically distributed and hence are correlated. Then, the role of pomeron correlation in pp multiplicity distribution has been examined. We have also explained how the mismatch between the Gribov-Regge theory and string models might be resolved by using the U-matrix technique.

In fact, this thesis adds to the body of knowledge in the field of high-energy hadronic interactions, especially when it comes to the study of cosmic ray physics and particle collisions at ultra-high energies. In particular, the choice of the U-matrix unitarization scheme as the focus of this research has been contributive as it has proved to be a useful tool, furnishing improved predictions for various cross-sections and shedding light on complex phenomena, such as multi-particle production and pomeron exchange. Additionally, the U-matrix scheme has demonstrated reliable extrapolation capabilities to ultra-high energy regimes, making it a promising candidate for future studies and applications.

Thus, implementing this scheme in Monte Carlo event generator codes could be a potentially fruitful avenue for future research, since these simulation codes are essential for the interpretation of experimental data and the prediction of particle collision results. Hence, this will furnish more accurate and reliable studies for future particle collider experiments and cosmic-ray physics.

Overall, this thesis has established a solid framework for further investigation into hadronic interactions at ultrahigh energies, offering novel

theoretical perspectives and useful techniques that will propel further developments in particle physics and astrophysics. In fact, this thesis is only a modest beginning in dealing with that probably never-ending task and challenge.

Bibliography

[1] A. Aab et al. The Pierre Auger Cosmic Ray Observatory. *Nucl. Instrum. Meth.*, A798:172–213, 2015.

[2] Alexander Aab et al. Measurement of the fluctuations in the number of muons in extensive air showers with the Pierre Auger Observatory. 2 2021.

[3] M. Aaboud et al. Measurement of the total cross section from elastic scattering in pp collisions at $\sqrt{s} = 8$ TeV with the ATLAS detector. *Phys. Lett.*, B761:158–178, 2016.

[4] G. Aad et al. Measurement of the Inelastic Proton-Proton Cross-Section at $\sqrt{s} = 7$ TeV with the ATLAS Detector. *Nature Commun.*, 2:463, 2011.

[5] G. Aad et al. Measurement of the total cross section from elastic scattering in pp collisions at $\sqrt{s} = 7$ TeV with the ATLAS detector. *Nucl. Phys.*, B889:486–548, 2014.

[6] R. Aaij et al. Measurement of the inelastic pp cross-section at a centre-of-mass energy of 13 TeV. *JHEP*, 06:100, 2018.

[7] et all. Abazov. Odderon exchange from elastic scattering differences between pp and $p\bar{p}$ data at 1.96 tev and from pp forward scattering measurements. *Phys. Rev. Lett.*, 127:062003, Aug 2021.

[8] R. Abbasi et al. IceTop: The surface component of IceCube. *Nucl. Instrum. Meth.*, A700:188–220, 2013.

[9] F. Abe et al. Measurement of $\bar{p}p$ single diffraction dissociation at $\sqrt{s} = 546$ GeV and 1800 GeV. *Phys. Rev.*, D50:5535–5549, 1994.

[10] F. Abe et al. Measurement of small angle $\bar{p}p$ elastic scattering at $\sqrt{s} = 546$ GeV and 1800 GeV. *Phys. Rev.*, D50:5518–5534, 1994.

[11] B. Abelev et al. Measurement of inelastic, single- and double-diffraction cross sections in proton–proton collisions at the LHC with ALICE. *Eur. Phys. J.*, C73(6):2456, 2013.

[12] T. Affolder et al. Double Diffraction Dissociation at the Fermilab Tevatron Collider. *Phys. Rev. Lett.*, 87:141802, 2001.

[13] Johannes Albrecht, Lorenzo Cazon, Hans Dembinski, Anatoli Fedynitch, Karl-Heinz Kampert, Tanguy Pierog, Wolfgang Rhode, Dennis Soldin, Bernhard Spaan, Ralf Ulrich, and Michael Unger. The muon puzzle in cosmic-ray induced air showers and its connection to the large hadron collider. *Astrophysics and Space Science*, 367(3), March 2022.

[14] T. Alexopoulos, E.W. Anderson, N.N. Biswas, A. Bujak, D.D. Carmony, A.R. Erwin, L.J. Gutay, A.S. Hirsch, C. Hojvat, V.P. Kenney, C.S. Lindsey, J.M. LoSecco, S.G. Matinyan, N. Morgan, S.H. Oh, N. Porile, R. Scharenberg, B. Stringfellow, M. Thompson, F. Turkot, W.D. Walker, and C.H. Wang. The role of double parton collisions in soft hadron interactions. *Physics Letters B*, 435(3):453–457, 1998.

[15] G. J. Alner et al. Antiproton-proton cross sections at 200 and 900 GeV c.m. energy. *Z. Phys.*, C32:153–161, 1986.

[16] G. J. Alner et al. UA5: A general study of proton-antiproton physics at $\sqrt{s} = 546$-GeV. *Phys. Rept.*, 154:247–383, 1987.

[17] N. A. Amos et al. A Luminosity Independent Measurement of the $\bar{p}p$ Total Cross-section at $\sqrt{s} = 1.8$-tev. *Phys. Lett.*, B243:158–164, 1990.

[18] N. A. Amos et al. $\bar{p}p$ Elastic Scattering at $\sqrt{s} = 1020$-GeV. *Nuovo Cim.*, A106:123–132, 1993.

[19] N. A. Amos et al. Diffraction dissociation in $\bar{p}p$ collisions at $\sqrt{s} =$ 1.8-TeV. *Phys. Lett.*, B301:313–316, 1993.

[20] L. Anchordoqui, M. T. Dova, A. G. Mariazzi, T. McCauley, Thomas C. Paul, S. Reucroft, and J. Swain. High energy physics in the atmosphere: Phenomenology of cosmic ray air showers. *Annals Phys.*, 314:145–207, 2004.

[21] R. E. Ansorge et al. Diffraction Dissociation at the CERN Pulsed Collider at CM Energies of 900-GeV and 200-GeV. *Z. Phys.*, C33:175, 1986.

[22] G. Antchev et al. First measurement of the total proton-proton cross section at the LHC energy of $\sqrt{s}$ =7 TeV. *EPL*, 96(2):21002, 2011.

[23] G. Antchev et al. Luminosity-Independent Measurement of the Proton-Proton Total Cross Section at $\sqrt{s} = 8$ TeV. *Phys. Rev. Lett.*, 111(1):012001, 2013.

[24] G. Antchev et al. Luminosity-independent measurements of total, elastic and inelastic cross-sections at $\sqrt{s} = 7$ TeV. *EPL*, 101(2):21004, 2013.

[25] G. Antchev et al. Measurement of proton-proton elastic scattering and total cross-section at S**(1/2) = 7-TeV. *EPL*, 101(2):21002, 2013.

[26] G. Antchev et al. Measurement of proton-proton inelastic scattering cross-section at $\sqrt{s} = 7$ TeV. *EPL*, 101(2):21003, 2013.

[27] G. Antchev et al. First determination of the ρ parameter at $\sqrt{s} = 13$ TeV: probing the existence of a colourless C-odd three-gluon compound state. *Eur. Phys. J.*, C79(9):785, 2019.

[28] G. Antchev et al. First measurement of elastic, inelastic and total cross-section at $\sqrt{s} = 13$ TeV by TOTEM and overview of cross-section data at LHC energies. *Eur. Phys. J.*, C79(2):103, 2019.

[29] X. Artru and G. Mennessier. String model and multiproduction. *Nuclear Physics B*, 70(1):93–115, 1974.

[30] C. Avila et al. A Measurement of the proton-antiproton total cross-section at $\sqrt{s} = 1.8$-TeV. *Phys. Lett.*, B445:419–422, 1999.

[31] C. Avila et al. The Ratio, ρ, of the Real to the Imaginary Part of the $\bar{p}p$ Forward Elastic Scattering Amplitude at $\sqrt{s} = 1.8$-TeV. *Phys. Lett.*, B537:41–44, 2002.

[32] Emil Avsar, Gösta Gustafson, and Leif Lönnblad. Diffractive excitation in dis and pp collisions. *Journal of High Energy Physics*, 2007(12):012, dec 2007.

[33] Saul Barshay. Geometric derivation of the diffractive multiplicity distribution. *Phys. Rev. Lett.*, 49:1609–1612, Nov 1982.

[34] Saul Barshay and Georg Kreyerhoff. Related power law growth of particle multiplicities near mid-rapidity in central Au + Au collisions and in anti $\bar{p}(p) - p$ collisions. *Nucl. Phys. A*, 697:563–568, 2002. [Erratum: Nucl.Phys.A 703, 891–891 (2002)].

[35] Alves Batista and all. Open questions in cosmic-ray research at ultrahigh energies. *Frontiers in Astronomy and Space Sciences*, 6:23, 2019.

[36] P. C. Beggio. A multiparton model for p p / p anti-p inelastic scattering. *Braz. J. Phys.*, 38:598–603, 2008.

[37] P. C. Beggio. Inelastic cross sections, overlap functions and C_q moments from ISR to LHC energies in proton interactions. *J. Phys. G*, 44(2):025002, 2017.

[38] P. C. Beggio and F. R. Coriolano. Energy dependence of the inelasticity in $pp/p\overline{p}$ collisions from experimental information on charged particle multiplicity distributions. *Eur. Phys. J. C*, 80(5):437, 2020.

[39] P. C. Beggio and Yogiro Hama. A new scheme for calculation of the multiplicity distributions in hadronic interactions. *Braz. J. Phys.*, 37(3B):1164–1170, 2007.

[40] P. C. Beggio, M. J. Menon, and P. Valin. Scaling violations: Connections between elastic and inelastic hadron scattering in a geometrical approach. *Phys. Rev. D*, 61:034015, 2000.

[41] P.C. Beggio and E.G.S. Luna. Cross sections, multiplicity and moment distributions at the lhc. *Nuclear Physics A*, 929:230–245, 2014.

[42] Atri Bhattacharya, Jean-René Cudell, Rami Oueslati, and Arno Vanthieghem. The proton inelastic cross section at ultrahigh energies. 12 2020.

[43] Atri Bhattacharya, Jean-René Cudell, Rami Oueslati, and Arno Vanthieghem. Proton inelastic cross section at ultrahigh energies. *Physical Review D*, 103(5), mar 2021.

[44] Christian Bierlich, Gösta Gustafson, and Leif Lönnblad. Diffractive and non-diffractive wounded nucleons and final states in pA collisions. *JHEP*, 10:139, 2016.

[45] R. Blankenbecler and M. L. Goldberger. Behavior of scattering amplitudes at high energies, bound states, and resonances. *Phys. Rev.*, 126:766–786, Apr 1962.

[46] M. M. Block. Sifting data in the real world. *Nucl. Instrum. Meth. A*, 556:308–324, 2006.

[47] K. G. Boreskov, A. B. Kaidalov, V. A. Khoze, A. D. Martin, and M. G. Ryskin. The Partonic interpretation of reggeon theory models. *Eur. Phys. J. C*, 44:523–531, 2005.

[48] M. Bozzo et al. Measurement of the Proton - anti-Proton Total and Elastic Cross-Sections at the CERN SPS Collider. *Phys. Lett.*, 147B:392–398, 1984.

[49] A Breakstone et al. *Phys. Rev. D*, 30:528–535, Aug 1984.

[50] M. Broilo, V. P. Gonçalves, and P. V. R. G. Silva. Model of diffractive excitation in *pp* collisions at high energies. *Phys. Rev. D*, 101:074034, Apr 2020.

[51] Hung Cheng and Tai Tsun Wu. High-energy elastic scattering in quantum electrodynamics. *Phys. Rev. Lett.*, 22:666–669, Mar 1969.

[52] T.T. Chou and Chen Ning Yang. Remarks on multiplicity fluctuations and kno scaling in pp collider experiments. *Physics Letters B*, 116(4):301–304, 1982.

[53] P. D. B. Collins. *An Introduction to Regge Theory and High Energy Physics*. Cambridge University Press, 1977.

[54] J.-R. Cudell. Elastic scattering, total cross sections and ρ parameters at the lhc. nov 2017. Paper presentation at the ATLAS collaboration meeting, Geneva, Switzerland.

[55] J.-R. Cudell, V. V. Ezhela, P. Gauron, K. Kang, Y. V. Kuyanov, S. B. Lugovsky, E. Martynov, B. Nicolescu, E. A. Razuvaev, and N. P. Tkachenko. Benchmarks for the forward observables at RHIC, the Tevatron Run II and the LHC. *Phys. Rev. Lett.*, 89:201801, 2002.

[56] J.-R. Cudell, K. Kang, and S. K. Kim. Simple pole fits to p p and anti-p p total cross-sections and real parts. *Phys. Lett. B*, 395:311–331, 1997.

[57] J.-R. Cudell, A. Lengyel, and E. Martynov. The Soft and the hard pomerons in hadron elastic scattering at small t. *Phys. Rev.*, D73:034008, 2006.

[58] J.-R. Cudell, E. Predazzi, and O. V. Selyugin. New analytic unitarisation schemes. *Phys. Rev.*, D79:034033, 2009.

[59] J.-R. Cudell, E. Predazzi, and O. V. Selyugin. New analytic unitarization schemes. *Phys. Rev. D*, 79:034033, Feb 2009.

[60] J.-R. Cudell and O. V. Selyugin. Saturation regimes at lhc energies. In *Proceedings, 4th Symposium on LHC Physics and Detectors: Batavia, USA, May 1-3, 2003*, volume 54, pages A441–A444, 2004.

[61] J.-R. Cudell and O. V. Selyugin. TOTEM data and the real part of the hadron elastic amplitude at 13 TeV. 2019.

[62] A Donnachie and P. V. Landshoff. Soft diffraction dissociation. 2003.

[63] A. Donnachie and P. V. Landshoff. pp and $\bar{p}p$ total cross sections and elastic scattering. *Phys. Lett.*, B727:500–505, 2013. [Erratum: Phys. Lett.B750,669(2015)].

[64] A. Donnachie and P. V. Landshoff. Small t elastic scattering and the ρ parameter. *Phys. Lett.*, B798:135008, 2019.

[65] I.M. Dremin and J.W. Gary. Hadron multiplicities. *Physics Reports*, 349(4):301–393, 2001.

[66] H. J. Drescher, M. Hladik, S. Ostapchenko, T. Pierog, and K. Werner. Parton based Gribov-Regge theory. *Phys. Rept.*, 350:93–289, 2001.

[67] Loyal Durand and Hong Pi. High-energy nucleon-nucleus scattering and cosmic-ray cross sections. *Phys. Rev. D*, 38:78–84, Jul 1988.

[68] David d'Enterria, Ralph Engel, Tanguy Pierog, Sergey Ostapchenko, and Klaus Werner. Constraints from the first lhc data on hadronic event generators for ultra-high energy cosmic-ray physics. *Astroparticle Physics*, 35(2):98–113, 2011.

[69] G.J. Alner et all. Scaling violation favouring high multiplicity events at 540 gev cms energy. *Physics Letters B*, 138(4):304–310, 1984.

[70] M. Bozzo et all. Measurement of the proton-antiproton total and elastic cross sections at the cern sps collider. *Physics Letters B*, 147(4):392–398, 1984.

[71] V. V. Ezhela, N. P. Petrov, V. A.and Tkachenko, and A. A. Logunov. On the ρ and σ_{tot} measurement by the TOTEM Collaboration: in the wake of recent discoveries. 3 2020.

[72] D.A. Fagundes, E.G.S. Luna, M.J. Menon, and A.A. Natale. Aspects of a dynamical gluon mass approach to elastic hadron scattering at lhc. *Nuclear Physics A*, 886:48–70, 2012.

[73] A. Fedynitch, F. Riehn, R. Engel, T. K. Gaisser, and T. Stanev. Hadronic interaction model sibyll 2.3c and inclusive lepton fluxes. *Phys. Rev.*, D100(10):103018, 2019.

[74] J. Finkelstein. AN IMPACT PARAMETER MODEL FOR MULTIPLICITY DISTRIBUTIONS. *Z. Phys. C*, 41:167, 1988.

[75] Christoffer Flensburg, Gosta Gustafson, and Leif Lonnblad. Elastic and quasi-elastic pp and $\gamma^* p$ scattering in the Dipole Model. *Eur. Phys. J. C*, 60:233–247, 2009.

[76] Christoffer Flensburg and Gösta Gustafson. Fluctuations, saturation, and diffractive excitation in high energy collisions. *Journal of High Energy Physics*, 2010(10), oct 2010.

[77] Christoffer Flensburg, Gösta Gustafson, and Leif Lönnblad. Inclusive and exclusive observables from dipoles in high energy collisions. *Journal of High Energy Physics*, 2011(8), aug 2011.

[78] Christoffer Flensburg, Gösta Gustafson, and Leif Lönnblad. Exclusive final states in diffractive excitation. *Journal of High Energy Physics*, 2012(12), dec 2012.

[79] Maria Beatriz Gay Ducati, M. M. Machado, and M. V. T. Machado. Investigating diffractive W production in hadron-hadron collisions at high energies. *Int. J. Mod. Phys. E*, 16:2956–2960, 2007.

[80] G. Giacomelli. Particle production in high energy collisions. 1 2009.

[81] R. J. Glauber. in lecture in theoretical physics. *Vol. 1, edited by W. E. Brittin, L. G. Duham (Interscience, New York, 1959).*

[82] M. L. Good and W. D. Walker. Diffraction dissociation of beam particles. *Phys. Rev.*, 120:1857–1860, Dec 1960.

[83] M. L. Good and W. D. Walker. Diffraction disssociation of beam particles. *Phys. Rev.*, 120:1857–1860, 1960.

[84] E. Gotsman, E. Levin, and U. Maor. Survival probability of large rapidity gaps in a three channel model. *Phys. Rev. D*, 60:094011, Oct 1999.

[85] E. Gotsman, E. Levin, and U. Maor. The Survival probability of large rapidity gaps in a three channel model. *Phys. Rev.*, D60:094011, 1999.

[86] E. Gotsman, E. Levin, and U. Maor. A comprehensive model of soft interactions in the LHC era. *Int. J. Mod. Phys.*, A30(08):1542005, 2015.

[87] E. Gotsman, E. M. Levin, and U. Maor. Diffractive dissociation and eikonalization in high-energy p p and p anti-p collisions. *Phys.Rev.D*, 49:4321–4325, 1994.

[88] N L Grigorov. Effect of inelastic interaction cross section increase on the shape of cosmic hadron spectrum. *Yadernaya Fizika*, 25(4):788–801, 1977.

[89] Jan Fiete Grosse-Oetringhaus and Klaus Reygers. Charged-particle multiplicity in proton–proton collisions. *Journal of Physics G: Nuclear and Particle Physics*, 37(8):083001, jul 2010.

[90] Gösta Gustafson, Leif Lönnblad, András Ster, and Tamás Csörgő. Total, inelastic and (quasi-)elastic cross sections of high energy pA and gamma-A reactions with the dipole formalism. *JHEP*, 10:022, 2015.

[91] M. Hatlo, F. James, P. Mato, L. Moneta, M. Winkler, and A. Zsenei. Developments of mathematical software libraries for the LHC experiments. *IEEE Trans. Nucl. Sci.*, 52:2818–2822, 2005.

[92] Kiyomi Itabashi. Koba-Nielsen-Olesen Scaling, Geometrical Scaling and Barshay-Yamaguchi Scaling. *Progress of Theoretical Physics*, 54(4):1168–1177, 10 1975.

[93] Syurei Iwao and Masaki Shako. Hadron-Hadron Interactions and their Interpretation as Critical Phenomena. 9 1974.

[94] László Jenkovszky, Rainer Schicker, and István Szanyi. Elastic and diffractive scatterings in the LHC era. *Int. J. Mod. Phys. E*, 27(08):1830005, 2018.

[95] H. Kawai et al. Telescope array experiment. *Nucl. Phys. Proc. Suppl.*, 175-176:221–226, 2008.

[96] V. A. Khoze, A. D. Martin, and M. G. Ryskin. Diffraction at the LHC. *European Physical Journal C*, 73:2503, July 2013.

[97] V. A. Khoze, A. D. Martin, and M. G. Ryskin. Elastic and diffractive scattering at the LHC. *Phys. Lett.*, B784:192–198, 2018.

[98] V. A. Khoze, A. D. Martin, and M. G. Ryskin. Elastic proton-proton scattering at 13 tev. *Phys. Rev. D*, 97:034019, Feb 2018.

[99] V. A. Khoze, A. D. Martin, and M. G. Ryskin. Multiple interactions and rapidity gap survival. *Journal of Physics G Nuclear Physics*, 45(5):053002, May 2018.

[100] Z. Koba, H.B. Nielsen, and P. Olesen. Scaling of multiplicity distributions in high energy hadron collisions. *Nuclear Physics B*, 40:317–334, 1972.

[101] R. S. Kolevatov and K. G. Boreskov. All-loop calculations of total, elastic and single diffractive cross sections in RFT via the stochastic approach. *AIP Conf. Proc.*, 1523(1):137–140, 2013.

[102] Hirak Koley, Arindam Mondal, Somnath Kar, Sreejita Mukherjee, Joyati Mondal, Argha Deb, and Mitali Mondal. Different degrees of complexity in multiparticle production at the LHC energies with the transition from soft to hard processes. In *65th DAE BRNS Symposium on nuclear physics*, 5 2022.

[103] Chou Kuang-chao, Liu Lian-sou, and Meng Ta-chung. Koba-nielsen-olesen scaling and production mechanism in high-energy collisions. *Phys. Rev. D*, 28:1080–1085, Sep 1983.

[104] C. S. Lam and P. S. Yeung. Possible connection between KNO and geometrical scaling. *Physics Letters B*, 119(4-6):445–448, December 1982.

[105] Paolo Lipari and Maurizio Lusignoli. Multiple parton interactions in hadron collisions and diffraction. *Phys. Rev. D*, 80:074014, Oct 2009.

[106] Fu-Hu Liu, Khusniddin K. Olimov, and Andrea Beraudo. Editorial: Particle production and system evolution in collisions from gev to tev. *Frontiers in Physics*, 10, 2022.

[107] A. A. Logunov, V. I. Savrin, N. E. Tyurin, and O. A. Khrustalev. Equal-time equation for two-particle system in quantum field theory. *Teor.Mat.Fiz.*, 6:157–165, 1971.

[108] E. Martynov and G. Tersimonov. Multigap diffraction cross sections: Problems in eikonal methods for the pomeron unitarization. *Phys. Rev. D*, 101:114003, Jun 2020.

[109] Hannu I. Miettinen and Jon Pumplin. Diffraction scattering and the parton structure of hadrons. *Phys. Rev. D*, 18:1696–1708, Sep 1978.

[110] M. Myska. Inelastic proton cross section at 13 TeV with ATLAS. *PoS*, ICHEP2016:1127, 2017.

[111] S. Ostapchenko. On the re-summation of enhanced Pomeron diagrams. *Phys. Lett. B*, 636:40–45, 2006.

[112] S. Ostapchenko. Monte Carlo treatment of hadronic interactions in enhanced Pomeron scheme: I. QGSJET-II model. *Phys. Rev.*, D83:014018, 2011.

[113] S. Ostapchenko. QGSJET-III model: physics and preliminary results. *EPJ Web Conf.*, 208:11001, 2019.

[114] Ostapchenko, Sergey. Qgsjet-iii model: physics and preliminary results. *EPJ Web Conf.*, 208:11001, 2019.

[115] Rami Oueslati. A multi-channel U-Matrix model of hadron interaction at high energy. *JHEP*, 08:087, 2023.

[116] A. Pandav, D. Mallick, and B. Mohanty. Search for the QCD critical point in high energy nuclear collisions. *Prog. Part. Nucl. Phys.*, 125:103960, 2022.

[117] F. Riehn, R. Engel, A. Fedynitch, T. K. Gaisser, and T. Stanev. Hadronic interaction model Sibyll 2.3d and extensive air showers. *Phys. Rev. D*, 102(6):063002, 2020.

[118] Felix Riehn, Ralph Engel, Anatoli Fedynitch, Thomas K. Gaisser, and Todor Stanev. Hadronic interaction model sibyll 2.3d and extensive air showers. *Phys. Rev. D*, 102:063002, Sep 2020.

[119] V. I. Savrin, N. E. Tyurin, and O. A. Khrustalev. The u matrix method in the theory of strong interactions. *Fiz.Elem.Chast.Atom.Yadra*, 7:21–54, 1976.

[120] O. V. Selyugin and J.-R. Cudell. Saturation effects in pp scattering in the impact-parameter representation. *Nucl. Phys. Proc. Suppl.*, 146:185–187, 2005. [,185(2004)].

[121] O. V. Selyugin, J. R. Cudell, and E. Predazzi. Analytic properties of different unitarization schemes. *Eur. Phys. J. ST*, 162:37–42, 2008.

[122] Chia C. Shih and Jing-ye Zhang. Particle production at high energy. i. geometrical orientated simulation of hadron-hadron collisions below 250 gev/c. *Phys. Rev. C*, 55:378–383, Jan 1997.

[123] A. I. Shoshi, F. D. Steffen, and H. J. Pirner. S matrix unitarity, impact parameter profiles, gluon saturation and high-energy scattering. *Nucl.Phys.A*, 709:131–183, 2002.

[124] Ranbir Singh, Lokesh Kumar, Pawan Kumar Netrakanti, and Bedangadas Mohanty. Selected Experimental Results from Heavy Ion Collisions at LHC. *Adv. High Energy Phys.*, 2013:761474, 2013.

[125] A. M. Sirunyan et al. Measurement of the inelastic proton-proton cross section at $\sqrt{s} = 13$ TeV. *JHEP*, 07:161, 2018.

[126] Albert M Sirunyan et al. Bose-Einstein correlations of charged hadrons in proton-proton collisions at $\sqrt{s} = 13$ TeV. *JHEP*, 03:014, 2020.

[127] M. Tanabashi et al. Review of Particle Physics. *Phys. Rev.*, D98(3):030001, 2018.

[128] Daniele Treleani. A multi-channel poissonian model for multi-parton scatterings, 2008.

[129] S M Troshin and N E Tyurin. Multiparticle production in the model with antishadowing. *Journal of Physics G: Nuclear and Particle Physics*, 29(6):1061, apr 2003.

[130] S. M. Troshin and N. E. Tyurin. Unitarity at the LHC energies. *Phys. Part. Nucl.*, 35:555–566, 2004.

[131] S. M. Troshin and N. E. Tyurin. The new scattering mode emerging at the LHC? *Mod. Phys. Lett. A*, 31(13):1650079, 2016.

[132] S. M. Troshin and N. E. Tyurin. Reflective scattering at the LHC and two-scale structure of a proton. *EPL*, 129(3):31002, 2020.

[133] S. M. Troshin and N. E. Tyurin. Reflective scattering at the lhc and two-scale structure of a proton. *Europhysics Letters*, 129(3):31002, feb 2020.

[134] L. Van Hove. Particle production in high energy hadron collisions. *Physics Reports*, 1(7):347–379, 1971.

[135] Arno Vanthieghem, Atri Bhattacharya, Rami Oueslati, and Jean-René Cudell. Unitarisation dependence of diffractive scattering in light of high-energy collider data. *Journal of High Energy Physics*, 2021(9), sep 2021.

[136] Arno Vanthieghem, Atri Bhattacharya, Rami Oueslati, and Jean-René Cudell. Unitarisation dependence of diffractive scattering in light of high-energy collider data. *JHEP*, 09:005, 2021.

[137] He Yudong, Wang Guangjun, Mu Jun, and Tai An. On the geometrical picture of multiparticle production in high-energy hadron-hadron collisions. *Europhysics Letters*, 9(7):645, aug 1989.